Green Flying

Final Report
DSE Group 08

TUDelft

This page was intentionally left blank

Green Flying

Final Report

by

DSE Group 08

Group members

Surname	Name	Student Number
Delgado Gosálvez	Marco	4268083
Ham, van	Jacomijn	4301145
Joosten	Sjoerd	4486048
Juschus	Daniel	4439317
Nieuwerth	Gerjan	4171047
Pelt, van	Tess	4465423
Smit	Lars	4479467
Takken	Michel	4431073
Wang	Yanbo	4352750
Ziere	Tijs	4088360

Version control

Version	Purpose/Changes	Responsibility	Date
0.9	Draft	Daniel Juschus (Project Manager)	27.06.2018
0.91	Updated Draft	Daniel Juschus (Project Manager)	29.06.2018
0.92	Updated Draft	Daniel Juschus	02.07.2018
1.0	Final Version		

Date: July 3, 2018
Supervisors: Prof. P. Groen, TU Delft, Principal Tutor
F. K. Leverone, Msc. TU Delft, Coach

TUDelft

Preface

Before you lies the culmination of the final results of the Green Flying project of the Spring Design Synthesis Exercise 2018. The DSE is the final step for Bachelor students in Aerospace Engineering at the Delft University of Technology towards obtaining their degree. Ten weeks of complex aerospace research, intensive coding and innovative design work by a team of ten students have led to this report and the results presented in it.

We had the honour to examine the future of flying. Most of us admire aircraft but also care deeply about the environment. Global warming and the depletion of fossil fuels are amongst the most pressing issues of today's modern society. The aviation industry is one of the industries which appears incapable of adopting the necessary changes to prevent the unsustainable use of our natural resources, as all commercially viable air transport solutions still rely on fossil fuels. In this project we had the chance to conduct research on emerging technologies which will enable a better future in which emission free flying is possible!

After ten weeks of hard work we are proud to present our work, into which we put all our knowledge, skills and energy. We would like to especially thank our principal tutor Pim Groen and our coach Fiona Leverone for their great support and very valuable help along the project. We would also like to express our gratitude to all other staff members, friends and family members who have supported us in these past weeks.

The future of green flying is blue. - Group 8

Abstract

Background

Twenty years ago, the possibility of electrical driving was still far out of reach. Now we see a rapid transition where electric cars become available and most manufacturers are investing heavily into this technology. The main driving force behind this transition is the need to slow down climate change, which requires a significant reduction of greenhouse gas emissions such as CO_2. In aviation however, commercially viable emission-free air transport solutions do not yet exist. This report aims to demonstrate the feasibility of emerging, sustainable technologies in this field.

Results

The analysis presented in this report shows that indeed by 2030, emission free passenger aircraft can be reality, by developing the concept of *The Greenliner: A novel propeller aircraft featuring distributed propulsion around its fuselage, with conventional (low) wing and tail configurations, which uses fuel cells in combination with liquid hydrogen as its source of energy.* After careful consideration of different criteria, hydrogen was selected as the main source of energy. To maximise the overall system performance, the most optimal hydrogen storage option was connected with the best-performing fuel cell type, resulting in the combination of cooled liquid hydrogen and a proton exchange membrane fuel cell. Liquid hydrogen has many important advantages and forms a crucial step towards the goal of emission-free flying: the aircraft's only direct product is pure water. In order to increase the propulsive efficiency it was decided to make use of a distributed electrical propulsive fuselage, which includes the promising concept of boundary layer ingestion.

Conclusions

It is concluded that the presented design is indeed emission free and is capable of fulfilling the requirements of completing a 500 nmi flight within 2 hours, while being economically viable.

List of Symbols

Latin	Explanation	Unit
a	Water vapour activity	[-]
a	Tank cross section radius	[m]
A	Aspect Ratio	[-]
A	Area	[m^2]
A_{e1}	Effective area of 1 propeller for 1 prop configuration	[m^2]
A_{en}	Effective area of 1 propeller for nth prop configuration	[m^2]
A_{cn}	Cross area for nth prop for nth prop configuration	[m^2]
A_{ten}	Total effective area of propellers for nth configuration	[m^2]
A_{tp1}	Total area covered by 1 propeller for 1 prop	[m^2]
A_{tpn}	Total area covered by n propellers for nth prop	[m^2]
ASR	Area-specific resistance	[Ω.m^2]
b	Wingspan	[m]
b	Tank sphere depth	[m]
$\bar{C}$/MAC	Mean aerodynamic chord	[m]
C_D	Drag coefficient	[-]
C_L	Lift coefficient	[-]
C_l	Airfoil lift coefficient	[-]
C_m	Moment coefficient	[-]
C_r	Root chord	[m]
c	Concentration	[mol/m^3]
c	Tank cross section height	m
cg	Centre of gravity position from nose	[m]
D	Diameter	[m]
D	Drag	[N]
E_0	Standard cell potential	[V]
E_y	Yong's modules	[GPa]
f_Ω	Rounds per second of propeller	[Hz]
F	Faraday's constant	[mol/s]
g	Gravitational constant	[N/kg]
I	Moment of inertia	[kg.m^2]
i	Incidence angle	[deg]
j	Current density	[A/m^2]
K	Limit stress	[Pa]
K_{uht}	Constant for unit horizontal tail	[-]
L	Rolling moment	[Nm]
L	Lift	[N]
l	Arm (length)	[m]
M/m	Mass	[kg]
M	Mach number	[-]
M	Pitching moment	[Nm]
$\dot{m}$	Mass flow	[kg/s]
N	Yawing moment	[Nm]
p	Pressure	[Pa]
p_c	Critical pressure	[Pa]
P	Roll rate	[rad/s]
P_a	Power available	[W]
P_s	Shaft power	[W]
Q_s	Shaft torque	[Nm]
q	Dynamic pressure	[Pa]
R	Universal gas constant	[J/mol.K]
R	Radius	[m]
Re	Reynolds number	[-]
S	Source or sink term	[-]
S	Wing area	[m^2]
s	tank wall thickness	[m]
t	Thickness	[m]
T	Temperature	[K]
T	Thrust	[N]
T_c	Critical temperature	[K]
u	Velocity vector	[m/s]
V	Voltage	[V]
V	Velocity	[m/s]
V_1	Input velocity	[m/s]
V_2	Output velocity	[m/s]
$V_{\Omega,tip}$	Propeller rotational tip velocity	[rad/s]
W	Weight	[N]
X_k	Molar fraction of species k	[-]
y_{max}	Gas and liquid H_2 volume ratio	[-]

Greek	Explanation	Unit
α	Transfer coefficient	[-]
α	Angle of attack	[deg]
β	Side slip angle	[deg]
Γ_0	Wing root circulation	$[m^2/s]$
Δ	Sweep angle	[deg]
δ_s	Control surface deflection	[-]
δ	Boundary layer thickness	[m]
ϵ	Porosity	[-]
ϵ	downwash angle	[°]
η	dynamic pressure ratio	[-]
η	Airfoil efficiency factor	[-]
η_{Act}	Activation overvoltage	[V]
η_{Conc}	Concentration overvoltage	[V]
η_{Ohm}	Ohmic overvoltage	[V]
η_p	Propulsive efficiency	[-]
κ	Permeability	$[m^{-2}]$
Λ	Tank length ratio	[-]
λ	water content	[-]
μ	Viscocity	[Pa.s]
ρ	Density	[kg/m^3]
σ	Conductivity	[S/m]
σ	Stress	[N/m^2]
τ_s	Control surface angle of attack effectiveness parameter	[-]
Φ	Potential	[V]
ϕ	Tank ellipsoidal axes ratio	[-]
ψ	Tank ellipsoidal axes ratio	[-]
Ω	Angular velocity of propeller	[rad/s]
ω	Molar mass	[kg/mol]

Subscript	Explanation
∞	Free stream
a	Anode electrode
a	Available
avg	Average
A/a	Aileron
BL	Boundary layer
c	Cathode electrode
csw	Control surface wing
D	Drag
d_0	Zero-lift drag
dg	Design gross
e	Electrolyte phase
E/e	Elevator
f	Fuselage
gap	Gap inside of ring of propellers
H_2	Hydrogen
H_2O	Water
h	Horizontal stabiliser
k	Species k
L	Lift
l	Rolling moment
l	Airfoil lift
lam	Laminar
m	Membrane
m	Pitching moment
m	Motor
misc	miscellaneous
MLG	Main landing gear
O_2	Oxygen
p	Proof
p	Hydraulic phase
pn	nth prop configuration
p1	One prop configuration
prop	propeller
R/r	Rudder
s	Solid phase
s	Shaft
sat	Saturated state
t	Total
tub	Turbulent
tip	Propeller blade tip
v	Vertical stabiliser
w	Wing
wall	tank wall
z	Axis pointing up

List of Abbreviations

Abbreviation	Explanation
ACL	Anode Catalyst Layer
ADT	Actuator Disk Theory
AFC	Anode Flow Channel
AOA	Angle Of Attack
APU	Auxiliary Power Unit
BV	Butler-Volmer
CCL	Cathode Catalyst Layer
CFC	Cathode Flow Channel
c.g.	Center of Gravity
CL	Catalyst Layer
DEP	Distributed Electric Propulsion
DOC	Direct Operational Costs
DP	Distributive Propulsion
FEM	Finite Element Modelling
GDL	Gas Diffusion Layer
GH2	Gaseous Hydrogen
GPU	Ground Power Unit
HOR	Hydrogen Oxidation Reaction
ICAS	International Congress of the Aeronautical Sciences
MAAMF	Hydrogen Tank Insulation Vapour Barrier
MEA	Membrane-Electrode Assembly
LH2	Cryogenic Liquid Hydrogen
ODE	Ordinary Differential Equation
ORR	Oxygen Reduction Reaction
PDE	Partial Differential Equation
PEM	Proton Exchange Membrane
PEMFC	Proton Exchange Membrane Fuel Cell
rpm	Round per minute
SF	Safety Factor
TE	Trailing Edge
TO	Take-off
TPD	Tonnes per Day

Executive Overview

In this project, 10 students were given 10 weeks to design an emission free aircraft according to customer requirements set by the project tutor. This Design Synthesis Exercise is the final part of the Aerospace Engineering Bachelor programme at the TU Delft. This report gives an overview of the project which focuses on assessing the challenge and developing a final concept.

The Challenge

Until today, the aircraft industry is incapable of adopting the necessary changes in order to reduce global warming and prevent the unsustainable use of our natural resources. At the current pace, the depletion of fossil fuels poses a real threat to the global industry, as it relies heavily on such resources. Furthermore, the damage done to the environment by the heavy use of these fuels is important and may soon reach a tipping point after which there is no perspective of recuperation. Since aviation is crucial to the modern globalised world, a viable alternative to fossil fuels must be found.

To reach this goal, new technology must be investigated. Research must be conducted in order to create a promising design and bring it to life, with a strong focus on sustainability. For this project, the following Mission Need Statement (MNS) and Project Objective Statement (POS) are formulated as follows:

> **Mission Need Statement**
>
> *Assess the possibility of emission free flying in a commercial passenger aircraft, while competing with existing aircraft in total cost of ownership.*

> **Project Objective Statement**
>
> *Design a cost competitive, emission free, small regional airliner, by ten students in ten weeks time.*

Final Requirements

After analysing the the project objective, the project requirements were established. As the design objective is an (emission free) aircraft, many requirements were defined that are not only relevant specifically for this project, but also to aircraft in general. Only the most significant project-specific and customer requirements are presented here.

> **Key Requirements**
>
> **Client Requirements**
>
> **GF-STK-CL-1** The aircraft shall seat 19 passengers.
>
> **GF-STK-CL-2** The aircraft shall not emit any harmful particles during operation.
>
> **GF-STK-CL-5-n** The aircraft shall have a nominal cruise range of at least 500 nautical miles.
>
> **GF-STK-CL-6-n** The aircraft shall be able to reach any destination within 500 nautical miles within 2 hours.
>
> **GF-STK-CL-7** The maximum runway length required for take-off for this aircraft shall be 1500 meters.
>
> **GF-STK-CL-8** The amount of harmful emissions emitted during manufacturing shall not exceed the amount of harmful emissions during manufacturing of conventional similar aircraft.
>
> **GF-SYS-EXT.1-1** The aircraft shall comply with the applicable regulations declared by EASA and ICAO.

GF-STK-CL-5-n, **GF-STK-CL-6-n** and **GF-SYS-EXT.1-1** are updated requirements and are justified below.

The updated range requirement follows from a short market analysis, in which it was determined that 80% of all regional flights have a range of less than 500 nmi. Subsequently, it was computed that it would be 70% more expensive to cover the additional 20% of the market with an aircraft designed for 1000 nmi. The speed requirement was thus changed concurrently.

The original noise requirement was formulated ambiguously and therefore not verifiable. First, the noise requirement does not specify how those 85 dB are measured. Furthermore, typically, the noise regulations are not given in dBs, but rather, as described by ICAO regulations, by dBAs, a unit which combines the noise dB levels with the frequency of the sound.

The requirements will be used to verify the final design presented in this report.

Final Design

In this part first the final design will be presented and then the selection process will be summarised.
After exploring all possible options and performing a trade-off the final concept was selected:

> **Final Concept**
>
> **The Greenliner**: *A novel propeller aircraft featuring distributed propulsion over its fuselage, with conventional (low) wing and tail configurations, which uses fuel cells in combination with liquid hydrogen as its energy source.*
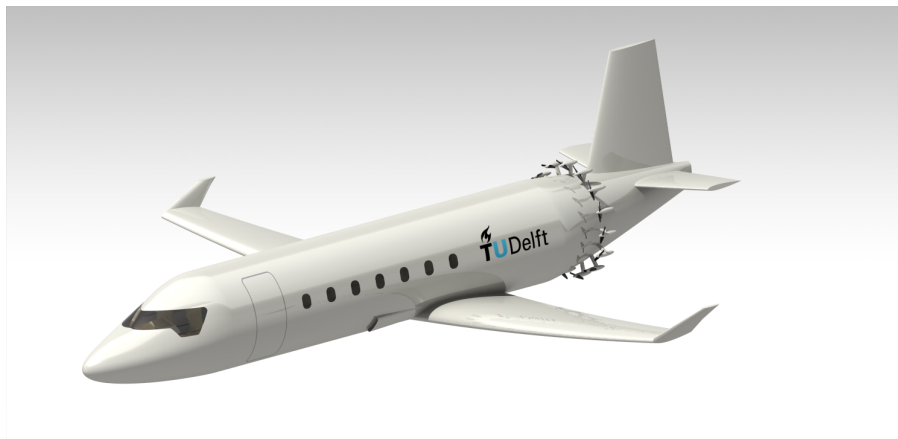
Figure 1: The Greenliner

This final concept comprises of **a propeller aircraft, which uses fuel cells and liquid hydrogen to power its electric motors** (render in Figure 1).

Since the main goal of this design project is to produce a commercially viable solution for emission free flying, the focus lies on a suitable propulsion system, as this is not yet available. As such, this subsystem must be carefully analysed and sized according to the overall performance needs of the Greenliner. To do so, the performance of the remainder of the aircraft must be known in detail and with high confidence. Because of this, it was decided to base the design on a standard configuration consisting of a circular fuselage and a fixed wing. It should also be noted that since the selected concept makes use of electrical motors, it was chosen to apply distributed propulsion on the fuselage, mostly because this increases the overall propulsive efficiency of the aircraft.

Fuel cells work based on the electrochemical half reactions presented here. A proton exchange membrane is coated with catalyst layers. At the anode side, hydrogen will react at the catalyst according to the first half reaction. The protons created, travel through the membrane. The electrons are conducted externally to the cathode where the second half reaction takes place at the catalyst. The external electron flow is the current that is used to power the aircraft.

> **Electrochemical half reactions**
>
> $$H_2 \rightleftharpoons 2H^+ + 2e^- \tag{1}$$
>
> $$\frac{1}{2}O_2 + 2H^+ + 2e^- \rightleftharpoons H_2O \tag{2}$$
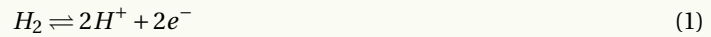
After careful assessment on different criteria, hydrogen was selected as the main energy source during the trade-off process. To maximise the overall system performance, the best hydrogen storage option was connected to the best performing fuel cell, resulting in the combination of cooled liquid hydrogen (LH2) and a proton exchange membrane fuel cell (PEMFC). The choice for liquid hydrogen has many important advantages and forms a crucial step towards the goal of emission-free flying.

One such advantage is the weight. After a preliminary total aircraft mass estimation, it was found that the hydrogen option would yield the lightest overall system: just 150 kg for a 500 nmi flight. Especially in Aerospace Engineering, such system properties are indispensable.

In terms of the system cost, one can observe that the hydrogen and fuel cell combination has been used in commercial transportation solutions (busses), also indicating high technical readiness. Most importantly, this will help to limit the retail price of the end product to an acceptable extent, creating competition with conventional air transport.

However, the most important property of hydrogen for the purpose of this project is that it has the potential to be produced emission free and on-site at the airport, if renewable energy sources are used for the electricity supply. Since water, which is needed to produce hydrogen, is readily available in many parts of the world, no scarce natural resources are used in the fuel production. This shows that the choice for hydrogen is ideal for the purpose of this sustainable project.

Sustainability

For the purpose of this design project, three key aspects of sustainability will be considered. The three aspects are based on the 3P (profit, people, planet) principle: financial, social and environmental sustainability. Financial sustainability focuses on the idea that any product or process must be designed such that it can function properly for a long time by receiving proper support. Social sustainability pertains to the impact of the product or process on society in general. Environmental sustainability plays a role whenever the natural environment of the planet is affected in any way. For each principle criteria were coined and the Greenliner was assessed based on these criteria. The result can be observed in Figure 2. This spider map shows the sustainability of the Greenliner and Dornier in the year 2030. The Dornier 228 is a reference aircraft because this is a commercial aircraft with similar specification and mission requirements.
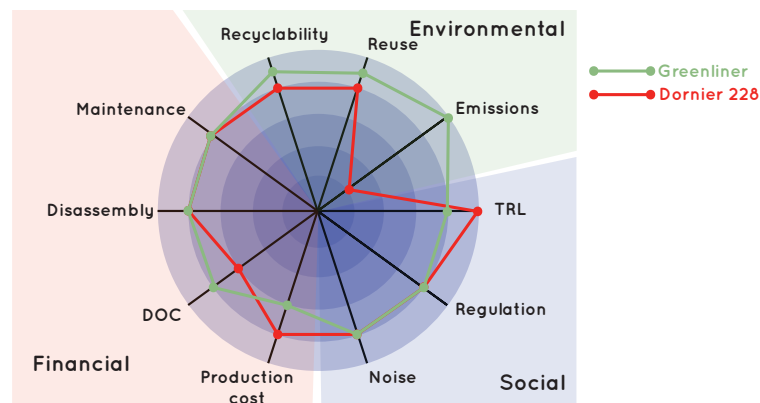

Figure 2: Spider map showing comparison between the Greenliner and Dornier 228

The result shows that in 2030, the Greenliner will be outperforming Dornier 228 in terms of sustainability. Both aircraft

are graded on a scale of 1 to 5 based on the ten criteria in Figure 2. The reasons are discussed below.

The Greenliner uses liquid hydrogen as a fuel, resulting in only water as its emission, while the Dornier uses kerosine. Therefore the Greenliner performs much better than Dornier 228 on environmental sustainability which has a high emission during operation.

A high level of recyclability and reusage of parts can be expected for Greenliner. Various metal alloys such as aluminium alloys and titanium are used for the aircraft structures and graphite is used for the PEM fuel cell. These metals are highly recyclable. Parts that are designed specifically for the Greenliner such as the hydrogen tank or fuel cell can be reinstalled in a new Greenliner if they are still within the service life. Compared to Dornier 228, which has composite propellers, the Greenliner performs slightly better in recyclablity and reuse.

Furthermore, the technical readiness level and regulation maturity are expected to improve in the near future. Since the Greenliner should be in service in 2030, it must be certified and the technology has to work. Besides, the international air transport association has set the ambitious goal of *a reduction in net CO2 emissions of 50% by 2050 relative to 2005 levels*. This means that both government and aviation regulatory bodies will push towards emission free flying.

The Greenliner is also financially sustainable: even though the production cost might be higher than for the Dornier 228, this will not be a restricting factor because it is expected that some are willing to pay more for an entirely emission free aircraft. Furthermore, As the direct operation costs are closely related to the fuel cost, airlines would prefer to use a cheaper fuel source. Even though liquid hydrogen (LH2) is currently 4 times as expensive as kerosene, it is expected that the LH2 price will be lower in 2030. Consequently, the Greenliner will perform better in terms of DOC. Concerning maintenance, disassembly procedures of the Greenliner are not expected to be more difficult than conventional aircraft. When lean engineering is applied throughout the design process, a highly time and energy efficient maintenance process can be obtained. Therefore, the Greenliner and Dornier 228 score the same on these two criteria.

Financial Analysis

To asses the financial viability of the Greenliner concept a return of investment prognosis was made. In order to do this first the investment costs and unit cost price have to be known. The selling price followed from the customer requirement that the price would not exceed 125% of comparable aircraft. These values are presented in Table 1 and discussed below.

|	price [million USD]
Selling price	12
R&D costs	±300
Unit cost price	±10.5 - ±5
Final Profit	±400

Table 1: Financial analysis Greenliner

In order to find the retail unit price, seven reference aircraft were analysed and based on the amount of passengers their retail price was scaled down. Then 25% was added to the average of these seven, resulting in 12 million USD as the unit price of the Greenliner.

The R&D costs and unit price were hard to assess, since because of harsh competition, aircraft manufacturers tend to keep these numbers secret. In order to make an assessment, the method of Willcox [105] was used, resulting in ±300 million USD for the R&D phase and an initial unit cost price of about 10.5 million USD. Furthermore, aircraft manufacturing tends to become cheaper when more units are produced, which is prescribed by the learning curve: as depicted in Figure 3a the unit cost price halves after about 140 units. When these values are known the RoI is calculated and as shown in Figure 3b, the break even point occurs in 2038 and a final profit of about 400 million is acquired after 150 units are sold according to prognosis.

Compliance

To evaluate the expected performance of the Greenliner, the compliance with requirements was examined. There are no requirements that are expect to remain unfulfilled. However, more research must be done to ensure that certain re-
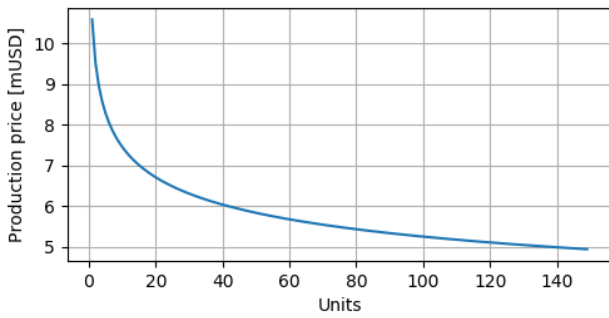
(a) Learning curve for production
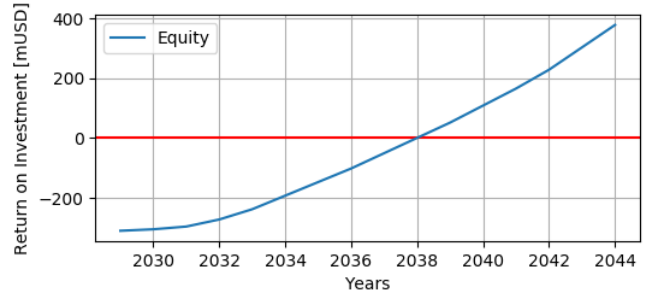
(b) Equity during selling phase

Figure 3: Financial analysis Greenliner

quirements are indeed fully met. These include most notably: complete compliance with EASA and ICAO regulations, a lifetime of 35,000 cycles, and an amount of emissions during manufacturing that does not exceed that of similar conventional aircraft.

Looking back at the mission statement, the Greenliner conceptual design certainly shows the possibility of emission free flying. Even as industry experts claim large electric aircraft may not fly before 2050, the Greenliner shows a real opportunity for developing a sustainable, cost competitive airliner that can enter the market as early as 2030.

Contents

1
Introduction

Climate change and the depletion of fossil fuels are among the most pressing concerns faced by the modern, globalised society. The aviation industry is a significant contributor to pollution and is projected to account for almost 5% of the remaining global carbon budget [73], which is the amount of emissions after which catastrophic climate change becomes certain. The depletion of fossil fuels is also a great concern: At the current pace of consumption, crude oil reserves will be depleted in the year 2051, making the commercial use of kerosene impossible [2]. In order to secure a long term market position, manufacturers and operators will therefore have to switch focus to green technologies. Although possible solutions for this challenge exist in theory or in smaller scale, no emission free commercial passenger aircraft has yet been produced. Therefore, extensive research into this topic is needed. Rather than being limited to the technology of subsystems such as the energy storage, a comprehensive assessment is needed of the feasibility of emission free flying. As a means of assessment, a Design Synthesis Exercise was completed by the authors of this report as the final part of the Aerospace Engineering Bachelor programme at the Delft University of Technology, in which the objective was to *design a cost competitive, emission free, small regional airliner.*

The aim of this report is to show how the design problem was approached and how the final design of the aircraft was synthesised, while focussing on the second half of the project. After first analysing the requirements, a final concept was selected through a trade-off procedure from a number of possible options. All subsystems were then sized and the results were integrated into a complete aircraft. The performance of this design was then analysed on different aspects such as sustainability, safety and technical risk. Finally, an outlook on future development was provided.

First, the context of the current phase of the project is given in chapter 2, where elements from previous reports such as the requirements analysis and the concept selection are summarised. Then, in chapter 3, sustainability assessment tools are developed. The integrated design approach is presented in chapter 4, whereas the detailed subsystem sizing methods follow in chapter 5, which also includes a discussion on the potential incorporation of solar panels. The final design is presented and analysed in chapter 6, after which the performance of the Greenliner is analysed in chapter 7. To confirm that a realistic system was designed, chapter 8 is devoted to the verification and validation of the design. Next, the future phases of the development of the Greenliner are explained in chapter 9. The operations and logistics are given in chapter 10, which includes a RAMS assessment. In chapter 11, the sustainable character of the final design is assessed, followed by a financial analysis in chapter 12 and the final requirements compliance matrix in chapter 13. The report ends with a conclusion and several recommendations in chapter 14.

2

Concept Selection

This chapter contains a summary of all design steps from the first three phases of the project, which were mentioned in previous reports. After discussing the name of the aircraft in section 2.1, the stakeholder requirements are presented in section 2.2. These requirements are then reviewed in section 2.3, followed by a functional analysis of the aircraft subsystems in section 2.4. Then, all design options which were considered in the early stages are shown in section 2.5. Finally, a trade-method for these options is established and a concept is selected in section 2.6. This concept then entered the Detailed Design phase, which is presented entirely in this report.

2.1. Naming the Aircraft

After initially just referring to the Greenliner as "the aircraft", it was decided to choose a name in order to better identify the specific aircraft that is being designed in this project. This also presents an opportunity to incorporate the main design characteristics into the identity of the final product. Furthermore, it presents an additional opportunity to create a clear difference to other, conventional aircraft.

Since the main characteristic of this design project is sustainability, most ideas for possible names included words such as "green" or "eco". After collecting many different possible names, a trade-off was conducted, based on parameters such as originality and simplicity. The outcome of this trade-off was the name "Greenliner". It was chosen because of its simplicity, its clear connection to (especially environmental) sustainability and the more frequent use of similar names in aviation. Furthermore, including the word "green" provides many opportunities to match other design elements such as the project logo to the actual name of the final product.

It should be mentioned that the name "Greenliner" has not been checked thoroughly for any possible existing trademarks or other protected names. In the case that these exist, it can be assumed that no serious conflicts will arise as the content of this report is created in an educational context.

2.2. Stakeholder Requirements

The Green Flying design project is based on the customer's project and mission definition, which includes a number of requirements. However, next to the customer, other stakeholders must be taken into account. Presented below is a list with the most important stakeholder requirements in their initial version. Unless specified otherwise, no changes were made to the requirements as presented below.

Client (Aircraft Manufacturer)

GF-STK-CL-1 The aircraft shall seat 19 passengers.

GF-STK-CL-2 The aircraft shall not emit any harmful particles during operation.

GF-STK-CL-3 The use of all resources in the manufacturing process shall be within acceptable boundaries, determined by similar conventional aircraft.

GF-STK-CL-4[1] The aircraft shall be able to fly safely with respect to altitude restrictions, using Europe as a reference.

GF-STK-CL-5[1] The aircraft shall have a nominal cruise range of at least 1000 miles.

GF-STK-CL-6 The aircraft shall be able to reach any destination within 1000 miles within 3.3 hours.

GF-STK-CL-7 The maximum runway length required for take-off for the aircraft shall be 1500 meters.

GF-STK-CL-8 The amount of harmful emissions emitted during manufacturing shall not exceed the amount of harmful emissions during manufacturing of conventional similar aircraft.

GF-STK-CL-9 The aircraft operations must be completed successfully without exterior influence (e.g. takeoff assistance, etc.).

EASA & ICAO

GF-STK-REG-1 The aircraft shall comply with the applicable regulations declared by EASA.

Airlines

GF-STK-ARL-1 The average maintenance costs shall not exceed those of conventional similar aircraft.

GF-STK-ARL-2 The average operational costs shall not exceed those of conventional similar aircraft.

GF-STK-ARL-3 The lifetime of the aircraft shall be at least of same length as conventional similar aircraft.

GF-STK-ARL-4 The airline shall be able to choose its desired interior cabin design option.

GF-STK-ARL-5 The nominal scheduled turnaround time shall not exceed that of conventional similar aircraft.

GF-STK-ARL-6 The retail price shall not be higher than 125% of the retail price of comparable conventional aircraft.

Airport

GF-STK-ARP-1 The airport shall be able to integrate the systems for replenishing and maintenance services.

Governments and Regulatory Authorities

GF-STK-GOV-1[2] The aircraft shall have a maximum noise level of 85 dB.

GF-STK-GOV-2 The aircraft shall be designed in such a way that its end-of-life is considered in terms of optimising the disassembly process and maximising recycling of components.

2.3. Requirements Discussion

After detailed analysis, some of these requirements are reviewed. First, an estimate for the total energy needed for the mission is used to change the initial cruise range and speed requirements (**GF-STK-CL-5** & **GF-STK-CL-6**). It was also determined that the noise requirement (**GF-STK-GOV-1**) is not accurate enough.

2.3.1. Range

In order to make an assessment on the range requirement, several steps are taken. A market analysis is first conducted, after which the total energy required is compared for different ranges to assess the increase in costs. Consequently, the analysis is concluded and the range requirement is updated.

Market Analysis

As shown in Figure 2.1a, 80 % of all commercial regional passenger flights have a range of below 500 nmi, with virtually all flights being below 1000 nmi. This is supported by other sources such as [8].

Required Mission Energy

Now that the typical range of regional aircraft is known, a preliminary energy analysis is conducted to find the energy required for the mission.

In Table 2.1, the energy required for both ranges can be found. The energy to fly 1000 nmi with the Greenliner that is designed for 500 nmi is calculated by multiplying the energy required to fly 500 nmi by three. This is a conservative estimate, including two intermediate stops. The energy to fly 500 nmi with the heavier 1000 nmi version of the Greenliner is equal to half of the energy needed to fly 1000 nmi. The average total energy is then calculated making use of Equation 2.1.

$$E_{total_{average}} = 80\% \cdot E_{500} + 20\% \cdot E_{1000} \tag{2.1}$$

As can be observed in the last column of Table 2.1, the average energy for the 1000 nmi Greenliner is 1.7 times the energy needed for the 500 nmi Greenliner. In other words, it will be 70% more expensive in fuel costs to capture the extra 20% of the market. Together with the customer this had led to the decision to change the original requirement.

---

[1]This requirement was modified at a later stage, as specified in subsection 2.3.1.

[2]This requirement was modified at a later stage, as specified in subsection 2.3.2.
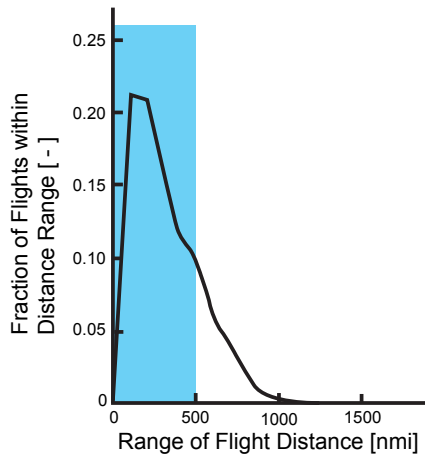
(a) Fraction of flights with a certain range for regional aircraft, from global statistics (adapted from[59])
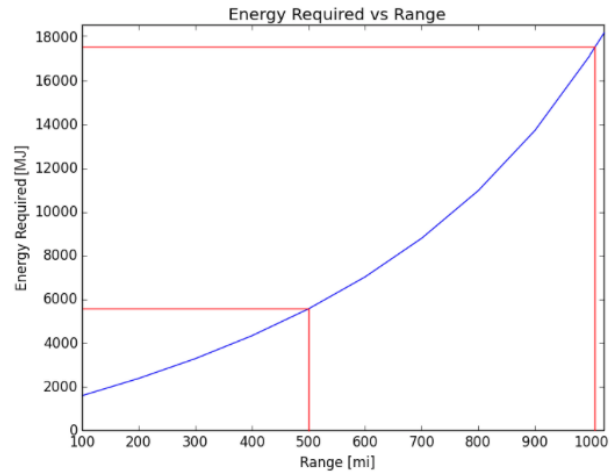
(b) Greenliner energy required against design range

Figure 2.1: Comparison of amount of flights and required energy versus range

Table 2.1: Energy needed for different ranges

Design Range Aircraft	Energy 1000 nmi	Energy 500 nmi	Average Total Energy
1000 nmi	20210 MJ	10105 MJ	12126 MJ
500 nmi	15225 MJ	5075 MJ	7105 MJ

New Range Requirement
After these findings were presented to the customer, a new range requirement was formulated and agreed upon:
   GF-STK-CL-5-n The aircraft shall have a nominal cruise range of at least 500 nautical miles.

In the same way, the cruise speed requirement had to be rewritten, as it depends on the range requirement:

   GF-STK-CL-6-n The aircraft shall be able to reach any destination within 500 nautical miles within 2 hours.

The 2 hours in **GF-STK-CL-6-n** were determined by the ratio between range and travel time from the original requirements.

2.3.2. Noise Regulations
The requirement **GF-STK-GOV-1** was specified as: "The aircraft shall have a maximum noise level of 85 dB." In addition, the airplane should, according to **GF-SYS-EXT.1-1**, comply with the applicable regulations declared by EASA. It was determined that these requirements are not accurate enough or even fallacious. First, the noise requirement does not specify how thz 85 dB are measured. Furthermore, the noise regulations are typically not set by EASA but by ICAO and are not specified in dB, but rather, as described by ICAO regulations, dBA. ICAO presents a clear method on how to measure all sound components and how to finally calculate the dBA level.

Given these issues regarding the noise regulations, in cooperation with the client, the requirements were modified as follows:

GF-STK-GOV-1-n The airplane noise performance shall be in accordance to ICAO regulations.

2.4. Subsystem Functional Analysis
In this section, the technical functionality of the aircraft is discussed and functional requirements are presented for the separate subsystems. First the desired functions of the aircraft during its lifetime are analysed in subsection 2.4.1. After the chronological order of the functions has been set, a functional breakdown structure is used in subsection 2.4.2 to analyse them in more detail. Hardware and Software Diagrams are presented to show the interrelation between several

hardware or software blocks. To conclude this chapter, the Electrical Block Diagram is shown to present an overview of all the subsystems that require power.

2.4.1. Functional Flow Diagrams

Functional flow diagrams are used to depict the functions of a product in a chronological matter, while also maintaining their interrelation. If the entire flow is completed, the function of the product is fulfilled properly. In Figure 2.2 the top level functional flow is presented. In sections 2.4.1 - 2.4.1, phases 2, 3, and 5 are explained. As designing (phase 1) the aircraft and delivering (phase 4) it to the customer are not direct functions of the product itself, these are not broken down. For the same reasons, the production phase is kept at a very basic level. The identifiers in the blocks reappear in the blocks of the functional breakdown structure (subsection 2.4.2). Also, the blocks are colour coded: red for top level, yellow for first level, blue for second level and purple for third level functions.
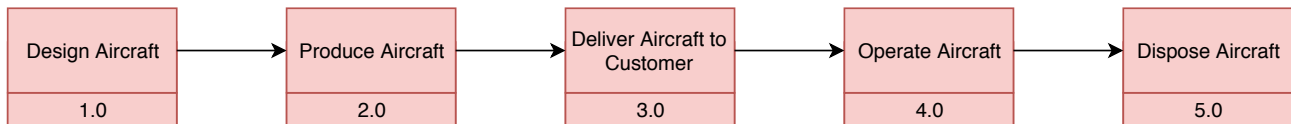

Figure 2.2: Top level functional flow diagram

Production Phase

The production phase can be observed in Figure 2.3. It consists of producing all necessary parts and assembling the aircraft, after which the aircraft goes to the next phase: delivery.
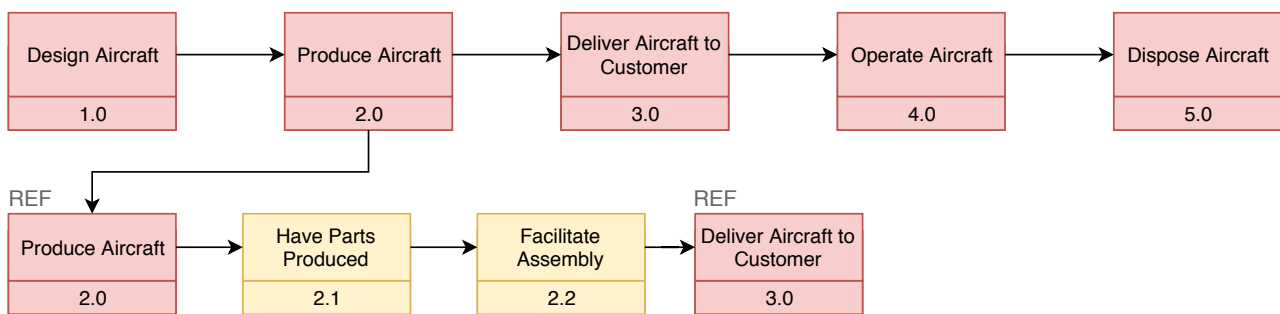
Figure 2.3: Production phase functional flow diagram

Operational Phase

The operational phase is the most important phase for the functional analysis of the product. The operational phase of the aircraft consists of performing the air transport. This is further broken down into performing pre-flight operations, performing flight and performing post landing operations sequentially. As this phase is the most important one, an additional level of detail is added, as can be observed in Figure 2.4.

Disposal Phase

The final phase of product life is disposal. After the useful life, the aircraft is disassembled. The parts that can be reused will be used for new aircraft, the reusable material will be processed and new parts will be manufactured. What is left of the plane after these steps have been taken needs to be disposed of, and is not further used. The functional flow of this phase can be observed in Figure 2.5.

2.4.2. Functional Breakdown Structures

The functional breakdown structure covers a complete set of functions needed to fulfil the product mission. This is done by subdividing functions into lower levels until the set is complete. In Figure 2.6 the top level functions for the mission are described. The design phase is not included, since it is not a function the aircraft itself has to perform. Besides, the delivery is not broken down for the same reason as in subsection 2.4.1.

Figure 2.4: Operational phase functional flow diagram

Figure 2.5: Disposal phase functional flow diagram

Figure 2.6: Top Level Functional Breakdown Structure

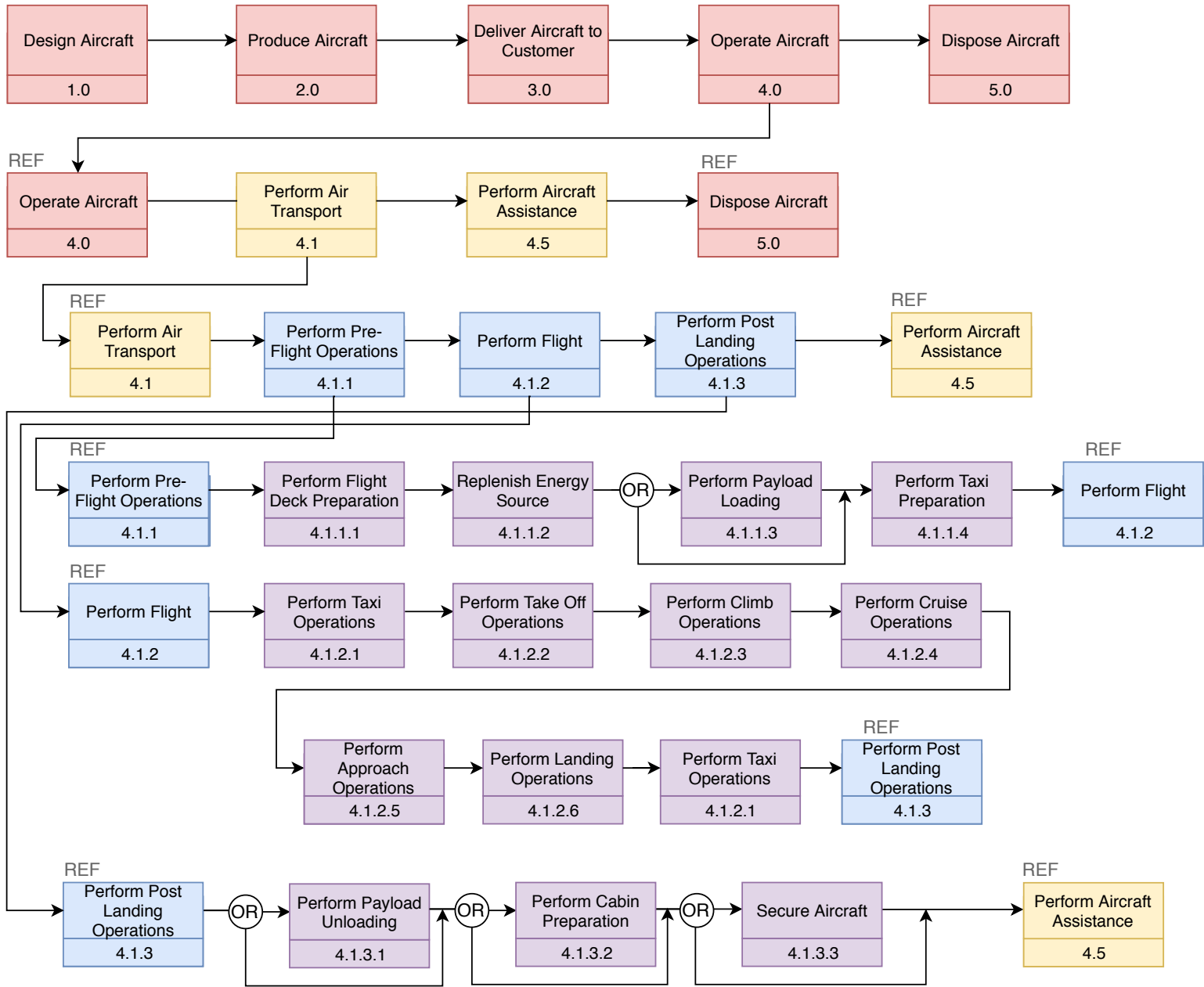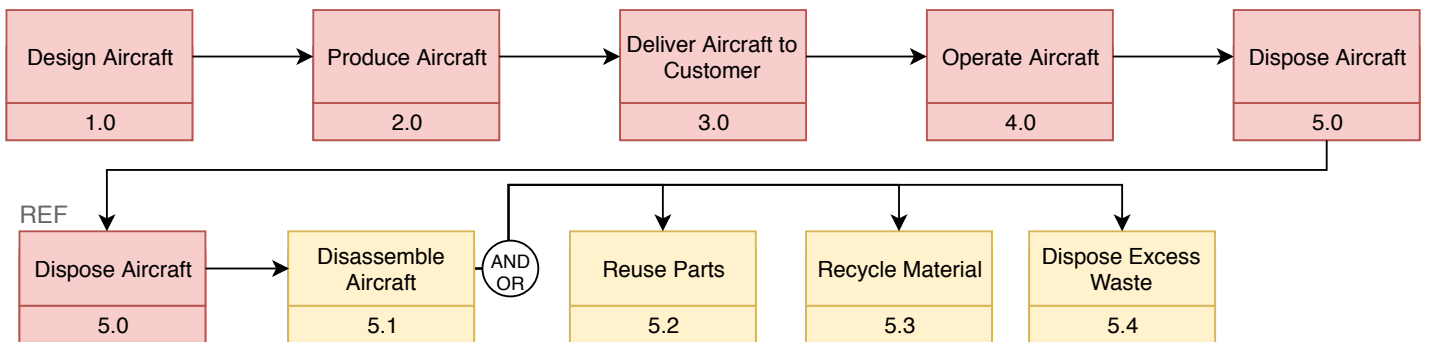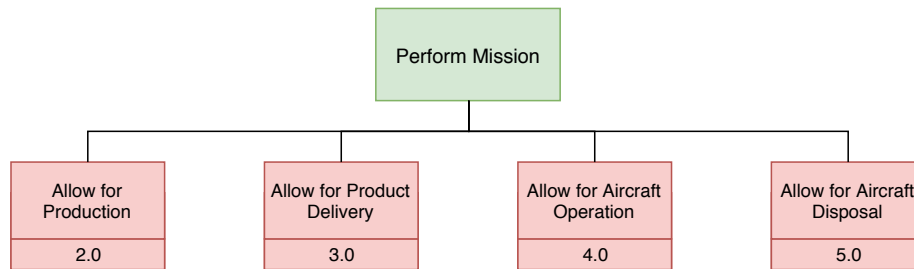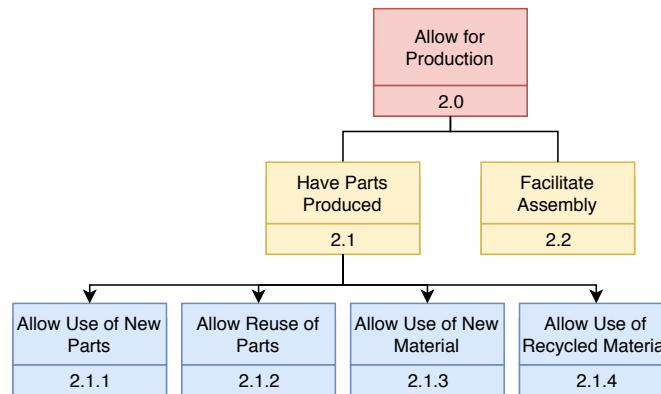Figure 2.7: Production phase functional breakdown structure

Production Phase
The breakdown of the production phase can be found in Figure 2.7. As mentioned earlier, the production phase is not elaborated in detail because it is not a direct function of the product. However, since sustainability should be implemented in production phase, the reuse of parts and use of recycled material are shown next to the use of new parts and new material.

Operational Phase
The functional breakdown structure for the operational phase is shown in Figure 2.8. From this figure only the "Perform Air Transport" block is present in the functional flow diagram (Figure 2.4 in Figure 2.4.1). This is due to the fact that a functional breakdown structure describes additional and exceptional cases under which the aircraft has to perform all of the functions in the functional flow diagram. For example, it should perform the mission in a sustainable manner, perform revenue and non-revenue flight and perform under abnormal operations (e.g. bad weather). Also the aircraft has to be able to be maintained and supported. This can be found under the "Enable Assistance" block. Finally, the aircraft has to provide communications with ground and other aircraft.

Disposal Phase
The functional breakdown structure of the disposal phase translates back to the functional flow diagram in Figure 2.4.1 and adds another layer of functionality, as can be observed in Figure 2.9.

2.5. Design Options
To establish a design that complies with all requirements, a design option tree (DOT) was constructed to conceive close to 150 different design options, after which the DOT was systematically pruned to leave only the most promising options. It was concluded that the propulsion and energy storage components are most critical for this project and therefore the viable combinations of these components were examined in greater detail.

The elements of the DOT were graded based on the defined criteria. The relative importance of each criterion can be recognised in the order of application, with the first being of greatest importance. The five options resulting from this process are listed above. The most important drivers for this selection were the maturity of the technologies, along with the mutual compatibility of the combinations. Electrical propellers are proven to be feasible propulsion options,
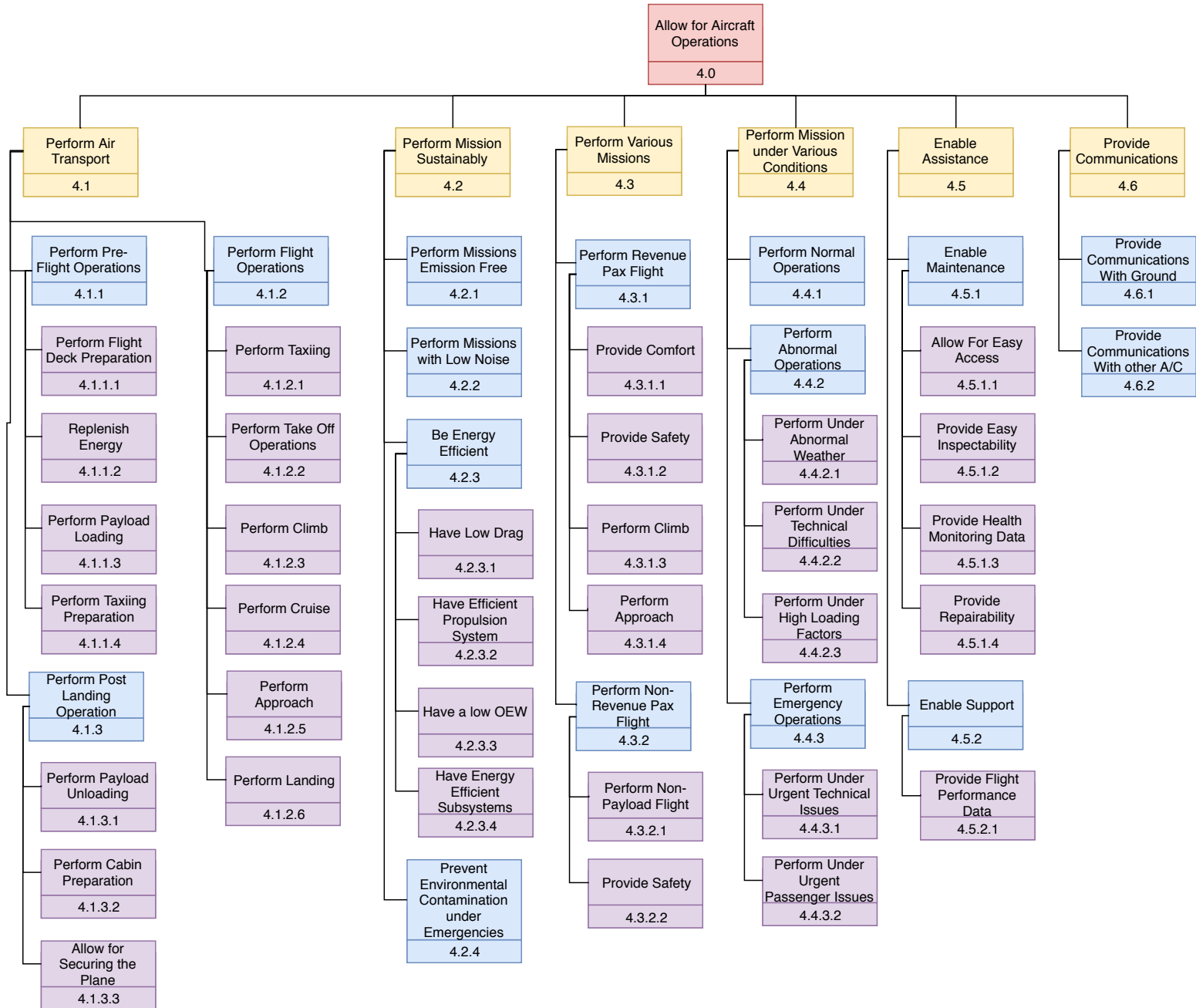
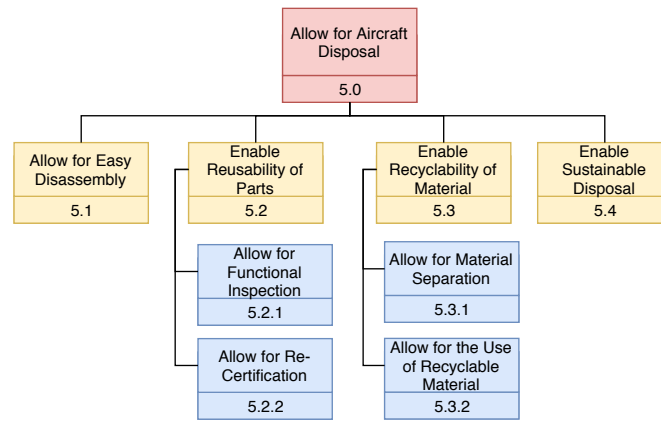Figure 2.8: Operational phase functional breakdown structure

Figure 2.9: Disposal phase functional breakdown structure

and can readily be combined with battery and fuel cell technology. As non-electrical options, hydrogen combustion remains as the only technology developed enough to be used for the main propulsion system. After conducting this first trade-off, the following five high level concepts were decided upon for further analysis, which are also presented in Figure 2.10:

1. **Propeller powered by batteries (electrical)**
2. **Propeller powered fuel cells (electrical)**
3. **Propeller powered by a hybrid battery and fuel cell combination (electrical)**
4. **Jet engine powered by hydrogen (combustion, non-electrical)**
5. **Propeller powered by hydrogen (combustion, non-electrical)**
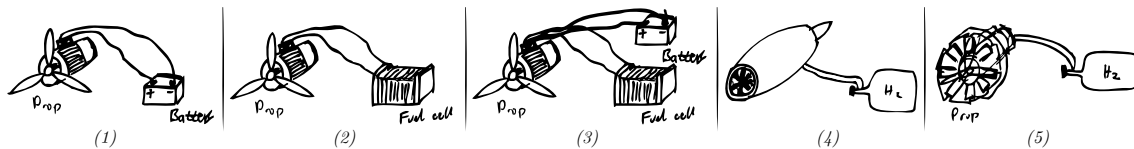
Figure 2.10: Sketches of the five concepts to be further analysed

The main focus of this design project is "green" flying, i.e. flying without harmful emissions, which is not possible without a suitable and well designed propulsion system. As such, this subsystem must be carefully analysed and sized according to the overall performance needs of the aircraft. To do so, the performance of the remainder of the aircraft must be known in detail and with high confidence. Because of this, it was decided to base the design on a standard configuration consisting of a fuselage and a wing, as analysis methods are readily available and have proven themselves. In the same way, this design option has proven itself in practical operations with decades of commercial flying. Therefore, this choice ensures that in the end, the goal of a commercially viable small emission free aircraft will be achieved.

2.6. Concept Trade-off and Selection

After the five most promising concepts were selected, a final concept had to be selected for the detailed design in this report. Yet again a trade-off procedure was developed and the final concept was then selected:

The Greenliner: A novel propeller aircraft featuring distributed propulsion over its low wing, with conventional fuselage and tail configurations, which uses liquid hydrogen and fuel cells as its energy source.

After careful consideration of different criteria, hydrogen was selected as the main energy source during the trade-off process. To maximise the overall system performance, the best hydrogen storage option was connected to the best performing fuel cell, resulting in the combination of cooled liquid hydrogen (LH2) and a proton exchange membrane fuel cell (PEMFC). The choice for liquid hydrogen has many important advantages and forms a crucial step towards

the goal of emission-free flying.

One such advantage is the weight. After estimating the total mass of the aircraft, it was found that the hydrogen option would yield the lightest overall system. Especially in Aerospace Engineering, such system properties are indispensable.

In terms of the system cost, one can observe that the hydrogen and fuel cell combination has been used in commercial transportation solutions, also indicating high technical readiness. Most importantly, this will help to limit the retail price of the end product to an acceptable extent, creating competition with conventional air transport.

However, the most important property of hydrogen for the purpose of this project is that it has the possibility to be produced emission free and on-site at the airport, if renewable energy sources are used for the electricity supply. Since water, which is needed to produce hydrogen, is easily available in many parts of the world, no scarce natural resources are used in the production. This shows that the choice for hydrogen is ideal for the purpose of this sustainable project.

As illustrated not only by these aspects, but also many more, which can be found in this report, the chosen final concept is very promising with respect to the goal of emission free flying. In the last phase of the project, the "Detailed Design Development" phase, this concept was further developed. More detailed sizing methods were used for all subsystems and after converging to a consistent design, it was further analysed on all important aspects, creating a complete concept for the Greenliner. Where necessary, several changes were made to the "final concept" presented in this section. The detailed subsystem sizing methods are presented in chapter 5 whereas the final results are presented in chapter 6.

3

Sustainable Development Strategy

Sustainability can be described using three principles: financial sustainability, social sustainability and environmental sustainability. Only if the design complies to all three principles, it can be classified as a fully sustainable design. Furthermore, the product life time can be divided into three distinct phases: development, operation and end-of-life. The three principles should be considered in all three product phases.

Sustainability throughout the three phases is realised by converting a linear economy into a circular one. The goal of a circular economy is to minimise waste and to revitalise the end-of-life product into a new phase. As depicted in Figure 3.1, a circular economy can be accomplished by applying various techniques. For example, the product can be recycled or reused after end-of-life. Another technique is to elongate the products life by proper maintenance planning.

This chapter begins with a description of the sustainability strategy in section 3.1. In section 3.2 it is then explained, how this strategy will be applied throughout the project.
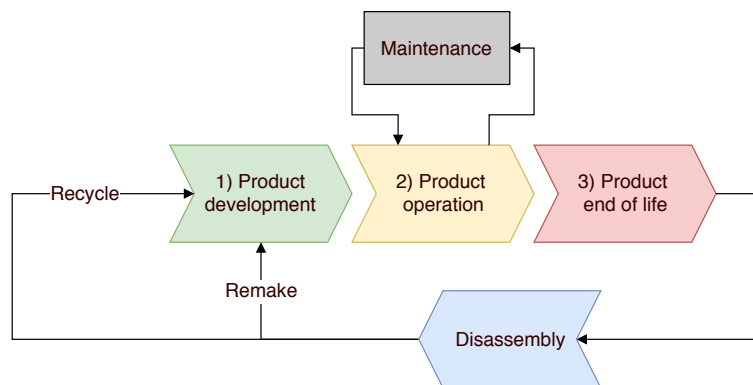
Figure 3.1: Flow chart indicating a circular economy

3.1. Sustainable Engineering & Tools

In order to make sure the design is sustainable, a sustainability strategy is developed. First, the 5S design approach is described and after that, the tools that are used to carry out the sustainability strategy are elaborated upon. These tools are: regulations, a materials map, a production planning chart and resource budget sheets.

5S approach

The 5S design approach is followed throughout the whole project. This approach makes use of a descriptive step-by-step table that consists of five phases: Sort, Set in order, Shine, Standardise and Sustain. However, 5S is said not to be a list of action items but an integrated concept of actions, condition and culture. When fully implemented into the design, the 5S process increases morale, creates positive impressions on customers and increase efficiency and organisation.[1] All of this results in lean manufacturing: a manufacturing process in which waste is minimised without sacrificing productivity[39].

---

[1] Retrieved from `https://www.isixsigma.com/tools-templates/5s/practical-approach-successful-practice-5s/` on 31 May 2018

Regulations

The first tool that is used to develop a sustainable design is the regulations documentation of EASA and ICAO. CS-23 of EASA and Annex 16 Volume 1 of ICAO and provide a basis for the requirements on sustainability because they consist of guidelines, recommendations and checklist that can be used during design of the product.

Materials Map

One tool that must be used to assure a sustainable design is a materials map [74]. This map lays out all possible materials to be used in aircraft and provides an overview of design possibilities. The materials map is a valuable tool because it initiates a thought process for sustainable material usage.
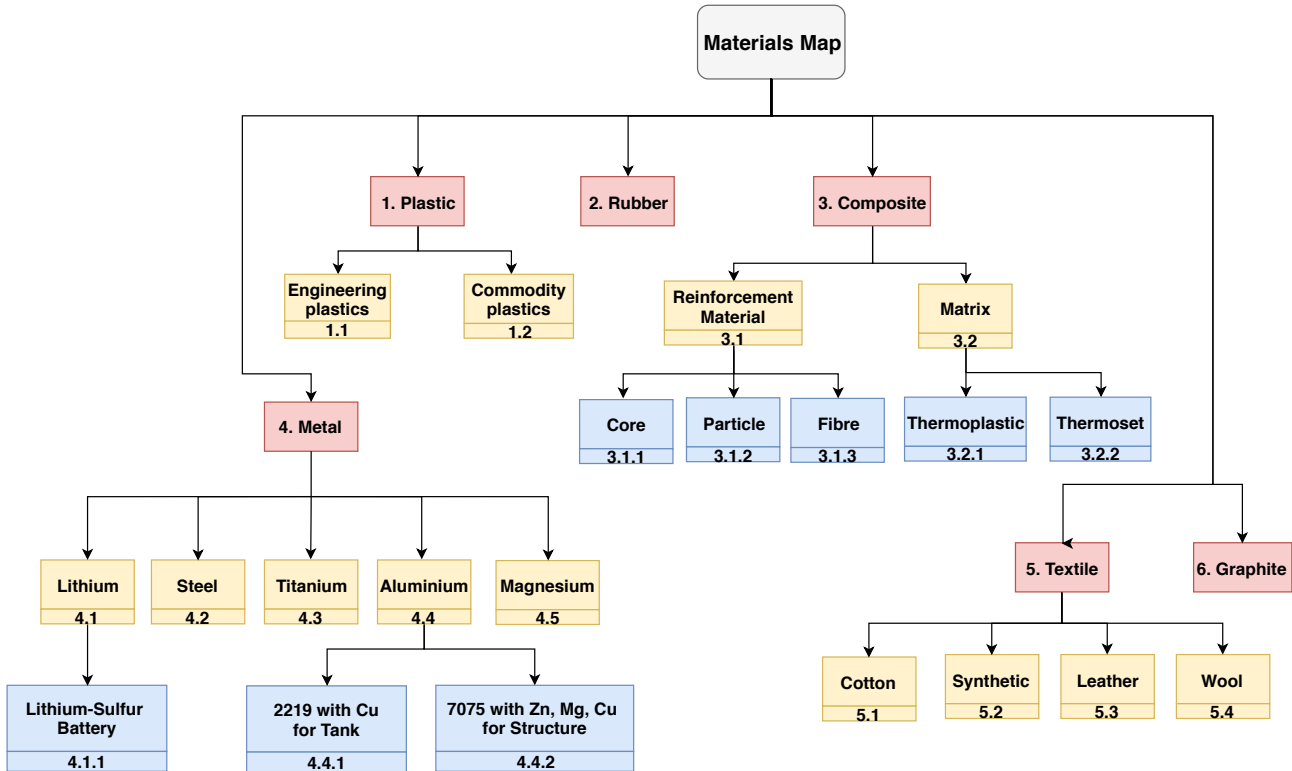
Figure 3.2: The materials map for materials in the Greenliner

Production Planning Chart

To minimise waste, a production planning chart is essential. A production planning chart is a tool that describes the production process in an illustrative manner so that it can be carried out smoothly, fast and efficiently. The assembly sequence of parts into (sub)assemblies is organised in terms of working days and visualised in a chart comparable to the Gantt chart. If the planning chart is properly created and applied, the production process will be cost effective, time efficient and lean in resource usage.

Resource Budget Sheet

To eliminate waste, keeping track of resources is of great importance. A resource budget sheet is used for that. In a resource budget sheet product elements such as cost, material availability and mass are planned, written down and evaluated.

3.2. Sustainability Analysis & Compliance Tools

During the design phase, a plan for sustainability compliance analysis must to be created. To do this assessment, various tools are created. The selected tools are a parts map, finance tools, quality function deployment and a PLATE spider map which are discussed in the following sections.

Parts Map

A parts map is used after the design of the aircraft is completed. The parts map includes all parts that the aircraft consists of. Using this map, one can make sure that every part is evaluated on all aspects such as mass budgets, cost budgets and material usage. The parts map is shown in Figure 3.3.

Finance Tools

To estimate cost and profit, various finance tools can be used. The total life cycle finance can be divided into two parts: production company finance and operational finance. For the production company, the production will consist of development cost and manufacturing cost and aircraft sales will result in revenue. The airlines that will operate the airplane will take into account the operational cost. For both parts, comparable tools can be used such as budget sheets, cost models and revenue models. A first estimate of the life cycle cost is made in chapter 12.

Quality Function Deployment

The social sustainability is assessed mostly based on a quality survey. This survey collects client and customer feedback after which the feedback can be implemented in redesigns, future products or operation plans.

PLATE Spider Map

Lastly, a PLATE spider map is developed. This spider map visualises the sustainability score of the overall aircraft design with respect to circular economy. Five criteria are mapped out in the spider map: recycle, future proof, disassembly, maintenance and remake. The map clearly indicates strong points of the design and points that still require improvement. If the aircraft has a high score on all aspects, it can be said to be a circular product design [74].
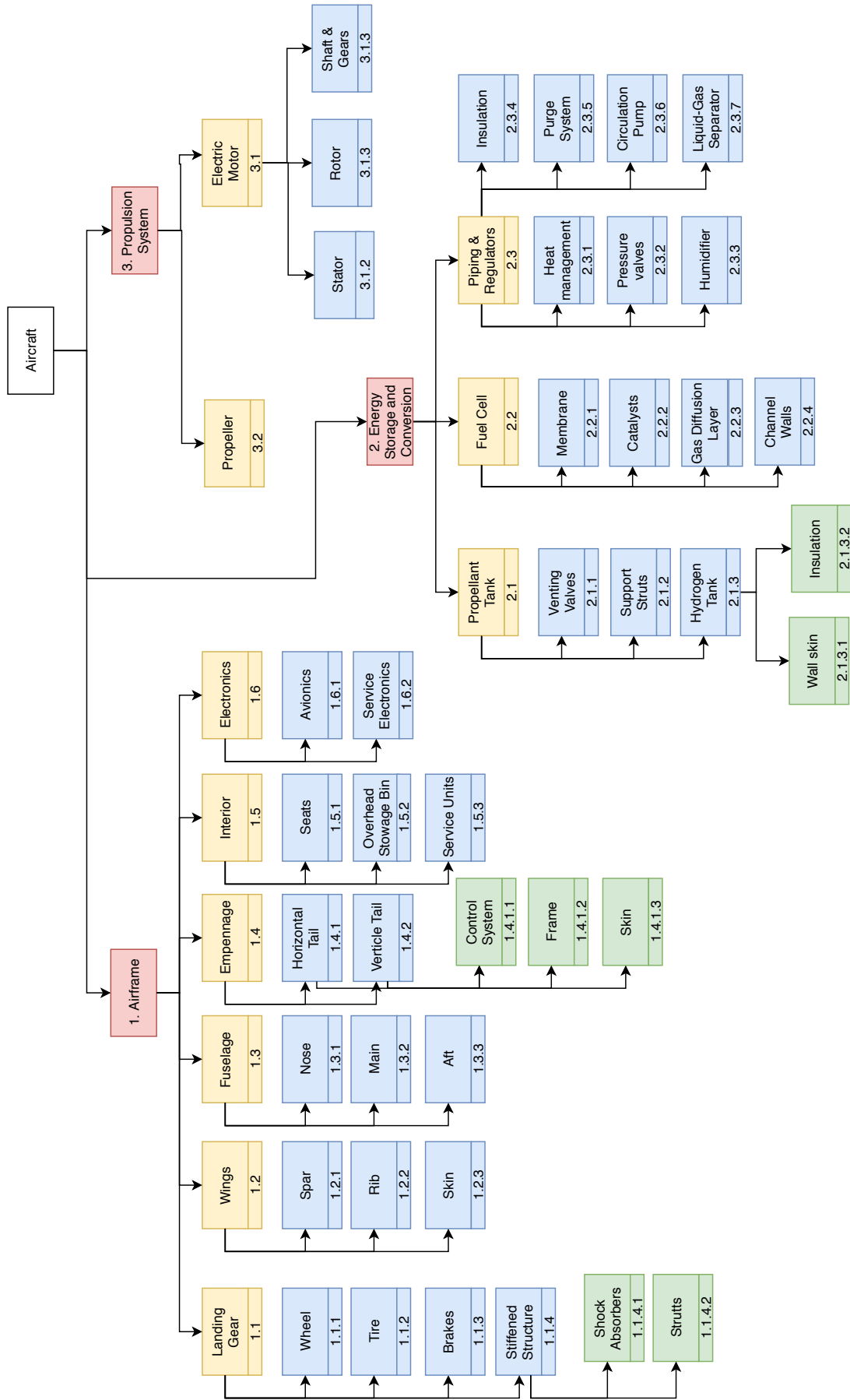
Figure 3.3: The parts map of the parts in the Greenliner

4

Integration Methodology

Rather than manually sizing all subsystems and assembling them after each iteration, the complete design approach including Class I and Class II estimation methods should be automised. The method of integration of all sizing and estimation methods is described in section 4.1, followed by a description of the mission profile analysis method in section 4.2.

4.1. Iteration Method

chapter 5 provides a complete picture of which subsystems must be sized and how this can be done however, these must still be assembled in order to form an actual aircraft. Because these subsystems mutually influence each other through their size, weight and drag, they must be sized in an integrated manner. A flow diagram of the integration is shown in Figure 4.1, which illustrates the structure of the main program. In the main, different functions are called, denoted here as separate Python (.py) files.

First, the OEM and MTOW are estimated through statistical Class I methods, which were presented in detail in the Midterm Report of this project.[21] Although these values, together with the known requirements, form a sufficient base for some of the subsystem estimations, some other values must be roughly estimated, such as an initial wing position or horizontal tail surface area. Then, through the mission profile module, which is explained in more detail in section 4.2, the required hydrogen mass and other important parameters such as the wing reference area, the cruise speed or the power required are calculated.

Next, semi-empirical Class II estimation methods, as presented in chapter 5, can be used to estimate the individual contributions of each subsystem to the overall weight, dimensions and drag. The individual subsystems and the order of the sizing procedures, which depends on the required variables, can be seen in Figure 4.1. Once this is done, the weights and zero lift drag coefficients can be assembled and the empty c.g. can be recalculated. From this, the tail surfaces can be resized, the landing gears can be resized and re-placed and the wing position can be re-determined, such that all stability and controllability requirements both during flight and on the ground are met. This is explained in detail in subsection 5.9.1. At this point, all relevant weights and dimensions are known.

However, these resulting values for the MTOW and OEM depend themselves on the initial MTOW and OEM estimates. Since the methods used in this process are much more detailed, the results have a high confidence, which also means that it can be expected that these numbers differ significantly from the very first estimates. A new estimate is then needed, which starts the typical snowball effect. Therefore, it is necessary to iterate this process, until all relevant values converge below a certain threshold, which should be set at below 1%, depending on the desired accuracy in terms of mass.

Furthermore, during the process, several "go/no-go" decisions are implemented, such as a function which checks if the fuel cells fit in the wing or if the control surfaces fit on the relevant lifting surfaces.

4.2. Mission Profile

For the iteration method to be implemented at the subsystem level, a model for the mission profile is set up. This model includes the phases that are identified in Table 4.1, based on the profile set out in Figure 4.2. The main outputs of this model are discussed here, as well as the most important assumptions.
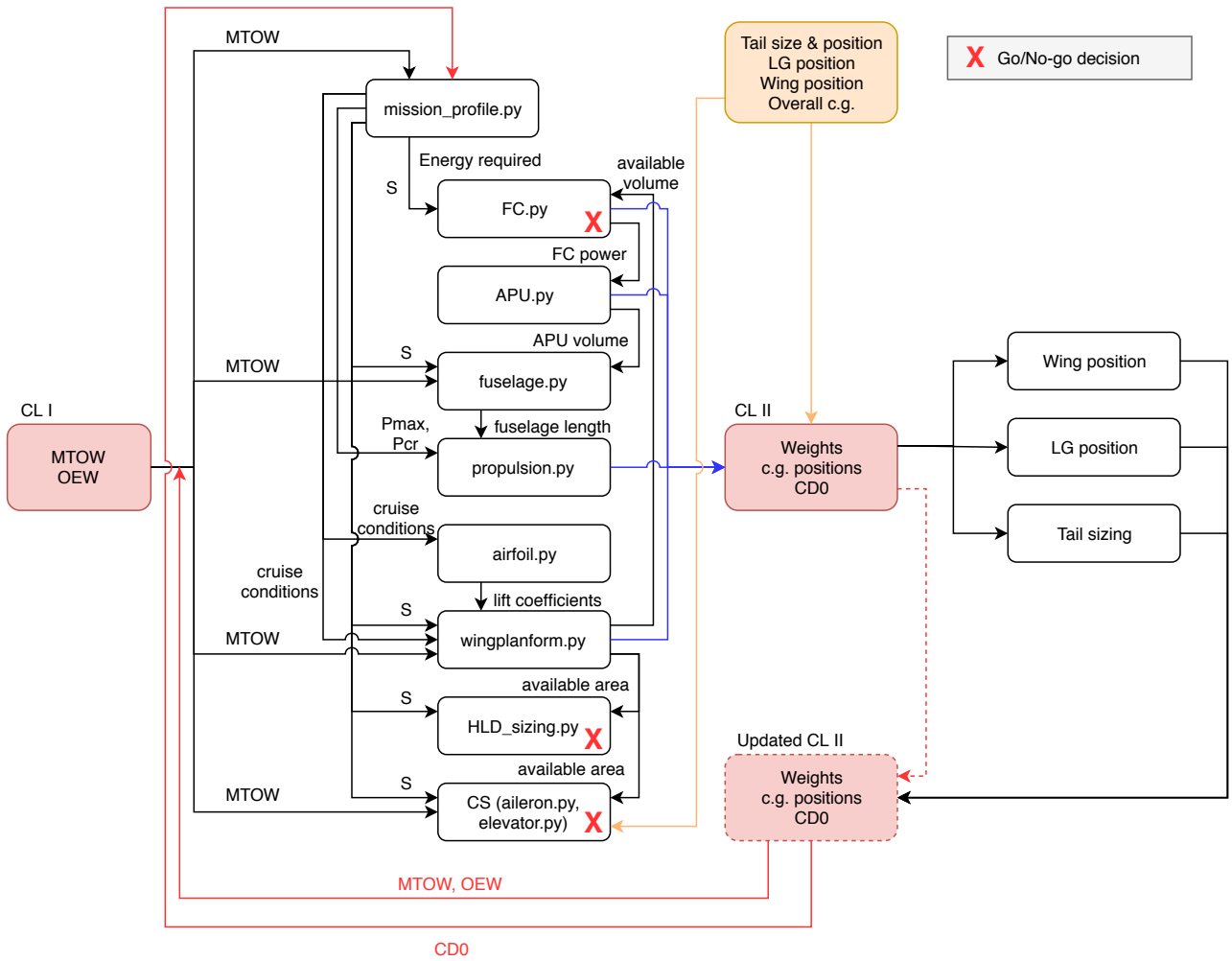
Figure 4.1: Flow chart of the main iteration program with outputs: Class II weight estimates and subsystem sizing and positioning

The goal of this model is to run through the entire mission with a time step of one second and calculate all relevant parameters for the subsystem sizing. The inputs are therefore the characteristics of the aircraft along with the mission requirements such as range and time. The most important outputs of this program are:

- **Airspeed**: The airspeed is important to calculate required power.
- **Altitude**: Needed to calculate ambient conditions.
- **Ambient Conditions**: The ambient air temperature, pressure, and density are calculated based on ISA conventions.
- **Required power**: The required power is calculated based on the mission phase, the airspeed, and ambient conditions.

The required power at each timestep is the most valuable outcome of this approach. Because the mission of the Greenliner is simulated with an accuracy of one second, the sizing of the subsystems can be based on energy and power calculations that are quite accurate for this stage of the design, especially because the subsystem sizing is used to update the inputs to the mission profile calculations.

In order to calculate the above listed parameters at every timestep, a number of choices and assumptions is made.

Climb: In this phase, the goal is to either operate the aircraft for minimal energy consumption or for maximum rate of climb. The latter option is chosen, because the cruise speed is considered limiting for the design, and therefore the time to climb should be minimal, to allow the cruise phase (which corresponds to the most efficient condition) to be as long as possible. For maximum rate of climb, the following equation is used:

$$RC_{max} = \frac{P_{max} - P_{req}}{W} \tag{4.1}$$

An additional assumption is that the aircraft climbs continuously up to cruise altitude. In reality, the climb will most likely occur in steps, but for the design considerations in this phase, the assumption of continuous flight is deemed acceptable, because it does not change the requirements on performance.

Cruise: There are two main parameters that were used to set up the cruise profile: the cruise altitude and the cruise velocity. The two are linked, because at any altitude, an aircraft has a certain optimum speed. This speed is optimised for minimal energy consumption over the entire cruise, and is given by:

$$V_{opt} = \sqrt{\frac{W}{S}\frac{2}{\rho}\frac{1}{C_{Lopt}}}, \text{ with} \tag{4.2}$$

$$C_{Lopt} = \sqrt{C_{d_0}\pi Ae} \tag{4.3}$$

The expression for $C_{L_{opt}}$ follows from stipulating maximum $\frac{L}{D}$. Since the cruise speed is determined by the mission time constraint, the optimal altitude can be found by rearranging Equation 4.2 to find the air density ρ, which in turn yields the optimal cruise altitude through ISA calculations.

Descent: Similarly to the climb profile, the descent is assumed to be continuous. The same reasoning applies as for the climb profile. An additional assumption is that a small fraction of the cruise power is used during descent. This is a conservative assumption, as kinetic energy recovery is currently being assessed for electric aircraft [111].
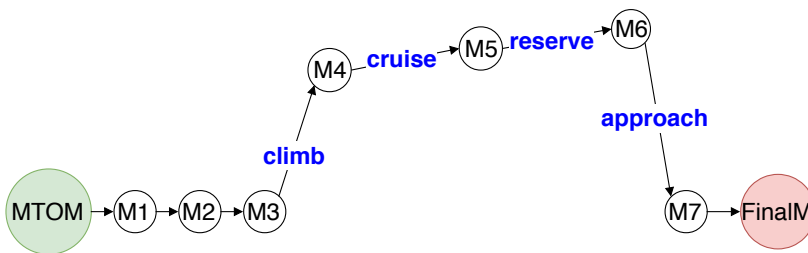
Figure 4.2: Schematic representation of the mission profile

From:	To:	Manoeuvre:
MTOM	M1	Warm up
M1	M2	Taxi
M2	M3	Take off
M3	M4	Climb
M4	M5	Cruise
M5	M6	Reserve cruise
M6	M7	Approach
M7	FinalM	Landing + Parking

Table 4.1: Mission profile elements

5

Subsystem Design Methods

In chapter 4, the mission profile is presented and the iteration method is introduced. In this chapter, the approach towards the Greenliner subsystem design is introduced, where the subsystems depicted in Figure 5.1 are discussed. In section 5.1, the fuselage cross section is chosen and the resulting fuselage dimensions are presented. Then in section 5.2, the cabin environment that ensures the passenger comfort is introduced, focusing on the air supply system design. After that, the airfoil of the wing and tail is selected in section 5.3. The wing planform approach is discussed in section 5.4. The propulsion system is introduced in section 5.5, where the benefit of using DEP is elaborated, the motor is selected and the sizing of propulsion unit is conducted. Then, the fuel cell subsystem model and sizing is discussed in section 5.6, together with corresponding systems such as air and hydrogen transfer systems and the water management system. After that, the LH2 storage is reviewed with proper insulation in section 5.7. The APU subsystem is discussed in section 5.8. Stability and control will be introduced in section 5.9 by sizing the tail and control surfaces and positioning the wing. After that, the landing gear design is presented in section 5.10. Lastly, the feasibility of using a solar panel is elaborated in section 5.11.

5.1. Fuselage

As the Greenliner is a commercial civil aircraft, it has the main function of delivering its passengers from point A to point B. Therefore, a comfortable cabin configuration is a important consideration in fuselage design. During the fuselage design process, there are two decisions to make before determining the weight and drag of the fuselage, namely the fuselage cross sectional shape and the number of seats abreast. Once the cross section geometry is given, the fuselage length including nose and tail cone can be estimated. The geometry of the complete fuselage is then used for the weight and drag calculations. Verification of these calculations is performed in section 8.1.

Fuselage Cross Section

In order to select the fuselage cross sectional shape, it should be decided if the cabin is pressurised or not. Since the aircraft flies at a high altitudes (explained in section 7.1), the pressure and temperature in the atmosphere is much lower than at sea level. Without adjustment, the cabin environment would not be suitable for transporting people. Therefore, cabin pressurisation is required. A circular fuselage is the most optimal shape in terms of pressurisation. On top of that, the propulsive fuselage configuration incorporated in the Greenliner (explained in section 5.5), will also influence the choice of cross sectional shape. As introduced in section 5.5, distributed propellers are mounted at the back of the fuselage. Therefore, the manufacturing process is challenging for irregular shapes. Concluding, a circular cross section is the best choice concerning both pressurisation and propulsion system mounting.

Now that a circular shape has been chosen, the cabin arrangement for 19 passengers can be determined by the number of seats abreast in the cabin. This number of seats abreast is used to calculate the the fuselage width. Because there should be no more than two seats accessed from one aisle, there will be three resulting options: two seats, three seats and four seats abreast. In Figure 5.2, these three options are presented. Logically, less seats abreast leads to a longer cabin. Because the fuel tank should also be located in the fuselage, the length will increase even more. Since the fuselage contributes greatly to the total aircraft weight, it should be optimised on this parameter. Concluding, the fuselage design must be optimised not only in terms of length but also in terms of diameter (seats abreast), because these two parameters determine the fuselage weight.

Fuselage Length

Fuselage length is generally divided into three compartments: the nose section, the cabin section, and the tail section. However, for the Greenliner, there is an additional compartment required to store the LH2 tank (discussed in
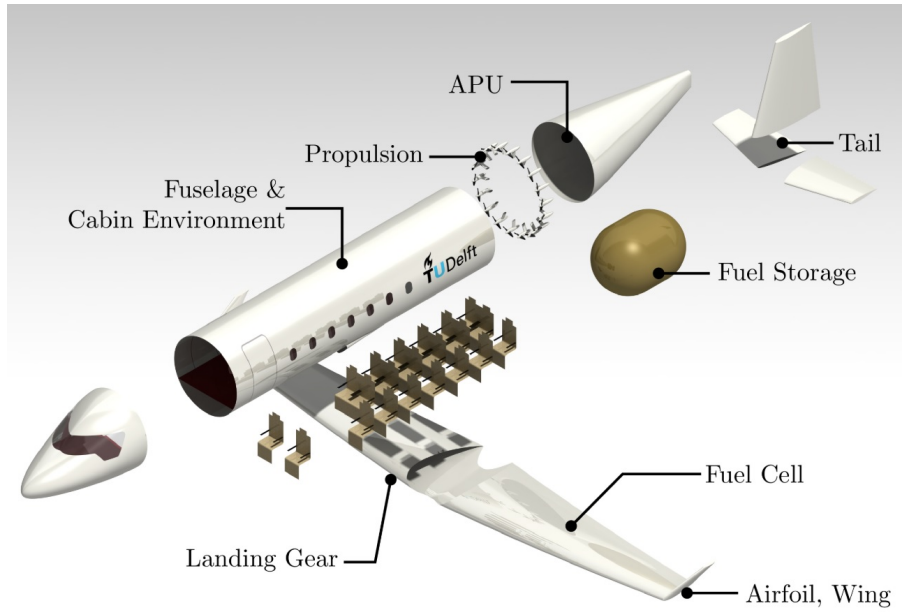
Figure 5.1: Exploded view of the Greenliner subsystems
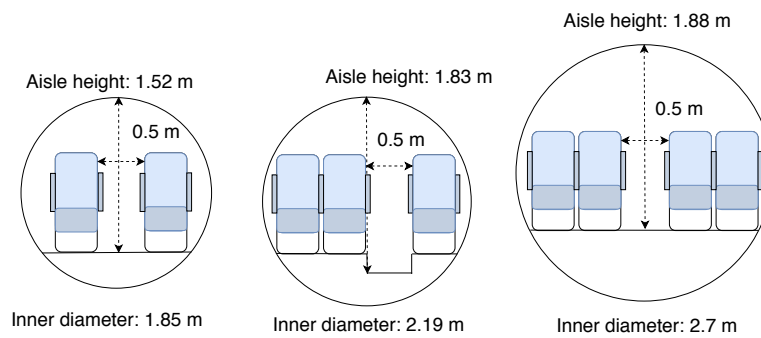
Figure 5.2: Cabin layout options: 2 seats abreast, 3 seats abreast, 4 seats abreast
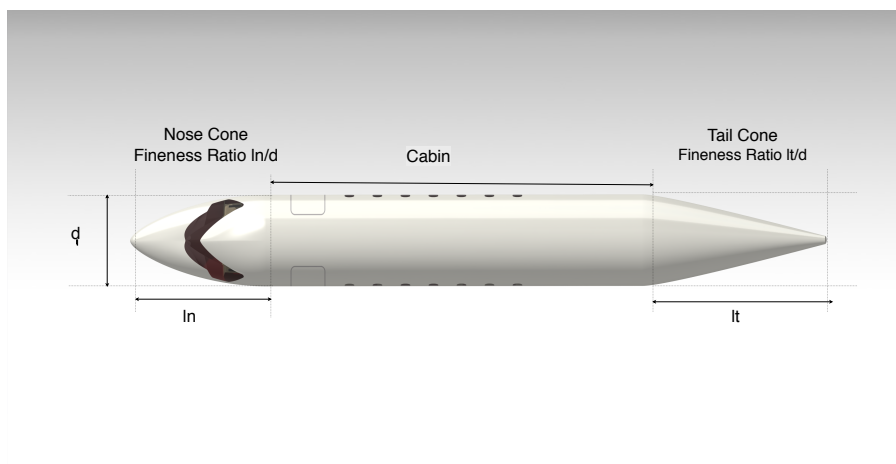
Figure 5.3: Definition of fineness ratio of the aircraft nose and tail

section 5.7) and APU. The length of the various compartments is discussed below.

The nose and tail length are estimated based on the drag-optimised fineness ratio range. The fineness ratio is defined as the ratio between the diameter and the length from a top view, as shown in Figure 5.3. For a subsonic aircraft, the nose fineness ratio is limited by fuselage drag [67]. Therefore, a nose fineness ratio is set to be 1.5 while a tail fineness ratio of 2 is used. The corresponding nose and tail length can be found in Table 5.1.

In the nose, where the cockpit is located, avionics are installed to control the aircraft during operation. The avionic types such as weather radar, flight-control system, communication are not described in detail in this report. However, to ensure the certification of the Greenliner, all avionic systems should be properly selected and installed so that the aircraft can be controlled. The tail design approach is discussed in more detail in subsection 5.9.1.

The spacing of the interior of the fuselage is determined more by market and passenger comfort consideration and less by regulations [77], so that the seat pitch, width and aisle width of the Greenliner is defined based on reference. The economic class seat sizing is used, so the seat pitch, width and aisle dimensions are 0.74 m, 0.5 m, and 0.5 m respectively. They are depicted in Figure 5.4. The combination of these dimension, determines the cross section diameter which results in 2.19 m for the three seats abreast configuration. Furthermore, based on FAA Regulation part 25, when 19 passengers are on board, the aircraft should have a Type II exit on each side of the fuselage. A Type II exit door has a dimension of 1.12 m in height and 0.5 m in width.
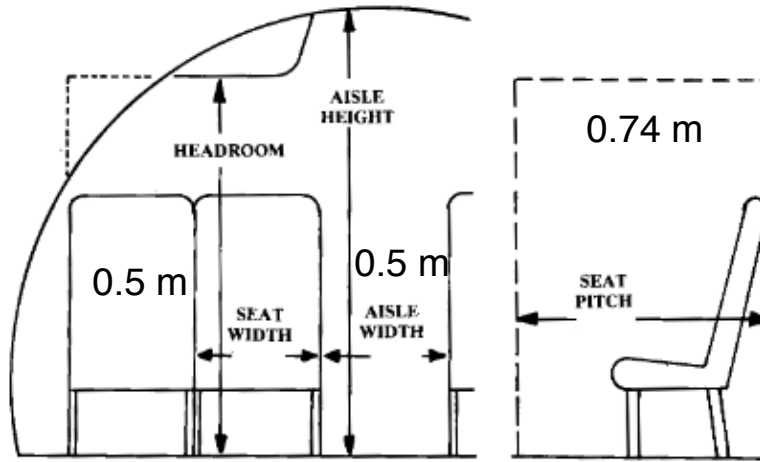
Figure 5.4: Seat dimension: seat pitch, width and aisle width[77]

Fuselage Mass

Fuselage mass estimation can be performed based on Raymer's statistical method. When calculating fuselage mass with Raymer's statistical method, Equation 5.1 is used [77]. This method does not use SI units nor conventional symbols so the output is converted for further design steps.

$$W_{fus} = 0.3280 K_{door} K_{LG} (W_{dg} N_z)^{0.5} L^{0.25} S_f^{0.302} (1 + K_{ws})^{0.04} (L/D)^{0.1} \tag{5.1}$$

Here, $W_{fuselage}$ is the estimated fuselage mass. The statistical values are retrieved from [77]: K_{door}, the coefficient for the cargo door, is 1.06 because one cargo door for luggage is chosen. K_{lg} is the coefficient for landing gear. Since wing mounted landing gear configuration is chosen in section 5.10, this value is set to be 1.0. W_{dg} is the design gross weight of the aircraft. N_z is the ultimate load factor which is 1.5 times the design load factor calculated in Equation 5.2.

$$N_z = 1.5 \ldots (2.1 + 24000/(W_{dg} + 10000) \tag{5.2}$$

This N_z value should not be greater than 3.8 based on regulation[25], therefore, the smaller value between the ultimate load factor and 3.8 is chosen for Equation 8.1. L and D are the length and diameter of the fuselage, which are

determined once the geometry is known. S_f is the fuselage wetted area given in m^2. Also K_{ws} is set to 0 because no sweep is considered for the wing.

For all three configurations depicted in Figure 5.4, these equations result in a different total fuselage mass. After analysis of the configurations and their mass, it is concluded that the optimal cabin configuration is the one with three seats abreast, the middle picture in Figure 5.4. This fuselage mass calculation is based on statistical approach.

Fuselage Drag

The drag of the fuselage is calculated through the following equations. As shown in Equation 5.3, the zero lift fuselage drag $C_{D0_{fus}}$ depends on fuselage drag coefficient c_{fus} and the ratio between wetted fuselage area, S_{wet}, and the aircraft reference area, S_{ref} [67].

$$C_{D0_{fus}} = (c_{fus} \cdot S_{wet})/S_{ref} \tag{5.3}$$

The variable c_{fus} is the product of three drag coefficients, namely the flat plate skin friction coefficient cf, the component form factor ff, and the interference factor if_c. The flat plat skin friction coefficient estimates the skin friction drag component. It is strongly dependent on the type of boundary layer flow, i.e. laminar or turbulent. There is no defined value for the ratio of laminar to turbulent flow. Based on [67], a ratio of 10% laminar cf to 90% turbulent cf is assumed. These values are calculated by Equation 5.4 and Equation 5.5 respectively, after which the weighted average is used as the flat plate skin friction coefficient cf.

$$cf_{lam} = \frac{1.328}{\sqrt{Re}} \tag{5.4}$$

$$cf_{tur} = \frac{0.455}{(log_{10}Re)^{2.58}(1+0.144M^2)0.65} \tag{5.5}$$

Re in Equation 5.4 and Equation 5.5 represents the Reyonlds number. This indicates the ratio of inertia forces to viscous forces in the flow. With a higher Reynolds number, a higher skin friction can be observed. However, when the flow is turbulent, there is a cut-off Reyonlds number after which the skin friction coefficient is constant. Therefore, the actual Reyonlds number is defined by the smaller value presented between Equation 5.6 and Equation 5.7. The skin roughness constant (k) is taken for a smooth surface as (0.634×10^{-5} m).

$$Re_{real} = \frac{\rho v l}{\mu} \tag{5.6}$$

$$Re_{cutoff} = 38.21(\frac{l}{k})^{1.053} \tag{5.7}$$

The component form factor ff estimates the pressure drag due to viscous flow separation. It can be calculated with Equation 5.8, which is for the fuselage component.

$$ff = \frac{60}{(\frac{L}{D})^3} + \frac{\frac{L}{D}}{400} \tag{5.8}$$

The last factor used to calculate c_{fus} is the interference factor if_c. This factor accounts for the interference caused by the thick boundary layer that occurs at the connection point of two components. As the propellers are far towards the back of the fuselage, this factor is chosen as 1.0 (negiligible interference).

Summary of the Three Options

The design choices lead to the fuselage dimensions shown in Table 5.1. The reasons for selecting a three-seats abreast design option are as following. A two-seats abreast option results in a very long aircraft, which has a higher drag comparing to the other two option. Meanwhile, the four-seats abreast option is heavier than the three-seats abreast.

Table 5.1: Summary of the fuselage layout for different seats abreast options

Seat Abreast/ Geometry	Aisle Height [cm]	Fuselage Diameter [m]	Nose Length [m]	Tail Length [m]	Fuselage Weight [kg]	Fuselage Induced Drag [-]
Two Seats Abreast	152	1.85	2.78	3.7	2419	0.007
Three Seats Abreast	183	2.19	3.29	4.38	2323	0.00638
Four Seats Abreast	188	2.7	4.05	5.4	2360	0.008

Fuselage Sustainability

Sustainability of the fuselage design is assessed in three different phases: production, operation and end-of-life.

Fuselage production can be divided into several sections: nose, forward, fuselage and wing joining, aft and lastly tail. Each section can be produced independently and assembled at a central location. For Greenliner fuselage production, the Fuselage Automated Upright Build (FAUB) system will be implemented, like the Boeing 777X and 777 model[1]. This process is faster, more precise and more cost beneficial than non-automated production processes; Less errors can be expected during production, therefore, the Greenliner will have a high reliability. This automatic production line will require a large investment on design and programming of the robots to adapt to the Greenliner production but in long term, the production of the Greenliner is more financially sustainable [102].

During operation, the fuselage of an aircraft generates about 20% of the total drag. The design approach to reduce drag introduces the following characteristics: Firstly, a circular shape cross section is used instead of a rectangular one like the reference aircraft the Dornier 228. Secondly, small propellers are installed at the back of the fuselage, which can reduce the boundary layer thickness along the fuselage. This corresponds to a smaller drag coefficient for the fuselage. Further analysis on the effect of propulsion choices can be found in section 5.5.

To be financially sustainable, the maintenance should be analysed in two aspects. One is the order of maintenance tasks and the other is the ease of accessibility of the components. The overall night maintenance plan and out of service operation plans should be constructed. In such plans, both sequential and concurrent tasks should be defined clearly so that the maintenance can be a repeatable event with schedule and milestones. Meanwhile, the fuselage should be easy to access, meaning that loading and unloading passengers and cargo should be comparable to conventional aircraft. More detail on maintenance tasks can be found in section 10.4.

At the end-of-life, the reuse and recyclability of the fuselage will determine the sustainability of its design. Since the fuselage is mostly made out of aluminium, the recycalbility of the fuselage is high. Within Europe there are many aircraft disassembling companies, such as Stolwerk Metaal BV and AELS (Aircraft End-of-Life Solution). Cooperation with these companies will be set up and maintained in the later phase of the aircraft design so that the environmental impact of the Greenliner at the end-of-life can be reduced.

5.2. Cabin Environment

Cabin environment is the most important area for the passengers as it influences the passengers' onboard experience during the flight. Essentially the cabin environment is the area where passengers are interacting with the aircraft. Therefore, having an easy-to-use and comfortable cabin environment will increase passenger satisfaction. Detailed information on seat arrangement and interior layout is presented in section 5.1 and it is not discussed here. In the following paragraphs, the cabin environment design of Greenliner is introduced, with the focus on air supply system, water and waste, food and galley, window design, and safety considerations.

Air Supply System

The air supply system has three main functions: to supply fresh air and remove pollutants, to pressurise the cabin, and to control the technical equipment. During flight operation, ventilation is required provide a sufficient amount of uncontaminated air to ensure that the crew members are able to perform their duties without discomfort, and to provide the passengers with a comfortable environment within the cabin. This means that the cockpit and the cabin should be free from harmful concentrations of gas or vapours. In reference [69], the maximum Carbon Monoxide (CO)

---

[1] Retrieved from `https://www.boeing.com/features/2017/02/faub-777-assembly-02-17.page` on July 2nd 2018

concentration should be less than 5% in the compartment occupied by the crew and passengers. Additionally, with the use of hydrogen as energy source, proper ventilation of hydrogen should prevent potential threat to the passengers on board [70]. On top of that the hydrogen tank is isolated from the cabin. A schematic for ventilation and re-circulation within the aircraft is presented in Figure 5.5. The specifics of this system are discussed below.
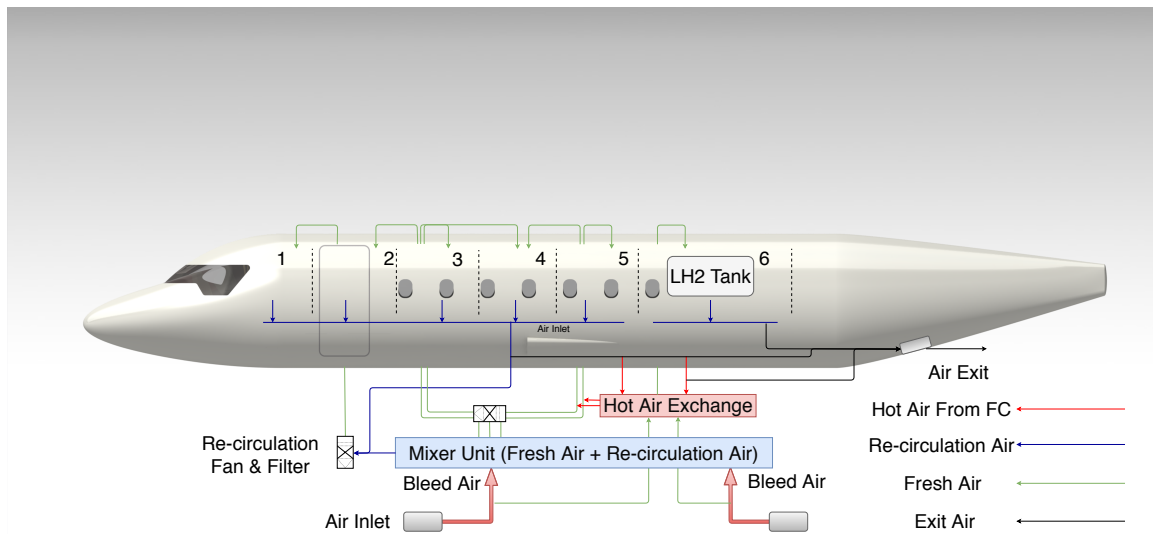
Figure 5.5: Ventilation and flow re-circulation inside the Greenliner cabin

Air Inlet

The air used in the circulation comes from external flow via air intake. The air supplied to cockpit and cabin is regulated via an environmental control system (ECS). The average air flow per passenger is required to be 20 m^3/min, which is regulated with half re-circulation air and half fresh air [112]. Conventionally, the air intake is absorbed via engines, where air is compressed and cooled before mixing with the internal re-circulating air. However, this does not apply to the Greenliner concept, as the motors do not take in air. In stead, the air inlet is designed to be along the fuselage in front of the wing, where it performs two functions: Firstly, providing fresh air into the cabin, and secondly, serving as oxygen supply for the fuel cells. The air inlet location is shown in Figure 5.5, while the geometry is shown in Figure 5.20.

Air Mixture

Once the make-up air, also known as the external air, is sucked and compressed in the air intake, it becomes the bleed air. The bleed air is first distributed into fuel cell use and cabin use. The cabin uses the fresh air combined with the recirculating air at the Mixer Unit after being cooled down. Then the breathable air mixture re-enters the cabin and cockpit with the assistance of a fan and filter, which removes unwanted substances introduced along with the bleed air and recirculated air. These unwanted substances include gases, vapours, smoke, fumes, and mist from bleed air, as well as anthropogenic constituents from crew and passengers such as dust and fibres from recirculated air. These particles are captured and filtered with a high efficiency particulate air (HEPA) filtration system. With the HEPA filtration system, dusts, fibres, bacteria cells and pollen grains with a size range of 0.3 μm to 10 μm are collected in the recirculated air. This cleaned air is then distributed throughout the cabin and cockpit and this process is regulated by the ECS with the objective of providing good air circulation and uniform temperature. The distributed air enters the cabin and flight deck through diffusers on the ceiling of the aisle or the over head baggage compartments. A uniform temperature throughout the cabin can obtained because the fresh air from the diffusers is at a consistent temperature level after going through the Mixer Unit. The temperature can be regulated by mixing with the hot air from the fuel cell.

Air Circulation in the Cabin

The fresh air enters the cabin through different diffusers and these diffusers are divided into three compartments, namely the cockpit, cabin, and fuel storage. The cabin is divided into different segments to maintain a high level of

quality in air circulation for all passengers. Five diffusers are used to ensure that different compartments will experience similar air conditioning. As for compartment 6, where the hydrogen tank is stored, there is a separate circulation diffuser. This ensures the cryogenic tank does not experience a heat exchange and increase temperature too much. The operation of the diffuser is dependent on the compartment conditions. Under normal conditions, there is a small amount of leakage, so the diffuser is turned on when hydrogen has a concentration of 2% inside the compartment. This is a safety control to ensure that hydrogen does not accumulate to a flammable density of 4% [49]. Under tank malfunction, where the tank has a crack, the diffuser is turned to maximum to ensure that the surrounding structure is not affected by the cold hydrogen. The air is expelled to the outside of the aircraft through an exit. This exit is also used to remove the unwanted air from the cabin or from the fuel cell. All re-circulation air either enters the loop or entering the air exit and expelled

Pressurisation

During operation, Greenliner flies at cruise altitude of 39000 ft. A pressurised cabin is used for Greenliner to maintain a high level of passenger comfort. The cabin pressure altitude is maintained at 8000 ft, at which supplementary oxygen supply is not required, and an ambient pressure of 0.76 bar is maintained. The circulated air also adjusts the pressure level throughout the mission. Especially during climb and decent, the ECS controls the required pressure by sucking in or expelling air.

Heat Exchange

As shown in Figure 5.5, cold fresh air is used to cool down the PEM fuel cell temperature. Meanwhile, in case of a higher temperature required for the cabin, heat released by the PEM fuel cell can be used to increase the cabin temperature. However, this heat exchange is not expected for the circulation line entering into the fuel cell compartment. This circulation line should not be turned on unless necessary as the higher the tank compartment temperature is, the higher the boil-off loss of LH2 becomes.

Water and Food Supply

Aside from air supply, other important aspects that help maintain a comfortable environment for the passengers include water and food supply, as well as the related waste. During operation, the fuel cell system generates H_2O as byproduct. The fuel cell water management system will transport this byproduct for lavatory use. The aircraft will have a water tank that can be filled during ground operation, which is located under the cabin floor. Additionally, there is the waste tank that connects the lavatory and galley waste disposal unit. As for galley and food storage, this is located at the front of the cabin. Since the whole mission duration is 2 hours, no meal is provided to the passengers.

Safety Considerations

The safety consideration regarding oxygen supply during emergency situations should be analysed. Different forms of oxygen supplies exist for aircraft application, including gaseous form, liquid form, chemical or solid oxygen, and Onboard Oxygen Generating Systems (OBOGS). Gaseous form or liquid form of oxygen are discarded because they requires a storage tank, which is three times heavier than a solid oxygen generator for the same quantity of oxygen available [29]. In a solid oxygen generator, sodium chlorate is used with a spring-loaded firing pin. Once the pin is pulled, oxygen is produced as the product of sodium chlorate burn. However, this option is not considered as safe because highly flammable hydrogen is stored on board. The option chosen for the Greenliner is the OBOGS which uses molecular sieve to separate oxygen from other gases in the air [29]. This option also has a high life cycle compare to GOX and LOX.

Sustainability

When using such environmental control system described above, a high level of passenger comfort can be maintained throughout the flight. While the aircraft presssure is maintained at 8000 ft cabin altitude, passengers and crews can also experience fresh air throughout the flight. When the passengers are informed about the separate air circulation compartment for the hydrogen storage, public concern regarding hydrogen safety will reduce. The HEPA filters ensure that the bacteria and dust will not enter the cabin, so that passenger do not need to worry about health issue. Furthermore, as no combustion engines are used and all propellers are installed at the back of the aircraft, the passengers on board will experience less noise. This shows that the Greenliner is socially sustainable.

5.3. Airfoil

In this section the selection process for the main wing and tail airfoils is described and both airfoils are presented.

5.3.1. Approach to Airfoil Selection

Selecting an airfoil can be a very time consuming process. Especially when the airfoil is designed from scratch, it will require a lot of testing, as well as financial means and human resources, before it actually can be used. In this stage of the design, it is therefore appropriate to select an existing airfoil from the NACA airfoil database in [1], based on the experimental data which this book contains for all the different airfoils.

An assessment of the NACA airfoils is done by examining three main characteristics: airfoil thickness, design C_l, and drag bucket. Then at the end of this section five airfoils will be selected for trade-off, which will be executed in Equation 5.3.1.

NACA 4, 5 or 6 Digits [92]
The different NACA versions are given in a series of digits. The numbers stand for geometrical values or aerodynamic characteristics of the airfoil. The amount of digits already gives information about the performance of the airfoil.

The NACA 4-digit airfoils have good stall characteristics, as after reaching the relatively high maximum lift coefficient they will only trend gradually to stall. The airfoils have relatively high drag, and therefore they are not suitable for the entire wing, but they can be used in the wingtip sections or tail wings due to their good stall behaviour. The NACA 5-digit airfoils (focusing on the 230-series) have high values for the maximum lift coefficient, but less favourable stall behaviour. The 6-digit airfoils have been designed to have very low drag values in a range of lift coefficients (drag buckets). These airfoils often have a lower maximum lift coefficient than the other two NACA versions, though this can be compensated by having a higher camber or thickness. A disadvantage of these airfoils is that they are very sensitive to dirt, which can significantly increase the drag. However, the NACA 6-digit airfoils are the most researched airfoils, which means that there is elaborate experimental data available, while the other two have less data available.

Wing Thickness Ratio
Since the fuel cells will be stored in the wing, firstly it should be considered if there is a minimum required wing thickness to fit them in the wing. The fuel cells are very thin and can be stacked, so it is expected that this will not be a constraint for the wing thickness.

Furthermore, the wing thickness has an influence on the following characteristics: drag, weight, and maximum lift [79]. As the drag tends to increase with thickness because of the profile drag, the maximum lift will also increase by increasing wing thickness. This will be subject to a trade-off by looking at the drag and lift curve of the particular airfoils. The weight is another consideration. The wing weight will decrease with increasing thickness ratio due to increased bending and torsional stiffness [79]. In conclusion, the goal is to find the airfoil with a high wing thickness ratio, while also striving for the optimal lift to drag ratio.

Design C_l and Drag Bucket
As mentioned before, the NACA 6-digit airfoils have drag buckets. This characteristic is very useful when choosing an airfoil. From the requirements a design lift-coefficient can be determined. C_{ldes} is determined by using the lift equation [66]. The main wing needs to take into account compensation for the down force of the tail wing, which is assumed to be 10% of the total lift [66]. This value can then be used in combination with the wing loading, cruise velocity, and density at cruise altitude implemented in Equation 5.9 to come up with the design C_l. C_{ldes} can be used to pick the most suitable airfoils by looking at the drag buckets of the airfoils. If the Cl value is within the bucket range, the airfoil is suitable to be used. As a note: the 5-digit airfoils also have some sort of drag bucket, but only less extensive.

$$C_{ldes} = 1.1 \frac{1}{q} \frac{W}{S} \tag{5.9}$$

Suitable Airfoils
For selecting the airfoils for the trade-off, firstly the airfoils of the reference aircraft from [20] were considered. Then from experimental data in [1] the airfoils were picked, which have a drag bucket which complies with the C_{ldes}. Since only one of the reference airfoils was suitable (only NACA 23018), there was decided to pick four other airfoils from [1], which also have favourable lift and drag characteristics. Now, the most suitable airfoil from these five airfoils can be selected by comparing different relevant parameters in a trade-off.
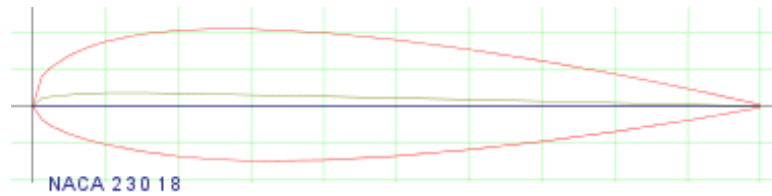
Figure 5.6: Shape of the NACA 23018 airfoil [37]

Airfoil Trade-off

In this section the airfoil trade-off is executed. The trade-off is performed by comparing five airfoils by means of the various relevant parameters. The trade-off is done in Table 5.2. The first column contains the parameter which is evaluated for each airfoil, the text in between brackets indicates the best option. For each parameter, the best performing airfoil is highlighted. At the time of airfoil selection, a lower cruise altitude was estimated than the current value, so that the $C_{l_{des}}$ was inside the drag bucket of all the airfoils. However, after some new calculations were published the cruise air density turned out to be lower (due to a higher cruise altitude), and thus the design C_l was increased. This is the reason for the three middle airfoils not having the C_l value inside their drag buckets.

From the trade-off, three airfoils received the highest score. Only two of these have a suitable drag bucket range, which is considered to be an important parameter in this stage of the design, due to the flexibility it offers. For this reason the airfoil with the highest drag bucket range, which is NACA 23018, is chosen as the most suitable airfoil for the Greenliner. Figure 5.6 gives the geometry of this airfoil.

Parameter	NACA 23018	NACA 63(3)618	NACA 64(3)618	NACA 64(4)421	NACA 65(3)618
Thickness ratio (high is best)	0.18	0.18	0.18	0.21	0.18
Sensitive to surface quality? (preferably no)	N	Y	Y	Y	Y
C_l for AOA=0 (closest to $C_{L_{cruise}}$ is best)	0.1	0.4	0.4	0.3	0.4
AOA for C_l=0	-1	-4	-4	-3	-4
$C_{l_{max}}$ (highest is best)	1.6	1.5	1.5	1.4	1.5
AOA of $C_{l_{max}}$ (highest is best)	16	12	18	20	18
Stall characteristics (A,B,C)	C	B	A	A	A
$C_{d_{min}}$ (lowest is best)	0.007	0.0055	0.005	0.00555	0.005
C_l of $C_{d_{min}}$ (closest to cruise is best)	0.3	0.2	0.3	0.1	0.3
$(C_l/C_d)_{max}$ (highest is best)	120	167	200	167	200
C_l of $(C_l/C_d)_{max}$ (lowest is best)	1.2	1	1	1	1.2
Cruise C_m (closest to 0 is best)	0	-0.1	-0.1	-0.07	-0.1
Drag bucket starts at C_l	-0.1	0.2	0.3	0	0.3
Drag bucket ends at C_l	1.2	1	1	1	1.2
Drag bucket length (largest is best)	1.3	0.8	0.7	1	0.9
Is $C_{l_{cruise}}$ inside drag bucket? (preferably yes)	Y	N	N	N	Y
Total	6	2	6	4	6

Table 5.2: Trade-off table for airfoil selection

5.3.2. Airfoil Horizontal and Vertical Tail

The airfoils for the horizontal and vertical tail are determined by taking the requirements of the performance of both tails into account. Firstly, they need to be able to exert a positive as well as a negative lift, so they require a symmetric airfoil. Next to that, it is favourable to have a high range of usable angles of attacks and a high slope of the Cl-alpha curve [92]. For these reasons it is decided to use the NACA 0012 airfoil for both the vertical and the horizontal tail. It is a symmetric airfoil with good stall characteristics.

5.4. Wing Planform

In this section the methodology for determining the wingplan parameters is given. The parameters that need to be selected are the aspect ratio (A), quarter chord sweep angle ($\Lambda_{0.25c}$), taper ratio (λ), the incidence angle (*i*), the wing

twist (ϕ), and the dihedral (Γ). The combination of parameters is optimised during an iterative process. This iterative process consists of assessing the wing performance on wing lift curve, drag polar, maximum lift coefficient, $C_{L_{max}}$, and stall angle of attack, α_s explained in subsection 5.4.1 and subsection 5.4.2. The results of this optimisation after iteration is given in section 7.2. Simultaneously, the design is assessed based on wing structural weight using the Raymer weight estimation method [77]. Then, the wing design is finalised by selecting the vertical position of the main wing and the wing tips. Additionally, the incidence angle, wing twist and dihedral are selected based on a suggested range of values depending on aircraft category [77]. Lastly, the process of arranging the wing structure is described.

5.4.1. Wing Lift Curve
The wing lift curve is computed by making use of the DATCOM method for estimating $C_{L\alpha}$, given in Equation 5.10.

$$\frac{dC_L}{d\alpha} = C_{L\alpha} = \frac{2\pi A}{2 + \sqrt{4 + (\frac{A\beta}{\eta})^2(1 + \frac{tan(\Lambda_{0.5c})^2}{\beta^2})}} \tag{5.10}$$

In this formula, β is a compressibility correction factor, given by:

$$\beta = \sqrt{1 - M_\infty^2} \tag{5.11}$$

After computing the lift curve slope, the maximum lift coefficient is calculated at landing conditions. To do this, the wing design is categorised as high or low aspect ratio. The wing has a high aspect ratio if the following holds:

$$A > \frac{4}{(C_1 + 1)cos(\Lambda_{LE})} \tag{5.12}$$

When using the current estimate of 10 for A in Equation 5.12, it can be concluded that the Greenliner is categorised as a high aspect ratio wing aircraft. Based on that fact, suitable formulas for CL_{max} and α_s are used, given in Equation 5.13 and Equation 5.14.

$$C_{L_{max}} = [\frac{C_{L_{max}}}{C_{l_{max}}}]C_{l_{max}} + \Delta C_{L_{max}} \tag{5.13}$$

$$\alpha_s = \frac{C_{L_{max}}}{C_{L_\alpha}} + \alpha_{0L} + \Delta\alpha_{C_{L_{max}}} \tag{5.14}$$

These formula are obtained from the Raymer method [77], in which also the corresponding graphs are presented to obtain the variables in the formula. When interpreting these graphs, it is assumed that CL_{max} occurs at landing, where the Mach number of the aircraft is lower than 0.2. After multiple iterations, the final lift curve can be constructed. The result is given in chapter 6

5.4.2. Drag Polar
Equation 5.15 and Equation 5.16 are used to construct C_D and C_L and thus the drag polar.

$$C_L = C_{L_\alpha}(\alpha - \alpha_{0L}) \tag{5.15}$$

$$C_D = C_{D0} + \frac{C_L^2}{\pi Ae} \tag{5.16}$$

$$C_{D0} = \frac{1}{S_{ref}} \sum C_{D_c} A_c + C_{d_{misc}} \tag{5.17}$$

The total zero lift drag (C_{D0}) presented in Equation 5.17 depends on the airfoil, fuselage, engine and mission characteristics. To calculate this value, the Raymer method presented in [67] is used. The final drag polar is given and explained in section 7.2.

High-Lift Devices

In order to take-off and land, high lift devices are installed. When considering high lift devices, a compromise has to made lift capabilities and complexity of the design. The more complex a high lift device, the larger the risk and the bigger the manufacturing and maintenance cost. Because the aircraft has a moderate take-off weight, it does not require high complexity lift devices such as triple slotted flaps. On the other hand, the increase in lift of basic high lift devices such as split flaps is much smaller than the increase in lift of slotted flaps. For this reason, an intermediate solution is chosen: single slotted flaps. An increase in lift is initiated by an extra upward air flow through the air gap over the upper surface of the flap. This extra air flow streamlines the flow over the surface and by doing that, energises the boundary layer, which leads to a higher production of lift.

5.4.3. Wing Structural Weight

To optimise the wing geometry, the weight of the wing is estimated. For quick estimation, the Raymer method that is based on statistical data is suitable [77]. For a cargo/transport aircraft, the formula for wing structural weight estimation is given in Equation 5.18. This method does not use SI units nor conventional symbols so the output is converted for further design steps.

$$W_w = 0.0051(W_{dg}N_z)^{0.557}S_w^{0.649}A^{0.5}(t/c)_{root}^{-0.4}(1+\lambda)^{0.1}cos(\Lambda)^{-1.0}S_{csw}^{0.1} \tag{5.18}$$

5.4.4. Finalising Wing Design

In conventional aircraft design, there are three main configuration options for the position of the wing: low wing, mid wing, and high wing. The choice is made to have a low wing configuration because of several advantages.

First of all, a low wing allows for a continuous wing structure in which the left and right wings are connected in the belly of the fuselage. Due to this, the wing structure is much stronger than in the case of a mid wing configuration. This structural advantage reduces the weight of the wing. Another advantage is that the main landing gear integration becomes much simpler and more efficient, which reduces the landing gear structural weight. The last main benefit is the accessibility of the wings. On a low wing, maintenance operations are more easily performed. A high wing configuration is mainly used in specific cases because of better wing clearance. For example, some aircraft are designed for STOL (Short Take-Off and Landing), or for unprepared runways. These aircraft thus require larger clearance, which leads to the choice for a high wing configuration. Since the Greenliner does not have wing mounted engines and does not require STOL or landing at extreme conditions, a high wing is not necessary.

During the wing design, the choice is made to add winglets to the wingtips of the aircraft. Although winglets are most effective in high speed flight and the Greenliner flies at moderate speeds, winglets still improve the performance. This is because winglets use the tip vortex energy to reduce the lift induced drag by increasing the effective aspect ratio of the wing [2].

To finalise the wing planform design, three design choices still have to be made: the wing incidence angle, the wing twist and the dihedral. The average wing incidence angle (twisted wings) for transport aircraft is set at the typical value of 1 degree [77]. Wing twist is an important parameter with respect to stall characteristics of the wing. A wing should stall from root to tip so that it is still controllable in stall. Therefore, the wing tip should have higher C_{Lmax} than the wing root. To assure this, the wing tip often has a lower angle of attack than the root. This characteristic is called washout. According to reference [77] it can be assumed that a twist of 3 degrees provides adequate stall characteristics. Lastly, the dihedral needs to be determined. The dihedral affects the stability of the Greenliner, since it has a restoring effect when banked. On top of that, the effect of the dihedral is dependent on the vertical position of the main wing. The low wing configuration, in combination with an unswept wing, results in a dihedral of 5 to 7 degrees (upwards), according to Table 5.3. The average of these values is taken, which sets the aircraft dihedral at 6 degrees.

5.4.5. Wing Structural Arrangement

The outputs of designing the structural arrangement of the wing are the locations of the spars and ribs in terms of chord- and spanwise locations. This structural arrangement requires as input the location of the moving surfaces and all the subsystems attached to the wing. With these known, the following steps can be taken to establish the structural arrangement [79]:

---

[2]Retrieved from: `http://aviationweek.com/blog/winglets-all-shapes-sizes-and-uses` on 02-07-2018

Wing Position	Low	Mid	High
Unswept (civil)	5 to 7	2 to 4	0 to 2
Subsonic swept wing	3 to 7	-2 to 2	-5 to -2
Supersonic swept wing	0 to 5	-5 to 0	-5 to 0

Table 5.3: Dihedral preliminary design guidelines [77]

1. On the lifting surface, identify the moving surfaces, such as flaps and ailerons

2. Position the rear and front spar leaving enough room for hinges on the moving surfaces

3. Determine potential cutouts in the wing for items such as doors or emergency exits and add ribs at these locations

4. Determine the location of the landing gear and add local ribs to support the attachment

5. Locate any other major masses, such as engines or fuel tanks which require ribs for attachment

6. Investigate whether items can be relocated to achieve structural synergism, meaning for instance ribs can be overlapped to attach multiple items

7. Fill in the empty spaces with the ribs according to standard spacing of 24 inches

This results in the final wing planform with the moving surfaces, cutouts and the spars and ribs. The only step left at that point is the material selection. For this selection three materials are considered; aluminium, titanium, and composites. The desired characteristics of the wing are a high strength and some flexibility. For this it is not worth it to pay the extra price for titanium or composites and their high stiffness. Because of this, the wing structure will be made out of aluminium, specifically Al 2024-T3.

5.4.6. Sustainability
Intrinsically, when comparing the wings of the Greenliner to those of conventional aircraft, they behave alike in terms of sustainability, due to the similarity in material usage. There are, however, steps to be taken to ensure an improved sustainability.

In terms of development, aluminium is easy and relatively cheap to manufacture. Also, since aluminium is so recyclable, the required aluminium production can all be from recycled aluminium, lowering the environmental impact. Additionally, to improve the production process automated production is strived towards. For the wing production, this presents a challenge. This is due to the internal structure, which consists of hollow cells, making the insides difficult to reach. At the Fraunhofer Institute for Machine Tools and Forming Technology IWU in Chemnitz, an automated robot arm has been developed for the assembly of, among other parts, the wing [3]. Making use of these machines will improve the production rate and costs.

During operations aluminium will have reasonable maintenance costs, because it is naturally resistant to corrosion. Also, the parts are closely monitored and separated, and it will be easier to simply replace a small broken part instead of having to replace a bigger portion of the structure, lowering maintenance times and costs. For the environmental aspect, the airfoil has in part been selected in such a way to fly with the lowest overall drag, lowering the fuel consumption.

And finally, after the lifetime of the aircraft, the parts that can not be reused can be completely recycled. It should be noted that reusing parts will be facilitated as much as possible since reusing a part will be more efficient than recycling it. Furthermore, because the parts are closely monitored and separated, the lifetime of the wing and thus aircraft will be maximised.

5.5. Propulsion
From the Midterm Report [21] it was concluded that the Greenliner should make use of distributed electric propulsion, since the benefits in propulsive efficiency are significant. However, the layout was not yet mentioned, nor how many propellers or motors are used to achieve that effect. This will finally be presented in the following section.
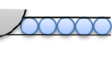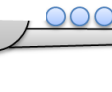
---

[3]Retrieved from `https://www.fraunhofer.de/en/press/research-news/2014/may/automated-assembly-of-aircraft-wings.html`[Accessed 20 June 2018]

First the type and layout of the selected Distributed Electric Propulsion is presented, along with the main working principles. This is then followed by the design and analysis of the Distributed Electric Propulsion, with the goal to analyse, size and integrate its components.

5.5.1. Choosing Type of Distributed Electric Propulsion

While the benefits of DEP are easy to understand in terms of theory, the actual research into implementing this technology for a full sized passenger plane is still quite young. The main reason is that such a system is not easily integrated into an airplane. Especially with current fuel based technology, the propulsion system would become prohibitively expensive, complex and heavy. Still, given that there is an ever increasing need to reduce the carbon footprint of air travel, a lot of research effort has been dedicated to this in the last decade. Additionally, an increased propulsive efficiency increases the chances that an airplane flying with an alternative, green energy source is actually possible. The ever increasing performance of electric components has already allowed the first breakthroughs, such as the Lilium [52].

As a kickoff to their research, in 2010 ICAS published an article discussing different DEP concepts [34]. Several other articles have been published where the different concepts are assessed on their own. However, in 2012, ICAS presented a feasibility trade-off considering several DEP concepts [27]. The concepts considered in their trade-off are shown illustratively in Figure 5.7a [27].

Concept	Description and Abbreviation
	Aft-mounted fans covering the upper part of a cylindrical fuselage (REVOLVE)
	BWB with embedded fans on top of the lifting body trailing edge (BWB)
	Tube and wing configuration with fans integrated within a split-wing (SPLIT)
	Tube and wing concept with fans mounted on the upper wing side (WING)
	Cylindrical fuselage with circumferential fan at the aft section (PROPFUS)
	Cross-flow fan embedded into the trailing edge of the wing (CROSS)

(a) Concepts considered in feasibility study of ICAS
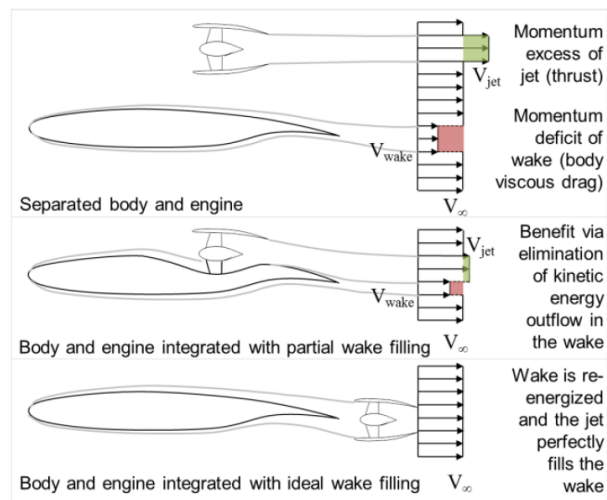
(b) Wake filling explanation from ICAS study

Figure 5.7: Propulsion concepts and wake filling principle

The 2012 article from ICAS first looks into the propulsive efficiency benefits each of the concepts could provide, and then combines this trade-off with an extensive list of criteria that include factors such as noise, maintenance and weight. From this trade-off it can be concluded that while installing the propellers on top of the wings adds a benefit to the propulsive efficiency, installing instead the propellers at the tail to form a propulsive fuselage is significantly more beneficial. Even with adding propellers to only one side of the fuselage (like on the top), the benefits still outperform the benefit of adding propellers to the wings.

The main reason for this added benefit in efficiency is again explained in the paper. While adding the motors on top of the wings improves the lift performance of the wings (by sucking air over the airfoil) and then indirectly also improves the propulsive efficiency, the propulsive fuselage focuses directly on the propulsive efficiency by **actively minimising the drag produced by the fuselage** (the largest drag component of the airplane). This is done by accelerating the flow inside the boundary layer, through so called boundary layer ingestion, and decrease thus the wake left behind by a

body flying through the air. See Figure 5.7b as an illustration on how to minimise the wake of an body through the air. The first case would indeed increase the lift performance. However, it performs badly in the reducing the wake left behind. The closer the propulsion unit is to the surface, the more the wake is reduced, with the best results achieved when the propulsion unit is added right where without it the biggest amount of wake deformation would occur.

Another reason why boundary layer ingestion is so beneficial to the propulsive efficiency is because **the air flow is reduced in velocity when close to the surface**. When taking a look at the propulsive efficiency equation Equation 5.19, one can observe why this is the case: For typical configurations, where the propulsion unit lies outside of the boundary layer formed by the body flying through the air, one can approximate the input velocity V_1 as $V_1 = V_\infty$. This implies that in order to improve propulsive efficiency, the only thing one can do is increase the velocity difference $V_2 - V_\infty$.

$$\eta_p = \frac{P_a}{P_s} = \frac{T V_\infty}{P_s} = \frac{V_\infty}{V_1 + \frac{(V_2 - V_1)}{2}} \approx \frac{V_\infty}{V_\infty + \frac{(V_2 - V_\infty)}{2}} \tag{5.19}$$

In the case however that one does install the propulsion unit in the boundary layer in order to make use of boundary layer ingestion, V_1 is no longer equal to V_∞, but, thanks to the surface slowing down the flow, smaller (So $V_1 < V_\infty$)! This flow deceleration, when checking Equation 5.19, acts as a second variable that affects the propulsive efficiency and is actually beneficial the slower the input velocity V_1.

Additionally, with the installation of a propulsive fuselage, the structure of the wings, already extremely aerodynamic, can now be fully optimised for lifting purposes only, while the loads of the propulsion system is now taken by the fuselage, which can offer a much larger moment of inertia in order to counteract the loads.

Given that the trade-off applied by ICAS conforms extremely well with the design goals of the Greenliner and its requirements, it was decided to follow the conclusions of ICAS's paper and install a propulsive fuselage to the Greenliner as well.

5.5.2. Analysis and Design of Propulsive Fuselage

The major design consideration now to investigate is how many propellers should be added in order to form the propulsive fuselage. The original idea as explained in ICAS's paper considers only one big fan around the fuselage (see PROPFUS in Figure 5.7a), but, as mentioned there as well, this causes the design to suffer from a single point of failure.

For safety reasons at least two propellers have to be installed, but the number of propellers used will directly impact the propulsive efficiency. The other DEP concepts that performed similarly to the propulsive fuselage (see REVOLVE and BWB in Figure 5.7a), did still have a very significant propulsive efficiency, yet were able to offer more redundancy and outperformed the propulsive fuselage with one big fan in some other criteria as well, such as maintenance.

Given that the propeller assembly, in order to create a propulsive fuselage, has a large impact on the propulsive efficiency, in the analysis to follow a series of configurations ranging from 1-50 propellers is considered in order to determine the optimum number of propellers. All of these configurations space the number of propellers evenly along the entire fuselage circumference and are sized for boundary layer ingestion.

Boundary Layer

Given that the propulsive fuselage is sized based on the boundary layer produced by the Greenliner, the propulsive fuselage analysis starts here with the goal to find the boundary layer thickness and average speed. The goal is to size the propellers to the thickness of the boundary layer produced by the fuselage in order to maximise boundary layer ingestion.

Unfortunately, boundary layer aerodynamics is quite complex. While laminar flow is still very predictable, the turbulent boundary layer is far harder to analyse, or as J. Anderson puts it in [7] when introducing the turbulent boundary layer theory: *"[...] no pure theory of turbulent flow exists."* Thus an approach has been taken that simplifies the scenario of the airflow flowing over the fuselage.

As a start, the assumption is made that **the flow over the fuselage is similar to the flow over a flat plate**, given the large length of the straight fuselage.

Additionally, **the air is assumed to be incompressible**, even when the cruise Mach speed of 0.4 exceeds the 0.3 Mach limit where one usually drops the assumption of incompressibility. However, when consulting Anderson [7] for the error produced when still considering compressible flow at 0.4 Mach, it ranges from 5% at the 0.3 Mach limit to 10% at the 0.4 Mach cruise speed. Given the complex nature of the boundary layer and the time constraint, it was decided that the error is acceptable. The assumption of incompressibility greatly simplifies the required equations to describe the boundary layer and allows for an initial sizing method for the propellers.

Applying these assumptions, according to Anderson [7] one can describe the thickness of the boundary layer as a function of the Reynolds number and the distance the flow has travelled over the flat plate. The equations for the laminar and turbulent cases are given by Equation 5.20 and Equation 5.21 respectively.

$$\text{laminar flow: } \delta = \frac{5.0x}{\sqrt{Re_x}} \tag{5.20}$$

$$\text{turbulent flow: } \delta = \frac{0.37x}{Re_x^{1/5}} \tag{5.21}$$

Given the Reynolds number and the length of the fuselage one can thus determine the thickness of the boundary layer. Figure 5.8a shows the boundary layer thicknesses produced by the fuselage length of the Greenliner during cruise conditions. The turbulent flow thickness is much more significant than the laminar flow.

(a) Boundary layer thickness of laminar and turbulent flow

(b) Boundary layer velocity profile
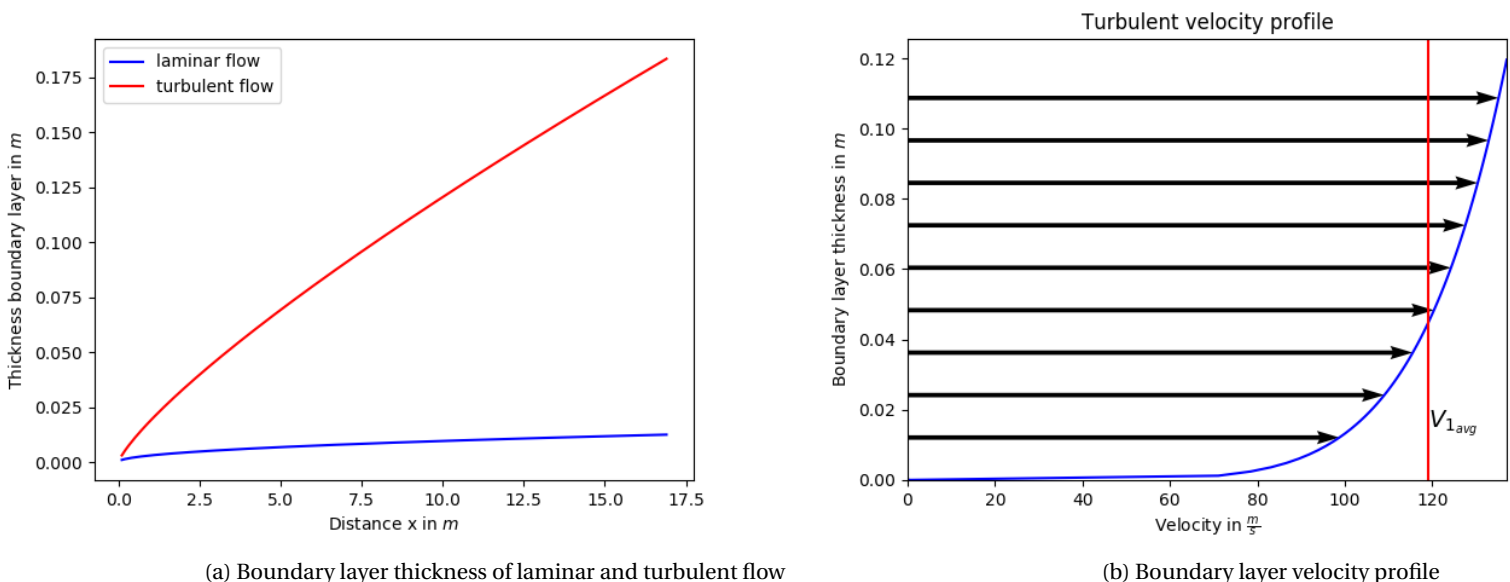
Figure 5.8: Boundary layer thickness and velocity overview

Additionally, given the large Reynolds number of the flow at the end of the fuselage, the nature of the flow is turbulent. **Thus, the propellers of the Greenliner are sized so that they match the thickness of the turbulent boundary layer**.

The next step is to find the speed reduction of the airflow inside the boundary layer, since, as mentioned in subsection 5.5.1, the speed reduction of the stream has a direct impact on the propulsive efficiency. Unfortunately it is already here where the analysis of the turbulent layer becomes much more complicated. This is due to the chaotic nature of the flow inside this type of boundary layer, where one can experience phenomena such as eddies and reverse flows.

Given the complexity of most methods, it was decided to apply the simplest one found [4]: an empirical relation that states that the velocity of the boundary layer flowing parallel to the surface is dependent on the distance from the fuselage skin through Equation 5.22.

---

[4]`http://www.cns.gatech.edu/PHYS-4421/lautrup/7.6/boundaries.pdf`, last retrieved on 28th June 2018
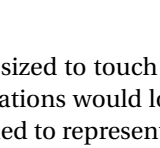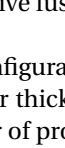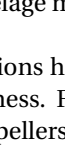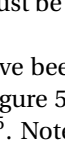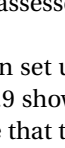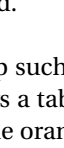
Number of unit circles	Enclosing circle radius	Density	Optimality	Diagram
1	1	1.0000	Trivially optimal.	
2	2	0.5000	Trivially optimal.	
3	$1 + \frac{2}{\sqrt{3}} \approx 2.154...$	0.6466...	Trivially optimal.	
4	$1 + \sqrt{2} \approx 2.414...$	0.6864...	Trivially optimal.	
5	$1 + \sqrt{2\left(1 + \frac{1}{\sqrt{5}}\right)} \approx 2.701...$	0.6854...	Trivially optimal. Also proved optimal by Graham (1968)[2]	
6	3	0.6667...	Trivially optimal. Also proved optimal by Graham (1968)[2]	

Figure 5.9: Circle packing for propeller fuselage configurations

$$\frac{V_{BL}}{V_\infty} = \left(\frac{y}{\delta}\right)^{\frac{1}{7}} \tag{5.22}$$

Thus the turbulent boundary layer velocity profile is created. Figure 5.8b shows this profile for cruise conditions, with the free stream velocity at the top, and as one moves towards the fuselage, the velocity is reduced more and more. From this profile the average boundary layer velocity can be calculated, shown as the red vertical line in Figure 5.8b. This average velocity will be considered as the input velocity for the propellers, such that $V_{BL_{avg}} = V_1$.

With these two values, the thickness of the turbulent boundary layer and its average velocity, the propulsion unit can be sized for boundary layer ingestion.

Geometry Setup of Propulsive Fuselage and First Predictions
As mentioned in subsection 5.5.1, the use of one large propeller to form the propulsive fuselage is not possible, since it suffers from the fact that it would remain a single point of failure. Thus other possible configurations to form the propulsive fuselage must be assessed.

The configurations have been set up such that the propellers used are always sized to touch the limit of the boundary layer thickness. Figure 5.9 shows a table of how the first series of configurations would look like with increasing number of propellers [5]. Note that the orange circle in the middle has been added to represent the fuselage. This area remains as an ineffective region for propulsion.

In the case of one propeller, the radius of the propeller matches the radius of the fuselage plus the thickness of the boundary layer, or $R_{pn} = R_{p1} = R_f + \delta_{BL}$. As one increases the number of propellers, the radius of the propeller reduces such that $R_{pn} < R_{p1}$. This causes a loss in the total effective area A_{ten} (the area between the boundary layer limit and the fuselage skin and covered by the propeller). Since the thrust equation of a thrust unit can be described through Equation 5.23, and from subsection 5.5.1 it follows that a smaller velocity difference improves the propulsive efficiency, the total effective area is already a good indicator for the propulsive efficiency, since the larger the total effective area of the propellers, the larger the mass flow and the smaller the required flow acceleration.

---

[5]Wikipedia article on circle packing: `https://en.wikipedia.org/wiki/Circle_packing_in_a_circle`, last retrieved on 26th June 2018.

$$T = \dot{m}(V_2 - V_1) \tag{5.23}$$

As the number of propellers increases from 2 onward, the total effective area increases again. From this one can already predict that the efficiency would improve as one increases the number of propellers.

Based on the given geometry for the configurations, Equation 5.24 can be derived, which describes the radius of 1 propeller per configuration. For verification purposes, the number of propellers per configuration can be put in, and indeed the same radius fractions are found as given in Figure 5.9.

$$R_{pn} = R_{p1} \frac{1}{1 + \left(\frac{1}{\cos\left(\pi(\frac{1}{2} - \frac{1}{n}) \right)} \right)} \tag{5.24}$$

Equation 5.24 can be used now to create a plot like shown in Figure 5.10a.

(a) Geometry values for different configurations

(b) Positioning of propellers on tail depending on number of propellers used.
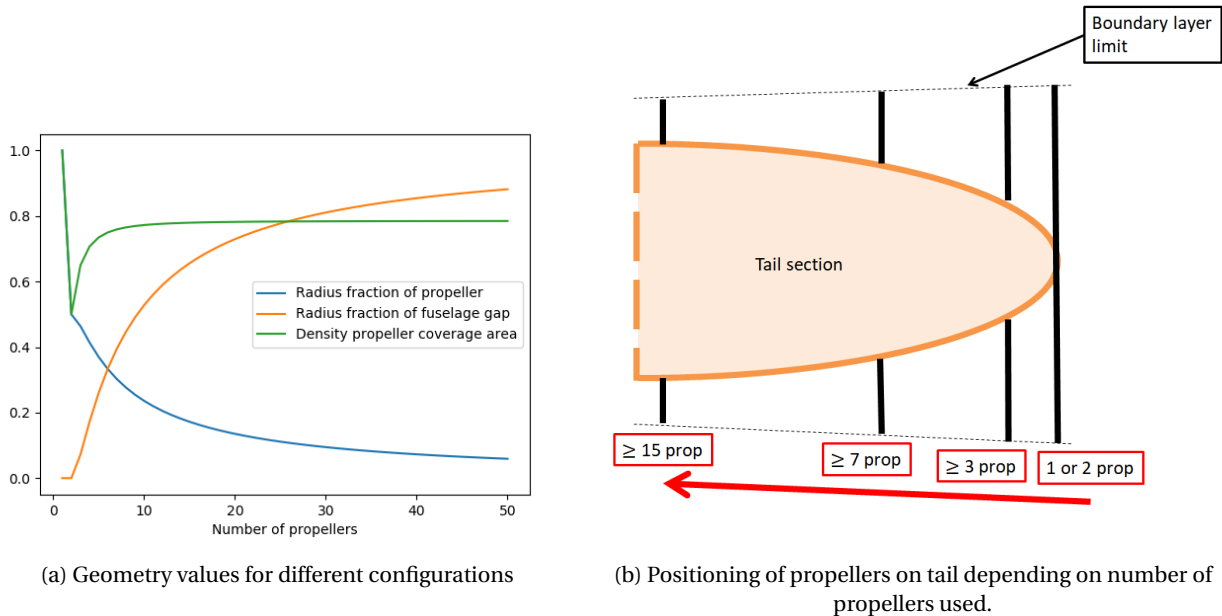
Figure 5.10: Geometry setup

The blue line in Figure 5.10a shows how the radius of the propellers decreases as the number of propellers per configurations increases. Especially for the first few configurations, the radius decreases drastically, and only later the radius starts to slowly level out.

The effect is that the space left out in the middle, by assembling the propellers around the fuselage, keeps increasing, as shown by the orange line in Figure 5.10a. This is a good effect, because after all, the area inside of the fuselage cannot be used.

In addition, the left out area can be used to indicate where on the tail the propellers have to be installed. This is shown in the top view of the tail section in Figure 5.10b. When installing only 1 or 2 propellers, if sized for the boundary layer, they have to be installed as far back as possible.
However, as the number of installed propellers increases, one can actually move the longitudinal position of the configuration forward, as shown illustratively in Figure 5.10b. This would offer the benefit of moving the center of gravity of the airplane forward and additionally offers the larger section of the tail, which can resist higher structural loads.

At this stage another important setup for the calculations must be mentioned: When assembling the configurations as shown in Figure 5.10a, the fuselage radius is kept constant; or in other words, the longitudinal position of the configurations has been fixed to the front part of the tail section, where it meets the fuselage.

The reason is that, according to the law of mass conservation (valid for compressible and incompressible flow), the airflow coming from the fuselage would slow down again as it passes over the tail section. In other words, **the narrowing shape of the tail section has an effect on the performance of the propulsion unit**. For the same reasons as to use the boundary layer to improve propulsive efficiency, the deceleration of the flow along the tail cone would improve even more the efficiency.

However, **in order to compare the performance of each propulsion unit under equal conditions, they have all been fixed to the same location at the front part of the tail section**. This allows the analysis to be completed without relying on the final shape of the tail cone and the need to assess the aerodynamic effects caused by its narrowing shape. Only for the detailed design for post DSE activities, to assess exactly the output performance of the propulsive fuselage, one can add a correction factor that takes into account the flow at the tail section.

Finally, only if one would size the fuselage radius for the space in the middle of the each configuration (this won't happen, as explained later on), one can calculate the area covered by the propellers in comparison to the area that is covered if only one propeller was used. The area density can be calculated through Equation 5.25.

$$\frac{A_{pn}}{A_{p1}} = \frac{nR_{pn}^2}{R_{p1}^2 - R_{gap}^2} = \frac{nR_{pn}^2}{R_{p1}^2 - (R_{p1} - 2R_{pn})^2} \tag{5.25}$$

The result is shown as the green line in Figure 5.10a, where one can observe that moving from 1 to 2 propellers immediately halves the area density fraction. As the number of propellers increases though, the area density is recovered until it reaches an asymptotic (constant) value just below 80%. From this, given that the total area covered by all propellers is an indicator for the propulsive efficiency, **it follows that trend for the efficiency for the different configurations will mimic the trend given by the green line shown in Figure 5.10a.**

The only difference would be at larger numbers of propellers. The space inside the circles would keep increasing, which in reality, as explained before through Figure 5.10b, means that the propeller configurations move forward towards the front part of the tail section.

At one point however, the largest part of the tail is reached, where the radius of the tail is equal to the radius of the fuselage. At that point, the space inside the circles stops increasing (the fuselage has a fixed radius), and the actual area covered by the propellers decreases again. Thus, **at a certain number of propellers the propulsive efficiency trends downwards again**, in stead of remaining as an asymptotic constant like the green line in Figure 5.10a.

With this one can confidently move to the actual analysis of the propulsive efficiency of each configuration with already some prediction of what the trend for propulsive efficiency looks like.

Propulsive efficiency of Propulsive Fuselage
With the configurations laid out as explained in the 2nd section of subsection 5.5.2, analysis for the propulsive efficiency of each of the configurations can begin.

For this, use is made of the actuator disk theory (ADT), used across several references and nicely summarised by [6]. The method replaces the propeller by a virtual disk that applies momentum to the air. See Figure 5.11a showing this virtual disk. Note that u_1 and u_2 in the figure are the same as V_1 and V_2 used in this report.

This method ignores the propeller shape itself and so allows for calculating the ideal performance of a single propeller. The actual design of the propeller will come later, where more detail will be added, with the goal to achieve the ideal performance that is found here.

The sizing is applied to each propeller used for each configuration, and the effect is later superimposed to represent the total performance of the configuration. This will allow completion of the initial sizing of the propulsion unit.

The ADT method states that the propulsive efficiency can be defined through Equation 5.19, as already shown in subsection 5.5.1.

---

[6]retrieved from `http://web.mit.edu/16.unified/www/FALL/thermodynamics/notes/node86.html` accessed 2 July 2018

(a) Actuator Disk used for initial propeller sizing

(b) Dimensions and areas for cross section of propeller configuration

Figure 5.11: Propulsion theory setup

In addition the thrust is defined through Equation 5.26. Note how the thrust consists of two parts: The mass flow of the average velocity $(V_2 + V_1)/2$, which is fixed by the intake area of the propeller, and then the acceleration of the flow, represented by the difference in velocity $V_2 - V_1$. In short, for constant thrust, the smaller the propeller, the larger the required air velocity acceleration. Recall from the discussion presented in subsection 5.5.1 that the higher the acceleration, the worse the propulsive efficiency.

$$T = \dot{m}(V_2 - V_1) = \rho A\left(\frac{V_2^2 - V_1^2}{2}\right) \tag{5.26}$$

Equation 5.26 can be rearranged as an expression for (input) shaft power P_s as shown in Equation 5.27.

$$P_s = T\left(\frac{V_2 + V_1}{2}\right) = \rho A\left(\frac{V_2^2 - V_1^2}{2}\right)\left(\frac{V_2 + V_1}{2}\right) \tag{5.27}$$

If now one solves for V_2, the mass flow of the propellers can be found, or, using Equation 5.19, the propulsive efficiency of the propeller. In this case, one would solve V_2 graphically by plotting the right and left sides of Equation 5.27 on a power vs. velocity graph.

However the shaft power P_s still remains an unknown! The only known power variable is the power available P_a, taken from the mission profile, as described in section 4.2.

Thus an iteration method is applied in order to find a solution for both the shaft power P_s and the exhaust velocity V_2. The iteration method applied here is shown as pseudo code in Figure 5.12, and explained below.

One starts with an estimate on efficiency, which with Equation 5.27 is corrected until it meets the condition that $P_s \eta_p = P_a$. The process ends with the correct values for both P_s and V_2. With P_s now known, the power can be plotted against velocity, as mentioned before, and shown in Figure 5.13a. Note that the graph changes depending on the current state of the airplane and the atmosphere it is flying through. The red line on Figure 5.13a shows the intersections of each of the power curves for the individual propeller for each configuration, from which the given exhaust velocity can be read. (Read the red line from top to bottom).

As predicted in the 2nd section of subsection 5.5.2, the setup of 2 propellers causes a huge jump in the required exhaust velocity, which would also indicate the lowest propulsive efficiency. In fact the jump in exhaust velocity is so high, that it passes the green line shown in Figure 5.13a, which indicates the speed of sound. Having passed this limit, the 2 propellers would be extremely heavily loaded by the shock waves produced.

Only by increasing the number of propellers further, the exhaust velocity is quickly reduced, approaching the ideal case of using only 1 propeller. At a certain point though, the red line turns around again, increasing the required ex-

```
#------------------
#INITIAL ESTIMATES:
#------------------
P_s = P_a # start assuming that p_eff = 1.0

calculate_eff():
        #Find V2 by applying power equation
        #calculate new p_eff for this exhaust velocity.
        P_s * p_eff = P_aE #calculate what P_a would be for given P_s
        Delta_P = P_a - P_aE #check difference in power available of what is required
and what is currently given.
|
#----------
#ITERATION:
#----------
if Delta_P >= 0.1:
        P_s = P_s + Delta_P #apply correction to input power
        calculate_eff() #repeat process above.
```

Figure 5.12: Iteration to find actual shaft power P_s and V_2

haust velocity. This is the point that was predicted in the 2nd section of subsection 5.5.2, where the position of the propellers has gone beyond the limit the fuselage radius can offer.

As mentioned before, the plot shown in Figure 5.13a shifts depending on the input parameters. Especially important to note is that if only the power requirement would increase, the red line shown in Figure 5.13a would shift to the right, to the point where all of the propeller configurations would have a supersonic exhaust velocity and be extremely loaded. At that point one would have to e.g. increase the fuselage radius in order to increase the circular area bound by the boundary layer limit.

In order to complete the efficiency calculations, the ineffective area of the propellers that is hid by the fuselage area needs to be accounted for. For this, the geometric assembly from the 2nd section of subsection 5.5.2 is taken as reference in order to calculate which areas are effective for propulsion. Figure 5.11b shows a more detailed layout of the relevant dimensions.

The dimensions of the fuselage are constant, while the boundary layer limit, to which the propellers are sized, is dependent on the current state of the airplane. The radius of the propeller, as discussed in the 2nd section of subsection 5.5.2, is dependent on the number of propellers that are to be fitted around the fuselage, but always touches the boundary layer limit. That is why only for a low enough number of propellers, there is actually a space of the propellers that crosses into the area covered by the fuselage radius; the ineffective area. For a number large enough though, the propellers will become so small that they do not cross anymore the fuselage area. In between these two cases, as predicted in the 2nd section of subsection 5.5.2, one will achieve a maximum of the effective area of one propeller. This will at the same time result in the maximum total effective area, since the total effective area is given as $A_{ten} = A_{en}n$.

Thus for low enough number of propellers, one needs to subtract the cross area A_{cn}. Reference [28] offers Equation 5.28 in order to calculate this area, for which use is made of the distance between the center of the propeller and the center of the fuselage, d_{pf}.

$$A_{cn} = R_f^2 \arccos \frac{d_{pf}^2 + R_f^2 - R_{pn}^2}{2d_{pf}R_f} + R_{pn}^2 \arccos \frac{d_{pf}^2 + R_{pn}^2 - R_f^2}{2d_{pf}R_{pn}}$$
$$-\frac{1}{2}\sqrt{(-d_{pf} + R_f + R_{pn})(d_{pf} + R_f - R_{pn})(d_{pf} - R_f + R_{pn})(d_{pf} + R_f + R_{pn})}$$

(5.28)

d_{pf} itself can be expressed as $R_{p1} - R_{pn}$. With this, the effective area of each propeller A_{en} and the total effective area for each configuration A_{ten} can finally be calculated. Therefore one can finally calculate the propulsive efficiency of each configuration.

The result is shown in Figure 5.13b. Note that again the plot depends on the airplane's state and the atmosphere it is flying through.

(a) Power curves to calculate exhaust velocity

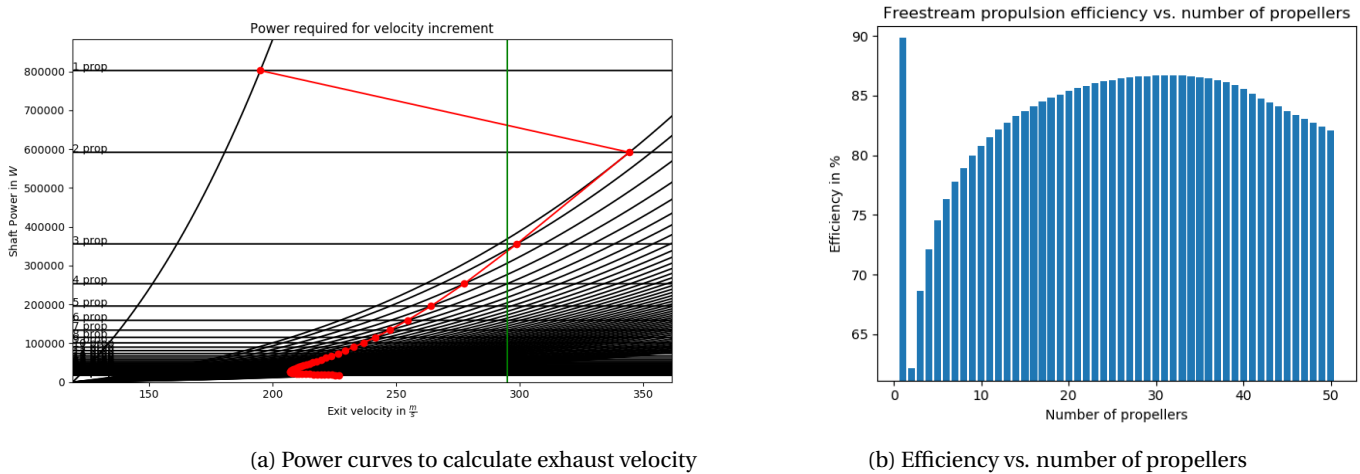(b) Efficiency vs. number of propellers

Figure 5.13: Power and efficiency plots

From this, it can be seen that the single propeller configuration still remains as the top performer. As predicted in the 2nd section of subsection 5.5.2, when moving to 2 propellers, a huge amount of efficiency has been lost. Already when installing a 3rd propeller, the trend reverses. One can keep adding propellers until one has almost recovered all of the efficiency!

In this case the optimum number lies at around 30 propellers, although choosing ±5 has only a minimal effect, as the trend flattens a lot around that area. Increasing even further the number of propellers however, as predicted by the 2nd section of subsection 5.5.2, causes the efficiencies to go down again.

With this, the performance of each of the configurations initially presented at the 2nd section of subsection 5.5.2 has been assessed. Additionally, information has been gained on the shaft power required for each configuration as well as the geometry properties of the propellers for each configuration. In other words, the sizing method of the actuator disk is complete and it is time to convert it into a propeller. The actual sizing of this propeller is explained in the upcoming section.

Propeller Sizing for Propulsive Fuselage

At this stage the basic sizing of the configurations is complete. In order to continue the sizing of the propellers a constraint is added to the tip velocity. The main reason behind this is that the tip of a propeller blade travels the fastest, and if the rpm's are too high, such that the tip velocity exceeds Mach 1, shock waves will be produced. This causes large amount of vibrations as well as a lot of noise. Therefore manufacturers will always design the propellers in such a way that the tip does not travel that fast. Reference designed the propellers for low noise by using a tip velocity constraint of 0.5 Mach. Given that a major design constraint set by ICAO is noise, one can directly optimise the propellers for low noise and use 0.5 Mach as well as a tip velocity constraint [7].

Given the tip velocity constraint V_{tip}, and the known radius of the propellers from the 3rd section of subsection 5.5.2, the rpm of the propellers can be calculated. Torenbeek [92] shows how the velocity components on a blade section (in this case the tip) can be broken down, as similarly shown in Figure 5.14. The velocity vectors can therefore be related through Equation 5.29.

$$V_{tip} = \sqrt{V_{\Omega,tip}^2 + V_1^2} \tag{5.29}$$

Then, solving for $V_{\Omega,tip}$, one can find the rotational velocity of the propellers through:

$$\Omega = \frac{V_{\Omega,tip}}{R_{pn}} = \frac{\text{rpm}\,2\pi}{60} \tag{5.30}$$

---

[7]Barnard Microsystems on propellers: `Retrievedfromhttp://www.barnardmicrosystems.com/UAV/engines/propellers.html`, on 29th June 2018
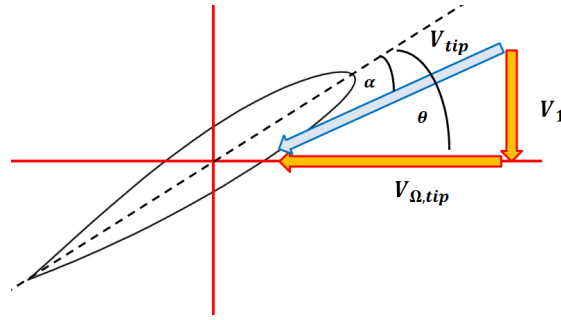
Figure 5.14: Velocity vectors on tip of propeller

Given the rotational velocity of the propellers, and the shaft power, the applied torque on the propeller can be found through $P_s = Q_s \Omega$.

Additionally, knowing all the velocity components, one can also continuously compute the required pitch angle for the blades using trigonometry; such that $\theta = \arctan(\frac{V_1}{V\Omega, tip})$.

As Torenbeek [92] mentions, **the ability to continuously adapt the blades allows one to maintain top propulsive efficiency** during the whole mission of the Greenliner. When reflecting back on the process done so far this makes sense, because the efficiency calculations directly relate to the pitch angle.

At this stage, the initial sizing of the propellers could be completed, as the manufacturers usually only need the required diameter and the rpm's in order to offer an adequate propeller. However, other parameters will aid in a more detailed design, since they will give an indication of the propeller loading. Once again, Torenbeek [92] presents the coefficients that would add this detail. These are:

- The advance ratio, expressed as $J = \frac{V_\infty}{f_\Omega D_{pn}}$

- The power coefficient, expressed as $C_P = \frac{P_s}{\rho f_\Omega^3 D_{pn}^5}$

- The thrust coefficient, expressed as $C_T = \frac{T}{\rho f_\Omega^2 D_{pn}^4}$

The combination of all of these parameters not only allows for selection of a propeller given by a manufacturer, but even design of a propeller that is optimised for the propulsion system used by the Greenliner.

Nevertheless, the actual design of the propeller is beyond the scope of conceptual design and will have to be left out for future development. The values calculated here will be used as reference for the more detailed design.

Components and Mass Analysis for Propulsive Fuselage
In order to complete the selection of the optimal configuration of propellers, the mass components that make up the propulsion unit need to be accounted for. In the following section the preliminary mass analysis of the propulsion subsystem is presented. The components that are included in this mass analysis are:

- Propellers
- Electric Motors
- Shaft connection with gear ratio
- Rest

The rest mass will be added with a constant safety factor to the total of the assembly of the first components to account for additional mass components such as motor installation or the mass of actuators. The safety factor here was chosen to be equal to 2, given that the biggest mass components are already taken into account here, and doubling the total mass should encompass plenty to fit the additional components. Doing this one arrives for the Greenliner at a similar mass fraction of the propulsion unit to the operative empty weight as for the reference aircraft, which lies at around 10%.

www.magnax.com		High-speed machines		
	AXF185	AXF225	AXF275	AXF350
max. rpm	12000	10000	8000	4000
Motor diameter (mm)	185	225	275	350
Motor length (mm)	75	86	86	86
Dry mass (kg)	8	14	26,5	42
Cooling	water	water	water	water
Peak power (kW)	100	170	300	480
Nominal power @ max rpm(kW)	50	85	150	240
Peak torque* (Nm)	100	250	500	1000
Nominal Torque* (Nm)	50	133	267	500
Efficiency at nominal (%)	95	95	94,8	94,5
max. efficiency (%)	98	98	98	98
Peak Power Density (kW/kg)	12,5	12,1	11,3	11,4
Nominal power density (kW/kg)	6,3	6,1	5,7	5,7
Peak Torque density (Nm/kg)	12,5	17,9	18,9	23,8
Nominal Torque density (Nm/kg)	6,3	9,5	10,1	11,9
Battery Voltage (V)	400 or 750	750	750	750
Expected availability	Q2, 2019	Q3, 2019	Q1, 2019	Q2, 2019
*depending on speed				

Figure 5.15: MAGNAX motor series specifications

With regard to the mass of the propellers, Equation 5.31 offered by Roskam [78] (pg.89) is used. Note that the units for Equation 5.31 here are not written in SI units and [78] should be consulted for the meaning of the symbols.

$$W_{prop} = K_{prop} N_p N_{bl}^{0.391} \left(D_p \frac{P_{to}/N_e}{1000} \right)^{0.782} \tag{5.31}$$

The mass of the motors depends on what electric motor is chosen. As can be seen when consulting the selection of industrial electrical motors offered by WEG [8], typical motors that can provide the shaft power required by the Greenliner are as heavy as the MTOM of the airplane itself! Fortunately, there has been much development in electric motors for aerospace applications that are lightweight and powerful. Just last year, 2017, Siemens has managed to propel a small airplane with an electric motor that had an incredible power density of 5.2 kW/kg [9]. In comparison, the motors from WEG only have a power density of around 0.2 kW/kg.

Obviously, maximising the power density of the motors is of top priority for the Greenliner if it is to be successful as an airplane. While the motors from Siemens would perform well with the power and weight requirements of the Greenliner, the motors from MAGNAX[10] would still outperform those ones with a nominal power density of 6.3 kW/kg. The outstanding performance of the MAGNAX motors is thanks to a new motor assembly that makes use of axial flux instead of the typical radial flux used in motors. In addition, they have implemented an integrated cooling system with which they can maintain top efficiency. Figure 5.15 shows some specifications of the motor series, which was kindly sent by MAGNAX, who have been very supportive in providing all important information.
The motor that was chosen then for the Greenliner is the MAGNAX AXF 185, given that it has the highest power density of their motor series. A great advantage of their motors as well is that they can be stacked, which, with regard to requirement **GF-SYS-INT.3-5** [20], further improves the possibility of keeping the motor assembly flexible. The motors themselves, as can be seen from Figure 5.15, will already be available next year 2019.

Given the motor selected and having calculated the required shaft power P_s from the 3rd section of subsection 5.5.2, one can now also calculate the number of motors that are required by simply dividing the shaft power by the nominal power output of the motors and rounding that number up to the next integer. The total mass of the motors is then the number of motors used times the mass of each unit, as shown in Equation 5.32. Note the fact that the nominal power

---

[8]WEG - Electric Motor Selection: `http://ecatalog.weg.net/TEC_CAT/tech_motor_sel_web.asp?cd_produto=33&CD_CATEGORIA_PRODUTO=5&cd_mercado=000I&cd_idioma_cat=EN&cd_empresa=110`; last retrieved on 2nd July 2018
[9]Article on Siemens electric flight: `https://www.siemens.com/press/en/feature/2015/corporate/2015-03-electromotor.php?content[]=Corp`, last retrieved on 2nd July 2018
[10]MAGNAX website: `https://www.magnax.com/`, last retrieved on 2nd July 2018

is taken and not the peak power, as the latter can only be sustained for a short time before serious damage is done on the electric motor. Sizing to nominal power also ensures a higher redundancy in case one electric motor fails.

$$M_{\text{total,motor}} = \lceil \frac{P_s}{P_{\text{motor,nom}}} \rceil M_{\text{motor}} \tag{5.32}$$

The next mass component is the shaft, which has to transfer the power from the motor to the propeller. In addition, the shaft may have to go through a gear ratio, which adapts the torque and rpm output of the electric motor to the torque and rpm values the propeller needs. **The efficiency of power transmission is assumed to be 100%**, given that properly designed mechanical links are able to approach this value very closely[11].

In order to design the gears the rpm values have been chosen to define the gear ratio. The rpm values of the propellers have to be maintained adequately, as otherwise the tip velocity of the propellers may exceed the 0.5 M constraint that was set in the 4th section of subsection 5.5.2. Additionally, according to typical dc motor characteristics, the electric motor runs most efficiently around 80% of its maximum rpm [12]. The torque requirement on the other hand is much more flexible. First of all, the motors already supply a large amount of torque at 50 Nm. However, in case the torque required by the propellers is higher, then the motors can be even be stacked together to increase the torque output.

Coming back to the shaft; a method has been developed to estimate its mass. Figure 5.16a shows how the mass components have been arranged. The shaft connecting the motor and propeller have been split into two equal length units of length L_s. Where these two propellers meet, at the dotted line in Figure 5.16a, the shafts are put side by side, without actually specifying how this connection is made. In addition, the shaft lengths that run horizontally are not taken into account. This rough assembly allows to keep the sizing very flexible without the need to actually specify the parts that make up the connection between the motor and propeller.

(a) Setup for shaft mass calculations

(b) Propulsion mass budget for propulsion unit
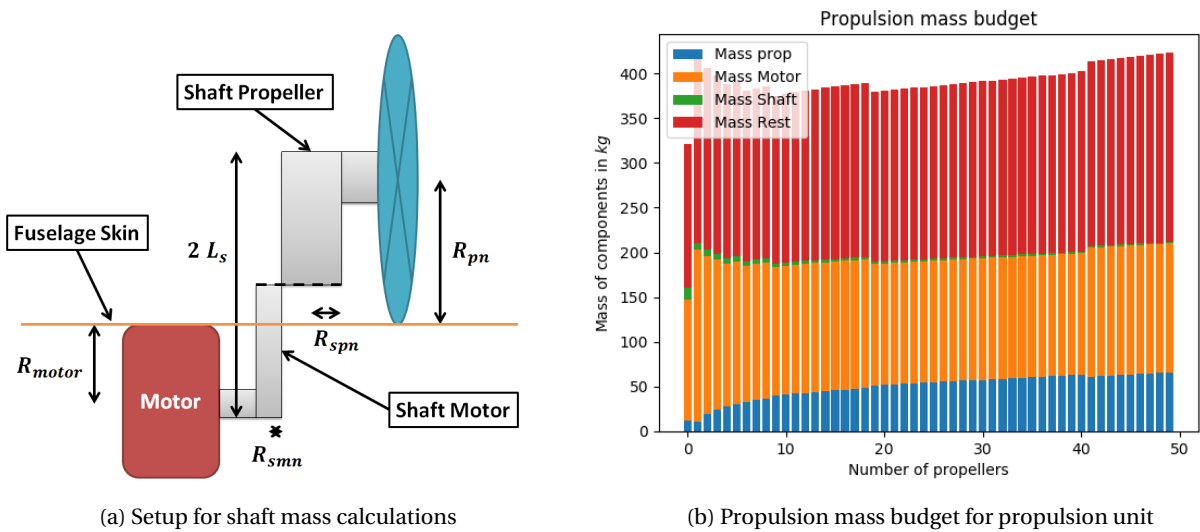
Figure 5.16: Mass calculations

The total length of the shaft has been taken as the sum of the radius of the motor R_{motor} and the propeller R_{pn}, such that the fuselage skin can run between the propeller that is installed on the outside and the motor that is installed on the inside. The main reason to put the motor on the inside is that the radius of the motor is relatively large; for high number of propellers even larger than the radius of the propellers themselves. However, how the motors are put in place is left for detailed designing. The goal here simply remains to set up a conservative estimate for the shaft mass. To add even more flexibility to the design a safety factor of 1.5 has been added to the length of the shaft such that the total shaft length now is described by Equation 5.33.

$$2L_s = 1.5(R_{\text{motor}} + R_{\text{pn}}) \tag{5.33}$$

---

[11]Quora on efficiency of mechanical links: `https://www.quora.com/Which-are-more-efficient-in-transforming-motion-gears-chains-or-belts`, last retrieved on 2nd July 2018

[12]Simple Electric Motors on DC motor calculations: `https://simplemotor.com/calculations/`, last retrieved on 2nd July 2018

The radius of the shaft is determined by the amount of torque it has to be able to resist and the maximum shear stress the material of the shaft can provide. **Assuming a circular solid shaft,** the relation between the torque and the radius of the shaft is given by Equation 5.34.

$$\tau_{\max} = \frac{Q_s}{\frac{\pi}{2}R^3} \tag{5.34}$$

The torque that the motor has to provide can be calculated from the torque value of the propellers found in the 4th section of subsection 5.5.2 and the gear ratio installed at the shaft connection to account for adequate rpm values, as described by Equation 5.35.

$$Q_{\text{smn}} = Q_{\text{spn}}\frac{\text{rpm}_{\text{pn}}}{\text{rpm}_{\text{mn}}} \tag{5.35}$$

Combining then Equation 5.34 and Equation 5.35 leads to the required shaft radius. The mass of the shaft can then be calculated by multiplying the volume of the shaft with the density of the material, as described by Equation 5.36.

$$M_s = \rho(\text{Vol}_{\text{smn}} + \text{Vol}_{\text{spn}}) = \rho\pi L_s\left(\left(\frac{2Q_{\text{spn}}\frac{\text{rpm}_{\text{pn}}}{\text{rpm}_{\text{mn}}}}{\tau_{\max}\pi}\right)^{\frac{2}{3}} + \left(\frac{2Q_{\text{spn}}}{\tau_{\max}\pi}\right)^{\frac{2}{3}}\right) \tag{5.36}$$

All the mass components can finally be put together to create the mass budget for each configuration. This is shown in Figure 5.16b. One can observe that the propeller mass does keep increasing as the number of propellers increases, although it levels out at higher numbers. The mass of the motors is highly dependent on the propulsive efficiency, where the smallest amount of motors is used for the most efficient cases. Despite this, they still make up a significant portion of the mass budget. In contrast, the mass of the shaft remains very small throughout all the configurations. The step changes in the total mass are mainly caused by the motors, where dropping one motor directly means a loss of 8 kg.

Final Selection
At this stage both the performance and the mass calculations have been completed for the preliminary sizing of the propulsion unit. The goal for optimisation is to maximise the efficiency over the propulsion mass.

When looking at Figure 5.17 it is clear that the 1 prop configuration still remains the most ideal case. As discussed in the 2nd section of subsection 5.5.2 this is not really an option, and thus the second best option, according to Figure 5.17, would be to use 20 propellers.

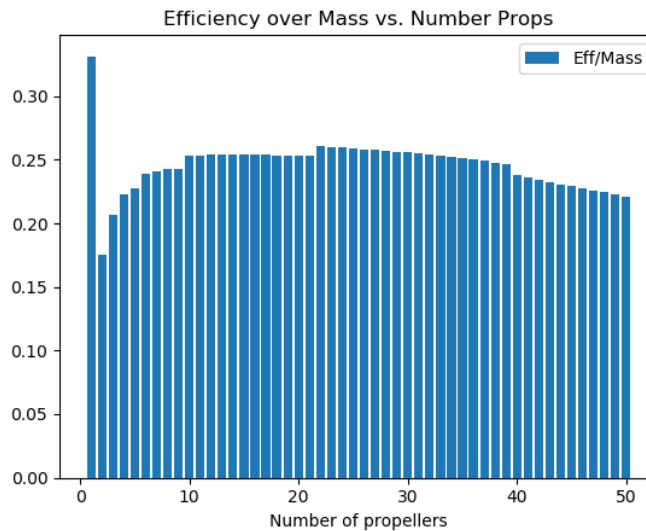Figure 5.17: Efficiency over mass plot for all configurations

A last assumption has been setup here, which is that **the number of propellers must match the number of motors** so that every propeller can be controlled independently. In this case most often the second best option shown in Figure 5.17 can also not be chosen. One instead needs to sort all the configurations based on their efficiency to mass
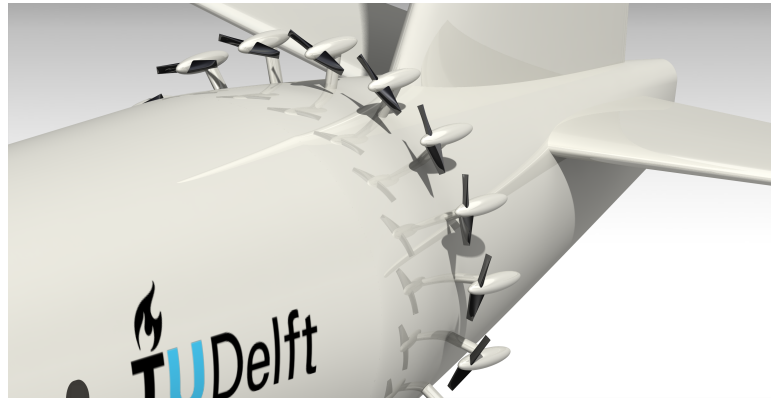
Figure 5.18: Conceptual view of the propulsive fuselage

performance and then select the configuration that has an equal amount of motors and propellers.

By applying the last assumption, the optimum design has a large dependency on the power required, since this has a direct impact on the number of motors required, as already discussed in the 5th section of subsection 5.5.2. The number of propellers, at first optimised for top efficiency, will be offset to higher or lower numbers depending on the amount of motors used. If this offset is too large the loss in performance is quite significant. Thus, in future design phases, the possibility of using one motor to propel several propellers should be assessed. More recommendations with regard to the propulsion part are presented in chapter 14.

This then finally concludes the sizing of the propulsion unit. To summarise: It has been found out that for a propulsive fuselage a high number of propellers can recover most of the propulsive efficiency that one large propeller could provide. In addition, the propellers for a propulsive fuselage were sized and a mass analysis has been completed. From this a best performing configuration can be selected, where one considers both efficiency and mass.

5.5.3. Sustainability
Figure 5.18 shows a conceptual view of propulsive fuselage based on the sizing method presented in the previous sections. The use of the multiple rotors instead of one large one means that the assembly and disassembly of the propulsion unit is easier, given that the components do not weigh as much. However the maintenance part is more intensive, since more components have to be checked before the airplane can be allowed to fly. Therefore financially the maintenance process is comparable to existing aircrafts.
Given that the propulsion system is made of so many independent units, it does add redundancy to the system. This not only means that a fault during maintenance is not as severe in consequence, but also during operation, when for example there is a sudden engine failure caused by a bird strike, the power loss is minimal compared to typical configurations. This will especially promote the financial and social aspect of sustainability.

Of course, there is the potential that during the bird strike mentioned above as an example, a propeller blade brakes off and flies into the tail section. Fortunately though, the tail section does not hold any passengers, so there is no danger of killing a passenger during this failure event. In addition, if the skin of the tail section cannot stop the blade from penetrating, all the electric motors are installed underneath. These units are essentially solid pieces of metal and are fully capable of stopping the blade, even if it means the failure of the motor itself as well.

The components themselves can be designed with a very high lifetime. The propeller blades, given that they are relatively small, can be designed to withstand well the moment of the high disk loading, while the electric motors already only have one large moving part. This reduces the frequency required to complete maintenance on the propulsion unit. Still, given that the system again is built of so many components, yet are connected quite simple, one can easily upgrade the parts in order to even further increase the lifetime of the propulsive fuselage. This will give the Greenliner a competitive edge with regard to financial and environmental sustainability.

Finally, most of the components used in the propulsion system can be designed with easily recyclable materials. The only exception is with regard to the electronics needed to control the electric motors, or any component that instead

of using alloys use for example carbon fibre components. These require a much more intensive recycling process. Thus, with regard to materials, one can achieve a high environmental sustainability performance as well.

5.6. Fuel Cell System

This section shows the design choices made for the fuel cell system in the aircraft. First, the fuel cell system layout is discussed, elaborating on the different parts and materials used. Secondly, the fuel cell system modelling and sizing are discussed, elaborating on the methods used and modelling done in order to size the fuel cell system.

5.6.1. Fuel Cell System Layout

This subsection shows the different aspects of the fuel cell system. First, the design of the different layers of the fuel cell is elaborated upon. Secondly, the design of the oxygen supply system to the fuel cell is discussed. Thirdly, the design of the hydrogen supply system is shown. Finally, an overview of the entire fuel cell system is given.

Fuel Cell Layers

A PEM fuel cell typically consists of seven layers. The middle layer consists of the proton exchange membrane enabling the chemical reaction, with on both sides a catalyst layer increasing the activity of this reaction. Next to both catalyst layers a gas diffusion layer is present, which allows diffusion of the reactants before reacting at the proton exchange membrane. Finally, the outer two layers are the flow channels through which the hydrogen and oxygen supply flows. Figure 5.19 shows this lay-out, with the middle three layers indicated as the membrane-electrode assembly (MEA).
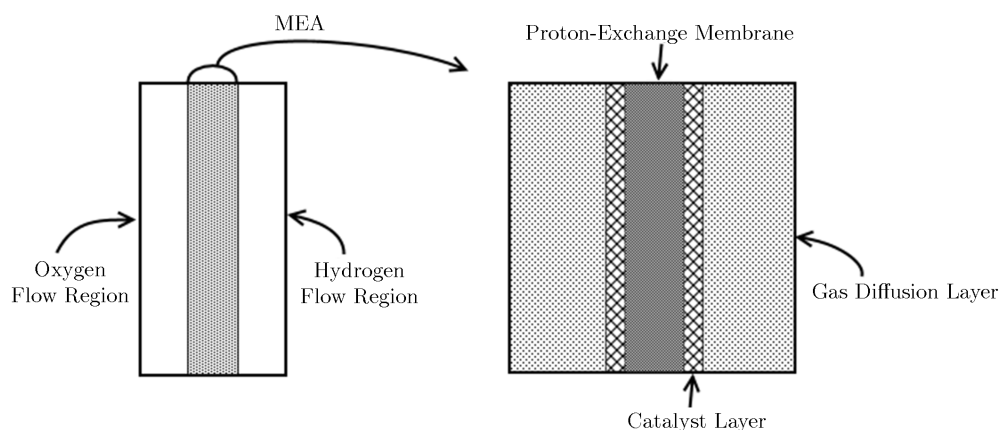
Figure 5.19: Nomenclature describing the different fuel cell layers

For the proton exchange membrane, a Nafion-117 membrane is chosen. This choice is made based on the performance of the membrane: the membrane has a high conductivity compared to competitors. Besides, the membrane is stable, durable and able to operate at the desired fuel cell operating temperature [65].

For the catalyst layers, the anode and cathode side have to be evaluated separately. For the anode catalyst layer a Pt/C (Platinum-Carbon) catalyst is chosen, due to the high catalyst activity of platinum at the anode. Although platinum is expensive, the combination with high-surface-area carbon powder increases the effectiveness of the platinum such that the costs remain limited [65]. Platinum has a lower catalyst activity at the cathode side than on the anode side. However, alternatives to platinum cathode catalysts are either not fully developed yet or bring along new complications such as accelerated degradation [65]. Therefore, the same catalyst (Pt/C) is chosen for the cathode as for the anode. More catalyst material is applied to the cathode side for an increased effectiveness.

For the gas diffusion layer a carbon fibre cloth layer is chosen. The choice is based on its high permeability and low density. Research is done on the use of metal-based gas diffusion layers, however due to challenges in the use of these, carbon fibre is still the standard gas diffusion layer. [65]

For the hydrogen and oxygen flow channels, expanded graphite is chosen as enclosing material. Next to providing a channel for the hydrogen and oxygen to flow through, graphite can function as bipolar plate when multiple fuel cells are stacked. The bipolar plate then functions as connection between individual fuel cells, while separating the required voltages between the fuel cells. Instead of using conventional graphite, expanded graphite is used due to its lower density while maintaining a high electric conductivity and a similar cost [108].

With the materials for the several layers of the fuel cell chosen, the properties in terms of volume, weight and costs could be found. The different layers are shown together with their properties in Table 5.4.

Table 5.4: Fuel cell layer properties

Layer	Material	Thickness [mm]	Weight [g/m^2]	Costs [\$/m^2]	Occurrence
Channel Walls [108]	Expanded Graphite	1 [13]	1000	50	2
Hydrogen & Oxygen Channels	-	0.762 [94]	-	-	2
Gas Diffusion Layers [65]	Carbon Fibre Cloth	0.35	132 [14]	300 [15]	2
Catalyst Anode [65]	Platinum Carbon	Negligible	0.5	21	1
Catalyst Cathode [65]	Platinum Carbon	Negligible	4	169	1
Membrane [65]	Nafion 117	0.183 [16]	360	400	1
Total		**4.407**	**2628.5**	**1290**	

Oxygen Flow System

In order to supply oxygen to the fuel cell, a system is designed to use the oxygen present in the ambient air as oxygen supply. This system is chosen over the possibility to take the oxygen either pressurised or liquefied on board. Due to the high molar mass of oxygen, taking the required oxygen for the whole mission on board would lead to an excessive fuel mass.

The oxygen intake system has to carry out several functions, depending on the state the fuel cell requires the air supply to be in. The incoming air requires a (by the fuel cell defined) level of purity, mass flow, pressure, temperature and humidity. Therefore, the air intake requires the following parts:

- An intake, ensuring a certain area of airflow is taken into the aircraft

- A filter, ensuring particles harmful to the fuel cell don't enter the system

- A fan, ensuring the mass flow of the air intake when the airspeed of the aircraft is insufficient

- A compressor, ensuring the pressure of the airflow needed

- A heating system, ensuring the temperature of the airflow needed

- A humidifier, ensuring the humidity of the airflow needed

An overview of the air intake system is shown in Figure 5.20. It shows the order of the different parts of the intake, and the directions the air gets guided to. It can be seen that not all air taken in goes to the fuel cell: a part of the air taken in goes to the cabin for environmental control, as discussed in section 5.2.

Aside from the internal air intake parts, the external layout of the intake has to be designed such that it minimises the drag induced. It was found that designing the intake in the free air stream around the aircraft leads to a significant increase in drag due to the high air velocity. Because of this, the air inlet is designed to take in air from the boundary layer of the fuselage. This air has a lower velocity due to the interaction with the fuselage, and thus generates less drag. For the sizing of the air intake, the protrusion distance from the fuselage is taken as a fraction of the boundary layer thickness, which is calculated in the same manner as in section 5.5. A fraction of this thickness is taken because it significantly reduces the average inlet airspeed compared to the free stream velocity, V_∞, according to Equation 5.37:

$$V_{avg} = \int_0^h V_\infty \left(\frac{y}{\delta}\right)^{\frac{1}{7}} = \frac{7}{8} \cdot \left(\frac{h}{\delta}\right)^{\frac{8}{7}} \cdot V_\infty \tag{5.37}$$

---

[13]retrieved from `https://www.zsw-bw.de/fileadmin/user_upload/PDFs/Vorlesungen/est3/WS_2017/ESTIII_WS_17_18_JS_Fuel_Cell_Components_Stack_Design_f.pdf`, accessed on 23 June 2018

[14]retrieved from `http://www.fuelcellsetc.com/store/DS/gas-diffusion-layer-properties.pdf`, accessed on 23 June 2018

[15]retrieved from `https://www.fuelcellearth.com/fuel-cell-products/carbon-cloth-cc4-plain/`, accessed on 23 June 2018

[16]retrieved from `http://www.fuelcellsetc.com/store/N117`, accessed on 23 June 2018
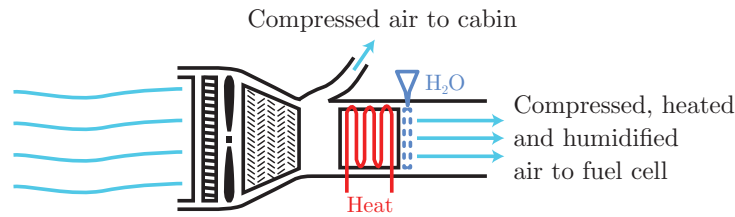
Figure 5.20: Air intake system overview

Here, $\left(\frac{h}{\delta}\right)$ is the ratio of protrusion to boundary layer thickness. While reducing the protrusion distance as much as possible benefits efficiency, too small a value will result in an unacceptably large inlet width in order to achieve the necessary inlet area. Therefore a ratio of protrusion to boundary layer thickness of 0.7 is taken. This leads to an average inlet velocity of $0.58V_\infty$.

Hydrogen Flow System
Transferring LH2 from the tank to the fuel cell involves a cooperation between the following key components: the pump driver, the tank pressure regulator and the delivery line. The following paragraphs introduce these components used in the transferring process.

Hydrogen is transferred to the fuel cell with a drive system as pump drive. A few options are considered by Brewer [15] including Bleed-air, electric motor, shaft drive with fixed or varying ratio. Bleed-air can be obtained through engine compressors, however, it is not applicable in the Greenliner as no engines are installed. Similarly, the shaft powered drivers using the power from engine gearbox is not selected for the Greenliner. Lastly, an electric motor drive pump is chosen because it has an advantage of using only electricity. Furthermore, the advantage of adjusting system power for electric motors allows the pump to deliver a higher fuel flow when necessary. Once the hydrogen is pumped out of the tank, it is transferred through fuel transfer valves and transfer tubes.

The hydrogen is released from the tank and pumped through a poppet-type absolute pressure regulator [15], which controls the amount of hydrogen that passes through the unit. This unit allows the fluid to pass in liquid form and then in gas form separately. After which LH2 is gasified when it passes through a heat exchanger, to achieve the desired working temparature for the PEM fuel cell. The pressure of GH2 is regulated such that it meets the working pressure of 3 bars at the PEM fuel cell.

The design of the line that carries the LH2 fuel from the tank to the PEM fuel cell is characterised by two parameters: the diameter of the line and the insulation system. The referenced fuel line from Brewer [15] is used to indicate the transfer system and the line has a diameter of 1 inch. This diameter was calculated based on a hydrogen flow rate of 0.351 kg/s in the design, which is approximately 8 times more than the required hydrogen flow rate for the Greenliner PEM fuel cell system. Thus a considerable smaller line diameter is expected for the Greenliner design. To simplify the calculation, half of the diameter value is chosen to fulfil the Greenliner requirement while maintaining a manufacturing feasibility. Therefore, a line diameter of 0.0127 m is used for the hydrogen flow rate of 0.047 m/s.

Furthermore, the insulation system is to be chosen. Two fuel delivery lines are considered, namely vacuum-jacketed (VJ) and rigid, closed cell foam. As much as VJ lines are efficient in heat loss, the drawback on manufacturing, installation and maintenance indicates its low sustainability. Meanwhile, the rigid closed foam is also the material used for the tank insulation design. Therefore, it is considered more convenient in terms of manufacturing. The same configuration for the reference line is considered for thermal insulation material: the rigid closed cell foam. Also for the insulation material half the thickness is assumed to be used for the Greenliner. The schematic cross section of the pump line is shown in Figure 5.21.

Once the hydrogen is supplied to the fuel cell, a circulating system for the hydrogen is used. Since only 1 out of 2.8 hydrogen molecules reacts as it passes through the fuel cell (a stochiometry ratio of 2.8 is determined) [94], the remaining hydrogen can be pumped back into the system. When the hydrogen flow is kept circular, it is possible to use almost all of the provided hydrogen, given that the water from the reaction is extracted out of the system and only pure hydrogen is provided to the system. Research shows that fuel utilisation percentages of 84.4 % to as high as 98.6
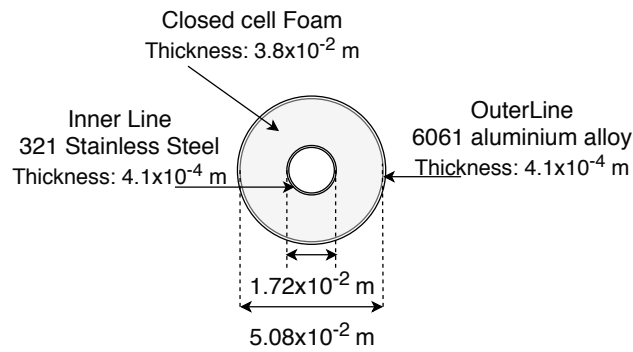
Figure 5.21: Hydrogen transfer line, from tank to fuel cell, cross section

% can be achieved [75]. For the Greenliner 90 % fuel utilisation is assumed as a safe estimate.

Figure 5.22 shows an overview on the circulation system, based on a fuel cell re-circulation system designed in [96]. The check valves function as monitor for the functioning of both the gas-liquid separator as the whole system. The gas-liquid separator removes the H_2O produced in the fuel cell from the circulation. The hydrogen pump controls the flow of the circulation. The purge system is only used when the hydrogen concentration in the flow reduces due to contamination of the flow. This reduces the functioning of the fuel cell, therefore the circulation system is then purged with hydrogen, ensuring the purity level of the circulating gas. Summarising, all hydrogen can now be used due to the circulation, except for the hydrogen which is used to purge the system: this part is expelled together with the contaminating gasses in the circulation system. Fortunately, this contamination can be avoided when only pure hydrogen is supplied from the fuel tank.
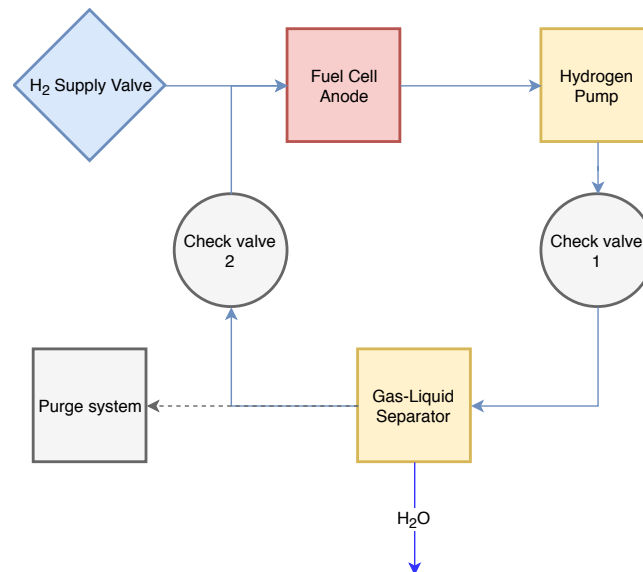
Figure 5.22: Hydrogen circulation system overview

Heat & Water Management
Since the different systems in the aircraft require or produce different amounts of heat and water, these flows have to be managed. The main systems that require heat are the hydrogen flow control, the oxygen flow control and the cabin environmental control. The main heat source is the fuel cell, which produces heat as byproduct since it does not function with 100% efficiency. During the sizing, the amount of heat produced by the fuel cell is compared to the heat needed by the other systems in order to assess if more heating is needed. If more heating is needed, extra power has to be generated by the fuel cell for active heating. If no extra heating is needed, the excess heat has to be transferred to the aircraft environment. Besides, if no extra heating is needed, the power use of the temperature regulation system is

assumed to be negligible with respect to the power needed for the propulsion of the aircraft, due to the relatively low power use of fluid pumps with respect to the propulsion system.

The main systems requiring water are the humidifier of the air intake and the fuel cell membrane. The water of the humidified air can be gained back at the air outlet by condensing the air if needed. Besides, the fuel cell also produces water as product of the chemical reaction occurring. Since the fuel cell operates at a temperature below the boiling point of water and in the middle to high current region, it is assumed that more water is produced than is required [11]. Water thus will be expelled from the aircraft and only the circulation and extraction have to be designed. The power use of this system is assumed negligible with respect to the power needed for the propulsion of the aircraft, also due to the relatively low power use of fluid pumps with respect to the propulsion system.

Fuel Cell System Overview

In order to have an overview on the complete fuel cell system before sizing it, the components and their interrelations were evaluated. Figure 5.23 shows the different parts of the system and their interactions. The air and hydrogen supply parts are both highlighted, indicating the different parts used before supplying the final air and hydrogen flow to the fuel cell. Based on this overview, the system modelling and sizing are done respectively in subsection 5.6.2 and subsection 5.6.3. First, a model is developed to address the design challenges associated with operating a fuel cell at the conditions encountered in the mission profile. Subsequently, this model will be implemented to size the complete fuel cell system for the Greenliner.
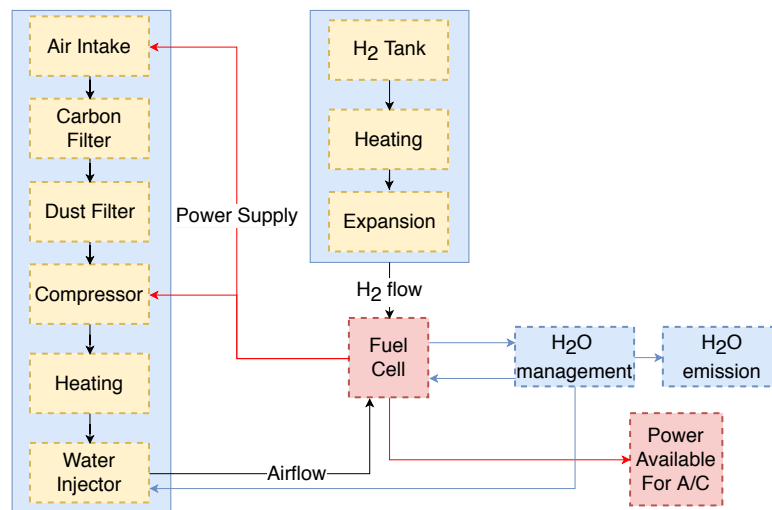
Figure 5.23: Fuel cell system overview

5.6.2. Fuel Cell System Modelling

The design of an aircraft that flies on fuel cell electricity is a difficult process in the sense that it is a rather novel area. Whereas in the automotive industry the application of fuel cells has already developed, the design of fuel cells in aviation is still in the conceptual phase.

For the design of the Greenliner, a fuel cell model was developed that could accurately represent the performance of a fuel cell during flight. The challenge in designing a fuel cell which powers an aircraft, is that the ambient pressure will change drastically during operations. The performance of a fuel cell strongly depends on the ambient pressure if the oxygen is taken from the air. Compared to the design of a fuel cell which is applicable in cars, the design of a fuel cell applicable in aircraft poses more challenges.

General Fuel Cell Modelling Approach

The creation of a model is a delicate process in which variables and conditions must be carefully chosen, such that all elements will work in harmony. The accuracy and complexity are strongly correlated for a fuel cell model. The first one-dimensional model of a membrane-electrode assembly (MEA) was done by Bernardi and Verbrugge [19]. This model forms the basis of the one-dimensional modeling approach of Ryan et al. [65]. A finite volume-based

isothermal two-dimensional model was applied by Um et al [94]. This model was adapted by Larbi et al. to study the influences of porosity and pressure on the fuel cell performance [9]. Haghayegh et al. present a three-dimensional, isothermal steady state model built in COMSOL which simulates a serpentine flow pattern based on the finite element method [54]. For the simulation of complex flow patterns such as serpentine and interdigitated flows, the use of three-dimensional models is necessary.

For the design of the Greenliner, a semi two-dimensional isothermal steady state model is developed for an accurate description of PEMFC behaviour during flight, based on the model developed by Um et al [94] and Larbi et al [9]. During climb, the pressure change is about 0.1% to 0.7% per second near the cruise altitude, and therefore it is reasonable to assume a steady-state fuel cell during flight. A semi two-dimensional approach was chosen because it provides more accuracy than a one-dimensional model, and it is not as complex as a three-dimensional model. This model can be used for parallel flow patterns only.
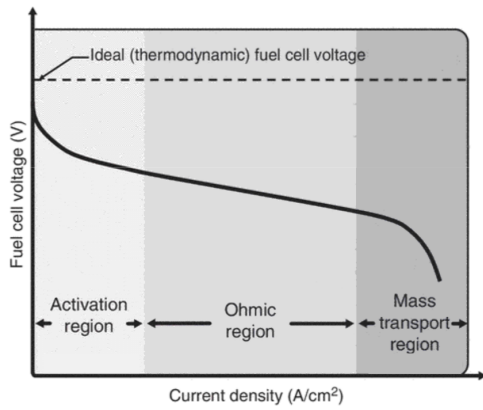
Figure 5.24: The standard shape of a current density curve of fuel cell [65]
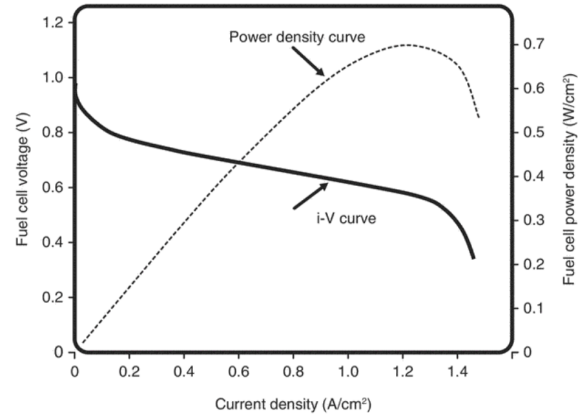
Figure 5.25: The standard shape of the power density curve of a fuel cell [65]

A fuel cell is designed using the characteristic current density curve which is shown in Figure 5.24. A basic fuel cell model can be explained using Equation 5.38 [65] and Figure 5.24: There is a thermodynamic limit to the energy that can be extracted electrochemically from hydrogen, this limit is given as E_0 and can be calculated using the Nernst equation of the form in Equation 5.39 [65]. There are three main types of fuel cell overvoltages which give the characteristic shape to the I-V curve. These are activation losses, ohmic losses and concentration losses; η_{act}, η_{ohm} and η_{conc} respectively in Equation 5.38. The activation losses set the vertical location of the current density curve by defining how the fuel cell behaves in the lower current density region. The ohmic losses describe the slope of the current density curve, and the concentration losses define the current density limit. Multiplying the voltage and current density will give the power density curve, shown in Figure 5.25. This power density curve is used to size for the fuel cell system, and the amount of required hydrogen during flight. The three overvoltages will now be discussed in more detail.

$$V = E_0 - \eta_{act} - \eta_{ohm} - \eta_{conc} \tag{5.38}$$

$$E_0 = 1.229 - \frac{RT}{2F} \cdot \ln\left[\frac{1}{(P_A X_{H2}) \cdot (P_C X_{O2})^{1/2}}\right] \tag{5.39}$$

1. **Activation Overvoltage**
   The activation losses are due to an overvoltage that is applied to the anode and cathode side. This overvoltage results in a higher current, but it requires a sacrifice in potential. This is because for the hydrogen oxidation reaction (HOR) and oxygen reduction reaction (ORR) there is a forward and a reverse reaction. Both of these reactions need a certain activation energy to be in activated state. From the activated state the reaction can go either forward or go backward. The reaction with the smaller activation energy will have a larger reaction rate. These unequal rates will however result in a build-up of charge, with e^- accumulating at the metal electrode, and H^+ accumulating at the electrolyte, until the reaction is in dynamic equilibrium. For a stimulation of the forward reaction at the anode and at the cathode electrode, an overpotential between the two must be

introduced to increase the current. The Butler-Volmer equation relates the overpotential and the reaction rate, hence current density, between an electrode and the electrolyte. Equation 5.40 [65] gives an adaption of the Butler-Volmer equation, which is used in the model to find the activation overpotential η_{act}.

$$\eta_{act} = \eta_{an} + \eta_{cath} = \frac{RT}{2\alpha_a F} \cdot \ln\left[\frac{j}{j_a^0 P_a X_{H2}}\right] + \frac{RT}{2\alpha_c F} \cdot \ln\left[\frac{j}{j_c^0 P_c X_{O2}}\right] \tag{5.40}$$

2. **Ohmic Overvoltage**

The second voltage loss is the ohmic loss, which describes lost energy due to charge transport. The ohmic overvoltage can be divided into two parts: The voltage loss due to electron transport and the voltage loss due to proton transport. The voltage loss of electron transportation is very small compared to proton transportation due to the difference in transport mechanisms. The voltage loss due to electron transport is therefore neglected in the model. The Ohmic overpotential is given by Equation 5.41 [65],

$$\eta_{ohm} = j \cdot ASR_m \tag{5.41}$$

where ASR_m is the area specific resistance of the membrane, resulting from the inverse conductivity integrated over the membrane thickness in Equation 5.42.

$$ASR_m = \int_0^{t_m} \frac{dx}{\sigma_m} \tag{5.42}$$

The membrane used in the fuel cell is Nafion-117 and its conductivity strongly depends on the water saturation. The conductivity σ_m can be calculated with the semi-empirical Equation 5.43 [9], where lambda is a function of water vapour activity a in Equation 5.44 [9]. The water vapour activity a describes the ratio of water in liquid and vapour form and is calculated using Equation 5.45 [9]. The saturation pressure p_{sat} of water in nafion is dependant on the temperature and is given by the semi-empirical Equation 5.46 [94].

$$\sigma_m = 100 \cdot e^{1268\left(\frac{1}{303} - \frac{1}{T}\right)} \cdot (0.005139\lambda - 0.00326) \tag{5.43}$$

$$\lambda(a) = \begin{cases} 0.043 + 17.18a - 39.85a^2 + 36a^3, & \text{for } 0 < a \leqslant 1 \\ 14 + 1.4(a+1), & \text{for } 1 < a \leqslant 3 \\ check, & \text{otherwise} \end{cases} \tag{5.44}$$

$$a = \frac{X_{H_2O}\, p}{p_{sat}} \tag{5.45}$$

$$p_{sat} = 10^{-2.1794 + 0.02953(T-273.15) - 9.1837 \cdot 10^{-5}(T-273.15)^2 + 1.4454 \cdot 10^{-7}(T-273.15)^3} \tag{5.46}$$

3. **Concentration Overvoltage**

The final voltage loss is due to a drop in product concentration. This loss is mainly caused by a depletion of oxygen at the cathode as the current density increases. The depletion of products affects the overvoltage in two ways as shown by Equation 5.47 [65]. There is a term with product concentration in the Butler-Volmer equation (Equation 5.40) and in the Nernst equation (Equation 5.39). The loss due to product depletion at the electrodes can be given as a function of the limiting current density [65]. However, it is far more accurate to calculate the concentrations of the products using governing equations over a domain. Using a set of governing equations and boundary conditions, a finite element estimation of a two-dimensional domain will be solved for species concentration. From this finite element estimation the activation loss and ohmic loss can be calculated since they are functions of hydrogen, oxygen and water concentration. The concentration overvoltage is thus incorporated in the finite element estimation.
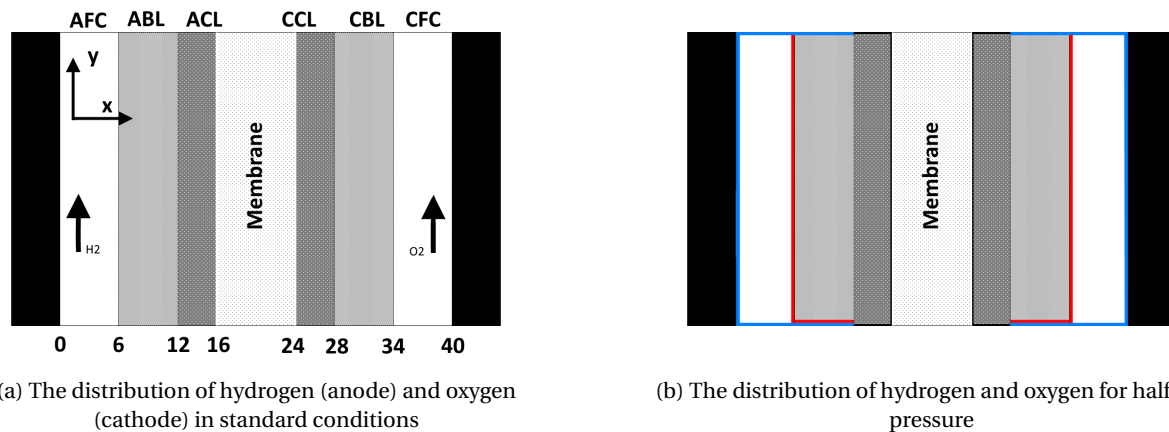
$$\eta_{conc} = \eta_{conc,BV} + \eta_{conc,Nernst} \tag{5.47}$$

Model Domain
Before the general approach of modelling a fuel cell is applied to the Greenliner's case, first the model domain is introduced. The domain consists of 7 layers (see Figure 5.26a), from left to right: the anode flow channel (AFC), anode backing layer (ABL), anode catalyst layer (ACL), membrane (MEM), cathode catalyst layer (CCL), cathode backing layer (CBL) and the cathode flow channel (CFC). The ABL and CBL represent the anode and cathode Gas Diffusion Layer (GDL) respectively. The domain is based on the domain used by Um et al. [94] and Larbi et al. [9], this means that the entire domain will be solved for simultaneously on all seven layers. There are however a few discontinuities in the domain, which are listed together with model assumptions:

- Hydrogen is only present in the AFC, ABL and ACL
- Oxygen is only present in the CFC, CBL and CCL
- In the membrane there is only water
- The model is isothermic
- The model is steady state
- No nitrogen is present in the CFC

Figure 5.26: Nomenclature of the MEA

(a) The distribution of hydrogen (anode) and oxygen (cathode) in standard conditions

(b) The distribution of hydrogen and oxygen for half the pressure

The dimensions of the layers are given in Figure 5.26a and are according to Larbi's model. The number of grid points of the domain is set to 40 in horizontal direction and 20 in vertical direction.

Several boundary conditions are applied to the model. The location of the boundary conditions is given in Figure 5.26b, with blue lines indicating boundary conditions for velocity and pressure, and the red lines indicating boundary conditions for species molar fractions. The lower and upper blue boundaries have a boundary condition for pressure of the flow coming in, and pressure of the flow going out. Additionally, the lower blue boundaries have a velocity boundary conditions equal to the flow inlet velocity. At the walls (indicated by the two vertical blue lines) the velocity is zero, assuming that there is no slip, and the pressure difference across the wall is also zero.

The two red lines at the anode side indicate a boundary condition for a hydrogen molar fraction of 0.9. At the cathode side the two red lines indicate an oxygen molar fraction of 0.18. All red lines indicate a water molar fraction of 0.1. It should be noticed that the molar fraction of oxygen in air does not change with altitude.

Species Distribution
The general approach for finding the current density curve has been given and the unknowns in Equation 5.40 to Equation 5.47 are identified as pressure, temperature and the molar fractions. All other parameters are constants or variables which depend on fuel cell configuration. In Table 5.6, all constants and variables can be found. The fuel cell model will output the current density curve for given anode and cathode operating pressures. Assuming that the temperature is held constant at 353K by the heat management system, the model will need to be solved for the species distributions.

A fuel cell model is described by a set of 4 governing equations. These equations are the incompressible Navier-Stokes equation (Equation 5.48), species equation (Equation 5.49), charge equation, and energy equation.

The charge equation solves for overpotential in the model domain. This is usually necessary because the activation overvoltage can be split into an anode part and a cathode part, giving a non-uniform overpotential distribution in the domain. This means that the current density terms j in Equation 5.40 are not equal for the anode and cathode side. For this model however, steady state is assumed, and in steady state the current density at anode and cathode are by definition equal [65].

The energy equation solves for heat, which is assumed to be constant in this model, making the energy equation redundant. It is however recommended that the energy equation be implemented into the model at a later stage to model for heat production in the fuel cell. The heat management system can then be designed more accurately.

The species distribution will be split up into two parts. First the solution for hydrogen and oxygen distribution will be discussed, and then the solution for distribution of water in the Nafion-117 membrane will be discussed.

$$\frac{\partial(\rho\epsilon)}{\partial t} + \nabla \cdot (\epsilon\rho\vec{u}) = 0 \tag{5.48}$$

$$\frac{\partial(\rho\epsilon\vec{u})}{\partial t} + \nabla \cdot (\epsilon\rho\vec{u}\vec{u}) = -\epsilon\nabla P + \nabla \cdot (\epsilon\mu\nabla \cdot \vec{u}) + \vec{S}u,$$

$$\frac{\partial(\epsilon X_k)}{\partial t} + \nabla \cdot (\epsilon\vec{u}X_k) = \nabla \cdot (D_k^{eff}\nabla X_k) + Sk \tag{5.49}$$

1.Hydrogen and Oxygen Distribution

The distribution of hydrogen and oxygen in the domain is solved by solving the weak form of the two governing equations, Equation 5.48 and Equation 5.49, on the domain. These governing equations have several source and sink terms within the domain. The source and sink terms can be found divided into regions in Table 5.5. The Navier-Stokes equation and the Species equation will now be discussed separately, including their source and sink terms.

The Navier-Stokes equation (Equation 5.48) has a few terms that require explanation. The density ρ is calculated using the ideal gas law in Equation 5.50, where the molar mass ω for a mixture can be calculated using Equation 5.51 [54]. The viscosity of the mix can be found using Equation 5.52 [54], where γ_{ij} is a dimensionless factor given by Equation 5.53 [54].

The first term of S$_u$ in Table 5.5 is caused by the porous nature of the GDL, CL and the membrane, which slows the flow down. This sink term is derived from Darcy's law for porous media. The permeability κ can be calculated using the Kozeny-Carman [47] [16] equation shown in Equation 5.54. The second term of S$_u$, which is only in the CL and membrane, defines the electro-osmitic drag phenomenon, which will be discussed in more detail in the water distribution section. This source term will be neglected, because the potential equation is not solved for in this model.

$$\rho = \frac{p\omega}{RT} \tag{5.50}$$

$$\omega = \sum_i \frac{M_i}{\omega_i} \tag{5.51}$$

$$\mu_{mix} = \sum_i \frac{\omega_i\mu_i}{\sum_j \omega_j\gamma_{ij}} \tag{5.52}$$

$$\gamma_{ij} = \frac{1}{\sqrt{8}} \left(1 + \frac{\omega_i}{\omega_j}\right)^{-1/2} \left[1 + \left(\frac{\mu_i}{\mu_j}\right)^{1/2} \left(\frac{\omega_i}{\omega_j}\right)^{1/4}\right]^2 \tag{5.53}$$

$$\kappa = a\frac{\epsilon^3 D_p^2}{(1-\epsilon)^2} \tag{5.54}$$

The species term depends on the effective diffusivity of hydrogen mixed with water, or oxygen mixed with water. The diffusivity of a mix can be found by using Equation 5.55, where a and b are 3.640 x 10^{-4} and 2.334 respectively for pairs involving water and non-polar gases [54]. The effective diffusivity of a mix is given by Equation 5.56, which accounts for the porous nature of a medium, and the tortuosity τ of the porosity.

The Species equation has sink terms at the ACL and CCL for hydrogen and oxygen respectively. Likewise, in the CCl there is a source term for water. The source and sink terms given by S$_k$ account for the electrochemical reaction that takes place in the catalyst layers. During a reaction one hydrogen and half an oxygen molecule disappears, and one water molecule appears. These source and sink terms are given by the reaction rate from the Butler-Volmer reaction in Equation 5.40. The concentration c is given by Equation 5.57

$$D_{ij} = \frac{a\left(\frac{T}{\sqrt{T_{ci}T_{cj}}}\right)^b \cdot \left(p_{ci}p_{cj}\right)^{1/3} \cdot \left(T_{ci}T_{cj}\right)^{5/12} \cdot \left(\frac{1}{\omega_i} + \frac{1}{\omega_j}\right)^{1/2}}{p}$$ (5.55)

$$D_{i,j}^{eff} = \epsilon^\tau \cdot D_{i,j}$$ (5.56)

$$c = \frac{p}{RT}$$ (5.57)

Table 5.5: Source and sink terms for the governing equations

	Su	**Sk**
GDL	$-\frac{\mu}{k}\epsilon^2 \vec{u}$	0
CL	$-\frac{\mu}{k}\epsilon\epsilon_{mc}\vec{u} + \frac{k_\phi}{k_p}z_f c_f F\nabla\Phi_e$	$-\frac{j}{2Fc}\Big|_{H_2}^{ACL} - \frac{j}{4Fc}\Big|_{O_2}^{CCL} + \frac{j}{2Fc}\Big|_{H_2O}^{CCL}$
Mem	$-\frac{\mu}{k}\epsilon_m \vec{u} + \frac{k_\phi}{k_p}z_f c_f F\nabla\Phi_e$	0

2. Water Distribution

The water distribution will be solved for differently than the hydrogen and oxygen distribution. This is done to reduce the complexity of the model, and to reduce computational time. The model becomes complicated because the water behaviour must be modelled in the membrane. There are two additional terms that influence the water distribution in the membrane, or rather, the saturation of Nafion-117.

Firstly, the protons that move through the membrane, move by reattaching themselves to adjacent water molecules. The protons usually drag some of the water molecules with them as they move. This phenomenon is called electro-osmotic drag [65]. Due to this drag, the water molecules accumulate at the cathode side of the membrane, which causes the second phenomenon that influences the water movement, namely back diffusion of water. If a certain species occurs in a high concentration, the diffusive forces become stronger, which causes a movement of the species [65].

It was decided to neglect these effects for the sake of simplicity. It is however recommended that the water distribution be modelled with these effects in a later stage of the design. The Nafion saturation is now calculated by taking the water concentration at the CCL-membrane border, which comes from the creation of water in this region from the electrochemical reaction. Neglecting S_k and the velocity term in Equation 5.49, the species equation takes the form of Equation 5.58. After applying the chain rule, this equation becomes Equation 5.59. Assuming that the water concentration will change across the membrane, $\partial X_{H_2O}/\partial x$ cannot be zero. This results in a homogeneous ordinary differential equation (ODE) for water diffusivity. The solution of this ODE is given in Equation 5.60, in which c_1 is found by solving the ode at the CCL-membrane border where the water concentration is known. From this water concentration the water diffusivity at the CCL-membrane border can be found from Equation 5.61 [9] where λ comes from Equation 5.44 and a comes from Equation 5.45. With the diffusivity at the boundary known, the diffusivity of water across the membrane can be solved for with Equation 5.60, and the conductivity of the membrane can be found with the diffusivity across the membrane from Equation 5.61 and Equation 5.43.

$$\nabla \cdot \left(D_k^{eff} \nabla X_k\right) = 0$$ (5.58)

$$D_K^{eff}\frac{\partial X_{H_2O}}{\partial x} + \frac{\partial D_k^{eff}}{\partial x} \cdot \frac{\partial X_{H_2O}}{\partial x} = 0$$ (5.59)

$$D_k^{eff}(x) = c_1 e^{-x}$$ (5.60)

$$D_w^m = \begin{cases} 3.1\cdot10^{-7}\cdot\lambda\left(e^{0.28\lambda}-1\right)\cdot e^{-\frac{2346}{T}}, & \text{for } 0 < \lambda < 3 \\ 4.17\cdot10^{-8}\cdot\lambda\left(161e^{\lambda}+1\right)\cdot e^{-\frac{2346}{T}}, & otherwise \end{cases}$$ (5.61)

Table 5.6: The values of constants and fuel cell parameters

Property	Units	Value	Property	Units	Value
F	mol/s	96485	ϵ_{GDL}	[-]	0.4
j_a^0	A/cm^2	0.01	ϵ_{CL}	[-]	0.4
j_c^0	A/cm^2	0.0001	ϵ_{mem}	[-]	0.28
p_{c,H_2}	atm	12.8	ϵ_{mc}	[-]	0.4
p_{c,O_2}	atm	49.7	κ_{GDL}	cm^2	1.76 x 10^{-7}
p_{c,H_2O}	atm	217.5	κ_{CL}	cm^2	1.76 x 10^{-7}
R	J/mol.K	8.3144	κ_{mem}	cm^2	10$^-$14
T	K	353	ω_{H_2}	g/mol	2.016
T_{c,H_2}	K	33.3	ω_{O_2}	g/mol	31.998
T_{c,O_2}	K	154.4	ω_{H_2O}	g/mol	18.015
T_{c,H_2O}	K	647.3	p_{Sat}	atm	0.4641
τ	[-]	1.5	μ_{H_2}	kg/m.s	9.83 x 10^{-6}
$X_{H_2,in}$	[-]	0.9	μ_{O_2}	kg/m.s	2.25 x 10^{-5}
$X_{O_2,in}$	[-]	0.18	μ_{H_2O}	kg/m.s	1.09 x 10^{-5}
$X_{H_2O,in}$	[-]	0.1			

Model Implementation

Now that the modelling approach has been explained, the programming environment can be discussed. The solving of the governing equations for the model using a finite element estimation was done in a program called Freefem++. Freefem++ is an open source partial differential equation solver. It has its own programming languange which is based on c++ and it "can solve non linear multiphysics systems in 2D and 3D" [35]. This program is very useful, there is however one drawback to its use. The partial differential equations (read: governing equations) must be expressed in their weak form.

It can be seen that the governing equations such as Equation 5.49 require a second order partial derivative to be solved. By considering an integral expression for Equation 5.49 this requirement can be weakened [62]. After using integration by parts the integral form of a partial differential equation can be expressed in multiple integral terms which represent an approximation of the strong form. The weak form of the Navier-Stokes equation is given in Equation 5.62 [35] and the weak form of the species equation is given in Equation 5.63, where $\vec{v}$ and v are the test functions.

$$\int_\Omega [(\vec{u} \cdot \nabla) \vec{u}] \cdot \vec{v} + \int_\Omega \mu \cdot \nabla \vec{u} : \nabla \vec{v} - \int_\Omega p \nabla \cdot \vec{v} - \int_\Omega q \nabla \cdot \vec{u} = 0 \tag{5.62}$$

$$\int_\Omega D_k^{eff} \cdot \nabla^2 X_k cdot \cdot v + \int_\Omega \nabla D_k^{eff} \cdot \nabla X_k \cdot v - \int_\Omega \nabla \cdot \left(\epsilon \vec{u} X_k^{n-1}\right) \cdot v + \int_\Omega S_k \cdot v = 0 \tag{5.63}$$

Model Iteration Process

To find the final velocity and species fields, a first estimate must be implemented. From this initial guess the velocity field can be calculated. It was chosen to add a convergence factor of 0.25 to make sure that the solution wouldn't overshoot the actual value and diverge. The best iteration method would be to calculate the velocity field, the species field and then to iterate to process until a converged value is found. It was however not possible to apply this method because both fields would start to diverge after a few iterations, no matter how small the convergence factor was made. It was therefore chosen to apply an iteration method as shown in Figure 5.27. First the solution was iterated for a convergence of the velocity field, and then with the resulting velocity field the species field was solved for by iterating until a converged value was found. The velocity field is not be updated in between. If the change between the nth iteration and the previous iteration is less than one percent, the solution is said to be converged.

Results

This model was used to get the current density curves for an input anode and input cathode pressure. With these current density curves, the optimal operating pressures could be found, and the necessity of compressing ambient air was assessed. A few examples of the distribution of hydrogen and oxygen are given in Figure 8.2, and a few examples of the velocity field are given in Figure 8.3. In section 8.2, this model is verified and validated. An output current density curve of this model is compared to that of Larbi [9] and O'Hayre [65] in Figure 8.4.
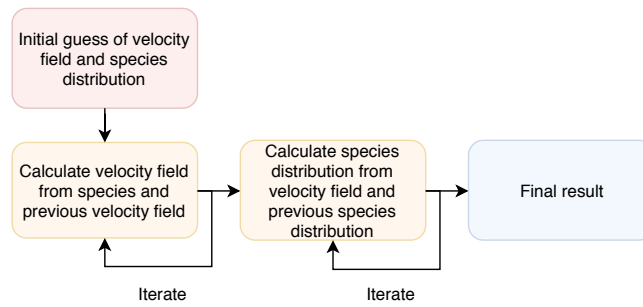
Figure 5.27: The iteration process of the FEM model

5.6.3. Fuel Cell System Sizing

As was discussed in subsection 5.6.2, there are several operating conditions which the Greenliner encounters that differ from those encountered in a car, most notably ambient temperature, air density and air pressure. These conditions need to be taken into account, and to do so, an iterative sizing program is used. The steps taken in this program are set out in Figure 5.28.
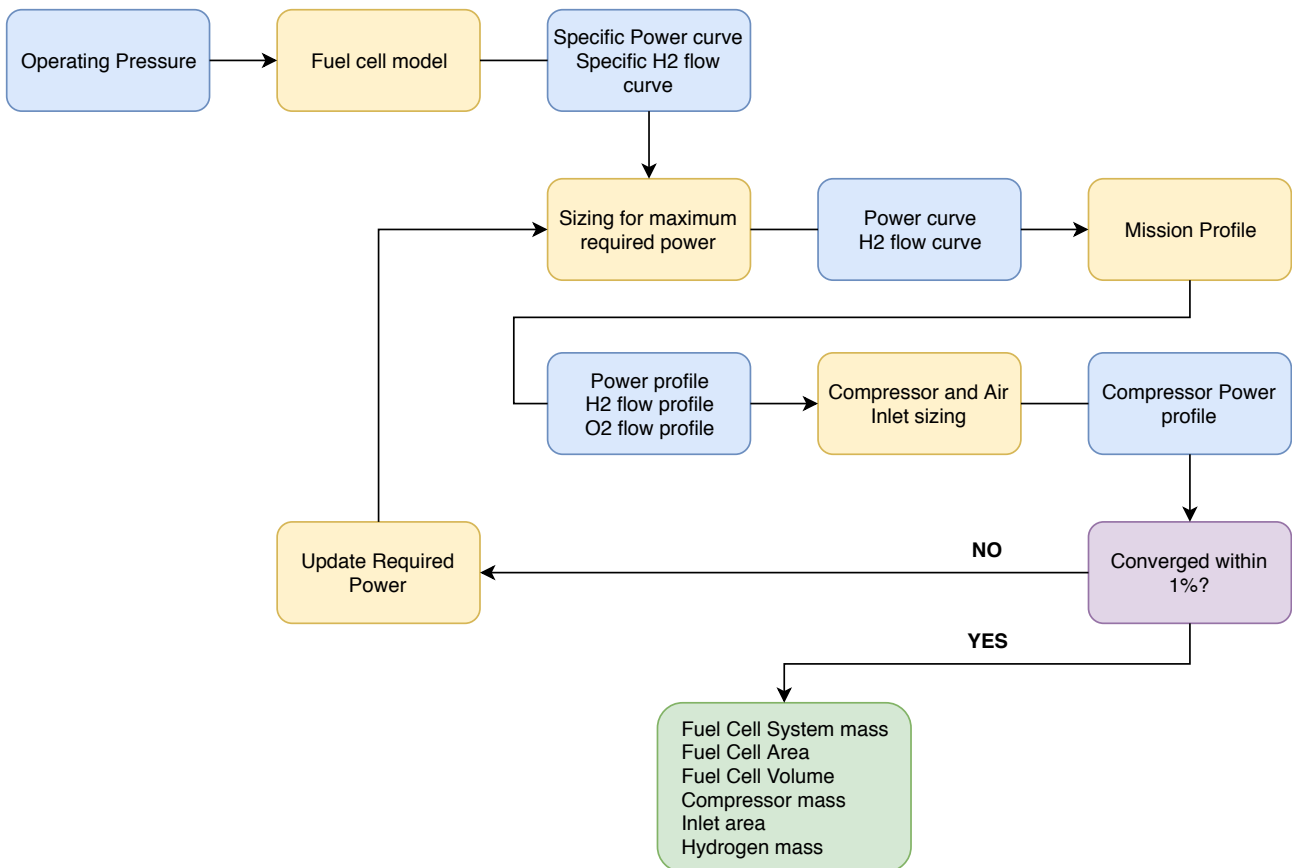
Figure 5.28: Flowchart describing the steps taken in the fuel cell system sizing

The most important input parameter for the functioning of the fuel cell is the operating pressure. The operating pressure on the anode side can be controlled by regulating the hydrogen supply from the fuel tank. However, the cathode side pressure is determined by the ambient air pressure. If no compressor were to be used, this would lead to cathode pressures of 0.2 to 0.3 bar at cruise altitude. From the fuel cell model, it was found that the chosen fuel cells lose much of their functionality at this level of cathode pressure. Therefore, it was determined that the incoming air needs to be compressed. A constant operating pressure is stipulated, which has the benefit of making the fuel cell operation predictable over the entire flight envelope. This means a compressor must work at varying levels throughout the mission,

providing a minimal cathode pressure of 1 atmosphere, since that is the ambient air pressure without compression at sea level.

The cathode operating pressure is used as an input to the fuel cell model, which examines the functioning of a single fuel cell. The anode operating pressure is fixed at 3 bar. This value is based on optimisation of the fuel cell model, and is validated by looking at operational pressure of current fuel cell applications [11]. For these conditions, the model calculates the power density curve and fuel consumption curve of a single fuel cell. Using these values along with the maximum power required during the mission, the total amount of fuel cells and their dimensions are determined. This gives the power curve and fuel consumption curve for the entire system.

The next step is running these curves through the mission profile: at each time step, the required power for the mission is matched with the fuel cell system power curve, which determines the hydrogen and oxygen mass flow at that time step. The power, fuel, and oxygen consumption profiles along the entire mission are now acquired. The fuel cells require an air inlet, which is sized to require zero active fan usage during cruise. The compressor can now be sized by calculating the power required to reach the desired cathode pressure at each time step in the mission. Of course, this power has to come from somewhere: the fuel cell system. Therefore, the compressor power profile is added to the mission power profile and used as an input for the following iteration. The iteration continues until the difference in results is below 1 %.

The flowchart in Figure 5.28 shows the procedure for sizing the system based on a specified cathode operating pressure. However, there will be a trade-off in determining the optimal pressure: higher pressure leads to higher efficiency of the fuel cell, but requires more power from the compressor. Therefore the sizing is done for a list of pressures, and the pressure that leads to the lowest total fuel consumption is chosen as the optimal pressure. The finalised sizing parameters for the fuel cell system can be found in chapter 6.

5.6.4. Fuel Cell System Sustainability

The fuel cell system sustainability is mainly dependent on the materials used and the production of the fuel cell. First, the materials and their recyclability and availability will be discussed. Second, the production process of the fuel cell will be elaborated upon. Finally, the overall durability of the fuel cell is discussed.

The main materials used for the fuel cell are (as indicated in Table 5.4): graphite, carbon fibre, platinum and Nafion 117. A main aspect of the sustainability of these materials is the recyclability. For graphite, recycling is still at lower stages of development due to the low price of the material. Graphite recycling thus is feasible[17], but not widely applied yet. For carbon fibre, recycling techniques are already applied [18]. In this way, carbon fibre parts can be reused in for example automotive industry. For the platinum catalyst, recycling of up to 95% of the metal is already possible [110]. Finally for the Nafion membrane, recycling techniques already make it possible to regenerate membranes from used membranes with comparable performance [107]. Summarising, all materials used in the fuel cell can be recycled in the production of new fuel cells, with mostly techniques which are already applied in industry.

Next to the recyclability of the materials, the availability of the materials is of importance for the sustainability of the fuel cell. This mainly applies to the platinum used: due to increased demand for platinum in for example the automotive industry, less platinum will be available in the next decades [5]. However, due to the recycling described in [110], the decreased availability is not considered a sustainability challenge.

The production process of fuel cells is (in terms of energy use) comparable to the production of conventional internal combustion engines [22]. However, during production research can be done in order to optimise the production process.

Finally, the durability of the fuel cell is an important aspect of the fuel cell sustainability. The operational lifetime of fuel cells generally is indicated in operational hours. In subsection 5.11.4, the total amount of flights in the lifetime of the aircraft is determined to equal approximately 58400 flights, with an average flight duration of 1.25 hours. Thus, the total operational lifetime of the aircraft equals approximately 73,000 hours. Fuel cells used in automotive applications already can operate more than 18,000 hours, and for stationary power generation already operational fuel cell lifetimes of 90,000 hours are reached [19]. Based on these it is expected that the fuel cells at least can be operative half of the life

---

[17]retrieved from `https://minerals.usgs.gov/minerals/pubs/commodity/graphite/graphmcs04.pdf` accessed 3 July 2018

[18]retrieved from `https://www.compositesworld.com/articles/recycled-carbon-fiber-update-closing-the-cfrp-lifecycle-loop` accessed 3 July 2018

[19]retrieved from `https://www.sintef.no/globalassets/upload/materialer_kjemi/energikonvertering-og-materialer/bilder/pemfc-overview-thessaloniki-fa-debruijn---f.pdf` accessed on 3 July 2018

time of the aircraft (36,500 hours), taking into account the improvement in fuel cell performance possible before the aircraft is operational in 2030. From this, it is estimated that the fuel cell system is likely to be replaced at most once in the lifetime of the aircraft.

5.7. Fuel Storage

Compared to conventional aircraft that carry kerosene, the Greenliner is facing distinctive challenges of storing cryogenic liquid hydrogen on board for the complete mission. In order to properly use cryogenic liquid hydrogen as fuel, a thorough analysis on the cryogenic liquid hydrogen tank design is performed. Firstly, cryogenic LH2 application on different vehicles is presented. In order to design a tank that holds the required amount of LH2, three aspects of the design are considered after that: geometry, mechanical and thermal insulation. Lastly, the sustainability aspect of using cryogenic LH2 and the corresponding tank is discussed.

5.7.1. Applications of Hydrogen as Fuel

Hydrogen storage is a challenge in all three product phases (production, delivery and operation). These challenges are introduced by material characteristics like volume, durability and cost. Hydrogen has been investigated in the Space program as a combustion fuel. Nowadays there are many cars like Hyundai Nexo, and aircraft like Rapid 200-FC which have shown the potential of using hydrogen as fuel. Even though in most of the applications hydrogen is stored in gaseous form or liquid form, there are other storage options such as solid metals [93]. Storing the gaseous form of hydrogen is considered very simple and common. One drawback of storing hydrogen in gas form is its low density which requires a large tank volume. Cryogenic LH2 has a few advantages such as high energy density and purity. Despite the extremely low temperature may cause cold burn when handled improperly, the low temperature could be used to cool down the fuel cell to maintain its working temperature. Hydrogen stored as a solid in combination with a metal is still in development, yet it remains an attractive alternative in the future. In the following paragraphs, the cryogenic LH2 will be focused on because the tank design is also based on this form of hydrogen storage.

5.7.2. Tank Sizing and Geometry

Before deciding on the size and geometry of the cryogenic tank, the tank volume must be calculated based on the hydrogen mass required. The required hydrogen mass is based on the required mission energy, given in section 4.2. After that, the tank geometry can be defined and optimised with respect to weight.

Firstly, the liquid hydrogen used consists of 99.79% para-hydrogen and only 0.2% ortho-hydrogen. This is because during liquefaction process, ortho-hydrogen is converted spontaneously into para-hydrogen under extreme conditions and temperatures [106]. Nuclei in a dihydrogen molecule can actually have two states of spinning: parallel (ortho-hydrogen) and anti-parallel (para-hydrogen). The latter, obtained during liquefaction process where energy is released. Therefore, in the following consideration, LH2 term is used to represent para-hydrogen. Furthermore, to reduce the disadvantage of low density of LH2, the LH2 is considered to be in saturated state at the given temperature. The corresponding pressure for LH2 and GH2 can be found in Figure 5.29. It can be seen that the saturated LH2 den-
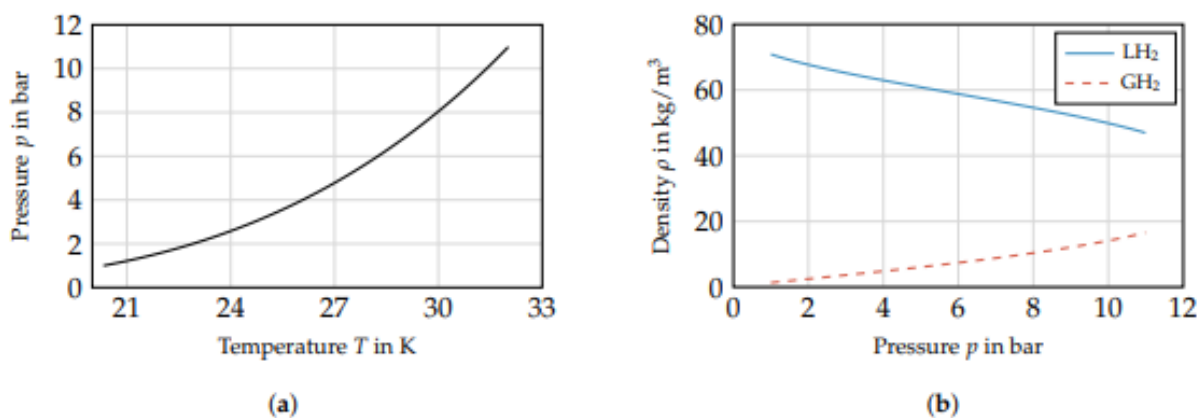

Figure 5.29: Density of saturated LH2 and GH2 vs pressure [106]

sity drops significantly with increasing temperature, while GH2 density increases only slightly. Due to heat exchange with the environment, the LH2 inside the tank will boil-off, turning into gas, which leads to a further increase of the temperature inside the tank. Therefore, a certain maximum venting pressure is required to properly vent the gas hydrogen out to reduce the pressure. This venting pressure dictates the amount of GH2 needed inside the tank. As a result, in order to obtain a high level of density, a venting pressure is selected based on Figure 5.30.
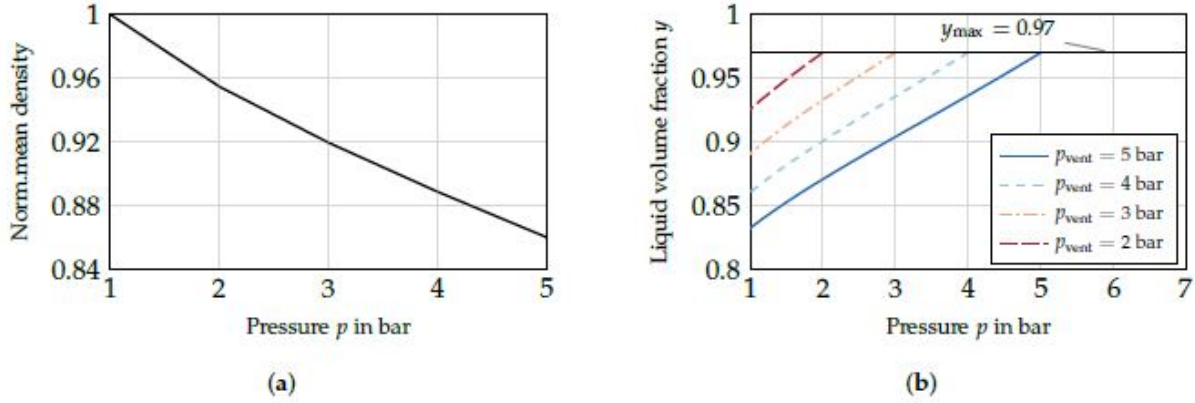
Figure 5.30: (a) Average hydrogen density for different pressure range. maximum (b) Liquid volume fraction VS pressure for varying venting pressure [106]

Three different performance requirements are considered for tank pressure. Firstly, the tank should be operated above ambient pressure in order to prevent air from flowing back into the tank, which would result in an air and hydrogen mixture. This mixture is a potential explosion threat that may cause structural failure. Therefore, the minimum pressure should be at least higher than ambient pressure. Secondly, in section 5.6, the PEMFC is designed to work under a pressure of 3 bar for the anode side which takes up hydrogen. To reduce the effort of compressing or expanding hydrogen, this pressure value is considered as a guideline when determining the tank pressure. Last but not least, the LH2 and GH2 density and volume ratio are considered for different pressure ranges. Combining Figure 5.29 and Figure 5.30, a tank pressure of 3 bar is considered, and a maximum allowed pressure of 4 bar is chosen. This leads to a volume fraction of LH2 and GH2 of 0.94 and 0.06 respectively. The LH2 density is read from Figure 5.29 (b) as 65 kg/m^3. Modified from the ideal gas law, the density of GH2 is calculated through Equation 5.64 as 3.04 kg/m^3.

$$\rho_{GH2} = \frac{P_{GH2}}{\frac{R}{m_{GH2}} \times T} = \frac{300000}{\frac{8.314}{2.02 \times 10^{-3}} \times 24} = 3.04 kg/m^3 \tag{5.64}$$

According to M. Hirscher [38], with today's tank installations, the LH2 evaporation loss is between 0.3-3% per day. Also stated by Brewer [15], allowance for boil-off of LH2 mass is about 3-4%. A more conservative contingency factor of 1.05 is taken for the LH2 mass stored on board which is sufficient for the tank design. With a liquid hydrogen volume fraction y_{max} of 0.94, the total hydrogen mass can be calculated from Equation 5.65.

$$m_{H2} = m_{LH2} + m_{GH2} = m_{LH2} + m_{LH2} \times \frac{\rho_{GH2}}{\rho_{LH2}} \times \frac{(1 - y_{max})}{y_{max}} \tag{5.65}$$

Before determine the tank geometry, integral or non-integral tank designs are decided. The integrated tank design serves as a part of the aircraft structure and carries fuselage loads additional to providing fuel containment. Meanwhile, the non-integral tank is designed to hold the containment and account of the load concerned with the fuel. The benefit of using a non-integral tank is the fact that the entire tank can be removed from the aircraft without damaging the surrounding structure. This is especially advantageous for the Greenliner, because as an novel design, the storage system should be easily accessible and replaceable.

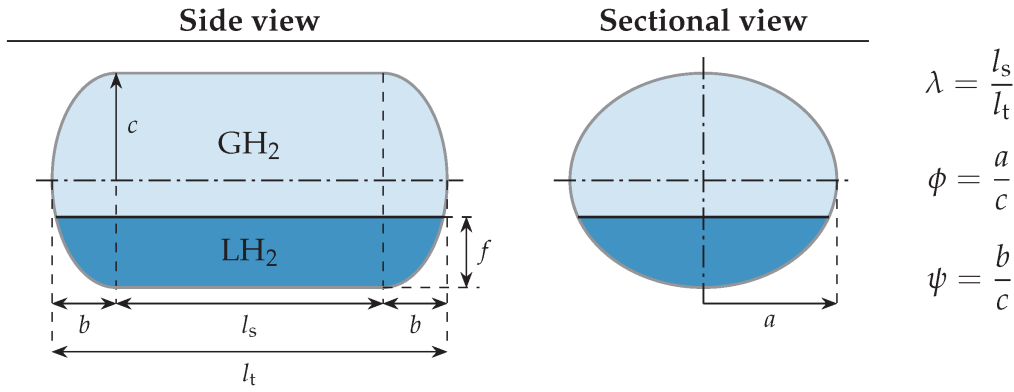Figure 5.31: Tank geometry parameter in side view and front view [106]

5.7.3. Tank Mechanical Design

As a general principle, aircraft material should be lightweight and possess high yield strength, stiffness and fracture toughness [58]. When considering cryogenic application, the density and critical crack size of the material are of particular interest. Once the material of the tank is selected, the corresponding tank thickness can be determined.

Four materials are considered: aluminium alloys 2021 and 2219, types 21-6-9 and 321 stainless steel. Aluminium alloy 2219 shows a high strength/density properties compared to the other two types of stainless steel. Moreover, there is more experience with using aluminium alloy 2219 than 2021. As NASA [58] has conducted a study for different tank materials, the aluminium alloy 2219 is considered as it fulfils all requirements the best among the others considered. The properties of this material include a density of 2825 kg/m^3, and a limited stress K of 172.4 MPa [106]. In the following design, both the spherical cap and the cylinder body use the aluminium alloy 2219 as the tank material. The tank wall thickness of the cylinder body is calculated based on accordance with official rules. The thickness s_{wall} can be calculated as shown in Equation 5.66,

$$s_{wall_c} = \frac{P_p \times d}{v(2K/SF_{tank} - P_p)} \tag{5.66}$$

Where P_p is the proof pressure determined by the venting pressure, considering a safety of 2.25, which is the maximum pressure inside a tank. This value is taken to be a bit higher than the normal regulated safety factor, because the stored tank is located right behind the passenger cabin. Usually a mandated safety factor of 1.4 to 2.0 is used for conservative material strength estimations [58]. While shown in the safety factor of statically loaded weld joints [20], butt welds loaded with a load have a safety factor ranging from 1.4 to 2.7. This is because the material strength is reduced by the cold operating temperature. Therefore, when using a weld factor of 0.8, a total safety of 2.8 can be achieved, which also verifies the safety taken in the Greenliner tank design. However, the method of welding determines the welding efficiency v and this welding efficiency should be further studied and elaborated upon. Lastly, d is the diameter of the tank.

The thickness of the cylinder body is compared to the thickness of the spherical cap and the higher thickness of the two determines the overall thickness of the tank such that a homogeneous tank surface can be achieved. The thickness of the spherical cap can be calculated with Equation 5.67.

$$\frac{K}{SF_{tank}} = P_p(\frac{a+c}{2s_{wall_s}}(1 + 2(1 + 3.6\frac{P_p}{E_y}(\frac{a+c}{2s_{wall_s}})^3)(\frac{a-c}{a+c})) + \frac{1}{2}) \tag{5.67}$$

When assuming a circular cross section for the tank, setting $\phi = 1$, a higher thickness of tank can be obtained for a given thickness. With this assumption, Equation 5.67 can be simplified to Equation 5.68. This assumption shows that a 25% reduction in spherical cap thickness s_{wall_s} is obtained with the latter equation. As a result, the tank is designed

---

[20]Retrieved from `https://knowledge.autodesk.com/search-result/caas/CloudHelp/cloudhelp/2017/ENU/Inventor-Help/files/` `GUID-C5A6A27F-8E81-4BD3-B9D9-8EDAE031B3B5-htm.html` on 25 June 2018
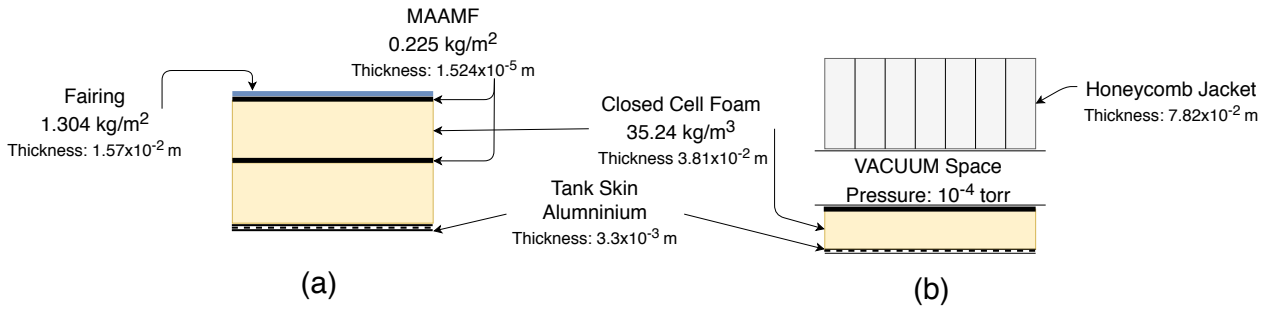
Figure 5.32: (a) The rigid closed-cell foam insulation layout. (b) The honeycomb jacket with vacuum insulation layout

efficiently in weight, while still being able to fulfil the structural requirement.

$$s_{wall_s} = \frac{a+c}{2} \frac{a+c}{\frac{K}{SFP_p} - 1} \tag{5.68}$$

5.7.4. Tank Thermal Insulation Design

To maintain LH2 at around 24 K, either an active refrigeration or a passive refrigeration system should be applied. Due to the weight penalty of the active refrigeration system, which uses additional components such as liquid nitrogen or mechanical refrigerator, a passive system is preferred. When using only thermal insulation materials around the tank, maintenance process is also simplified. The purpose of the thermal insulation of the tank is to reduce the heat exchange between the cryogenic LH2 in the tank and the ambient temperature of the for both integrated and non-fuselage-integral tank design. Only the non-integral options are considered in this report. For the Greenliner the two best performing options from [15] are considered on the basis of the DOC, performance and the safety. These options are discussed below.

Firstly, a rigid closed-cell polyurethane foam can be found in Figure 5.32 (a). This option has been demonstrated in Apollo flight program for S-II, where 69400 kg LH2 was stored in six tanks with a diameter of 10 m [43]. This proven rocket fuel storage tank demonstrates the possibility of using polyurethane foam as insulation. Unless polyurethane is placed under a temperature of 350 K, it has a low thermal conductivity, around 0.0028 W/mK. Such a low thermal conductivity means that it requires smaller a thickness to provide sufficient insulation comparing to other materials. The layout of such design includes a closed-cell polyurethane foam, a MAAMF vapour barrier. The MAAMF vapour barrier is used to prevent hydrogen gas from escaping the tank. It consists of a layer of Mylar layer, two aluminium foils series, followed by another Mylar layer and glass net fabric. The second option has three layers (see: Figure 5.32 (b)). Beyond the tank wall, there is a layer of closed cell foam, covered by a MAAMF vapour barrier. Then, there is a vacuum space between the foam and the aluminium honeycomb jacket. This option has also been demonstrated in the space shuttle [15].

The corresponding surface density and thickness for different layers in both thermal insulation options are given in Figure 5.32. Comparing these two options, the thickness of the honeycomb results in a heavier design. Furthermore, the vacuum space used in the latter option presents a higher level of difficulty in the manufacturing and maintenance process. Therefore, the rigid closed-cell foam insulation option is preferred. The thickness of such foam material should be decided upon, in order to calculate the overall mass of the tank. Since the Greenliner has a mission duration for about 3 hours, the time duration between refilling will be no more than 6 hours. This is considerably shorter compared to other applications. Therefore, for an initial estimate, a reference insulation thickness is applied for the Greenliner. From Brewer [15], the rigid closed-cell polyurethane foam with a thickness of 3.8 cm is chosen for a tank containing 3000 kg of liquid hydrogen. However, as a recommendation, this exact thickness required for such a small application in the Greenliner should be evaluated.

5.7.5. Venting System

Since LH2 boil-off is expected during operation as the temperature difference inside and outside of the tank is very large, GH2 will generate as time passes. Consequently, the internal pressure is building up if no measure is taken. The

tanks should be maintained at a constant temperature. To achieve this, a pressure relief system with venting valves is required. For redundancy purpose, two valves should be installed, a primary valve and a secondary valve. The secondary valve has a slightly higher venting pressure than the primary valve. This is because in case of the failure of the primary valve, this pressure difference would indicates the abnormal conditions.

Furthermore, the transfer between the tank to the fuel cell is still to be designed. This transfer system is further elaborated upon in subsection 5.6.1. The nonintegral tank design is supported by struts, connected to the fuselage. The structural design of such struts are not considered here in the report, but they should be designed in such a way that the cryogenic tank can be easily removed and replaced.

5.7.6. Sustainability of Cryogenic LH2 and Tank
While using liquid hydrogen as fuel is far more environmental friendly compared to traditional aircraft fuel, the potential high cost of production and operation is still to be studied. The production of LH2 is discussed in subsection 10.2.2, where different production methods are discussed as well as different possible delivery methods that airport can use. The environmental effects of water and hydrogen emission are discussed in subsection 11.1.1. When using non-integral tank design, the aircraft production and maintenance can be comparable to conventional aircraft.

5.8. Auxiliary Power Unit
The Auxiliary Power Unit (APU) is a secondary power source within the aircraft that is not used for propulsion. On the ground, when the engines are turned off, it can be used to power the cabin lighting, air conditioning or cabin instruments. Whereas in flight the APU can be used to provide additional power to the engines in case of turbulence or manoeuvres. A downside of using the APU on the ground, however, is that the additional mass of energy storage and the power unit itself have to be carried in flight where it is not used. In order to save this weight and have lower production and depreciation costs the APU of the Greenliner will not be used during ground operations. In flight, on the other hand, the APU will be used in case the fuel cells require additional power in a short period of time.
In conventional aircraft the APU is a turbo shaft placed in the back of the aircraft. For the Greenliner, this system can not be applied as it brings about harmful emissions. Thus, a battery will be used. Specifically, a Li-S battery as this type offers a great specific energy, price and specific heat capacity [21].

5.8.1. On Ground
Since the APU is not used on the ground, another energy source is required. For this the aircraft will make use of a Ground Power Unit (GPU) provided by the airport. This can either be done by a portable electrical generator or via cabling present at the gate. Upon arrival at the gate, this GPU will be connected, allowing the fuel cells and the APU to be turned off, while also recharging the APU for the next flight.
One consideration is that it is now required that the airport be in possession of a GPU. As of now, many airports are already making use of these. Additionally, some airports are taking active actions against the noise and polluting emissions of APUs. Both at Heathrow [26] and Zurich [95], restricted APU times and proposed alternatives, such as the GPU and ASU is experimented with. Because of this trend, it is assumed that airports will be able to supply the Greenliner with energy on the ground.

5.8.2. In Flight
The Greenliner will have an APU that functions as a back-up to the fuel cells in flight. Normally, all the instruments in the cockpit, the cabin lighting and air conditioning will be powered by the fuel cells. However, when necessary the APU can power all of these. This is chosen as it forms a redundancy of power supply of the vital instruments. On top of this, the APU might also be needed to feed power to the fuel cell a peak power exceeding the maximum power output is required. These situations might occur when the aircraft is experiencing some heavy turbulence. The APU will be sized according to the estimate on power required to assist the fuel cells.

5.8.3. Sustainability
Both production and product costs will be lowered with the reduction in size and weight. Also, the production of the smaller battery will be less polluting than the production of a generic turbo shaft which powers the aircraft on the ground.

During operation, reduced mass means less fuel is consumed. Since batteries have a relatively low specific energy a smaller reduction in required energy can bring a significant reduction is mass of the APU. This means that the fact that

the APU is not used during ground operations can result in a lower fuel consumption, which also requires less hydrogen to be produced, benefiting the environment. Additionally, opting for a battery instead of a turbo shaft means the noise emission during the turnaround time will now be negligible, which is highly desired by airports. Economically, however, it will not be a major benefit, as the fuel reduction can be roughly negated by the cost of utilising the GPU and the corresponding labour [85].

At the end of life, the battery is also far easier to replace in the aircraft than a conventional turbo shaft in the rear of the aircraft would be. Recycling it, on the other hand, is slightly more costly because of the chemicals in the battery. This one downside, however, is by far out weighted by all of the benefits.

5.9. Tail and Control Surfaces

Stability and control are important aircraft characteristics, because it defines the missions it can fly.
Stability will be determined by tail sizing and wing positioning in subsection 5.9.1. Control will be assessed by sizing the control surfaces in subsection 5.9.2.

5.9.1. Tail Sizing

In order to minimise drag during cruise, it is optimal to have the smallest possible horizontal tail in combination with the best longitudinal main wing position. On the other hand, the horizontal tail needs to be large enough for the aircraft to be stable and small enough to be controllable. To determine the optimum horizontal tail surface, first an aircraft loading diagram is constructed to find the most front and aft aircraft centre of gravity positions, and then this is used in a scissor plot to find the optimal horizontal tail surface and the main wing position according to the method of Dr.ir. G. La Rocca, provided in [31].

Aircraft Ground Loading Diagram

When people, cargo and fuel are loaded in an aircraft, the centre of gravity (c.g.) shifts. In flight, the aircraft should be operable for each possible c.g. In order to find these most extreme centre of gravity positions, loading from the back to front and front to back is assessed:

Back to front sequence

1. Fill passengers starting in the back

    (a) Start with window seats back to front
    (b) Then middle seat in the back
    (c) Finally aisle seats back to front

2. Fill cargo bay
3. Fill with fuel

Front to back sequence

1. Fill passengers starting in the front

    (a) Start with window seats front to back
    (b) Then middle seat in the back
    (c) Finally aisle seats front to back

2. Fill cargo bay
3. Fill with fuel

To find the shift in c.g. during loading, the contribution of each component (cargo, individual passengers and fuel) is assessed:

$$\Delta cg = \frac{\sum x_i \cdot W_i}{\sum W_i} \tag{5.69}$$

This Δcg is then added to the cg_{OEW} for each component during loading to construct the loading diagram. Finally a 2% margin is added to account for in-flight variations (i.e. moving passengers, moving flight crew, etc.).

Scissor Plot

A scissor plot shows the relation between the horizontal tail size and the maximum allowable front and aft c.g. position to guarantee stability and controllability [31]. The most aft c.g. curve is generated by Equation 5.71: the stability equation. The controllability equation in Equation 5.70 determines the maximum allowable front c.g., as observable in Figure 5.33. In order for an aircraft to be stable and controllable, the cg-range that follows from the loading diagram has to be in the green area.

$$\bar{x}_{cg} = \bar{x}_{ac} - \frac{C_{m_{ac}}}{C_{L_{A-h}}} + \frac{C_{L_h}}{C_{L_{A-h}}} \frac{S_h l_h}{S \bar{c}} \left(\frac{V_h}{V} \right)^2 \tag{5.70}$$

$$\bar{x}_{cg} = \bar{x}_{ac} + \frac{C_{L_{\alpha_h}}}{C_{L_\alpha}} \left(1 - \frac{d\epsilon}{d\alpha}\right) \frac{S_h l_h}{S\bar{c}} \left(\frac{V_h}{V}\right)^2 - 0.05 \tag{5.71}$$
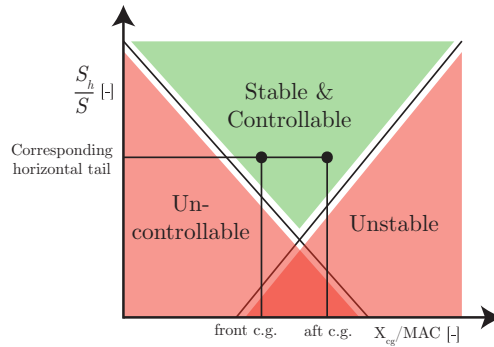
Figure 5.33: Layout of a generic scissor plot

Horizontal Tail Surface Area

The optimal size for the horizontal tail is the smallest possible size for which the aircraft is still both stable and controllable. As explained, the cg-range has to be in the stable and controllable region. To minimise the tail surface, the possibility exists to modify the longitudinal position of the wing (group) with respect to the fuselage, changing the cg at OEW and therefore the front and aft cg positions.

As can be observed in Figure 5.34, the smallest S_h/S occurs when the c.g. range line just intersects the scissor plot on both sides, (Figure 5.34c). This situation occurs for a certain main wing position which is thus used for the final design.
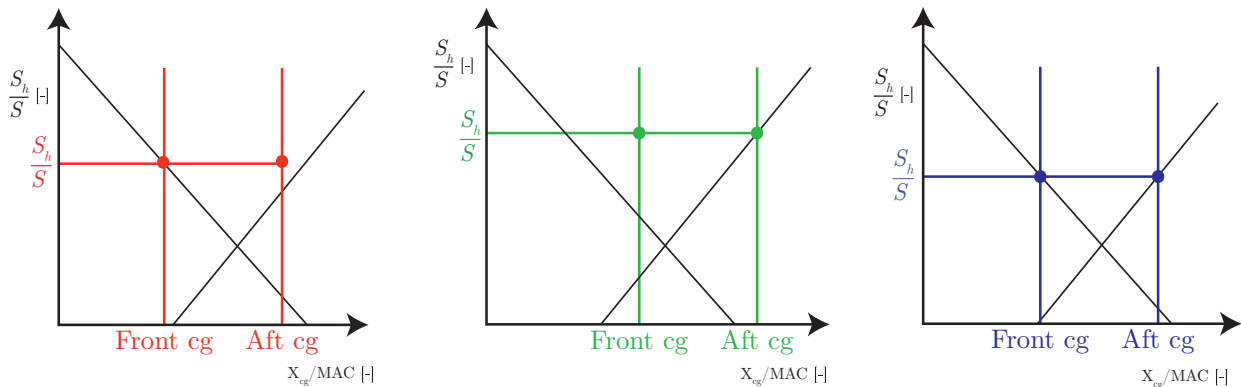
(a) Main wing position in front of optimal (resulting in high S_h/S)

(b) Main wing position aft of optimal (resulting in high S_h/S)

(c) Optimal position of the main wing: smallest S_h/S

Figure 5.34: Varying main wing longitudinal position, changing cg-range and determining S_h/S

Horizontal Tail Geometry

Now that the horizontal tail surface area is sized, the geometry can be determined. To determine the aspect ratio, quarter chord sweep angle, taper ratio, incidence angle, twist and dihedral, a comparable approach as for the main wing is used. First, an estimate for the given values is assumed. After that, the lift curve and drag polar are constructed to optimise the design. The results are presented in chapter 6.

For the estimation of the weight of the horizontal tail, Equation 5.72 is used [77]

$$W_h = 0.0379 K_{uht} (1 + \frac{F_w}{B_h})^{-0.25} W_{dg}^{0.639} N_z^{0.1} S_h^{0.75} L_t^{-1} K_y^{0.704} (cos(\Lambda_h))^{-1} A_h^{0.166} (1 + \frac{S_e}{S_h})^{0.1} \tag{5.72}$$

Vertical Tail Design

To estimate the vertical tail surface area, the tail volume coefficient (c_{vt}) is used. This coefficient for sizing takes into account wing parameters such as wing span and wing area but also the vertical tail length (L_{vt}). The equation for calculating the vertical tail surface is given in Equation 5.73.

$$S_v = \frac{c_v b_w S_w}{L_v} \tag{5.73}$$

The value of the vertical tail volume coefficient is based on statistical data from [77].

To determine the vertical tail geometry, data of reference aircraft is used [92]. From these reference aircraft, the aspect ratio (A_v), taper ratio (λ_v) and quarter chord sweep angle (Λ_v) are determined. Now that the $S_v, A, \lambda_v, \Lambda_v$ are known, parameters such as the vertical tail span, root chord and MAC can be calculated.

For the class II weight estimation, the weight of the vertical tail is computed. This is done with a weight estimation shown below Equation 5.74 [77].

$$W_v = 0.0026(1 + \frac{H_t}{H_v})^{0.225} W_{dg}^{0.556} N_z^{0.536} L_t^{-0.5} S_v^{0.5} K_z^{0.875} cos(\Lambda_{vt})^{-1} A_v^{0.35} (\frac{t}{c})_{root}^{-0.5} \tag{5.74}$$

5.9.2. Control Surfaces

The control surfaces are one of the last parts to be designed of an aircraft. They enable the Greenliner to perform manoeuvres, to take-off and land under harsh conditions and to trim it. Without control surfaces the aircraft will be very difficult to control. Due to the fact that a conventional airframe configuration is chosen, the control surfaces (aileron, elevator, rudder) will also be conventional. In this section, the control surfaces will be sized. This will be done by looking at the manoeuvres for which a specific control surface is used. Then, this flight condition is analysed and the equations of motion are determined from which the geometry can be calculated. First the aileron will be considered, then the elevator and at last the rudder.

An important parameter which is applicable to all three control surfaces is the control surface angle of attack effectiveness parameter (τ_s). It is a relation between the angle of attack and the deflection angle of the control surfaces for the major control derivatives. Equation 5.75 is the mathematical representation of the parameter as a function of the chord ratio of the control surface (C_S/C) [84].

$$\tau_s = \frac{0.8}{\sqrt{0.7}} \sqrt{\frac{Cs}{C}} \tag{5.75}$$

Aileron

The ailerons are the control surfaces positioned at the wing tips. Due to an increase of lift on one side and a decrease of lift at the other side, the aircraft produces a rolling moment, which in turn makes the aircraft roll as shown in Figure 5.35. This change in lift is produced by rotating the ailerons up and down, this rotation changes the shape of the airfoil. The aileron rotating down has a positive effect on the lift and the aileron rotating up a negative effect. From CS23 [24] the aircraft should be able to achieve a bank angle of 45° within 1.4 seconds, this will define the size of the aileron. The method used is from [68].
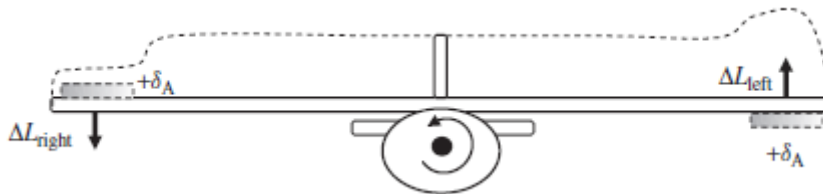

Figure 5.35: Front view of aircraft with displayed effect of aileron deflection [84]

Equation 5.76 gives the aerodynamic rolling moment as a function of aerodynamic pressure (q), wing area (S), wingspan (b) and rolling moment coefficient (C_l). C_l is a function of the aileron control derivative $C_{l_{\delta_A}}$, the roll damping coeffi-

cient C_{l_p}, the side slip angle and the rudder deflection. However, for these calculations, it is assumed that the aircraft is flying with zero side slip and no rudder deflection, so these coefficients are omitted from the equation. Then, δ_A is the aileron deflection, P the roll rate in rad/s and V the velocity in m/s. The rolling moment is zero because it is a function of the time rate of change of the roll rate which is assumed to be zero because of a steady roll rate.

$$L = qSbC_l = qSb\left(C_{l_{\delta_A}}\delta_A + C_{l_p}\frac{Pb}{2V}\right) = 0 \tag{5.76}$$

When Equation 5.76 is rearranged the following equation is derived:

$$P = -\frac{C_{l_{\delta_A}}}{C_{l_p}}\delta_A\frac{2V}{b} \tag{5.77}$$

The roll rate was given as a requirement and is 0.56 rad/s. Then the only unknowns are the aileron deflection, the aileron control derivative and the roll damping coefficient. These coefficients are given by Equation 5.78 and Equation 5.79.

$$C_{l_{\delta_A}} = \frac{dC_l}{d\delta_A} = \frac{2C_{l\alpha}\tau_a}{Sb}\int_{b_1}^{b_2} C(y)y\,dy \tag{5.78}$$

$$C_{l_p} = \frac{4\left(C_{l\alpha} + C_{d_0}\right)}{Sb^2}\int_0^{b/2} y^2 C(y)\,dy \tag{5.79}$$

The chord length as a function of wing location is given by Equation 5.80. This equation is a function of the geometry of the wing, with λ as the taper ratio.

$$C(y) = C_r\left[1 + 2\left(\frac{\lambda-1}{b}\right)y\right] \tag{5.80}$$

The aileron geometry is determined by an iterative process. To start the iteration, a first estimation of the geometry is required. Since flaps already have a large surface, it is assumed that the inboard location of the ailerons is just a bit further (5%) than the outboard location of the flaps. The outboard location of the ailerons is determined by the end of the wings but, as vortices are present at the wingtip which would disturb the flow over the ailerons, the aileron surface does not continue till the wingtip. The aileron chord is limited by the wingbox rear spar. The initial maximum aileron deflection is taken to be 12°. With these initial values the iteration can be performed until the requirement is met.

From the chord ratio the control surface effectiveness can be determined. With this effectiveness and the other geometry values the coefficients can be calculated. From the coefficients, the general wing geometry and the mission characteristics, the roll rate can be determined. Then the acquired roll rate can be compared to the required roll rate till the required roll rate is larger than the calculated one. The easiest adaptation when this is not the case, is the maximum deflection angle: with a new angle the roll rate can be calculated and compared again. However, there is a limit to the maximum deflection angle. This angle is at 25° and is limited by stall. When the iteration would require a larger angle than that, the other parameters can be tweaked, starting with moving the inboard location of the aileron closer to the flap.

Adverse yaw appears when using ailerons, caused by the higher induced drag due the higher lift coefficient at one wing and the lower induced drag at the other wing. This can be counteracted by deflecting the down deflected aileron less than the up deflected aileron. For this reason the maximum down deflection will be 25% less than the maximum up deflection.

Elevator
The elevator is positioned on the horizontal stabiliser, it causes a pitching moment when deflected. A positive deflection makes the aircraft pitch up and a negative deflection gives a pitch down moment. The elevator is used at take-off to let the aircraft pitch up when reaching the take-off velocity. It is also used during cruise for longitudinal trim. In the next section the elevator will be sized for these flight conditions using the method from [84].
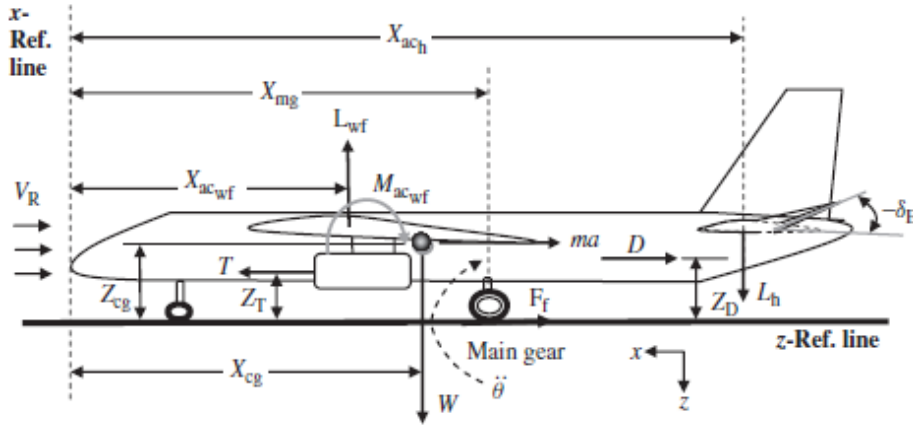
Figure 5.36: Side view of aircraft with present forces and moments at take-off [84]

For normal general aviation the rotation time at take-off is required to be between 1 to 3 seconds and the angular acceleration between 8 to 10 deg/s^2 [84]. For this flight condition the equations of motion are written down using Figure 5.36 in Equation 5.81, Equation 5.82 and Equation 5.83 (around the landing gear, where I_{yy} is the moment of inertia around the y-axis). From the equilibrium equations, the required lift from the horizontal stabiliser can be calculated. From Equation 5.84 the lift-coefficient (C_{L_h}) of the horizontal stabiliser can be acquired. V_R denotes the linear forward speed. In the most critical case this is the stall speed.

$$\sum F_x = m\frac{dV}{dt} = ma = T - D - F_f \tag{5.81}$$

$$\sum F_z = 0 = L_{wf} - L_h + N - W \tag{5.82}$$

$$\sum M_{cg} = I_{yy}\dot{\theta} = M_W + M_D - M_T + M_{L_{wf}} + M_{ac_{wf}} + M_{L_h} + M_a \tag{5.83}$$

$$C_{L_h} = \frac{2L_h}{\rho V_R^2 S_h} \tag{5.84}$$

As can be seen in Equation 5.85, C_{L_h} is a function of the angle of attack of the tail, the elevator deflection and geometry of the horizontal stabiliser. The airfoil of the tail is symmetric, which means that $C_{L_{h0}}$ is zero. $C_{L_{h_{\delta E}}}$ can be rewritten with the angle of attack effectiveness (τ_E) to a more general coefficient.

$$C_{L_h} = C_{L_{h0}} + C_{L_{\alpha_h}}\alpha_h + C_{L_{h_{\delta E}}}\delta_E = C_{L_{\alpha_h}}\alpha_h + C_{L_{\alpha_h}}\tau_e\delta_E \tag{5.85}$$

$$\alpha_h = \alpha + i_h - \epsilon \tag{5.86}$$

To determine the angle of attack of the tail Equation 5.86 can be used. Here i_h denotes the incidence angle of the horizontal stabiliser and ϵ the downwash angle produced by the main wing. Then this value can be implemented in Equation 5.85, with a first assumed value of the elevator deflection of -25°. Now, only one unknown is left in the equation, τ_e. After calculating this value, the elevator chord ratio can be obtained with Equation 5.75.

The next step is to trim the aircraft in cruise with the elevator (steady straight symmetric flight). For this, Figure 5.37 is used. The equations of motion are given in Equation 5.88, 5.87 and 5.89.

$$\sum F_z = 0 = L - W \tag{5.87}$$

$$\sum F_x = 0 = T - D \tag{5.88}$$
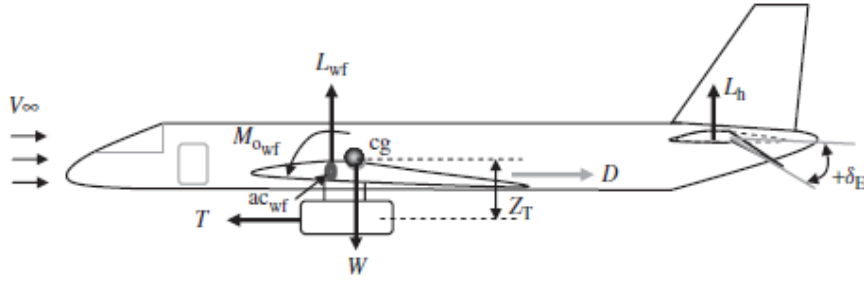
Figure 5.37: Side view of aircraft with present forces and moment at cruise [84]

$$\sum M_{cg} = 0 = M_A + Tz_T \tag{5.89}$$

For a straight flight the lift is thus equal to the weight. This can be rewritten in the lift formula and put down in non-dimensional derivatives. The same accounts for the moment equation. These equations are displayed in Equation 5.90 and 5.91. The elevator effectiveness is given by three non-dimensional derivatives ($C_{m_{\delta E}}$, $C_{L_{\delta E}}$ and $C_{L_{h_{\delta E}}}$), from the first two derivatives the equations are given in 5.92 and 5.93. $\bar{V}_h$ denotes the horizontal tail volume, which is a function of the tail length, volume and mean aerodynamic chord and η_h is the dynamic pressure ratio between the main wing and tail wing (normally between 0.85 and 0.95). After calculating these two values only two unknowns are left in Equation 5.90 and 5.91, the elevator deflection and the angle of attack. Now, the trim elevator deflection can be calculated for different velocities.

$$W = qSC_L = qS\left(C_{L_0} + C_{L_\alpha}\alpha + C_{L_{\delta E}}\delta_E\right) \tag{5.90}$$

$$0 = qS\bar{C}C_m + Tz_T = qS\bar{C}\left(C_{m_0} + C_{m_\alpha}\alpha + C_{m_{\delta E}}\delta_E\right) + Tz_T \tag{5.91}$$

$$C_{m_{\delta E}} = \frac{\partial C_m}{\partial \delta_E} = -C_{L_{\alpha_h}}\eta_h \cdot \bar{V}_h \cdot \frac{b_E}{b_h}\tau_e \tag{5.92}$$

$$C_{L_{\delta E}} = \frac{\partial C_L}{\partial \delta_E} = C_{L_{\alpha_h}}\eta_h\frac{S_h}{S}\frac{b_E}{b_h}\tau_e \tag{5.93}$$

The maximum and minimum velocity give the maximum elevator deflections, only these will be considered for the design of the aircraft. The required elevator deflection versus the velocity can be displayed in a graph, which is included in the flight manual. It gives the pilot information on how to trim the aircraft at different velocities.

Now, only thing left is to check if the horizontal stabiliser does not stall when the elevator is deflected maximally at take-off, the elevator namely has a negative influence on the stall angle of attack. The angle of attack at take-off can be calculated with Equation 5.94. Then this value can be compared to the stall angle of attack which can be obtained from Equation 5.95. $\Delta\alpha_{h_E}$ is the decrease in stall angle of attack caused by the elevator deflection and is obtained from empirical values [84]. When the stall angle of attack turns out to be smaller than the take-off angle of attack, the aircraft is considered as uncontrollable and a redesign of the horizontal stabiliser or landing gear should be considered.

$$\alpha_{h_{TO}} = \alpha_{TO}\left(1 - \frac{d\epsilon}{d\alpha}\right) + i_h - \epsilon_0 \tag{5.94}$$

$$\alpha_{h_s} = \pm\left(\alpha_{h_{s:\delta E=0}} - \Delta\alpha_{h_E}\right) \tag{5.95}$$

Rudder

The rudder is the control surface on the vertical stabiliser. It is the main contribution to control a yawing manoeuvre. When the rudder is deflected a side force is generated by the tail, this provides a yawing moment around the centre of gravity. The rudder should be able to counteract the moment created by the engines when one-engine (or multiple engines) is inoperative, this is a way to size the rudder (from [84]). However, since the engines will probably be placed

on the fuselage this effect will not be very decisive for the aircraft controllability. Furthermore, the aileron also has an effect on yaw, which makes it difficult to get an outcome only for the rudder. So for the rudder geometry the rudder geometries of reference aircraft are also be considered.
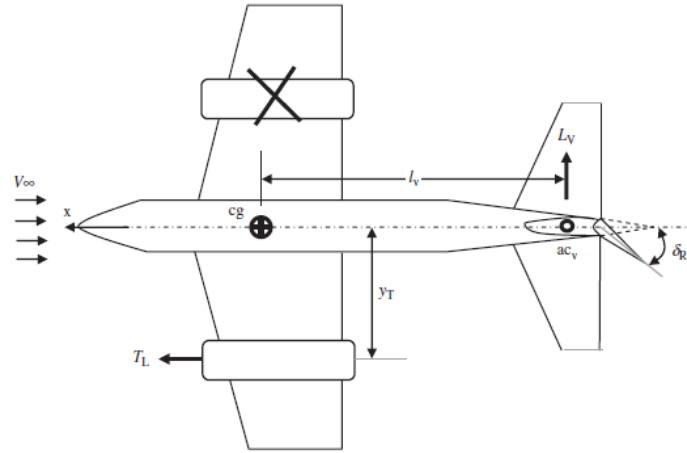
Figure 5.38: Top view of aircraft with present forces with one-engine inoperative and rudder deflection [84]

Figure 5.38 shows the forces which are present when one-engine is inoperative and the rudder is deflected. The equation of motion for the moment around the centre of gravity is given by:

$$\sum N_{cg} = 0 = T_L y_T + L_v l_v \tag{5.96}$$

The moment from the vertical tail is a function of the aircraft geometry, sideslip, aileron deflection and rudder deflection. For this flight condition there is no sideslip angle, the aileron is not deflected and it is assumed that the aircraft is symmetric. So that gives the final expression in Equation 5.97. $C_{n_{\delta R}}$ is the directional control derivative given in Equation 5.98 and it is dependent on the size of the vertical tail, rudder and on the vertical tail volume ($\bar{V}_V$). For the rudder span ratio it can be assumed that it is one, the rudder spans the whole vertical tail. This is taken from references and will later be validated.

$$L_v l_v = N_A = qSb\left(C_{n_0} + C_{n_\beta}\beta + C_{n_{\delta A}}\delta_A + C_{n_{\delta R}}\delta_R\right) = qSbC_{n_{\delta R}}\delta_R \tag{5.97}$$

$$C_{n_{\delta R}} = \frac{\partial C_n}{\partial \delta_R} = -C_{L_{\alpha_V}}\bar{V}_V\eta_V\tau r\frac{b_R}{b_V} \tag{5.98}$$

After rearranging, Equation 5.99 can be obtained, which gives the rudder deflection as a function of the control derivative and the thrust moment. As this aircraft will have distributed propulsion, it is interesting to calculate the rudder deflection when all the engines at one side of the aircraft become inoperative, this will give the most critical case and thus the maximum required rudder deflection.

$$\delta_R = \frac{\sum_{i=1}^n T_{Li} y_{Ti}}{-qSbC_{n_{\delta R}}} \tag{5.99}$$

5.10. Landing Gear

The landing gears have to be positioned carefully to allow the steering capability of the nose wheel while maintaining stability in preventing any tipping over of the aircraft in any direction. Additionally, the gears have to be sized in such a way to be able to withstand the high impacts occurring during landing.

5.10.1. Landing Gear Selection

It is decided whether the landing gear should be retractable or not. After this, the gear arrangement will be determined.

Retractability Trade-Off

This first trade-off is between a retractable and fixed landing gear. For the retractable landing gear, the gear is stowed in either the wing or fuselage after take-off. A fixed landing gear, on the other hand, will remain in the same position during all phases of the flight.

The main trade-off is done based on the lower weight, complexity and maintenance costs of the fixed gear versus the minimal drag of the retractable gear. For smaller aircraft with shorter ranges the fixed gears are most often opted for. However, bigger and faster aircraft will generally always make use of retractable gears to remove this additional drag component.

In general, aircraft that fly with a cruise speed above 150 nautical miles an hour have retractable gears as the drag penalty is far greater than the negative consequences in terms of structural weight and maintenance costs [80]. Since the Greenliner has a cruise speed of around 270 nautical miles an hour, which is significantly greater than 150, the retractable gear is selected. This means that in the design, the space required for the stowing of the landing gear has to be taken into account as well as the accessibility for maintenance.

Gear Arrangement Trade-Off

Several arrangements for landing gears are used in aircraft design. The most common are: tricycle, bicycle (with outriggers) and tailgear configurations. Each different configuration has its pros and cons, which are graded in Table 5.7, the scores are taken from [80] and adapted.

Table 5.7: Gear arrangement trade-off table. Scoring: 3: Good, 2: Medium, 1: Poor [adapted from [80]]

	Gear type	Weight	Tricycle	Bicycle	Tailwheel
Weight		4	2	1	3
Ground operations	Stability during groundloop	1	3	2	1
	Steering after touchdown	1	3	2	1
	Steering while taxiing	1	2	2	1
Passenger comfort	floor attitude on the ground	2	3	2	1
take-off difficulty	visibility over the nose	0.3	3	3	1
	Take-off rotation	0.3	2	1	2
	Take-off procedure	0.3	3	3	2
	Weighted average		**3.1**	**2.0**	**2.3**

The configurations are assessed on, from most to least important and linearly weighted: total mass (weight 4), ground operations (weight 3), passenger comfort (weight 2) and take-off difficulty (weight 1). A final score is determined by multiplying the weight by the score and taking the average of the sum. In a sensitivity analysis of the weighting factors, it is concluded that in all combination of the four weighting factors (24 different combinations), the best option is the tricycle landing gear, therefore this is selected.

5.10.2. Landing Gear Sizing

With the configuration of the landing gears, they can now be sized accordingly. This is done with two assumptions for the calculations. Firstly, in order to account for impurities in materials and uncertainties in operations, a safety factor of 1.07 [80] is applied to the forces induced by the impact of landing and the friciton forces of braking. Secondly, the nose landing gear will take 10% of the MTOW to enable the steering capability [80].

Strut Sizing

On top of the static loads during the operations on the ground, struts have to carry a greater load during the braking in the landing phase. Both the nose and main landing gears will endure a moment because of the friction force between the wheels and the runway. Also, while braking, the nose wheel will be subjected to an additional force as the momentum change causes the aircraft to lean forward.

In order to evaluate the stresses within the struts it is necessary to establish assumptions on the loads induced by the braking which is the most critical loading case. The forward horizontal force on the wheels because of the braking is equal to 0.2 times the static load [18] and the dynamic vertical load on the nose gears due to the braking motion is

equal to 1.5 times the static load [80].

The total stress in the struts can then be calculated according to Equation 5.100, where the struts are assumed to be cylindrical shaped with a radius R, area A and moment of inertia I. Then, for the specific yield strength of the material, the minimum radius of the strut can be computed.

$$\sigma_{strut} = \frac{F_y}{A} + \frac{MR}{I} \tag{5.100}$$

Because of the high impacts on the landing gear, the material used in the struts should have a relatively high strength. Combining this with striving for low weight, a high strength-to-weight ratio is desired. The perfect material in this case is titanium, which is 45% lighter than steel with the same strength [21]. The main disadvantage is however the cost of titanium, which is significantly higher than that of steel. In the end, because struts are not expected to be a major component of the aircraft in terms of weight, Ti-10V-2Fe-3Al has been selected as the alloy for the struts, as this alloy has an ideal combination of strength, ductility, fracture toughness and fatigue cycle strength [40].

Shock Absorber Sizing

The shock absorber is the most important part of the landing gear. Without it absorbing the kinetic loads, the gear would break during landing. Generally, three different shock absorbers exists for aircraft: a solid, a fluid or a combined solid-fluid shock absorber. The solid has the lowest efficiency, the combined the best and the fluid has an efficiency that is in between the two others. Since the Greenliner is a relatively small and lightweight aircraft, the advantage of using a simple, reliable, easy to maintain and low cost solid-spring absorber outweighs the cost penalty [18]. This decision is strenghtened by the fact that the comparable Twin-Otter uses the same shock absorber.

In order to estimate the shock absorber size, the necessary shock stroke has to be determined. A conservative estimate for the shock stroke in meters (not taking into account tyre deflection) is presented in Equation 5.101 (adaptation from [36]).

$$S = \frac{V_{sink}^2}{2gN\eta_s} \tag{5.101}$$

The most common load factor (N) used during landing is 1.2 [36] and the shock absorber efficiency is 60% [18]. The sink speed (V_{sink}) comes from regulations [36].

Since the maximum thickness of the rubber disks should not exceed 1.5 inches [18], the amount of disks can now be deduced from the required shock stroke. The diameter of the shock absorber can be estimated with Equation 5.102 [80], in which P_m is the maximum static load per main gear.

$$d_s = 0.041 + 0.0025\sqrt{P_m} \tag{5.102}$$

Since now the volume is known, the weight of the shock absorber can be calculated making use of the densitiy of rubber ($1255 kg/m^3$ [22]). The shock absorber is placed conventionally, as can be observed in Figure 5.39.

Tyre Sizing

Besides carrying the loads between the ground and the aircraft, the tyres also have the important function of protecting the runway. This also means that the intended runway surface influences the tyre selection process. The maximum tyre pressure depends the intended runway surfaces. In order to be able to land at as many airports as possible, the tyre pressure is selected to be able to land on at least small tarmac runways with poor foundation. The corresponding maximum pressure is equal to $5 kg/cm^2$, or $70 psi$ [80]. Higher pressure tyres can not lower the impact of the landing aircraft enough to sufficiently protect the runway.

Then, for the main landing gear, the tyres are selected based on the combination of the static load and the maximum pressure. For the front tyres, on the other hand, the maximum dynamic loads are considered. Finally, the tyres can be selected using the combination of the load and the inflation pressure with the method presented by Torenbeek [92].

---

[21]Retrieved from `https://www.dorsetware.com/steel-vs-titanium/` [Accessed 7 June 2018]

[22]Retrieved from: `https://www.aqua-calc.com/page/density-table/substance/rubber-coma-and-blank-manufactured` [Accessed 6 June 2018]
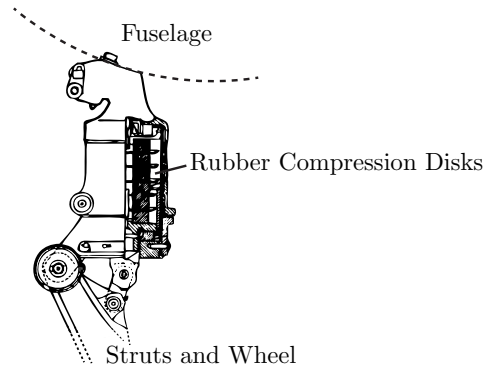
Figure 5.39: Shock absorber placement, adapted from [18]

5.10.3. Landing Gear Disposition
Enabling the steering capability of the nose wheel is not the only way the landing gear has to be positioned. There are also several phenomena that have to be prevented by carefully placing the undercarriage.

Lateral Tip-Over
While the aircraft is turning on the ground, the c.g. will move in the lateral direction. If it moves beyond one of the struts of the main landing gear, the aircraft may tip over. To avoid this, the wheelbase must be sufficiently wide. This is calculated according to Equation 5.103 [80], where for hard surfaces the lateral tip-over angle $\psi = 55°$. In the equation l_n and l_m are the distances from the c.g. to the nose and main landing gears respectively and h_{cg} is the height of the c.g. from the ground.

$$y_{MLG} > \frac{l_n + l_m}{\sqrt{\frac{l_n^2 tan^2\psi}{h_{cg}^2} - 1}} \tag{5.103}$$

Longitudinal Tip-Back
In the moments before take-off the aircraft will tip back. If the undercarriage has not been properly positioned it is possible that the c.g. will then be more aft than the main landing gear. In this case the aircraft will uncontrollably tip back and scrape over the floor. Note that conventionally the corner of the tailcone will be the critical point that can scrape the runway. The Greenliner, on the other hand, has propellers around the tailcone shifting the critical point to the propellers on the bottom side of the fuselage.

To prevent the aircraft from uncontrollably tipping back, the angle between the vertical and the line through the landing gear and the c.g. shall be at least 15° [80]. This will be implemented in the integrated design.

Additionally, in case the propellers do touch the runway it is important that the aircraft can be easily tipped forward again. To allow this, the scrape angle has to be smaller than the tip-back angle meaning the aircraft will inherently want to tip forward.

5.10.4. Braking
Aircraft brakes are used primarily for stopping the aircraft during landing. The factors that influence the braking capability are the diameter of the braking disks and the material used [18].

In order to stop the aircraft, the kinetic energy has to be dispersed. Having the same assumptions as Currey [18] (250 stops at design landing weight (with 10 ft/s^2 deceleration), 5 stops at maximum landing weight (with 19 ft/s^2 deceleration) and a single rejected take-off (RTO) stop (with 6 ft/s^2 deceleration) at the maximum take-off weight) and using the semi-empirical formulas (eqs. (5.104) to (5.106)) from Currey [18], the mass, in *lb*, of the brake system per wheel is found:

$$W_{brake,RTO} = -0.1581 \cdot E_{K,RTO}^2 + 6.8971 \cdot E_{K,RTO} \tag{5.104}$$

$$W_{brake,5stops} = -0.375 \cdot E^2_{K,maxlanding} + 10.5 \cdot E_{K,maxlanding} \tag{5.105}$$

$$W_{brake,250stops} = -0.9746 \cdot E^2_{K,Landing} + 20.699 \cdot E_{K,Landing} \tag{5.106}$$

The final brake weight per wheel is then found by averaging these weights. Furthermore, the brake volume, in cubic inches, can be approximated with Equation 5.107 [18].

$$V = 2.625 W_{brake} \tag{5.107}$$

If the volume is found, the rim diameter of the brakes can be found making use of Heerens, p23 [36]. If carbon brakes are used instead of steel, the volume increases by a factor 1.28 and the weight decreases by a factor 2.5 [36]. Since weight plays an important role in this project, carbon brake plates are selected. In normal conditions (no icy runway), landing distance is shorter than take-off distance[23], it is assumed that if the brakes are sized with the presented method, it will comply with the landing distance requirement.

5.10.5. Recommendations
Furthermore there are several aspects that are recommended to be analyse further in the detailed design phase:

- Heat build up during braking
- Brake cooling
- Skid control
- Elaborate on different load cases presented by EASA (such as one-wheel landing, lateral drift landing, etc.)

5.10.6. Sustainability
In terms of production, the chosen materials do not achieve a great financial sustainability. Both titanium and carbon fibre, the primary materials in the landing gear, are costly products to purchase and manufacture.

When considering the operational period, the landing gears perform better. The retracted landing gears mean less noise is produced and thus released to the environment and the passengers inside. Additionally, the carbon fibre in the brakes is more corrosion resistant than conventional metals, lowering maintenance times and costs.

Another benefit of the chosen material is the long lifetime. This will postpone the end of life of a product, increasing the sustainability. There is, however, one more downside to using carbon fibre which is that the percentage that can be recycled is lower than for conventional metals. However, with the usage of carbon fibre constantly increasing, there is also a lot of research being done into more efficient recycling. Because of this, in the future carbon fibres and other composites are expected to perform much better in terms of their recyclability [72].

5.11. Solar Panel Feasibility
The addition of solar panels to the aircraft will extend the operational range but will also add weight to the aircraft. To check if solar panels on the aircraft would increase the range of the Greenliner, a back-of-the-envelope feasibility study is conducted. Also, the economics are analysed to check if it is a good idea economically.

5.11.1. Theoretical Power Output
The theoretical available area for installing solar cells is the entire upper side of the aircraft. The wing and tail areas are known, for the fuselage a cylinder of constant diameter over the entire cabin length is assumed (Equation 5.108).

$$A_{total} = A_w + A_h + \frac{l_{cabin} \cdot (\pi \cdot d_{fus})}{2} \approx 68m^2 \tag{5.108}$$

The average solar irradiance reaching earth is 1361 W/m^2. Currently, solar panels have an efficiency of 14%[24]. Therefore a theoretical power output of 55 kW is acquired (Equation 5.109).

---

[23]Retrieved from `https://www.skybrary.aero/index.php/Landing_Distances` [accessed 2nd July 2018]

[24]Retrieved from `https://news.energysage.com/what-are-the-most-efficient-solar-panels-on-the-market/` [Accessed 22 June 2018]

$$P_{theoretical} = \eta_{panel} \cdot 1361 \cdot A_{total} = 0.14 \cdot 1361 \cdot A_{total} \approx 13 kW \tag{5.109}$$

5.11.2. Solar Panel Selection

As weight is a driving issue for aerospace, it is important to select a lightweight solar panel. Currently, solar panels are being developed that weigh 3.6 g/m^2[42] with about the same efficiency as conventional, glass-based solar cells[25]. For the area calculated in subsection 5.11.1, this yields 342 grams, since this is a prognosis and just the panel weight, a large safety factor of 10 is used to account for the other components (Maximum power point tracker, wiring, inverters, battery management system, shunts, etc). The weight becomes 3.42 kg. Still, this is not a lot and it is considered negligible with respect to the aircraft weight.

5.11.3. Range Including Solar Panel

Since the Greenliner needs about 1400 kW for cruise, and the solar panels produce 13 kW, this is only 0.9% of the total required power. A preliminary value for the extra range is calculated by assuming a linear relationship between power available, OEW and range. It is assumed that OEW does not change, so the relation reduces to Equation 5.110. For the current power settings the Greenliner is able to travel 500 nm, when solar panels are installed the new theoretical range is 520 nm.

$$Range_{new} = \frac{P_{old} + P_{Panel}}{P_{old}} \cdot Range_{old} \approx \frac{1400 + 13}{1400} \cdot 500 = 505 nm \tag{5.110}$$

So, when assuming a very small weight and a 14% efficiency, one would be able to extend the range by approximately 1%.

5.11.4. Economics

Another option to increase the range is to simply bring more hydrogen. For small fuel increments it is assumed that the OEW does not change and that for a 1% more range, 1% more hydrogen is needed. It is assumed that liquid hydrogen costs about \$4,- per litre. Furthermore it is assumed that the lifetime of the solar panels is 20 years[26], therefore the aircraft over a span of 20 years is assessed. For the amount of flights in this 20 year period, the following assumptions have been made:

- The flight hours are between 06:00 and 22:00
- Average flight time is 1.25 h [8]
- Turnaround time is 45 minutes [46]
- The aircraft will be used 365 days a year

These assumptions render the amount of flights over the 20 year span, resulting in 58400 flights. These values are reasonable when compared to other aircraft [27].

$$N_{flights} = \frac{hours_{day}}{T_{avg,flight} + T_{turnaround}} \cdot days_{year} \cdot years = \frac{16}{1.25 + 0.75} \cdot 365 \cdot 20 = 58400 \tag{5.111}$$

When assuming \$4.-/kg for the liquid hydrogen section 12.4, the amount of money one is able to save if solar panels are installed is:

$$C_{H_2} = 1\% \cdot M_{H_2} \cdot C_{H_2/kg} \cdot N_{flights} = 1\% \cdot 150 \cdot 4 \cdot 58400 = \$350,400.- \tag{5.112}$$

In order to compare this to the cost of the solar panels, the price of the photovoltaics is calculated. Current photovoltaics cost 3\$ per watt[28]. Therefore:

$$C_{pv} = P_{solarpanels} \cdot \$3 = 13,000 \cdot \$3 = 39,000.- \tag{5.113}$$

Therefore, under the assumption that the solar panels do not add additional weight and do not increase the operational costs, it is possible to save about $350,000 - 39,000 = 311,000$ USD. Therefore it is recommended to add solar panels to the Greenliner. Also, since a lot of assumptions are being made it is also recommended to conduct a better study.

---

[25]Retrieved from `https://www.livescience.com/54192-ultrathin-lightweight-solar-cells.html` [Accessed 2nd June 2018]

[26]Retrieved from `http://energyinformative.org/lifespan-solar-panels/` [Accessed 22 June 2018]

[27]Retrieved form `https://www.telegraph.co.uk/travel/travel-truths/a-week-in-the-life-of-a-plane/` [accessed 26 June 2018]

[28]Retrieved from `https://www.solarreviews.com/solar-panels/cost-of-solar-panels-per-watt/` [Accessed 22 June 2018]

Final Design Results

After the integration of all subsystem sizing methods presented in chapter 5 into the general iteration method shown in chapter 4, resulting values for the main system parameters of the Greenliner could be obtained, which are presented in section 6.1. After an examination of the resulting system interfaces in section 6.2, the sensitivity of the final results is examined in section 6.3.

6.1. Final Sizing Results of the Design

After a description of the convergence of the final design along with the values of the main parameters, the results of the most important subsystem sizing methods are presented in this section.

Weight Convergence of the Final Design

Using the iteration process explained in Figure 4.1, the Greenliner converges to a final preliminary design after 10 iterations with a convergence threshold of 0.05 %, corresponding to about 2 kg in empty mass. The evaluation of the OEM during this process is shown in Figure 6.2. The final values are **4410 kg for the OEM** and **63500 N for the MTOW**. A rendering with an accurate presentation of the dimensions of the final design is shown in Figure 6.1.
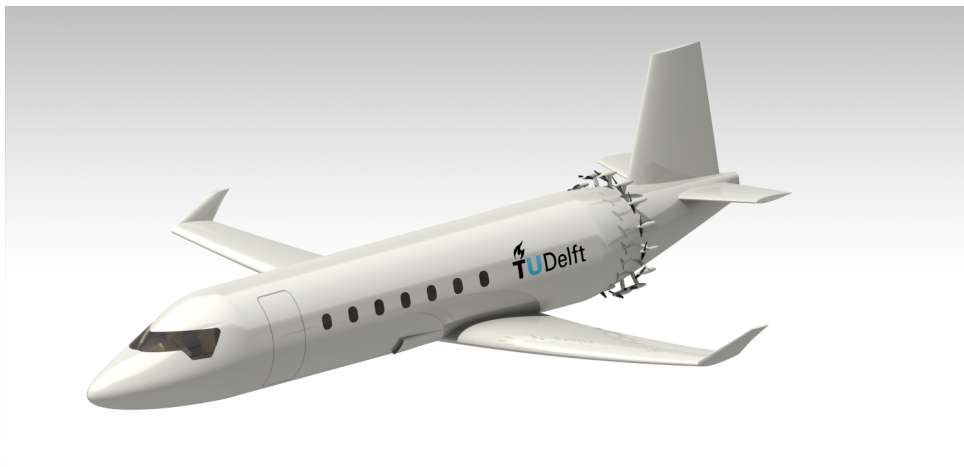
Figure 6.1: Rendering of the final design of the Greenliner. The actual dimensions are used in this model, even though the image as it is presented in the report is not to scale.

The first value, labelled "iteration 0" corresponds to the preliminary estimates obtained through simple statistical relations from Class I estimation methods. After that, a steep increase in OEM can be observed, which is caused by the first Class II estimate of the weight. In each subsequent iteration, the difference in OEM to the subsequent iteration decreases, until the specified threshold is reached. In Figure 4.1, this effect can be observed from the horizontal asymptote which the curve approaches. The initial peak created by the first iteration indicates that there is a clear difference between the empty weight estimates between the Class I & II methods. After this peak, the curve becomes more smooth, since only one method is now used.

Another reason for this seemingly smooth convergence is the fact that most variables such as the wing reference area or the hydrogen mass change continuously, since not only integers but all real numbers are allowed. However, there is

one important variable which does change in a discrete way, which is the number of propellers. Although this cannot be clearly seen in Figure 6.2, this value changes from 27 in the first iteration to the final value of 23 in the fifth iteration, going through discrete steps in between. Still, this can be used as a secondary explanation to why the slope is highly negative in the first few iterations, since the mass of a complete propeller and electric motor assembly is saved each time.

Resulting Fuselage Design
The final results for the sizing of the fuselage are presented in Table 6.1. While the (outer) diameter was set to a fixed value based on the number of seats abreast in section 5.1, the length changes continuously during the iterations, mainly due to change in tank length. It should also be noted that the nose length relates to the length of the non-cylindrical part at the front of the aircraft, while the tail length relates to the same length at the back of the aircraft. These parameters depend directly on the fuselage diameter through a specified fineness ratio and are therefore fixed as well.

Table 6.1: Final results for the sizing of the fuselage.

Parameter	Value	Unit
Total fuselage length	16.72	[m]
Fuselage diameter	2.2	[m]
Nose length	3.3	[m]
Tail length	4.4	[m]

Resulting Wing Design
Table 6.2 contains the final results for the wing, obtained during the overall sizing process. While the wing reference area and the wing span change continuously during the iteration, the other parameters presented in the table depend on preliminary design decisions, as shown in section 5.4. Finally winglets were added to the wing to reduce vortex drag and increasing lift creating area, therefore improving lift-to-drag ratio, increasing aerodynamic efficiency [30].

Table 6.2: Final results for the sizing of the wings.

Parameter	Value	Unit
Wing reference area	25.9	[m^2]
Wing span	16.1	[m]
Aspect ratio	10	[-]
Taper ratio	0.4	[-]
Quarter chord sweep angle	0	[deg]

Resulting Empennage Design

In Table 6.3, the final results for the sizing of the empennage, i.e. the vertical and horizontal tails, are shown. Similarly to the wing, only the surface area and span are changed continuously during the iterations.

Table 6.3: Final results for the sizing of the empennage.

Parameter	Value	Unit
Horizontal tail surface area	5.95	[m^2]
Horizontal tail span	6.05	[m]
Horizontal tail aspect ratio	4	[-]
Horizontal tail taper ratio	0.6	[-]
Horizontal tail three-quarter chord sweep angle	0	[deg]
Vertical tail surface area	5.29	[m^2]
Vertical tail height	2.82	[m]
Vertical tail aspect ratio	1.5	[-]
Vertical tail taper ratio	0.5	[-]
Vertical tail three-quarter chord sweep angle	0	[deg]

Resulting Propulsion System Design

Table 6.4 shows the final values of the main design parameters of the propulsion system. Although the number of propellers can only assume discrete values, it is not fixed and can still change during the iterations. Furthermore, the propulsion system mass includes all elements of the system, i.e. the motors, propellers, shafts, gears and fairings.

Table 6.4: Final results for the sizing of the propulsion system.

Parameter	Value	Unit
Number of propellers	23	[-]
Propeller radius	0.16	[m]
Propulsion system mass	446	[kg]

Resulting Fuel Cell System & Hydrogen Tank Design

In Table 6.5, the values for the final design of both the fuel cell system and the hydrogen tank are shown. Regarding the fuel cell volume, it should be noted that the available volume inside the wing, taking into account the restrictions by the front and back spar, is about 2.6 m^3. The fuel cells therefore easily fit into the wing, as initially decided.

Table 6.5: Final results for the sizing of the fuel cell system and hydrogen tank.

Parameter	Value	Unit
Total hydrogen mass	151	[kg]
Fuel cell system mass	526	[kg]
Fuel cell volume	0.767	[m^3]
Fuel cell area	174	[m^2]
Fuel cell maximum produced power	1.43	[MW]
Inlet area	0.0615	[m^2]
Tank mass	148	[kg]
Tank length	2.59	[m]

Resulting Landing Gear Design

Below, in Table 6.6, the final result of the landing gear design is shown. The total mass includes both the main and the nose landing gear and all additional systems such as the brakes, hydraulics and tyres. The strut length is measured from the ground to the beginning of the cylindrical part of the fuselage, at full shock absorber compression.

6.2. System Interfaces

The interfaces between various subsystems are presented in this section.

Table 6.6: Final results for the landing gear design.

Parameter	Value	Unit
Distance nose to nose landing gear	2.35	[m]
Distance nose to main landing gear	9.85	[m]
Strut length (ground to fuselage)	0.95	[m]
Total landing gear system mass	105	[kg]
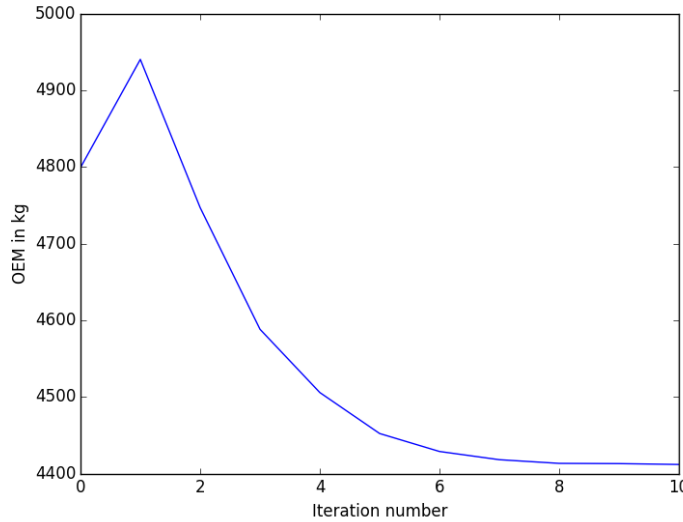
Figure 6.2: Graph showing the estimated OEM after each iteration.

Electrical Block Diagram

The electrical system layout shown in Figure 6.3 illustrates the flow between the electrical components of the Green-liner. This diagram has been updated since the previous report [21]. The power required for the propulsion system is now divided between the engines and the active intake.

Data Handling Block Diagram

The data handling diagram shows the way data is processed and used in the aircraft. The diagram is presented in Figure 6.4. Avoiding a massive diagram, two branches are giving as an example of the data handling. Firstly, the navigational branch is presented. Every five seconds the location is automatically broadcast through the *Automatic Dependant Surveillance - Broadcast* (ADS-B), made then available for everyone. The main advantage of this system is the fact that this can contain a lot of information such as flight information from airports, weather reports and traffic
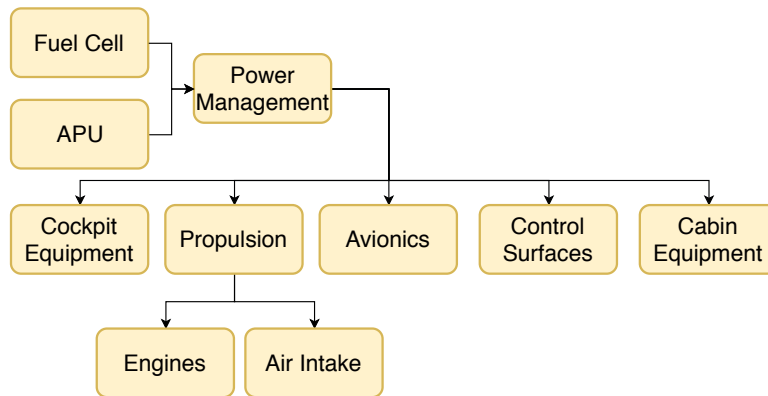
Figure 6.3: Electrical System Block Diagram
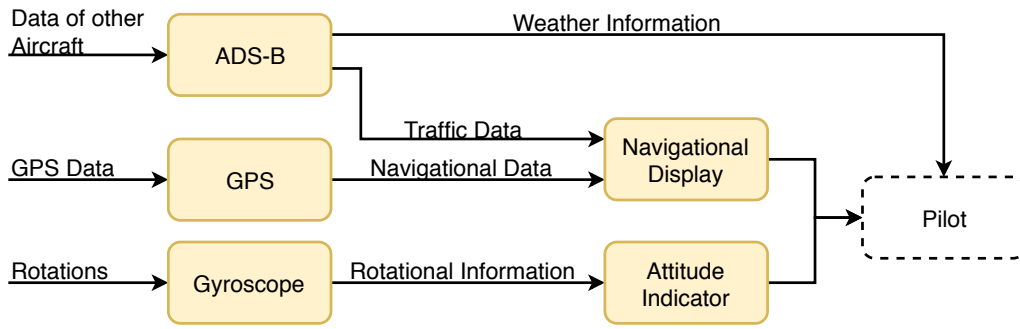
Figure 6.4: Data Handling Block Diagram
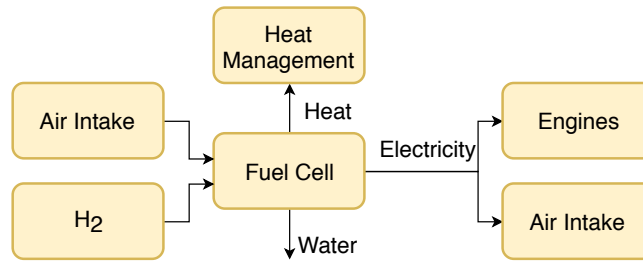
Figure 6.5: Fuel System Block Diagram

information broadcast by other aircraft. As the name suggests, the ADS-B is dependant however, on a GPS navigation source. Another system to be included in this branch is the TCAS. This was however omitted for the purpose of this example. And finally, the gyroscope is providing the data on the attitude of the aircraft, which is the second branch.

Fuel System Layout

The layout of the fuel system is given in Figure 6.5. It shows the two inputs into the fuel cell, namely the hydrogen from the tank and the air that is brought in via an the intake. As a product of the reaction in the fuel cell, water is produced, which is simply disposed of during flight. Also, heat is produced within the system. This will be managed and can possibly be used to maintain the temperature of the fuel cell. Finally, the produced electricity will mainly be used for the propulsion system via the engines and for the active air intake.

Hydraulics System Layout

The hydraulics system layout consists of a simple feedback loop, which is given in Figure 6.6. Beginning with the input of the pilot or possibly the autopilot, the controller acts on an actuator which in turn applies the required external load. During this process, the feedback loop continues to monitor if the desired external load has been applied.

Environmental Control System Layout

The environmental control system is the system which monitors and controls the environment within the cabin. It controls the pressure, temperature, air supply, smoke detection and so on. The layout of the system is given in Figure 6.7. The aforementioned parameters are measured by the system after which the values are compared to reference values to determine whether they are critical. The process is looped if the values are non-critical and the corresponding control units are activated in case the values are critical.

Figure 6.6: Hydraulics System Block Diagram of the Greenliner

Figure 6.7: Environmental Control System Block Diagram of the Greenliner

Figure 6.8: Hardware Block Diagram of the Greenliner

Hardware and Software Block Diagrams

In order to gain an overview of the interrelation of hardware and software components, a Hardware Block Diagram and a Software Block Diagram is constructed. In the Hardware Block Diagram, the different hardware components are shown together with the pilot and their interrelation. The same is done for the different software components in the Software Block Diagram. The Hardware Block Diagram is shown in Figure 6.8, and the Software Block Diagram is shown in Figure 6.9.

6.3. Sensitivity Analysis

To investigate the feasibility of the final design, a sensitivity analysis is done. This analysis varies the key requirements and looks at the impact on the aircraft characteristics. The requirements whose impact on the design parameters are investigated are the range and the runway length. In order to assess the sensitivity, three output parameters are considered: OEM, MTOW, and the liquid hydrogen mass.

The approach to the analysis is as follows: One of the input parameters is varied from -10% to +10% of its original value, the design iteration is redone for each new parameter value and the corresponding percentage change in output parameters is then examined. A categorisation of the sensitivity level is given by Table 6.7

Both increasing and decreasing the runway length was found to have no impact on the design parameters within the investigated range. The sensitivity of the design to runway length is therefore categorised as negligible. This result has two possible causes. Firstly, the runway length is not limiting for the design and therefore does not influence the output parameters when changed. The second explanation is that runway length is not fully integrated into every design aspect. It is explicitly used in the takeoff and wing loading calculations, in which it might not be limiting, but the runway length can of course also be limiting in the landing phase. In that case, high lift devices may need to be

Figure 6.9: Software Block Diagram of the Greenliner

Table 6.7: Categorisation of sensitivity levels of the response to a change in input

Response to a 10% input change	Sensitivity level
< 1%	Negligible
< 5%	Small
< 10%	Significant
< 20%	Large
> 20%	Extreme
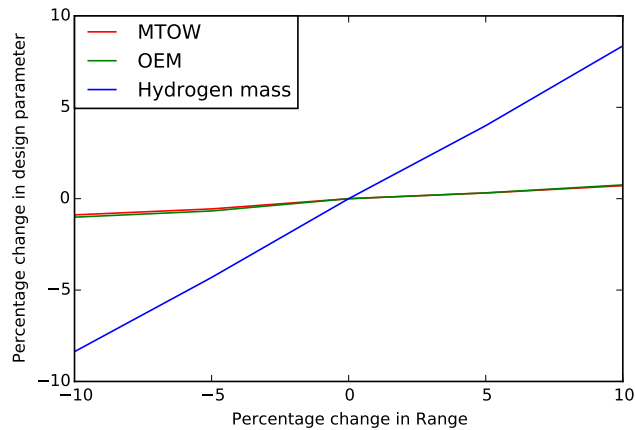
Figure 6.10: Sensitivity of design parameters to changes in range

redesigned, and the aspect ratio increased to provide the required aileron moment to cope with this change. The fact that this parameter is of negligible influence in the current calculations is cause for further investigation in future development phases.

The influence of range variations on the design parameters can be seen in Figure 6.10. This effect is close to linear. As expected, the hydrogen mass sensitivity to a change in range is significant. However, it scales by less than a full one-to-one ratio. This is as expected, because the requirement for reserve fuel does not change. The sensitivity of MTOW and OEM to a change in range is classified as negligible to small. This can be explained by the fact that hydrogen mass is actually a small fraction of the total mass, much smaller than the fuel fraction of a conventional aircraft. The 8 % increase in hydrogen mass shown in the graph, for example, only constitutes a 12 kg increase in fuel mass. Of course, the tank mass also increases slightly, which explains the higher OEM.

Overall, the system responds as expected to changes in requirement inputs. A recommendation for further development is to take more input and output factors into account.

7

Aircraft Performance

After presenting the final design parameters and values for the sizing of the Greenliner, the resulting performance can now be analysed. First, the flight profile will be investigated in section 7.1. This is followed by an analysis of the aerodynamic characteristics in section 7.2 and of the structural and material characteristics in section 7.3. Next, the stability and control performance of the aircraft is checked in section 7.4, after which the noise produced during operation is analysed in section 7.5. Finally, the resource allocation and budget breakdown are reviewed in section 7.6.

7.1. Flight Profile

Normally at this stage of the design, the final design parameters of the aircraft are run through the mission profile for the first time in order to assess the performance of the system. However, the design approach taken with the Greenliner already includes this assessment in the iteration, as explained in chapter 4. The results of the final iteration through the flight profile are shown here, including a payload-range diagram and an assessment of the climb performance.

Flight Profile Diagram
Figure 7.1 shows the complete flight profile of the Greenliner, with the altitude plotted on the vertical axis versus the distance travelled on the horizontal axis. It can be seen from the flight profile that the Greenliner is capable of completing the required 500 nmi (925 km) mission . The ideal cruise altitude is 12 000 m, calculated through the method explained in section 4.2.
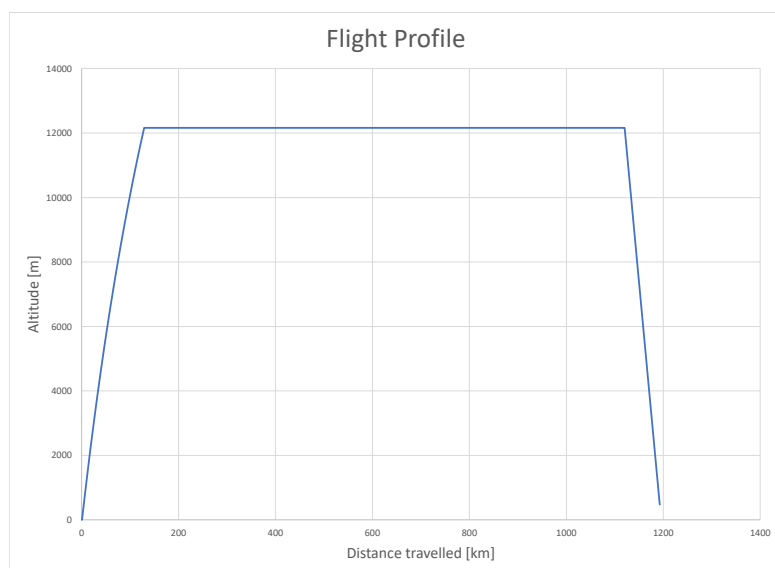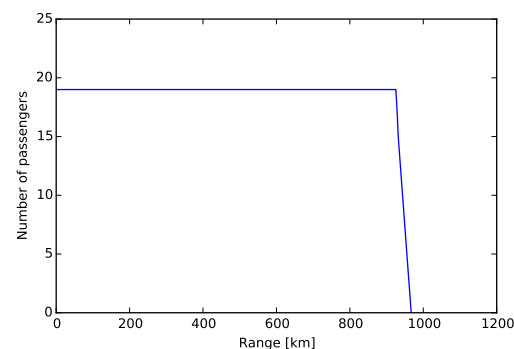

Figure 7.1: The flight profile of the Greenliner

Figure 7.2: Payload vs range diagram of the Greenliner aircraft

81

Payload - Range Diagram

For a hydrogen powered aircraft, constructing a Payload Range diagram takes a slightly different approach compared to conventional configurations. The total energy density of the storage system is considerably lower than that of kerosene based aircraft. However, a very small fraction of the storage mass is actually the hydrogen itself, of which the specific energy is high. This means that the mass fractions over the different mission phases all approach 1. Additionally, the energy storage system is not likely to be designed for more than the required range. While a conventional aircraft can quite easily design the fuel tanks to have a volume higher than required for the mission, the hydrogen storage capacity is limited and drives the total mass of the storage system to a significant extent. The assumption is therefore made that there is no possibility to trade passenger weight for fuel weight. Therefore the only benefit to the range of decreasing passenger number is the reduction in aircraft takeoff weight and thus the required energy for the mission. In Figure 7.2, the effect of removing passengers on the range can be seen.

In the assessment of climb performance, two parameters of interest are examined: Firstly, the average rate of climb in the climb phase, and secondly, the service ceiling of the aircraft. The average rate of climb can be simply calculated by the following equation:

$$RC_{avg} = \frac{h_{cruise}}{t_{climb}}, \text{with} \tag{7.1}$$

$$h_{cruise} = 12000m \tag{7.2}$$

$$t_{climb} = 825s \tag{7.3}$$

This leads to an average rate of climb of 14.8 m/s, or in a more conventional figure: close to 3000 ft/min.

7.1.1. Climb Performance

To determine the service ceiling, the maximum altitude is examined at which the aircraft can fly. This altitude is calculated by examining the condition for zero maximum rate of climb, derived from Equation 4.1:

$$P_{req} = P_a \tag{7.4}$$

When increasing altitude, the air density decreases, and thus the airspeed required for providing lift increases. This leads to the increase in required power shown in Figure 7.3. At the same time, the available power decreases with altitude, again because of the decrease in air density which reduces the mass flow through the propellers. The intersection of the two curves yields a theoretical ceiling of 12 210 m. However, to leave room for manoeuvring at cruise, the service ceiling is set at the altitude that allows a maximum rate of climb of 100 ft / min. The service ceiling is determined to be 11 980 m through this method, which is marginally lower than the cruise altitude determined through the mission profile. This means the aircraft is capable of flying at cruise altitude, but in order to allow for manoeuvres in cruise, the propeller sizing should be increased. This is a recommendation for further design.
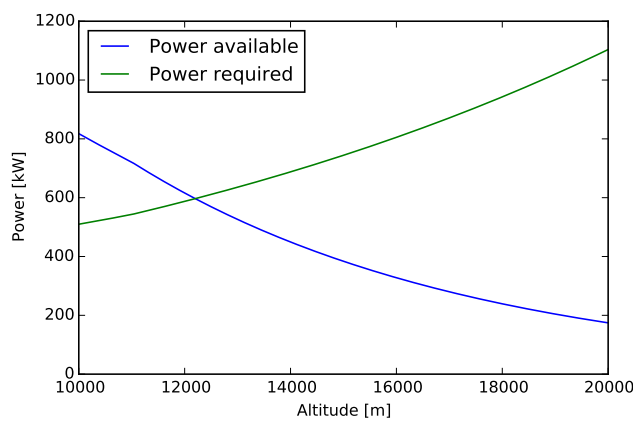

Figure 7.3: Power available and power required plotted against cruise altitude

7.2. Aerodynamic Characteristics

To assess the Greenliner's lift and drag performance, a lift curve and a drag polar are constructed, as described in section 5.4. The optimised results are shown in Figure 7.4 and Figure 7.5. From the lift curve, it can be deduced that the maximum lift coefficient is 1.44 and occurs at an angle of attack of 17 °. Also, the drag polar shows the best C_L over C_D ratio of 14.2 at the design lift coefficient, 0.94, which corresponds to an angle of attack of 9.2 degrees.
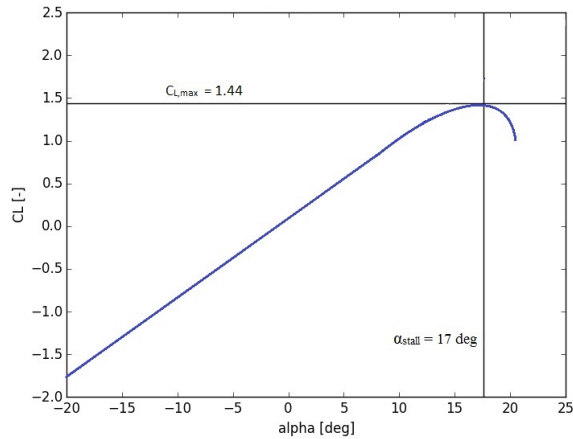
Figure 7.4: Greenliner Lift Curve
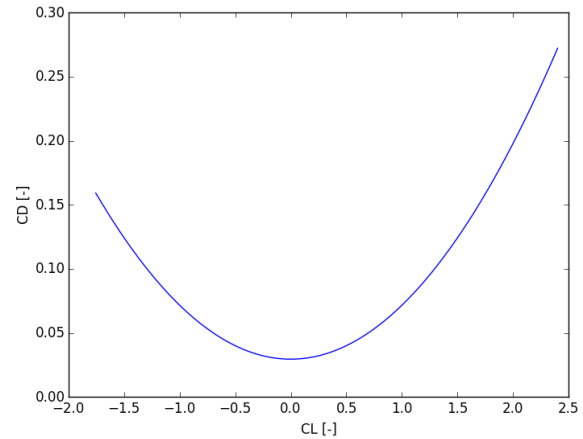
Figure 7.5: Greenliner Drag Polar

7.3. Structural & Material Characteristics

In order to further justify the feasibility of the design, the chosen materials are discussed and a structural analysis is performed on the wings and fuselage.

Material Characteristics

For every selected material, the usage on the aircraft is discussed and the important physical properties are evaluated, such as the yield and fatigue strength. The material properties are also linked to the usage of the specific part when applicable. The three alloys that are primarily used are compared in Table 7.1 [1].

Alloy	σ_y [MPa]	σ_f [MPa]	E [GPa]	ρ [kg/m^3]
Al 2024-T3	345	138	73.1	2780
Al 2119-T62	290	103	73.1	2840
Ti-10V-2Fe-3Al	1160	1270	107	4650

Table 7.1: Physical properties of the used materials

Aluminium Alloys

Aluminium alloys are the most used material in the Greenliner. They can be found in parts such as the fuselage, the wings and the hydrogen tank. This is mainly due to the fact that it is a relatively cheap material that can be easily recycled. Additionally, the material is not only lightweight, but also corrosion resistant. The outer layer oxidises with oxygen which then creates a thin protective layer preventing further corrosion. Because of this, it is excellent to use for the fuel tank minimising the damage from oxidation.

Titanium Alloys

The only parts to use a titanium alloy are the struts of the landing gear. This expensive material has the advantage of being extremely strong while being lightweight. From Table 7.1 it can be deduced that per unit weight Ti-6Al-4V is 60% stronger than Al 2024-T3. Additionally, the fatigue strength is 2.3 times greater per unit weight. As a result the material is ideal for the high impacts that occur during landing.

---

[1] Retrieved from `http://www.aerospacemetals.com/contact-aerospace-metals.html` [Accessed 26 June 2018]

Usage of Composites

Notably, no major part of the Greenliner is made out of composites. Despite the advantageous physical properties, there are several reasons why this is the case.

To begin with, the usage of composites is still relatively new compared to metals and estimation and analysis methods are therefore less readily available, compared to metal alloys. If found, these methods are often highly complex and don't produce results with high confidence. Since the Greenliner is a proof-of-concept for emission free flying with a heavy focus on the propulsion, it was opted to make use of more traditional materials.

Additionally, as much more is known these conventional aerospace materials, they are also generally easier and more efficient to recycle, which contributes positively to the sustainability of the Greenliner.

Finally, an added benefit is that metals, especially aluminium alloys are often cheaper. This again positively influences the compliance with the requirement that the aircraft shall not be more than 25 % more expensive than a comparable conventional aircraft.

7.3.1. Structural Characteristics

In order to evaluate the structural characteristics, a structural analysis is performed. This analysis will provide the structural arrangement, loading diagrams and stress distributions for both the wing and the fuselage.

Wing

Firstly, the structural arrangement is made following the steps provided in subsection 5.4.5. The final arrangement is shown in Figure 7.6. The rear spar has been positioned at 57.5 percent chord to leave enough room in front of the control surfaces for the hinge placement. This is fairly far forward, as the rear spar is normally between 65 and 75 percent of the chordline [79]. The front spar is usually positioned between 15 and 30 percent of the chordline [79]. Since the rear spar is relatively far forward, the front spar has been positioned at 15 percent chord.
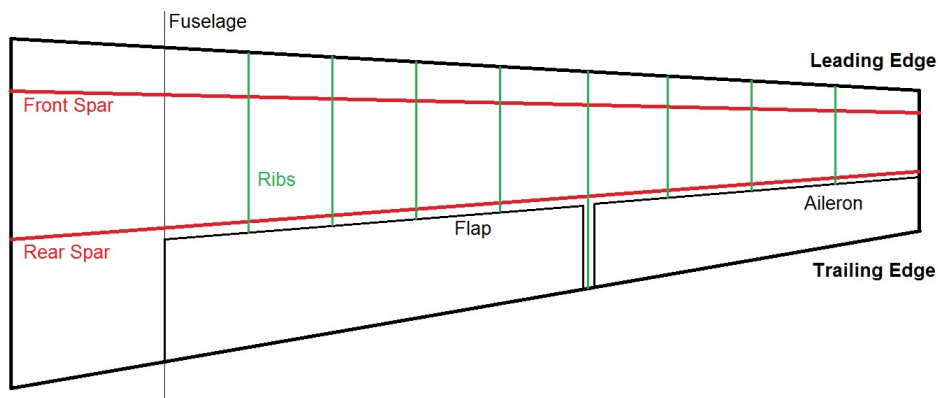
Figure 7.6: Structural arrangement of the wing

The next step is to determine the loads on the wing. For this the lift is first modelled as an elliptical lift distribution as shown in Equation 7.5 [7]. Γ_0 is the circulation at the wing centre at $x = 0$, which is calculated in such a way that the integral of the equation over the entire wingspan is equal to the lift.

$$L'(x) = \rho V_\infty \Gamma_0 \sqrt{1 - \left(\frac{2x}{b}\right)^2} \tag{7.5}$$

The stress relief due to the weight of the wing is neglected, which also results in a more conservative analysis. Then, integration of the lift distribution results in the experienced shear within the wing. Another integration yields the internal moment distribution. These results are shown in Figure 7.7. These values are including the ultimate loading factor of 3.8 to which the structure is sized. It is assumed that the ribs and the skin will carry the torques and that the bending moment is the main loading of the wing. Also, it is assumed that the bending moment will be carried by the spars, modelled as two I-beams. The final step is to compute the corresponding bending stress within the wing. This
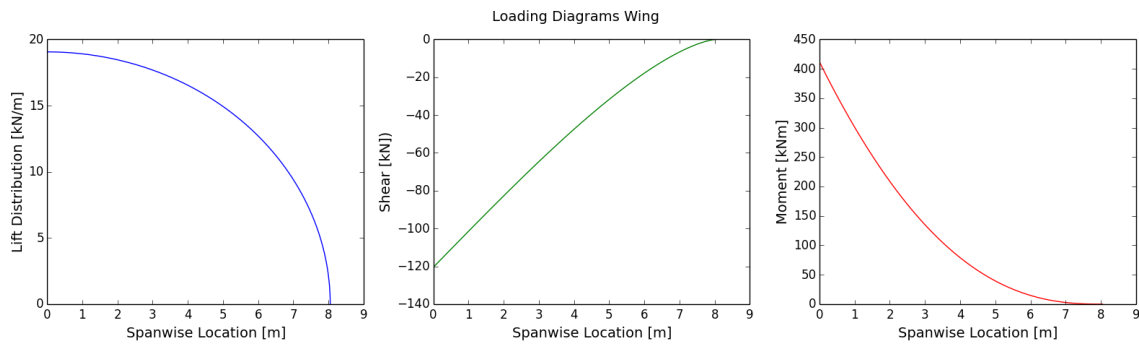
Figure 7.7: Loading diagrams of the wing versus the spanwise location

is done using the moment distribution and Equation 7.6, where M is the bending moment, y is the distance from the neutral line and I is the moment of inertia of the cross-section.

$$\sigma = \frac{My}{I} \tag{7.6}$$

Then, including the ultimate load factor, the required thickness at the root is calculated so that the maximum stress in the cross-section just reaches the yield strength of the Aluminium Alloy 2024-T3, namely 345 MPa [2]. This yield strength should just be reached as to not over design the structure and make it unnecessarily heavy. Then, the dimensions of the spar are varied linearly along the wing corresponding to the taper ratio. The resulting maximum stress distribution is presented in Figure 7.8. It can be seen that the maximum stress at the root is equal to the yield strength when the ultimate loading factor is applied.
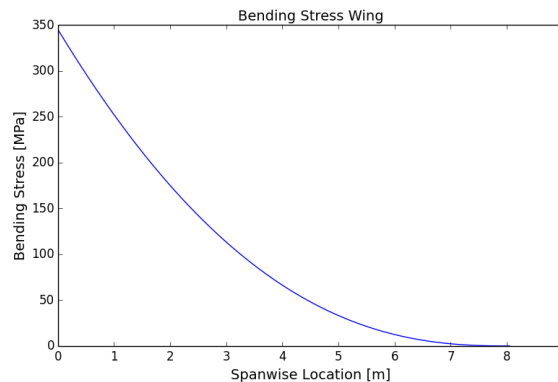
Figure 7.8: Maximum bending stress in the wing versus the spanwise location

Fuselage
For the fuselage the structural analysis is performed on the stresses carried by the skin. These stresses are caused by the bending of the fuselage due to the downwards gravity and upwards lift and also due the pressurisation of the fuselage.

For the bending moment, the weight of the aircraft is assumed to be evenly spread throughout the length of the fuselage, creating an evenly distributed force downwards. Then, the wing produces the same amount of force upwards as the total force downwards, with an additional moment to keep the aircraft levelled. The resulting loading diagrams are shown in Figure 7.9. The jump in the shear diagram is because of the lift of the wing and the jump in the moment diagram is due to the moment of the wing. Then, the stress in the skin can be calculated using Equation 7.6.
The pressurisation of the fuselage causes a pressure difference that acts on the skin. Older generations of aircraft kept the cabin pressurised at a pressure comparable to that of an altitude of 2400 m, but newer aircraft such as the Boein

---

[2]Retrieved from `http://www.amesweb.info/Materials/Aluminum-Yield-Tensile-Strength.aspx` [Accessed 21 June 2018]
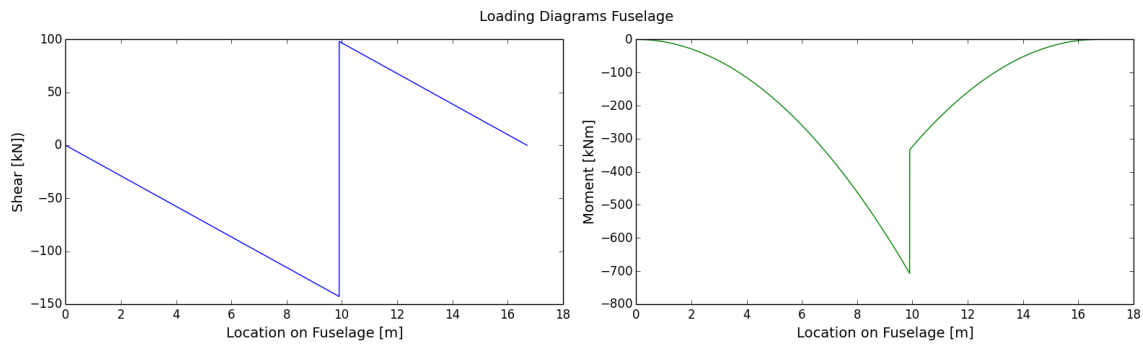
Figure 7.9: Loading diagrams of the fuselage versus the longitudinal position from the nose

787 are pressured at the pressure of 1800 m for an increased level of comfort [86]. This pressurisation causes stresses in three ways as presented in Figure 7.10[3]. The radial stress is simply equal to the pressure difference and is negligible as this will never be higher than 1 atm, or around 100 kPa. The circumferential, or hoop stress can be calculated using Equation 7.7 and the axial stress can be calculated using Equation 7.8, where Δp is the pressure difference, R is the fuselage radius and t is the skin thickness.
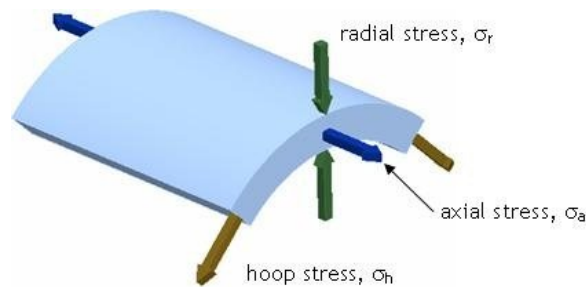
Figure 7.10: Radial, hoop and axial stresses due to pressurisation of the fuselage

$$\sigma_{circ} = \frac{\Delta pR}{t} \tag{7.7}$$

$$\sigma_{axial} = \frac{\Delta pR}{2t} \tag{7.8}$$

For the stress analysis of the fuselage the stresses of the bending and the axial stress due to pressurisation are added together, whereas the circumferential stress is evaluated separately as this acts in the perpendicular direction. Sizing the fuselage skin, again using the ultimate loading factor and the material property, the required skin thickness is only 0.45 mm. However, the skin needs relative hardness to be protected against impacts such as stones or debris on the ground. Therefore, a skin thickness of 1 mm is opted for, which is also easier to produce than a very thin skin. This then results in the stress distributions given in Figure 7.11.

7.4. Stability & Control

The stability and control characteristics of the Greenliner are assessed in subsection 5.9.1. First, the loading diagram is constructed, then the scissor plot. With these two graphs, the optimal longitudinal wing position and the horizontal tail size is determined. The loading diagram can be found in Figure 7.12a and the scissor plot can be found in Figure 7.12b. The results are summarised in Table 7.3.

The values in Table 7.3 are used to size the horizontal tail. As explained, the optimum wing position and the corresponding optimum horizontal tail surface occurs when the intersection of the vertical lines with the controllability and stability curves are on the same line. As can be seen in Figure 7.12b, this is (almost) the case. The results are presented in Table 7.2.

---

[3]Retrieved from `https://www.quora.com/What-is-radial-tangential-and-axial` [Accessed 21 June 2018]
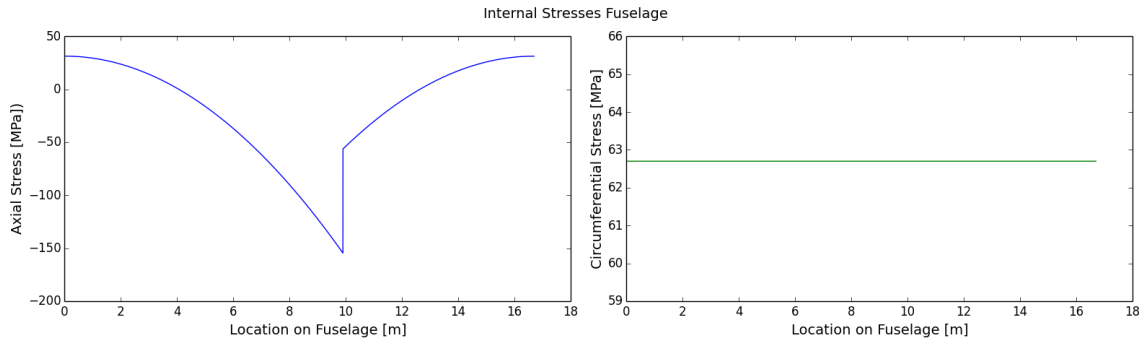
Figure 7.11: Maximum internal stresses in the fuselage versus the longitudinal position from the nose

(a) Greenliner loading diagram

(b) Greenliner scissor plot
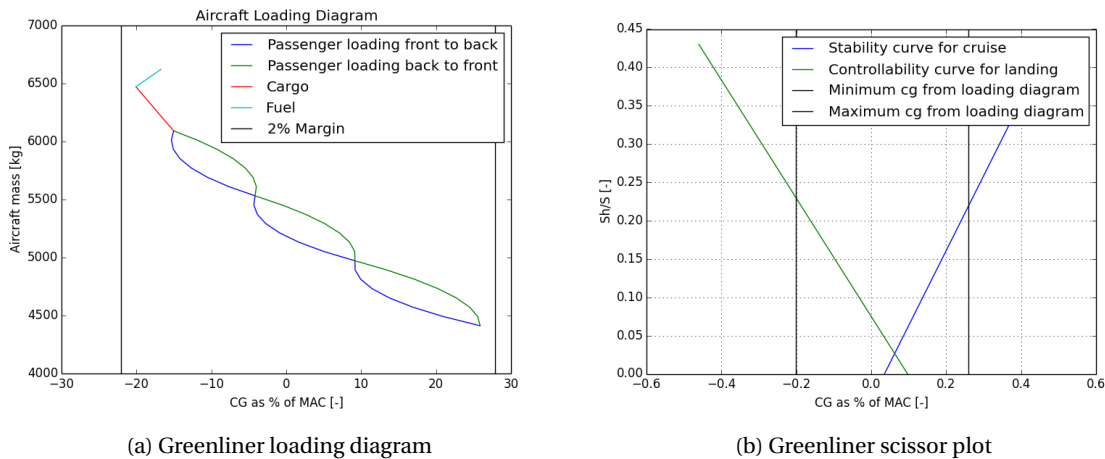
Figure 7.12: Assessing stability and control for the Greenliner

7.5. Noise

In this section, the reasoning and methods for estimating the noise level are explained. After that, the results are presented and checked against the noise requirements.

ICAO has developed noise regulations to which every aircraft should comply in order to be allowed to fly. Based on ICAO regulations, system requirement GF-STK-GOV.1-n was formed, as mentioned in section 2.2. This requirement specifies that the Greenliner should comply to ICAO noise regulations which are given in ICAO Annex 16 Volume I.

7.5.1. ICAO Regulations

The maximum take-off noise level depends on the aircraft development year and maximum take-off weight. Furthermore, noise can be defined in several ways. To meet the noise requirement mentioned above, a closer look has to be taken into ICAO Annex 16 Volume I. Chapter 10, section 10.4.a of this document states all noise regulations a propeller-driven aeroplanes not exceeding 8618 kg and developed after 1988, should comply to:

ICAO Annex 16 Volume I, 10.4 a)
for aeroplanes specified in 10.1.2 and 10.1.4, a 76 dB(A) constant limit up to an aeroplane mass of 600 kg varying linearly from that point with the logarithm of aeroplane mass until at 1400 kg the limit of 88 dB(A) is reached after which the limit is constant up to 8618 kg [71].

This noise level is measured at the take-off reference point: the point on the extended centre line of the runway at a distance of 2500 m from the start of take-off roll [71]. From the mission profile, the exact conditions during every second of take-off can be extracted. Taking into account that the measurement reference point lies at a distance of 2500 m from the start of take-off roll, the instant at which the aircraft is closest to that reference point can be determined. The distance between this instant and the reference point is used as an input for to calculate the highest

Table 7.2: Extreme c.g. values (including 2% margin) during loading and the c.g. at OEW for the Greenliner.

	% MAC	Loading conditions
Most forward c.g. position	-22%	After all the passengers and cargo are loaded
Most aft c.g. position	28%	c.g. at operation empty weight (incl. margins)
C.g. at Operational Empty Weight	26%	

Table 7.3: Horizontal tail size and wing position parameters for the Greenliner

Ratio horizontal tail surface / main wing surface (S_h/S)	0.23 [−]
Main wing surface (from section 5.4)	26 m^2
Longitudinal position main wing w.r.t. the nose	8.6 m
Horizontal tail surface	6 m^2

noise level the Greenliner is emitting. The A-weight is applied because the human ear perceives a different loudness at different frequencies because the ear is less sensitive to low audio frequencies [10].

7.5.2. Noise Estimation Method

Various researches demonstrated that there are two factors that contribute most to aircraft noise: engine noise and (aerodynamic) airframe noise [48]. An estimate for the component noise distribution is shown in Figure 7.13. Because of the fact that high noise levels dominate the total aircraft noise, only engine noise (including propeller noise and motor noise) and airframe noise are estimated and added to determine the Greenliner's noise level.
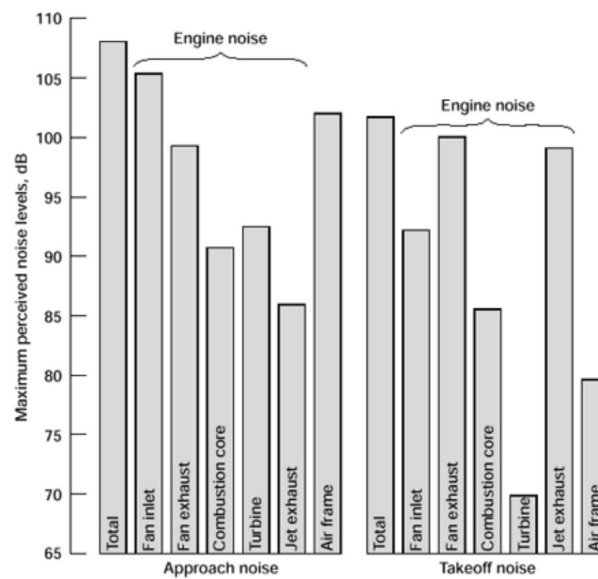
Figure 7.13: Component noise distribution of the Greenliner

Propeller Noise

NASA has developed a method for estimating the far-field sound pressure level (SPL) of propellers, which will be used to estimate the noise level of the propellers on the Greenliner [57]. This method consists of 9 steps:

1. Obtain a reference level L_1 from figure B-2 in [57] based on shaft power.

2. Calculate the correction factor for the number of blades (B_{prop}) and propeller diameter (D_{prop}).

$$Correction_B = 20log(\frac{4}{B_{prop}}) \tag{7.9}$$

$$Correction_D = 40log(\frac{15,5}{D_{prop}}) \tag{7.10}$$

3. Obtain the propeller rotational speed correction factor from figure B-3 from [57], based on rotational speed (Ω_{prop}), tip Mach number (M_t) and the distance from radial reference point to the propeller disc (Z).

4. Obtain the sound propagation correction factor from figure B-8 from [57], based on the angle with the heading of the propeller (θ).

5. Calculate the normal spherical spreading of sound correction factor, based on the distance from the centre of the propeller (r).

$$Correction_{soundpropagation} = -20log(r-1) \tag{7.11}$$

6. Sum the values of steps 1.-5. which gives the SPL at the point of interest.

7. Calculate the fundamental blade passage frequency (f_0) and obtain the corresponding harmonic distribution correction factor from figure B-6 from [57].

$$f_0 = \frac{B*n}{60} \tag{7.12}$$

Now subtract the harmonic distribution correction factor from the SPL obtained in step 6. to obtain the harmonic level.

8. Categorise the frequencies in preferred octave passbands and obtain the octave band levels by adding the correction factors of fig. B-7 from [57] to the highest harmonic level obtained in step 7.

9. Obtain the correction factor for attenuation due to molecular absorption of sound in air using the values in figure B-9 from [57]. Subtract this correction from the octave band levels obtained in step 8. to determine the corrected octave band levels in [dB].

The result of this step is a list of octave band levels for each preferred octave passband in decibels. In order to compare this noise level to regulations (which are given in dBA), A-weights have to be applied to the octave band levels. This is done by adding the A-weight described by Equation 7.13 and Equation 7.14 to the octave band levels. The maximum noise level of the propellers is then the maximum A-weighted octave band level.

$$R_A = \frac{12194^2 * f^4}{(f^2 + 20.6^2)\sqrt{(f^2 + 107.7^2)(f^2 + 737.9^2)(f^2 + 12194^2)}} \tag{7.13}$$

$$A = 20log(R_A) + 2.00 \tag{7.14}$$

Electric Motor Noise
From measurement data, a general formulation for predicting motor noise is developed in [17]. This method estimates the electrical motor noise level as a function of shaft power (P_{shaft}), shaft rotational speed (Ω_{shaft}) and the conformal surface area (S) in A-weighted decibels (dBA). Equation 7.15 shows the equation for an electric motor with less than 40 kW shaft power at a measurement distance of 1 m.

$$SPL_{A_{motor}} = 16 + 17log(P_{shaft}) + 15log(\Omega) + 10log(S) \tag{7.15}$$

This motor noise level is adjusted to the number of motors used on the Greenliner and the take-off measurement point before it can be added to the propeller noise level.

Airframe Noise
The last major aircraft noise contributing factor is the airframe noise. This noise is estimated by use of a NASA research on airframe noise [50]. The equation is based on the aircraft cruise speed (V_{cruise}) and the aircraft weight (W) and is given in Equation 7.16 and the solution is given in dBA.

$$SPL_{A_{airframe}} = 10log(V_{cruise}^5) + 10log(W) - 74 \tag{7.16}$$

7.5.3. Results and Compliance
The result of the calculations described in Figure 7.5.2 is a propeller noise level of 81.5 dBA. Furthermore, the engine adds an A-weighted noise level of 64.5 dBA at that same reference point. The last major contributing factor, the airframe, has an estimated noise level of 66.8 dBA. Since acoustic levels behave logarithmic, these values are not directly added, but evaluated on a logarithmic scale. The result of the addition of the propeller noise, engine noise and airframe noise is a total of 81.8 dBA. As specified before the aircraft falls into the category that should have a noise level lower than 88 dBA. The noise requirement is therefore met.

7.6. Resource Allocation & Budget Breakdown

Technical Performance Measurement (TPM) is a process through which one can measure risks that are inherent to a given design project. It represents critical technical thresholds or goals that should be followed for the success of the project.

Since TPM parameters follow from key performance parameters, the following parameters have been selected: emissions, range, MTOW, costs, take-off length, number of engines. These parameters, including their contingencies and relative importance, are listed in Table 7.4. Contingencies are adapted from [63] and [100], scaled to the risk the specific parameter imposes to the project.

In Table 7.4, the current contingency values are presented in bold. As can be observed, the confidence for the emissions is at 0%, as the Greenliner was designed especially for no harmful emissions. The same argument is used for the range, but since a lot of research has be to put into Class III estimations, the current contingency factor is close to the preliminary phase. A lot of time was spend on producing good estimations for the weight, which is why the contingency factor is lowered to 20%. For the financial analysis (see chapter 12) many uncertainties remain, therefore the contingency factor is increased to 50%. Additionally, since the propellers need to be analysed more thoroughly, as for now, a simplified ideal model was used (see section 5.5). The take off depends greatly on the power these propellers provide, therefore the contingency is increased. For the same reasons, the contingency factor for the number of engines is kept the same.

Table 7.4: Contingencies per design phase including relative importance in percentages

	Emissions	Range	MTOW	Cost	Take-off length	Number of engines
Conceptual	10	65	35	35	20	20
Current values	**0**	**30**	**20**	**50**	**40**	**20**
Preliminary	5	35	23	23	15	15
Detailed design	0	20	15	15	5	5
Manufacturing	0	13	10	10	3	3
Flight test	0	9	7	7	2	2
Production	0	0	0	0	0	0
Relative importance	30	30	20	10	5	5

The TPM-parameter per phase is calculated by multiplying the contingency by the relative importance and summing all the parameters, as can be observed in Equation 7.17.

$$TPM_{phase} = \sum (contingency \cdot relative\ importance) \tag{7.17}$$

The result of this process can be observed in Figure 7.14. As shown, while taking into account the new contingencies, the current TPM value is above the target value, meaning that there are less uncertainties than expected.
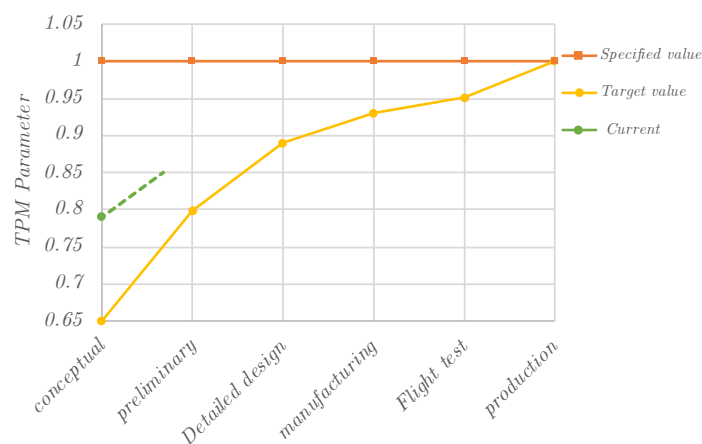

Figure 7.14: Technical Performance Measurement Prognosis

<div align="right">

8

</div>

Verification and Validation

Verification and Validation are an integral part of the design process of any complex product, such as an aircraft. Therefore, after presenting the general approach in section 8.1, the results of the verification and validation processes for the Greenliner are presented in section 8.2.

8.1. Verification and Validation Approach

Throughout the entire design process, the (numerical) computer models must be verified and validated to ensure that the numerical solution actually depicts the modelled problem and the modelled problem accurately describes the real life situation. These verification and validation approaches will be described in this chapter. First the verification and validation methods are presented in subsection 8.1.1 and subsection 8.1.3 respectively. Then, the results of these models are presented in section 8.2.

8.1.1. Model Verification

The verification process focuses on making sure that the numerical solutions represent the models created for the computations. There are several ways of performing this step.

Code Verification

The first step in verifying the results is verifying the used code. This is to be done every time a code is used to reach a solution in the design process.

First, the so-called unit tests have to be performed. During unit tests, smaller individual blocks of code will be run with a known set of controllable input data. These tests are set up in such a way that the outcome can easily be verified by a trusted source, such as a simpler analytic model or a manual computation. Due to the possibility of using different assumptions or a different general approach, the results will not necessarily match perfectly, however they are expected to behave similarly. This process will determine whether the code is doing what it is supposed to do and will give an indication on the accuracy of the code.

Another way of verifying the code is to perform a check on the units used in the code. Errors can easily be found if the computations between parameters with certain units do not coincide with the units of the outcome. If, for instance, Newtons and meters are multiplied with each other, the outcome should be in Joules, but if the result is in Joules per second, a mistake must have been made somewhere.

System Tests

After the smaller blocks of code have been verified, the integration of these blocks is analysed and by doing that, the entire system is tested. This is done in order to confirm that the code is finding the correct solutions to the modelled problem. One form of a system test is the "sanity check". This is the quickest and simplest, but most inaccurate test that can be done. If the solution of the model is obviously regarded as false due to absurd results, the model can be shown to be incorrect. However, if the results do not show obvious mistakes, the sanity check will not be an accurate verification.

During another form of the unit test, the numerical solution is compared to an analytical solution. Again, these results are not expected to be identical but should be in the same order of magnitude. The similarity between the two results will be used as an indication that the numerical model is performing as intended.

8.1.2. Design Verification

In any design process, the final product must meet the requirements. Checking the compliance of the designed system with the requirements ensures that the design process is heading to the right direction.

Each system requirement will be categorised according to the method of verification as presented in Table 8.1. The four possible methods of verification are defined as follows:

- **Inspection**: Visual observation to check whether the system meets the specified requirements.
- **Analysis**: Mathematical models and/or numerical simulations are established to analyse whether the system performance meets the specified requirements.
- **Demonstration**: Without the use of elaborated instrumentation or test equipment, the functional operation of the system is evaluated to check compliance with the specified requirements.
- **Test**: With the use of special equipment, instrumentation, or simulation techniques, system compliance to specified requirements is checked.

Table 8.1: Verification of the design with system requirement using inspection, analysis, demonstration, and testing.

Inspection	Analysis	Demonstration	Test
GF-SYS-INT.1-1	GF-SYS-INT.2-2	GF-SYS-INT.3-1	GF-SYS-EXT.1.1-3
GF-SYS-INT.3-5	GF-SYS-EXT.1-1	GF-SYS-INT.3-2	GF-SYS-EXT.1.1-4
GF-SYS-EXT.1.2-1	GF-SYS-EXT.2-1	GF-SYS-INT.3-3	GF-SYS-EXT.1.3-1
	GF-SYS-EXT.1.1-1	GF-SYS-INT.3-4	GF-SYS-EXT.1.3-2
	GF-SYS-EXT.1.1-2	GF-SYS-EXT.1-2	GF-SYS-EXT.1.3-3
	GF-SYS-EXT.1.2-2		GF-SYS-EXT.1.2-3

A compliance matrix will be constructed and displayed in chapter 13 to confirm that the design meets all system requirements mentioned in section 2.4.

8.1.3. Validation

After the verification has established that the numerical solutions are accurately describing the proposed model, the validation process can begin. This process will determine whether the proposed model correctly depicts the real life situation.

Validation Process

The validation process will compare the numerical solutions of analysis methods to the real life performance. Since the aircraft is not in the test phase yet, these real life performance data will be retrieved in the form of data on existing aircraft or other relevant machines. For simpler calculations, such as the MTOW, required thrust or surface area the data can directly be obtained from reference aircraft. However, some outputs, especially on the newer concepts used in the design, might require a more creative approach.

In the case of more innovative solutions, it will be required to look outside of the aerospace industry and base conclusions on different products, while still taking into account the difference in application. As an example, gathering data on hydrogen fuel tanks might be more of a challenge. Although hydrogen tanks are used in various fields, the usage in the field of aerospace engineering is close to none. For this reason, one could look into the automotive industry to collect data about fuel tanks and validate chosen solutions.

Error Analysis

A certain error is expected to be found during validation of the subsystem results. In fact, these validation errors are expected to be of a larger magnitude than the verification errors since the Greenliner is very innovative.

8.2. Verification and Validation Results

The results of the verification and validation approach described in section 8.2 are presented in this section, for each subsystem.

Fuselage

Fuselage weight verification is done comparing the output values of the method used (Raymer) to the output values of two other estimation methods shown in Equation 8.1 and Equation 8.2. These two equations are a fast Raymer [77] and a Torenbeek statistical fuselage weight estimation method.[92]

$$m_{fus_{verify1}} = 2.5 \times S_f \times 0.454 \qquad (8.1)$$

$$m_{fus_{verify2}} = 0.12 \times MTOW/g \qquad (8.2)$$

The fuselage weight estimated by the original method is 975 kg. The weight estimated by Equation 8.1 and Equation 8.2 are 1096 kg and 776 kg respectively. The result of the original method is therefore within range of the verification methods. This means that the method used is indeed correct and that the fuselage weight is verified.

The estimated fuselage CD_0 can be verified based on a simple calculation shown in Equation 8.3 with the wetted area of the aircraft and the equivalent skin friction coefficient cf_e which equals 0.0026 for civil transport aircraft.[77] If the estimated $CD_{0_{fuselage}}$ does not deviate more than 25% from the verifying value, then the estimation can be considered correct.

$$CD_{0_{fuselage}} = C_f e \frac{S_{wet}}{S_{ref}} \qquad (8.3)$$

The drag coefficient resulting from section 5.1 is 0.0087 while the drag coefficient calculated above is 0.009. This leads to the conclusion that the drag coefficient is in the correct range.

To validate the Greenliner fuselage design, in Table 8.2, the fuselage width and length are compared to the reference aircraft, the Dornier 228 and the DHC-6 Twin Otter. It shows that the Greenliner is wider than the reference aircraft, which is because of its three seat abreast arrangement. When comparing to other aircraft with the same configuration such as the Embraer ERJ 145 which has a fuselage width of 2.28 m, the fuselage diameter of the GReenliner can be deemed reasonable. In terms of fuselage length, the Greenliner is very similar to the reference aircraft. However, additional space is taken up by the tank and due to the seating configuration, the passenger cabin is shorter. Due to this, the fuselage cabin length validation does not produce confident results.

Table 8.2: Fuselage comparison

Aircraft	Year	Length [m]	Width [m]	Seats abreast
Greenliner	2̄030	16.7	2.19	3
Dornier 228	2015	16.56	1.33	2
DHC-6 Twin Otter	2003	15.77	1.75	2

Airfoil

The airfoils selected for the main wing and the tail surfaces are both part of the NACA airfoil database. These NACA airfoils have been extensively tested and frequently used in many aircraft designs such as the Dornier 228, which uses the exact same NACA 23018 airfoil for the main wing. Another example is the Cessna 402C which has a capacity of 9 passengers and a maximum speed of 266 mph (428 km/h) [1]. As a last example, the Embraer 120 Brasilia is also designed with the NACA 23018 airfoil. This aircraft has a maximum speed of 378 mph (608 km/h) and can carry 30 passengers. These examples can be seen as a validation method for the airfoil choice.

Wing Planform

The wing planform parameters are initially estimated based on statistics. These initial parameter values are used to construct two graphs: the wing lift curve and the drag polar. After the initial estimate, the aspect ratio, taper ratio and sweep angle can be varied in order to optimise these graphs. The lift curve and drag polar can be verified by inspection. It is well know that the lift curve and drag polar are proven tools to assess the performance of an aircraft. Furthermore, it is also known how the lift curve and drag polar are supposed to look. To conclude, for verification, the

---

[1] Retrieved from: `http://seattleclouds.com/myapplications/daly365/TwinsJets/BCessnaG401.html` on 28-06-2018

shape of the lift curve and drag polar are used.

The validation of the wing parameters can be done by comparing them to wing parameters of reference aircraft. The comparison is shown in Table 8.3.

Table 8.3: Wing planform comparison

Aircraft	Aspect ratio [-]	Quarter chord sweep angle [deg]	Taper Ratio [-]	Reference area [m^2]
Greenliner	10	0	0.4	25.9
Dornier 228	9	0	0.7	39
Twin Otter	10.1	0	1	32

As can be seen, the aspect ratio and the quarter chord sweep angle of all three aircraft lie very close to each other, from which one can conclude that the aspect ratio and sweep angle of the Greenliner are validated.

One notable fact is that both the Dornier and the Twin Otter both have a larger taper ratio than the Greenliner. This may be due to the fact that the Dornier and Twin Otter are designed for short take-off and landing and for the operation in extreme conditions. These extreme conditions require good stability characteristics. However, a low taper ratio increases the possibility of tip stall and an additional moment, which negatively affects the aircraft stability. Since the Greenliner design is not focused on extreme conditions, a low taper ratio is possible and favourable over a high taper ratio in terms of structural stiffness and structural weight.
Furthermore, the two reference aircraft have much larger wings in terms of the reference area. This is again due to the short take-off and landing characteristics, which prescribe a lower wing loading.

Propulsion
The detailed design of a propulsion system is a complex and time-consuming process. Therefore, in the conceptual design stages, a number of assumptions must be done, as explained in section 5.5. For the validation of the propulsion subsystem design, some of the assumptions that go into this design are revisited, and their consequences evaluated.

1. **Ideal velocity profile inside boundary layer**
   A simplified assumption is done on the boundary layer velocity profile: it is approximated by Equation 5.22, assuming turbulent flow. In reality, a turbulent velocity profile will likely include unsteady fluctuations, which need to be taken into account in detailed design. The effect of these fluctuations is difficult to predict. A possible consequence are unacceptable vibration loads on the propeller blades.

2. **Uniform flow speed through propellers**
   To size the propellers, actuator disk theory is implemented. This assumes a uniform velocity profile entering the propeller, and the velocity differential over the propeller then determines the thrust. The model therefore uses the average velocity over the boundary layer as an input. In reality, the flow speed is variable. The effect of this assumption could be quite large. When following a fixed point on the propeller blade through a full rotation, the incoming airspeed will vary in reality. To estimate the extreme case for airspeed differential, an example calculation is shown here, illustrated by Figure 8.1b.

   In the extreme case, the tip of the propeller encounters the cruise airspeed on the outside of its rotation (Situation 1), while the airspeed attached to the fuselage is zero (Situation 2). With a tip velocity of 0.5 M at a cruise velocity of 137 m/s, V_{Total_1} is equal to 201 m/s, while V_{Total_2} is equal to 148 m/s, leading to a velocity differential of 53 m/s. This is a major design concern for future development. Firstly, it is difficult to design the propeller blades for optimal functioning in both velocity fields simultaneously, because the pitch would likely have to be adjusted within every rotation. Secondly, the loading on the propeller will vary continuously. This is a concern because it will likely introduce structural vibrations, as well as increased noise due to pressure changes. In the following design phase, the propeller design will therefore likely need to be adjusted. Designing propellers for these varying conditions is a topic of current research by NASA and others [32]. Ideas for improving this design aspect can be found in chapter 14.
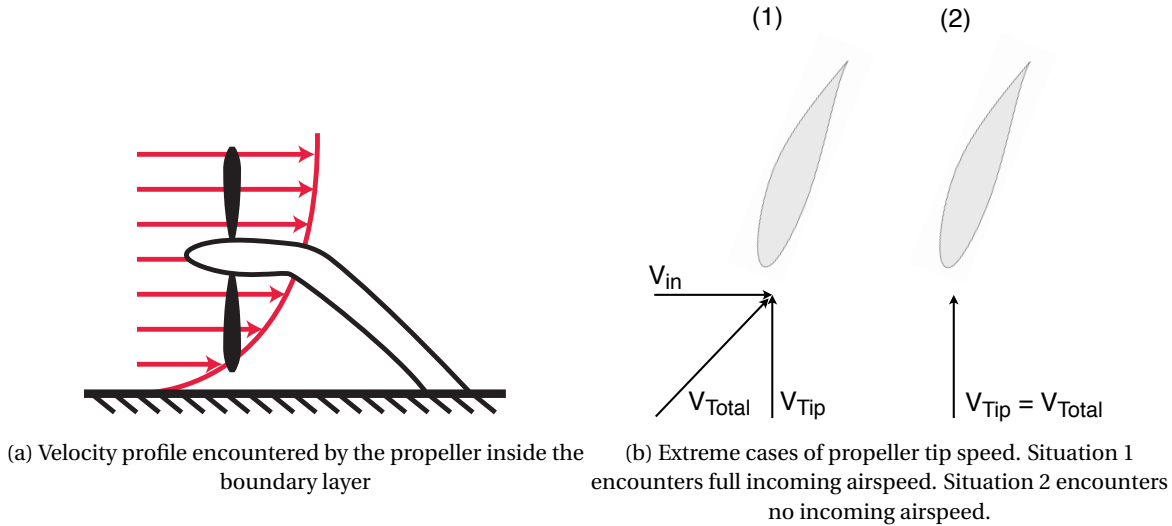
(a) Velocity profile encountered by the propeller inside the boundary layer

(b) Extreme cases of propeller tip speed. Situation 1 encounters full incoming airspeed. Situation 2 encounters no incoming airspeed.

Figure 8.1: Illustration of airflow differential encountered by propeller tip

3. **No influence of propellers on tail surfaces**
   With the focus of the Greenliner design being on the power generation and propulsion, conservative and conventional choices were made with respect to the airframe configuration. An example of this is the standard tailplane layout. However, the tail surfaces will in reality be influenced by the propeller exhaust, due to their proximity [13]. This needs consideration in the continuation of the design.

4. **No limit on allowed exhaust velocity**
   In the current model, the emphasis is put on achieving maximum efficiency by placing the propellers inside the fuselage boundary layer. This means there is a limited area available for propellers. The actuator disk theory can be used to examine the effect of limiting this area.

$$T = \dot{m}(V_2 - V_1) \text{ , with} \tag{8.4}$$

$$\dot{m} = \rho \, A \, V \tag{8.5}$$

Equation 8.4 suggests that the exhaust velocity of the propeller may become too high. To examine this, a calculation is done based on the total propeller area and the required thrust at cruise. With an effective propeller area of 1.158 m^2, and a required thrust of 4338 N, it can be shown that the required velocity differential over the propellers is approximately 104 m/s. The total exhaust velocity will then be approximately 224 m/s, which is Mach 0.76 at cruise altitude. This is deemed an acceptable exhaust velocity, because the likelihood of shock waves and drag divergence is low.

5. **No limit on propeller blade loading** The tip speed of the propellers is limited to Mach 0.5. However, the high velocity differential that the propeller needs to provide leads to high loading on the blades, because the tip velocity limits the RPM. This high blade loading will have to be considered during the detailed blade design.

In the process of verifying the propeller exhaust velocity, an error was found in the propeller sizing model. This error resulted in a higher estimation for exhaust velocity than is actually the case. Because exhaust velocity is an important parameter in the efficiency calculation of the propeller, this error carries through to the selection of the total propeller number and radius. After correcting the error, it was found that in fact, a configuration with 15 propellers of 22 cm diameter produced even better results than the current design. Because this error was found after fixing the final design parameters, the conceptual design is kept according to the original specifications. This design is still valid, because the propellers are indeed capable of providing the necessary thrust, as proven by the exhaust velocity calculations above. The improved configuration of 15 propellers is taken as a recommendation for further design.

To confirm the feasibility of using electric motors, research is done on vehicles that already use (distributed) electric propulsion. Firstly, the electrification of aircraft is thoroughly discussed in [12]. This article emphasises that, even though fossil fuel propelled aircraft are in the majority, electric propelled aircraft have a huge potential.

Secondly, Table 8.4 shows that already now, electric aircraft are in the production phase and are performing fairly well. The aircraft in this table are proof that electrical motors can be implemented in aviation. Furthermore it should be noted that the electric engines have a high efficiency which indicates great potential.

Table 8.4: Electrically Propelled Aircraft

Aircraft	MTOM [kg]	V_{cruise} [km/h]	Motor Power [kW]	Best Motor Efficiency [%]
Alpha Trainer [97]	550	185.2	85	95
Rui Xiang RX1E [88]	480	140	30.6	93
FEATHER [61]	800	126	60	95

Fuel Cell

The process of designing a good fuel cell is as complex as the design of an aircraft. It is a multiphysics problem that requires good understanding of its functioning. The development of an accurate fuel cell model is crucial in the process. In this subsection the proposed fuel cell model and the fuel cell system will be verified and validated.

Fuel Cell Model Verification

The verification of the fuel cell model from subsection 5.6.2 is done in five parts. The distribution of hydrogen and oxygen will be tested in terms of effects due to the porosity layer, the catalyst layer, pressure difference, inlet velocity and inlet molar fraction. These tests will be substantiated with the use of velocity fields from Figure 8.3.

In Figure 8.2 four different hydrogen and oxygen distributions are given where Figure 8.2a is the distribution under standard conditions. The hydrogen distribution is given at the anode side (left of the membrane) and the oxygen distribution is given at the cathode side (right of the membrane). The distribution for the standard conditions, as given in Figure 8.2a, is done at an anode operating pressure of three bars and a cathode operating pressure of one bar; the inlet velocities are respectively for the anode side and cathode side, five and one centimetres per second; the molar fraction at the anode inlet is 0.9 for hydrogen, and at the cathode 0.18 for oxygen. In Figure 8.2 the red indicates 0.9 molar fraction at the anode side, and 0.18 molar fraction at the cathode side, unless stated otherwise. The molar fraction is then gradually decreasing, where orange (see membrane) indicates zero at both sides.

1. **The porosity of the Gas Diffusion Layers**
   The GDL and CL are porous layers in contrast to the flow channels. The effect of this porosity is that diffusion becomes the main movement method instead of advection. The expected behaviour is that the molar fraction of species gradually change in x-direction across the porous medium.

   It can be seen in Figure 8.2a that the hydrogen and oxygen in the respective GDL decrease gradually as they progress through the GDL. At the bottom of the GDL the molar fractions decrease rapidly. This can be explained by the fact that the flow channels provide easier flow, and that therefore the species will flow to the flow channels in the beginning. As the flow progresses the molar fractions of hydrogen and oxygen diffuse more into the diffusion layer. This is also explained by the fact that the flow diverges from the walls as the flow progresses (see Figure 8.3a).

   Although the flow does not exactly behave as expected, this deviation can be explained, and therefore the model is verified in terms of porosity effects.

2. **Reaction in the Catalyst Layers**
   In the CL the electrochemical reactions happen, and therefore a reduction or even depletion of the reaction products, hydrogen and oxygen, is expected. In Figure 8.2a the fractions are indeed significantly lower in the CLs. At the cathode side the oxygen fraction becomes larger at the cathode as the flow progresses. This is explained by the improved diffusivity as the flow progresses.

   In terms of CL effects, the model is verified.

3. **Operating Pressure Difference**
   It is vital for the design of the Greenliner that the fuel cell behaviour at different operating pressures can be modelled correctly, because the aircraft operates at a range of ambient pressures, and the fuel cell behaviour strongly depends on the operating pressure. In Figure 8.2b the distribution of hydrogen and oxygen is given at 1.5 bars and 0.5 bars at the anode and cathode side respectively. From Equation 5.57 it is expected that a lower operating pressure will result in a lower concentration of products. The depletion of products will therefore happen

sooner, and the molar fractions of hydrogen and oxygen in the CLs are expected to be lower compared to the standard conditions. Especially the molar fraction of oxygen is expected to be lower, because the concentration of oxygen is already comparatively low, due to the fact that it's extracted from the air.

The distribution of oxygen in Figure 8.2b clearly shows the expected behaviour for the cathode side. At the anode side, however, an increment in hydrogen is found. This is due to a better diffusion at lower pressure, as can be conducted from Equation 5.55, and due to the fact that hydrogen doesn't deplete as fast as oxygen. The improved diffusion is also visible from Figure 8.3b, where the velocity vectors have a more horizontal orientation, indicating improved diffusion.

Even though the hydrogen is distributed differently than expected, the model can be verified in terms of pressure behaviour. There is good reasoning for the hydrogen behaviour, and the oxygen is behaving exactly the way it was expected to.

4. **Inlet Velocity Difference**
   To verify the model for inlet velocity effects, the anode and cathode inlet velocities have been halved to 2.5 and 0.5 centimetres per second respectively. As the inlet velocity becomes lower, this should result in a depletion of oxygen at the CCL, since the moles of oxygen flowing into the model is lower.

   In Figure 8.2c the result of halving the inlet velocities is that there is an improved diffusivity at especially the cathode. This improved diffusion is also shown in Figure 8.3c where the velocity vectors have a more horizontal orientation compared to the standard conditions, indicating better diffusivity. This diffusivity is thought to be caused by the velocity term in the species equation Equation 5.49, however the physical reasoning behind this behaviour is unclear.

   Since the model behaves differently than is expected, the model cannot be verified based on inlet velocity behaviour.

5. **Inlet Molar Fraction Difference**
   Finally, the model will be tested on its behaviour due to a difference in inlet molar fraction. The inlet molar fraction of hydrogen at the anode has been lowered from 0.9 to 0.4, and the molar fraction of oxygen at the cathode has been increased from 0.18 to 0.4. This automatically means that in Figure 8.2d the red at the anode and cathode side now indicates a molar fraction of 0.4. Orange still indicates a molar fraction of zero. A lower molar fraction means less moles that can react. It is therefore expected that this test will show a depletion of hydrogen and an increment in oxygen.

   At the cathode side of Figure 8.2d it is clearly visible that there is more oxygen in the GDL and CL. Although not as clear as for the cathode side, the anode side shows a slight depletion of hydrogen. The velocity field in Figure 8.3d shows no difference with Figure 8.3a. This is because the velocity solution is based on an initial guess of species distribution, which hasn't changed here.

   From this molar fraction test it can be concluded that the model is verified for the solution of hydrogen and oxygen distribution, but not for its solution of the velocity field.

These five tests have provided enough information to verify the model, because they discuss the model's behaviour based on parameters that are most relevant to the model. The conclusion is that the model is verified for use in the design of the Greenliner, although there is still room for improvement, especially in the modelling of the velocity field.

Fuel Cell Model Validation
Now that the model has been verified, it can be validated. This is done by comparing the obtained current density curve with the results that are obtained by Larbi's two-dimensional model [9], and with the current density curve that is presented by O'Hayre et al. for a one-dimensional model [65]. The current density curves for the model, Larbi's model and O'Hayre's model, are given in Figure 8.4. It shows that the model actually gives values that are a bit too high. Apart from that, the data after a current density of 1.2 A/cm^2 is clearly wrong. It is interesting to note however that Larbi's data, on which the model is based, ends at 1.0 A/cm^2. Apart from the fact that the model gives to high values, the slope is actually comparable with Larbi's data in the lower current density region, and with O'Hayre's data in the higher current density region.

The conclusion that can be drawn is that the activation overpotential is actually modelled wrongly. In a fuel cell current density curve, the slope is given by the ohmic overvoltage, the vertical placement of the curve is given by the activation overvoltage, and the limit current density by the concentration overvoltage. The activation overpotential
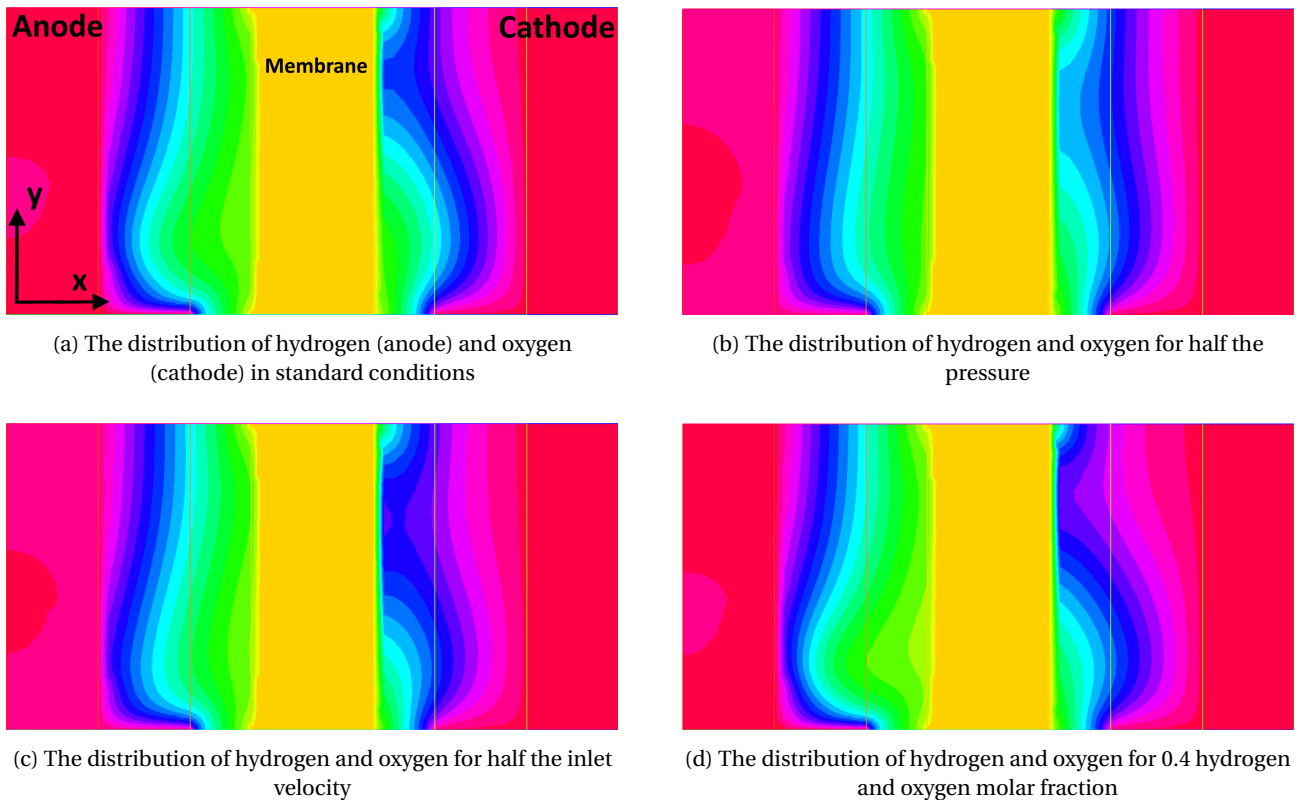
(a) The distribution of hydrogen (anode) and oxygen (cathode) in standard conditions

(b) The distribution of hydrogen and oxygen for half the pressure

(c) The distribution of hydrogen and oxygen for half the inlet velocity

(d) The distribution of hydrogen and oxygen for 0.4 hydrogen and oxygen molar fraction

Figure 8.2: The distributions of hydrogen (anode side) and oxygen (cathode side) for four different conditions

equation Equation 5.40 shows that the species fraction is in the denominator. This means that the model actually gives a lower molar fraction distribution than there is in reality. This model can be used for the design of the Greenliner, since it is still in a rather preliminary phase, but it is recommended that the distribution of the species given by the model is scrutinised, to find the mistake(s).

Fuel Cell System
In order to verify and validate the design of the fuel cell system, several parts of the system can be verified and validated separately.

In order to verify the fuel cell power calculations, the power output of the fuel cell is plotted against the mission time. By checking the feasibility of this plot, it is verified that the code representing the fuel cell is able to generate the correct power output to the aircraft propulsion system based on the power it is required to deliver. The code takes into account several aspects, such as compression power and the optimal power on the fuel cell operating power curve. Because of this, the total power profile will not be equal to the power required by the aircraft. Figure 8.5 shows the total power produced by the fuel cell during the mission in blue, and the power required for propulsion in red.

The differences between the total power produced and the power required for propulsion occur due to several factors. Firstly, the difference in magnitude mainly occurs due to the electric motor and propeller efficiency. The power output of the fuel cell has to be larger than the power required for propulsion in order to overcome these efficiencies. Secondly, the differences in shape occur mainly during climb (approximately from t = 800 to t = 2000) and descent (approximately from t = 8800 to t = 9500): there the power required is constant while the total power produced either is increasing or decreasing. This difference occurs due to the change in air density at each height: at higher altitudes the air density decreases, which leads to higher compression needed in order to keep the fuel cell at the desired operating pressure. Because of this the power needed for compression increases during climb, which leads to an increase of total power produced by the fuel cell. For descend, the decreasing compression power needed leads to a decrease in total power produced by the fuel cell. This both does not influence the power required for propulsion, which is defined by other aircraft parameters, thus leads to the difference occurring. Summarising, the total power generated by the fuel cell responds to the power required as expected, which indicates the fuel cell code works as needed.

(a) The velocity field of the flow in standard conditions

(b) The velocity field for half the pressures

(c) The velocity field for half the inlet velocities

(d) The velocity field for 0.4 species molar fractions
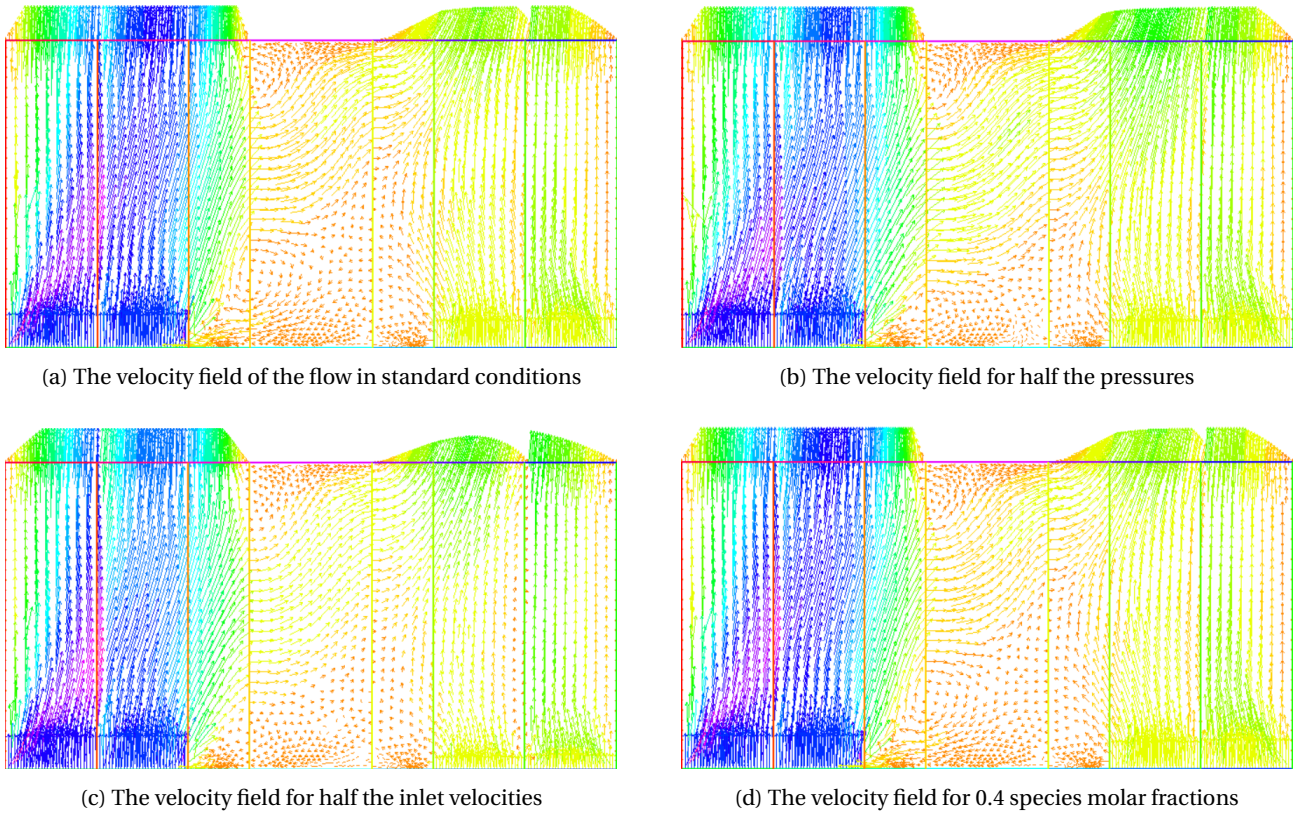
Figure 8.3: The velocity fields for four different conditions

At first, this power output seems quite high, compared to the voltage of 1V of a fuel cell, since this means a current of above 1000 A would be required. However, the configuration of the fuel cells can be adapted by placing them in parallel and in series corresponding to the design current and voltage, thus being able to provide the power that is necessary.

To validate the fuel cell calculations, a calculation is done on the total fuel cell efficiency, after which this value is compared to that of existing systems. The efficiency of any system is given by the following relation:

$$\eta_{system} = \frac{E_{out}}{E_{in}} \tag{8.6}$$

In the case of the Greenliner fuel cell system, the output energy is simply found by integrating the power output over the mission profile. This yields a total energy of E = 10760 MJ. To calculate the total input energy, the theoretical maximum of the electrical energy provided by the hydrogen is examined. This is done by the following derivation:

$$E_{in} = H_{2_{in}} * \frac{J}{mol}, \text{ with} \tag{8.7}$$

$$\frac{J}{mol} = \frac{J}{C} \cdot \frac{C}{mol} \tag{8.8}$$

Here, $H_{2_{in}}$ is the total mol of hydrogen used, and C is the charge in Coulomb. The fractions $\frac{J}{C}$ and $\frac{C}{mol}$ can be expressed as V (voltage) and F (Faraday's constant) respectively, reducing the complete equation to:

$$E_{in} = V \cdot F \cdot 2 H_{2_{in}} \tag{8.9}$$

The factor of 2 comes from the fact that two electrons react for every hydrogen molecule. Using an optimal fuel cell voltage V of 1.23 V, this leads to a theoretical energy of 237.2 kJ per mol H_2. This calculation is verified by the Gibbs free energy determined in [65], which is 237 kJ per mol. The Gibbs free energy is defined as the total energy a system

Figure 8.4: The validation of the model compared to Larbi et al.[9] and O'Hayre et al. [65]
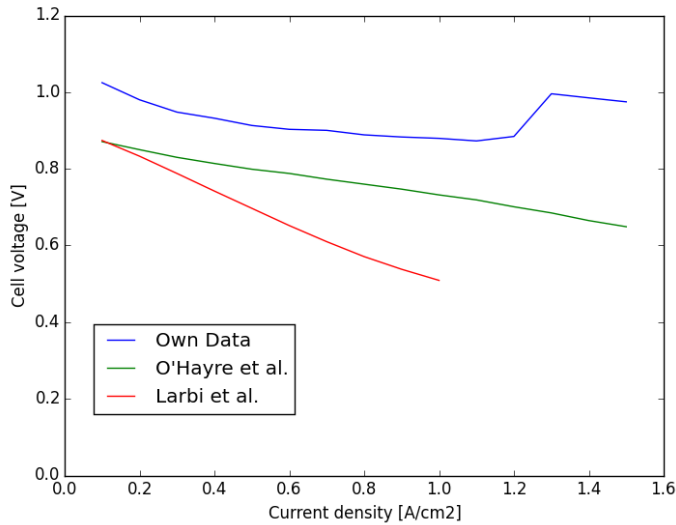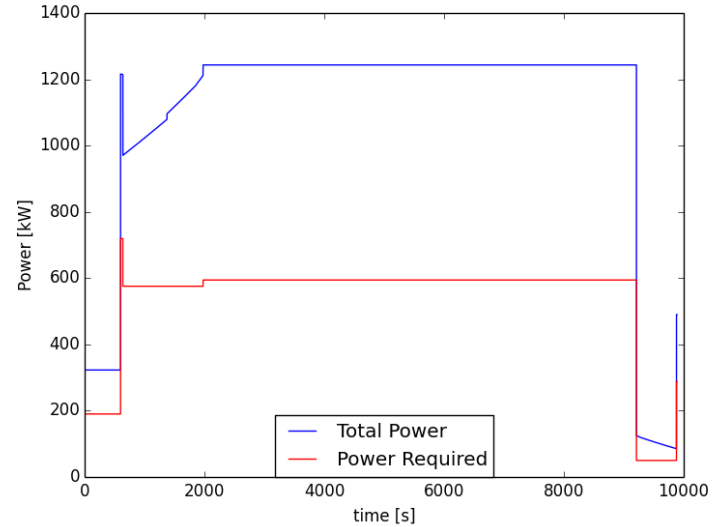

Figure 8.5: Power profile showing the required power for propulsion of the aircraft and total power generated of the fuel cell during the mission

can provide after making room for itself. Multiplying the theoretical energy value with the total amount of hydrogen used (150.98 kg gives 75 490 mol) provides the total used energy:

$$E_{in} = 17906 MJ \tag{8.10}$$

Finally, the total fuel cell system efficiency is calculated through Equation 8.6:

$$\eta_{FC} = 60.0\% \tag{8.11}$$

This is within the range of efficiency quoted in [91]. In conclusion, validation shows that the fuel cells perform within expectations set by existing systems and references. However, it is on the high end of these values.

Next to the fuel cell efficiency validation, the specific power can be validated. Based on the maximum power and fuel cell mass (determined in section 6.1, shown in Table 6.5), the specific power in kW/kg can be determined. With a maximum total power of 1.43 MW and fuel cell system mass of 525 kg, the specific power equals 2.72 kW/kg. Since fuel cells are not widely applied in aircraft, the specific power is compared to that of automotive design. An example in the automotive design is the Toyota FCV Mirai, which uses a fuel cell stack with a specific power of 2.0 kW/kg. although the order of magnitude is complying, it is recommended to improve the weight estimation for the fuel cell system.

Fuel Storage
Verification of the final fuel tank geometry requires a simplified model that can be solved by hand calculations. The fuel tank code is than modified to size a spherical tank instead of a cylindrical tank with semi-spheres on the ends. Then custom values are inserted for the temperature, pressure and required hydrogen mass. The corresponding result is then compared to the result of the hand calculations using the same input values. When these match, the code is verified to be accurate for spherical tanks. Then, to verify the functionality of the code for cylindrical tanks, the length of the cylinder in between the semi-spheres is gradually increased to inspect the change in volume and required thickness and compare this to what changes are expected with the changes in dimensions.

Before the tank geometry is validated using other applications of hydrogen storage in tanks, the required insulation is evaluated. the thickness of the insulation for the fuel tank in the Greenliner has been retrieved from Brewer [15] which bases the method on data of other aircraft, thus validating the approach.

For validation of the fuel tank geometry it is not possible to compare it to other aircraft, as the only aircraft to have flown using liquid hydrogen, such as the HY4 [2], have released very little information on their entire system. However,

---

[2] Retrieved from `http://hy4.org/` [Accessed 29 June 2018]

in essence the fuel tank of the Greenliner is the same as other pressurised tanks with a similar pressure. So the fuel tank can be compared to regular pressure vessels that are supplied [3] to the public. Comparing these values, they do fall within the same range of numbers. Additionally, the methods used are also validated by realising the similarity to regular pressurised vessels.

Tail and Control Surfaces

The calculations concerning aileron, elevator and rudder characteristics can be verified by performing a unit test: comparing the output stability derivatives to theoretical values. Table 8.5 summarises the calculated values and reference values.The Greenliner's stability derivatives, C_{l_p}, $C_{m_{\delta e}}$ and $C_{n_{\delta r}}$ have the same sign and are in the same order of magnitude as the reference aircraft, which confirms verification. One peculiar fact is that $C_{l_{\delta a}}$ has the opposite sign. This is due to the difference in reference frame used for the Greenliner and reference aircraft. The convention used to calculate the Greenliner's $C_{l_{\delta a}}$ takes right aileron up, left down as positive while the reference aircraft uses the other way around.

Table 8.5: Asymmetric and Symmetric Stability and Control Derivatives Comparison [60]

Aircraft	MTOM [kg]	Pax [-]	$C_{l_{\delta a}}$ [-]	C_{l_p} [-]	$C_{m_{\delta e}}$ [-]	$C_{n_{\delta r}}$ [-]
Greenliner	6460	19	0.28	-0.69	-1.06	-0.32
Cessna 500	4310	6	-0.23	-0.34	-1.55	-0.13
Fokker F-27	19773	56	-0.086	-0.6	-1.8	-0.086

The second unit test is the example unit test. The equations that are used to calculate the control surface geometry of the aircraft in subsection 5.9.2, include an example calculation. Only if the example inputs result in the same outputs, the program is verified. This was the case.

For validation, the geometry of the aileron, elevator and rudder of the Greenliner are compared to control surfaces of reference aircraft. This comparison is shown in Table 8.6. The aileron chord ratio is slightly smaller than that of reference aircraft but approaches it well. The elevator area ratio and chord ratio show the same behaviour. The rudder dimensions overshoot the reference dimensions and this may be due to the fact that, as explained earlier, the c.g. position of the Greenliner is in the back of the aircraft. Due to this, the tail arm is smaller and the force (thus rudder area) must be bigger to overcome the same moment.

Table 8.6: Geometry parameter comparison of the Greenliner with reference aircraft

Aircraft	MTOM [kg]	C_A/C	S_E/S_h [-]	C_E/C_h [-]	S_R/S_v	C_R/C_v
Greenliner	6460	0.19	0.26	0.24	0.36	0.38
Cessna Citation III	9979	0.3	0.37	0.37	0.26	0.27
Gulfstream 200	16080	0.22	0.28	0.31	0.3	0.32

Landing Gear

First, the dimensions of the landing gear are verified by a simple hand calculations of the forces on the struts and the corresponding stresses. The location of the gears is verified by taking a look at aircraft drawings and measuring the angles to verify that all clearances are met.

Then, for validation the configuration and material is compared to other aircraft. First of all, the retractibility of the gears has been established to be common for aircraft flying at speeds above 150KTS [80] and the Greenliner will have a cruise velocity of around 260KTS so that is a definite indication that a retractable gear is desired.

Secondly, the usage of titanium is validated, as it as used in most commercial passenger aircraft. On the small side of the spectrum of all aircraft, the Cessna 180 and 182 for instance use titanium landing gears too [4]. On the other hand, the Boeing 777 and 787 and the Airbus A380 all use at least partially titanium landing gears too [5]. This shows that the size of the aircraft does not change the fact that the landing gears will be under heavy impacts and that titanium is truly a weight-efficient material for this application.

---

[3]Retrieved from `http://www.winegrowers.info/wine_equip/tanks_stst/3%20bar%20pressure%20tanks.htm` [Accessed 29 June 2018]

[4]Retrieved from `https://www.thelandinggearworks.com/`[Accessed 28 June 2018]

[5]Retrieved from `http://www.tms.org/pubs/journals/JOM/1005/boyer-1005.html`[Accessed 28 June 2018]

Solar Panel Feasibility

In terms of verification, no unit tests are performed as all of the original calculations are already done by hand so no code can be verified. As a way of still verifying, some input parameters have been varied to see the effect on the final outcome to evaluate the method used. Additionally, actual tests are done on the units of all the values to see if they correspond to each other. For instance, that the power per unit area multiplied by the area will in fact give a result in power and not another unit.

There are currently only a few solar powered aircraft that are actually flying. The most famous one is the Solar Impulse 2, which started a flight around the globe in 2015 [6]. Additionally, the Helios Pathfinder Plus from 2003 is an interesting aircraft to consider [7]. These aircraft are used to validate the inputs used for the calculations on the solar panels for the Greenliner. A comparison on the power retrieved from the solar panels is shown in Table 8.7. First of all, the comparison shows how the technology of solar panels has improved considerably in the past decades. Secondly, the used power output of the solar panels on the Greenliner are shown to not only be reasonable but even conservative as it can be expected that by 2030 the efficiency will have gone up considerably.

Table 8.7: Solar power comparison

Aircraft	Year	Power [kW]	Solar Panel Area [m^2]	Power with 68 m^2 [kW]
Greenliner	2030	13	68	13
Solar Impulse 2	2015	66	269.9	16.6
Helios Pathfinder Plus	2003	12.5	88	9.7

Structural & Material Characteristics

The outputs of the structural analysis are the structural arrangement within the wing, the fuselage skin requirements and the loading and stress diagrams of both the fuselage and the wing.

The structural arrangement is verified and validated by the fact that the arrangement was made making use of Roskam [79], which is based on average values of reference aircraft and the general taken approach.

Then, the loading diagrams for the wing were computed and verified by the combination of a "sanity check" and a hand-solved simplified model using a point load for the lift instead of an elliptical lift distribution. Similarly, The fuselage loading was also checked via a simple hand calculation showing the feasibility of the results. Then, for the wing stress calculations, the required moment of inertia at the root was calculated. The height of the spar was set by the airfoil thickness, the width of the flange was selected as a ratio of the height and then the thickness of these parts was computed to match the required moment of inertia. Then the result was again verified by a hand calculation.

Finally, the thickness of the fuselage is validated. The analysis showed that a thickness of 0.4 8mm was required but in order to facilitate riveting and easier manufacturing, a thickness of 1 mm was opted for. Comparing to the Boeing 757 which has a skin thickness of around 1 mm [104] and the much bigger Boeing 777 with a thickness of 2-2.3 mm [109], shows that the thickness is reasonable and within a expected range. Additionally, an example design calculation of the University of Liege shows how the required skin thickness was a maximum of 0.67 mm but 1 mm was chosen to allow for riveting [53].

Noise

The equations used to estimate the noise can be verified by performing unit tests. The first unit test applied to the noise code is a dependency test. Aircraft noise is dependent on multiple clear variables: number of motors/propellers, distance to propeller and power input. In case you increase the number of motors/propellers or the power input, the noise level should go up. In case you decrease the distance to the source, the noise level should go up too. On top of that, one knows that the loudness of a source is measured in decibels which is a logarithmic scale. By now increasing or decreasing the above mentioned variables, the change in noise level can be checked. The sign of the change in noise level is known, as well as the order of magnitude.

---

[6]Retrieved from `https://en.wikipedia.org/wiki/Solar_Impulse#Solar_Impulse_2_(HB-SIB)` Accessed 28 June 2018

[7]Retrieved from `https://web.archive.org/web/20030810185046/http://www.dfrc.nasa.gov/Newsroom/FactSheets/FS-034-DFRC.html` Accessed 28 June 2018

The second unit test is the example unit test. The equations that are used to estimate the sound level of the aircraft in section 7.5, include an example calculation. Only if the example inputs result in the same outputs, the program is verified. This was the case.

The noise level estimation values can be validated by comparing them to the noise level of similar aircraft. For reference, the Dornier 228 and Twin Otter aircraft noise levels are used. As can be seen in Table 8.8, the Greenliner has a(n) (A-weighted) noise level extremely close to the reference aircraft. A lower noise level could be explained by the fact that the Greenliner has very small engines and propellers. However this decrease in noise is compensated by the fact that so many propellers and engines are used. To demonstrate, an increase in noise level of the whole aircraft of 10 dB is induced by the fact that 23 engines and propellers are used in stead of just one.

Table 8.8: Noise level comparison

Aircraft	Maximum Take-off Mass [kg]	Noise Level [dB(A)]	Noise Limit [dB(A)]
Greenliner	6460	81.7	88.0
Dornier 228	6575	78.5	88.0
Twin Otter	5670	84.5	88.0

<div align="right">

9

</div>

Future Development

After the development of a complete design for the Greenliner in this report, more detailed design tasks must be carried out in subsequent phases. Although this project is concluded at the end of the DSE, these tasks, which are presented in section 9.1 would be carried out in a real-world engineering process. Furthermore, a production plan is given in section 9.2 and a technical risk assessment is carried out in section 9.3.

9.1. Project Continuation

This section will lay out the steps to be taken after the DSE to finalise the project of the Greenliner. A Gantt chart including all subsequent phases is shown in Figure 9.1. Each phase is explained below.
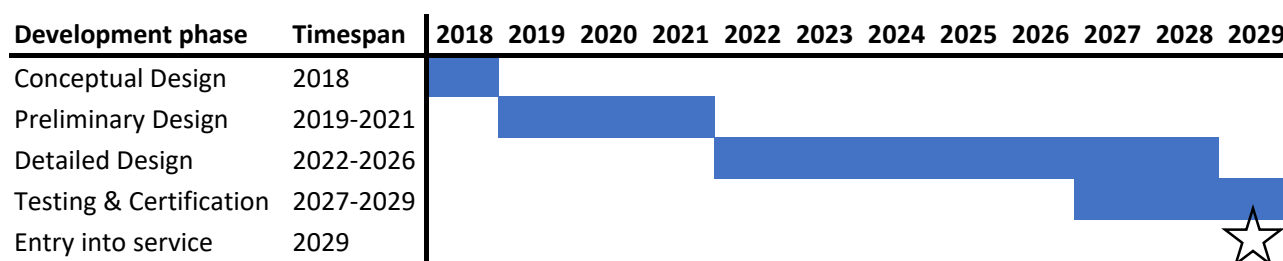
Development phase	Timespan	2018	2019	2020	2021	2022	2023	2024	2025	2026	2027	2028	2029
Conceptual Design	2018												
Preliminary Design	2019-2021												
Detailed Design	2022-2026												
Testing & Certification	2027-2029												
Entry into service	2029												

Figure 9.1: Gantt chart showing the planning of the future development processes of the Greenliner. Each phase is explained in the section.

9.1.1. Designing

A typical aircraft design process consist of conceptual design, preliminary design and detailed design sequentially. In this design project, only the conceptual design is completed. The other two phases should therefore take place after the DSE, followed by the remaining processes explained in this chapter.

Conceptual Design

In the conceptual phase, most sizing methods are largely based on statistics, although the influence of the main design parameters is included in the corresponding formulas. Furthermore, the performance analysis methods depend on many initial assumptions, which decreases the confidence level. An initial compliance check of the requirements can however still be performed. Although the DSE is officially finished halfway through the year of 2018, this design phase should ideally be extended to investigate several important effects which are mentioned in chapter 14.

Preliminary Design

The preliminary design process can be observed in Figure 9.2. With the final result of the conceptual phase, detailed aerodynamic, control and stability and structural analysis is performed, along with wind tunnel tests. If any issues arise, the design is modified until the desired performance is achieved. The preliminary design ends with a go/no-go moment in which a decision has to be made if the Greenliner is actually going to be built. This phase is expected to last around three years, similar to other modern aircraft development programs such as the Bombardier CS300 [1] or the Airbus A350. [2]

---

[1] Retrieved from `https://www.bombardier.com/en/media/newsList/details.404-bombardier-updates-market-on-status-of-its-cseries-commer` `bombardiercom.html` Accessed 29 June 2018

[2] Retrieved from `http://www.airbus.com/newsroom/press-releases/en/2006/12/a350-xwb-family-receives-industrial-go-ahead.` `html` Accessed 29 June 2018
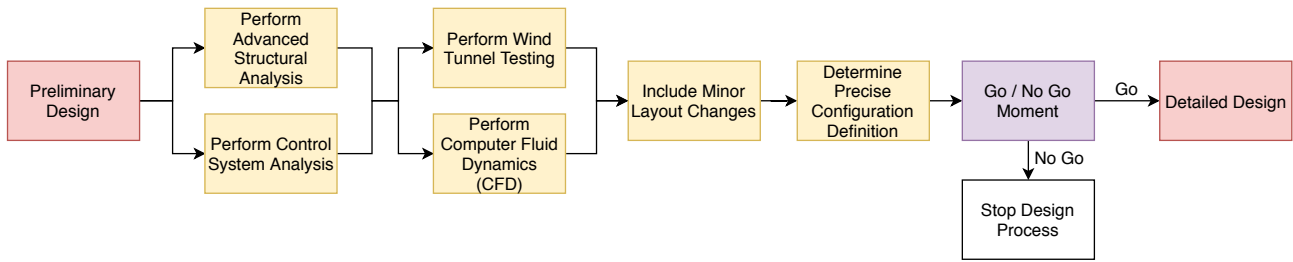
Figure 9.2: Preliminary Design Phase, adaptation from [6]

Detailed Design

The detailed design process can be observed in Figure 9.3. It is the process in which every part of the aircraft is designed in the smallest detail possible. More specifically this phase focuses on the number and locations of all the structural elements, such as the ribs, spars and other sections. Then, with all the specific characteristics from the preliminary design only the manufacturing remains. For this, the manufacturing tools and jigs have to be designed for the final assembly. In a separate but parallel process, the flight simulator is developed. As shown in Figure 9.1, this phase would last a minimum of five years, similar to recent aircraft programs such as the Bombardier CS300. [3] However, it is likely that first testing procedures would already begin during this phase, for instance in a smaller technology demonstrator aircraft. Since no hydrogen powered aircraft of this size has flown before or is planned to fly within the next few years, many question remain answered only in theory. Therefore, before the construction of the first full prototype can begin, initial testing must be conducted, in addition to possible redesign procedures.
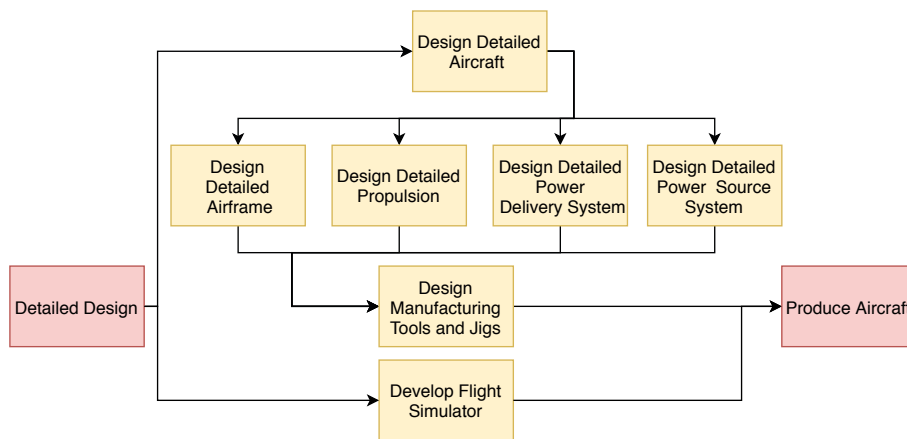
Figure 9.3: Detailed Design Phase, adaptation from [6]

9.1.2. Certification

Before production can begin at full speed, the aircraft has to be certified. A type certification will allow the Greenliner to be used for scheduled civil transport flights as is the intended purpose of the aircraft. These certifications are issued by organisations such as FAA and ESEA depending on the region of the world. So, in order to fly in every region, certification has to be received from the corresponding authorities. Generally, the certification procedures are fairly similar between the authorities, however all procedures do have to be done separately.

The certification will be done on several prototypes that are to be build. Multiple prototypes are required to perform different functions. One prototype can be equipped with measurement instruments to identify the flight dynamics of the aircraft, whereas another can be used to actually test the aircraft filled with the intended payload and verify the requirements are met. This can be done with a single prototype, but to save valuable time processes can be done simultaneously by using multiple prototypes. The tests involve taking the aircraft to its extremes and verifying if it can withstand these. For instance, it is tested if the aircraft performs normally on a runway filled with water. Another test

---

[3] Retrieved from `http://www.airbus.com/newsroom/press-releases/en/2006/12/a350-xwb-family-receives-industrial-go-ahead.html` Accessed 29.06.2018

is to take off under the so called 'hot and high' circumstances, meaning at a high altitude with warm weather. This results in a relatively low density, thus being the most critical situation to take off.

After all tests are performed successfully and the test hours have been achieved, the certification is granted and pilots can be awarded a type rating based on the type certificate finally allowing the civil transport flights. The entire certification process, with the official ESEA steps, can be observed in Figure 9.4 [4].

For the Greenliner, it is expected that the total certification process would take about three years. Although this is significantly longer than the eight and a half months of flight testing which is required for modern aircraft such as the Boeing 787[5], this is to be expected as certification authorities are likely to impose additional flight tests and certification requirements for the entry into service of any fundamentally new technology in aviation such as fuel cells. The first revenue flights can then take place in 2029, in line with the assumptions made in section 12.3.
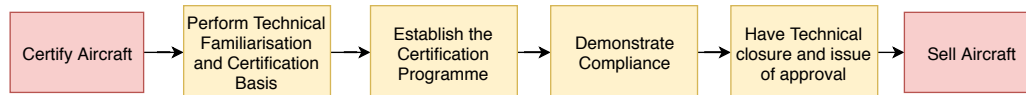

Figure 9.4: Certification Phase

9.2. Production Plan

After the certification process, the production of the Greenliner can start. Typically, an assembly process is used for aircraft which are produced serially. In this process, the aircraft is separated in many different parts called assemblies, which are then again separated into subassemblies. These separations are made either using mounting or manufacturing divisions. Mounting divisions are used for movable parts such as the control surfaces or the propellers of the Greenliner, but also for parts which need to be exchanged or inspected, such as the electrical motors or fuel cells. Manufacturing divisions however are those which are needed for efficient manufacturing. This includes for instance the connections of the wing to the fuselage, as then the fuel cells can be installed in a separate process.

The sequence of assembly of the Greenliner will be as follows. First, the tail cone is assembled, after which it is joined together with the assembly of the cylindrical part of the fuselage. This assembly already includes the tank subassembly. Next, the nose cone including the flight deck is added. Although the fuselage is now complete, it only contains the flight deck and the hydrogen tank. In the next step, the lifting surfaces assemblies are produced in a separate station and then joined with the rest of the aircraft in the main production line. Again, the fuel cells will already be integrated into the wing during the creation of the wing assembly from other subassemblies. Finally, all elements of the passenger cabin will be integrated, simultaneously with the installation of the motors and propellers. This is similar to a typical process found in other civil passenger aircraft.

This assembly process makes the manufacturing process quite efficient, as complex tasks can first be completed off the main assembly line, after which they can simply be connected with the rest of the aircraft. Furthermore, this process is needed because of the large size of some components and the required accessibility. Since the Greenliner will be produced by a relatively small company compared to Airbus or Boeing (due to the total market volume), the factory will be rather small and likely contain less station. Furthermore, except for the parts which are bought from external companies, such as the motors or flight deck instruments, almost all of the aircraft will be produced at the main factory.

9.3. Technical Risk Assessment

In this section, the risks which may occur during the next phases of the project are identified. Next, all risks are evaluated based on their severity and likeliness and shown in a technical risk map. With this technical risk map mitigation strategies are developed and a new technical risk map is shown with the mitigation strategies applied. First technical risk will be discussed in general, after which the risks are categorised into the three phases the Greenliner still will go through: the detailed design, certification and production.

---

[4]adapted from `https://www.easa.europa.eu/easa-and-you/aircraft-products/aircraft-certification` [accessed on 6 May 2018]
[5]Retrieved from `https://www.flightglobal.com/news/articles/787-first-flight-is-just-the-start-for-gruelling-pro-336319/` Accessed 29.06.2018

9.3.1. General Risk

Technical risk can be assessed on three aspects: costs, schedule and technical performance. Generally, improvement on one of these aspects will have the opposite effect on one of the others.

Costs have a significant impact on each project. It occurs frequently that a design process involves more costs than expected, which can lead to termination of the design process. Besides, a risk also exists of losing money when one of the investors decides to stop investing, which can have the same effect. For this reason there should always be enough reserves to take in such incidents.

Next, scheduling also contributes significantly to a project. A schedule is predefined for all project phases, and can therefore influence the outcome of these phases. The design phase schedule for example can influence the quality of the design by constraining the options considered. For this reason, sufficient contingency has to be built in into the project schedule, in order to allow for unforeseen circumstances.

Finally, the technical performance level required also has a significant impact on the project: if the design does not fulfil its desired purpose, more time and budget is needed. On the other hand if less time and budget is available, the technical performance of the design can be significantly less.

9.3.2. Detailed Design Risk

During the detailed design phase, several risks exists. Firstly, the detailed design can provide more challenges than expected, for example due to unconventional aspects of the aircraft, leading to a delay in completing the detailed design. This delay can lead to an increase in costs, or a decrease in income, thus forms a risk to the entire project. Secondly, estimations from the preliminary design phase can turn out inaccurate due to incorrect assumptions made. This will complicate the design, which can also delay the process. Finally, the design can turn out to be unfeasible as a whole. This will be assessed at the final stage of the preliminary design: the go or no-go part as discussed in the detailed design subsection of subsection 9.1.1.

9.3.3. Certification Risk

Several risks can lead to the aircraft not begin certified for operations. The certification is based on testing a prototype of the aircraft, as discussed in subsection 9.1.2. From this test, two risks appear: firstly, the prototype used may be flawed compared to the design made, and a new prototype has to be built. Second, the test may be performed incorrectly, which can also lead to the aircraft not being certified. Next to the prototype, the aircraft itself can be under-designed due to design mistakes made. This can lead to the aircraft not being certified, due to insufficient performance.

9.3.4. Production Risk

The production is the final phase of the aircraft before operations start. During production, the risks exist on three aspects. Firstly on the parts and materials, secondly on the human resources and thirdly on assembly.

For the parts and materials, the main risk is unavailability. When the required parts or materials for production are not available, the production will come to a stop. Next to part and material unavailability, an unexpected increase in costs for these also forms a risk. With increased costs for parts and materials, other aspects such as testing can be cut on budget, decreasing the final technical performance of the aircraft.

For human resources, multiple risks can be defined. Firstly, under-educated employees can weaken the design during production. Since a significant part of the aircraft is unconventional, this risk is larger than for conventional aircraft: new, unavailable, education is needed in order to produce the aircraft. Second, the employees can become unavailable, for example due to a strike. This will stop the production process. Finally, an unexpected increase in employee wages will lead to decreasing budget for other production aspects.

For assembly, the main risk consists of delays in the process. These can occur due to insufficient assembly ease, flaws in the production line or the delivery of parts being delayed. In either case, delays during assembly will lead to a decreased customer satisfaction, or even a loss of income due to less aircraft being sold.

9.3.5. Technical Risk Map

In this section, the technical risks discussed in the previous sections will be estimated on their probability of occurrence, and assessed on their severity. The risks discussed are given an overview together with an identifier assigned in table Table 9.1.

Next, the risks are plotted in a technical risk map, using their identifier as assigned in Table 9.1. The risk map is shown in Table 9.2, with the likelihood of the risk occurring ranging from impossible to most likely, and the consequence of

Table 9.1: Main risks with assigned risk ID

Risk ID	Risk
1.1	Delay due to design of unconventional aircraft subsystems
1.2	Delay due to incorrect assumptions
1.3	No-go in detailed design phase
2.1	Flawed prototype for tests
2.2	Test performed incorrectly
2.3	Aircraft under-designed
3.1	Required part unavailable
3.2	Required material unavailable
3.3	Increase in material costs
4.1	Under educated employees
4.2	Employee strike
4.3	Increase in employee wages
5.1	Insufficient assembly ease
5.2	Production line flaws
5.3	Delayed deliveries

the risk ranging from negligible to catastrophic

Table 9.2: Technical risk map prior to mitigation

Project Risks	Negligible	Marginal	Critical	Catastrophic
Most likely				
Likely				
Moderate		1.1, 5.1, 5.2, 5.3	1.2, 2.1, 4.1	1.3, 2.3
Improbably			2.2, 3.1, 3.2, 3.3, 4.3	4.2
Impossible				

With the risk map, the highest risks (risks with a combination of high probability of occurrence and large severity) are given a mitigation strategy. From Table 9.2, the two risks indicated in red are chosen: a no-go in the detailed design phase and the aircraft being under-designed when tested for certification (risk 1.3 and 2.3). In order to prevent a no-go in the detailed design phase, intermediate feasibility tests can be performed on the aircraft design. This can for example be done by testing separate subsystems on their functionality, ensuring the subsystems perform as required. In order to prevent the aircraft from being under-designed when tested for certification, a safety factor can be applied during the detailed design of subsystems sized for meeting the regulations. These mitigation strategies will limit the likelihood of both risks from moderate to improbable. The risk map after mitigation is shown in Table 9.3.

Table 9.3: Technical risk map after mitigation

Project Risks	Negligible	Marginal	Critical	Catastrophic
Most likely				
Likely				
Moderate		1.1, 5.1, 5.2, 5.3	1.2, 2.1, 4.1	
Improbably			2.2, 3.1, 3.2, 3.3, 4.3	1.3, 2.3, 4.2
Impossible				

<div align="right">

10

</div>

Operations and Logistics

While the Greenliner should follow standard aircraft operational procedures, there are special operational procedures that the Greenliner has due to its unconventional subsystems used. In this chapter, the operations and logistics of the Greenliner are introduced, where general operational design is combined with additional procedures. Two main operations are considered here, Ground Operations in section 10.1 and Flight Operations in section 10.2. After these, the RAMS (Reliability, Availability, Maintainability and Safety) characteristics of the aircraft operation are assessed, focused on the unconventional subsystems.

10.1. Ground Operations

The ground operations of an aircraft include all processes leading up to the line-up at the runway for take-off, starting from the moment when the runway is vacated from the previous flight or from the cold-and-dark state if there was no previous flight on the same day. Many different procedures are completed during the ground operations, as shown in Figure 10.1.

After vacating the runway, the aircraft must taxi to the parking position. As only a fraction of the maximum thrust is needed for taxiing, the majority of the motors could be turned off which would reduce the hydrogen consumption during that phase. Other than that, no differences to conventional aircraft can be found during this phase.

Once the Greenliner reaches its parking position, the parking brakes are set and the fuel cells can be turned off by cutting off the hydrogen supply. Although the APU certainly could take over the electricity supply for the cabin systems required on ground such as the air conditioning or the lighting for a certain time, the aircraft should as soon as possible be connected to ground power. This could either be done by a direct connection to the airport's electricity grid via a cable, or by a mobile ground power unit. In the latter case, units making use of conventional combustion engines should be avoided, as this would again introduce emissions into the overall process.

Next, the passengers and luggage can be unloaded and the servicing of the cabin such as cleaning or refilling of drinks and food can be completed. As the configuration of the Greenliner is fairly conventional, no differences to conventional aircraft arise during these operations. Although such regulations do not exist yet for the operation of hydrogen powered aircraft, it can be assumed that just as for conventional aircraft, the refuelling may not be completed with any passengers onboard the aircraft due to the risk of fire. However, it is not expected that the refuelling of hydrogen will take more time than the refuelling of kerosene, even though specialised vehicles and trained personnel will be necessary. Again, two different options exist for the refuelling. In the case of big airports with a large occurrence of hydrogen powered aircraft, an underground refuelling system could be installed, to which the aircraft could be simply connected via a pumping truck. Alternatively, a special hydrogen refuelling station could be installed. In the case of small scale operations, as it wil be the case in the beginning, most airports would most likely opt for the option of applying liquid hydrogen fuel trucks, which also has the additional advantage of high flexibility. However, these vehicles should again not produce any direct harmful emissions. Instead, they could also be powered by hydrogen, as explained in subsection 10.2.2.

After the refuelling, new passengers and payload can be loaded into the aircraft. Before the aircraft can taxi to the runway for the next flight, the fuel cells must first be brought to their operating temperature of 80 °C. Still, the push back procedure can already begin during this process, since the now fully charged APU can take over the electricity supply after the disconnection of the ground power. However, if time allows, this should be prevented to keep the APU fully charged for the upcoming flight. Once the fuel cells have finally reached working temperature, the taxiing to the runway can begin.
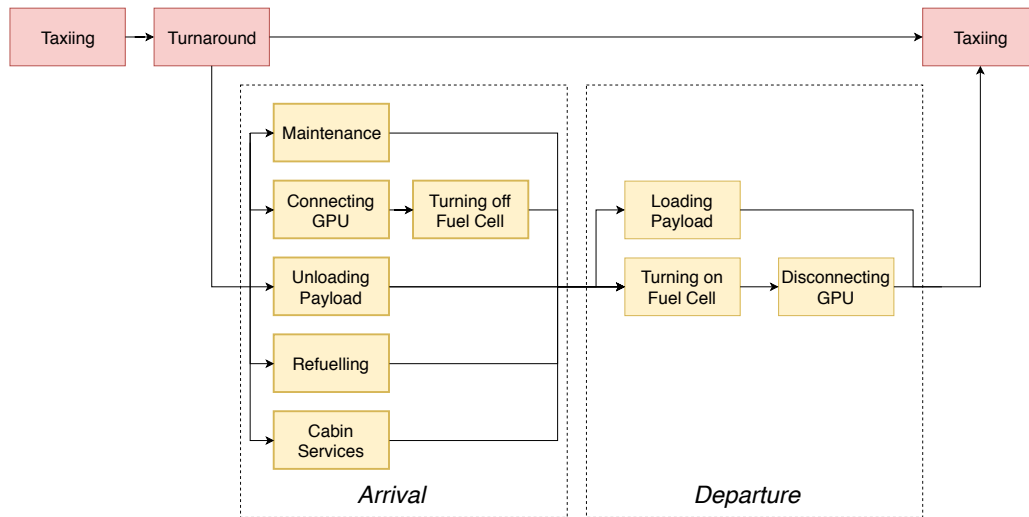
Figure 10.1: Operations flow chart showing the steps during ground operations

10.2. Flight Operations

In this section, the flight operations of the Greenliner are described.

10.2.1. Mission Profile

The profile of the flight mission of the Greenliner, presented in Figure 4.2, is designed such that during flight operations, no significant differences with conventional kerosene powered aircraft arise. Climb, cruise, approach and holding procedures are performed in the same way, with similar vertical speeds and at similar altitudes. As for any aircraft, it is desirable to fly at the highest possible cruise altitude, which guarantees the lowest fuel consumption. During the cruise phase, one interesting difference to other aircraft does however occur. Due to the high fuel mass fraction of kerosene powered aircraft, the optimal cruise altitude increases significantly throughout the cruise range, which is why a step climb is advisable to stay close to the optimal conditions. For the Greenliner however, because of the relatively low hydrogen mass, this change in optimal altitude would not be high enough to reach a new flight level.

10.2.2. Hydrogen Production

Rather than directly producing liquid hydrogen, first gaseous hydrogen (GH2) is produced and then cooled down. In order to achieve sustainable production and operation of the Greenliner, the GH2 production must be powered by renewable energy sources such as solar and wind energy. The current production method is mainly based on steam reforming, where hydrocarbons are split into hydrogen and carbon dioxide. However, this production procedure does not meet the green production requirements of the mission objective. Therefore, the alternative electrolysis method is considered, where water is split into oxygen and hydrogen when electricity is applied. With no harmful emissions produced, this method will be used during the Greenliner operation to maintain high environmental sustainability. Once GH2 is produced, the liquefaction process is conducted.

The storage of liquefied cryogenic hydrogen is a proven and tested technology [38]. The mostly refrigeration processing techniques for LH2 production are with a helium Brayton Cycle or a hydrogen Claude Cycle. For the helium Brayton Cycle, helium is used to achieve refrigeration with an expansion turbine. The helium Brayton Cycle has a low production efficiency, resulting in a higher energy consumption of 12.3 to 13.4 kWh per kg LH2 produced [44]. It also has a low production capacity of 3 tonnes per day (TPD), therefore, this is a suitable production method for distributed production plants. As for the hydrogen Claude Cycle, it has a higher energy efficiency as it uses recycling compressors that require less power. This method uses the combination of expansion turbine and Joule-Thomson valves, and the energy consumption is in the range of 10.8 to 12.7 kWh for 1 kg LH2 produced [44]. Hydrogen is cooled from 30 K to 20 K during expansion, based on the positive Joule-Thomson effect. Then the LH2 can be cooled down below the boiling point of 20.8 K. Both processes use liquid nitrogen to pre-cool the compressed GH2 to low temperature and release liquid nitrogen back to the air, hence no emission is created. These two liquefaction techniques can be used for different production plant sizes.

The production plants of liquid hydrogen production can be grouped in three types, namely central production, distributed production and semi-central production. In the centralised production, a large capital investment is required as well as extensive hydrogen transport and delivery infrastructure. On the contrary, distributed production requires less investment as small, on-site production infrastructure can be built in a short amount of time. Especially for the beginning, when only small amounts of hydrogen are needed, this option becomes attractive. Semi-central production combines the advantages of both centralised and distributed production strategy. Meanwhile, a production strategy should be chosen based on the local production. Nowadays, there are various sizes of hydrogen production plants in different parts of the world, in [83], a summary of hydrogen liquefaction plants can be found. The small production plants have a capacity ranges from 0.3 - 5 TPD, while some large production plants can obtain a 10 - 35 TPD. The produced liquid hydrogen can be transported towards the airport by LH2 trucks. Even though this pathway is still costly, the large delivery capacity will likely reduce the cost when combined with large scale of production plants [23].

An LH2 production method for the Greenliner is first chosen based on the short term goals and then at a later stage on the long term goals. In the short term, meaning from 2020 to 2035, only a small market share is expected, where less investment on LH2 production would result in a higher financial benefit. Therefore, it is advisable to opt for distributed production, off-site with the produced LH2 being delivered to the airport using trucks. This method will result in a low airport adaption cost, and small investment on infrastructure. In the long term, from 2035 to 2050, a centralised production plant is expected. It should be located close to the airport, meanwhile the infrastructure of delivery should be built, where pipe line or local plant production are considered.

10.3. End-of-Life

With any product an aircraft loses value when in it is in use. Regularly, an aircraft has a lifetime of 20-25 years[1]. After a certain point the maintenance cost become higher than the revenue gained from operating the aircraft. Furthermore, it becomes more and more difficult to keep to aircraft in compliance with regulations from government organisations [41]. Then, it is time for the aircraft to be disassembled. First, the separate parts should be assessed on reusability: parts can be used for other purposes or other aircraft. Second, it is priority to recycle as much as possible from what is left of the aircraft. Reusability and recyclability of the aircraft will be assessed in subsection 11.1.1. What cannot be recycled or reused will be dumped on a landfill[2]. However, with the current technologies / end-of-life solutions it is already possible to recycle and reuse over 90% of the aircraft parts[3].

10.4. RAMS Characteristics

In order to assess the operational performance of the Greenliner, the RAMS (Reliability, Availability, Maintainability and Safety) characteristics of the system are evaluated for the complete aircraft. For this analysis the general approach is to assess the RAMS characteristics for the unconventional subsystems of the Greenliner, since conventional subsystems are assumed to perform properly.

Reliability

The reliability of the Greenliner mainly depends the on unconventional aspects of the aircraft: the conventional parts are assumed to be reliable due to their proven designs in other aircraft. Because of this, only the reliability of the unconventional aspects is evaluated.

Electrical motor failure

Due to the unconventional system chosen for the propeller configuration (23 propellers at the back of the fuselage, as elaborated upon in section 6.1, the motor configuration is also unconventional. 23 motors are used to power the 23 propellers, which is not widely applied in aircraft. The unproven flight design can thus lead to unexpected failures, decreasing the aircraft reliability.

Although the configuration is unconventional, the use of electric motors is already widely applied in for example automotive industry. However, the electric motors for the Greenliner will operate at significantly different temperatures due to the altitudes the aircraft will fly at. When the motor temperatures are not regulated properly, this can have motor failure as a consequence, thus decreasing the reliability of the aircraft. However due to the configuration of 23

---

[1]Retrieved from `https://aviationbenefits.org/environmental-efficiency/end-of-life/` [cited on 03-07-2018]

[2]Retrieved from `https://www.icao.int/Meetings/EnvironmentalWorkshops/Documents/2014-GreenTechnology/3_Elliff_Envisa.pdf` [cited on 03-07-2018]

[3]Retrieved from `https://aviationbenefits.org/environmental-efficiency/end-of-life/` accessed 3 July 2018

motors chosen, single motors can fail without leading to mission failure.

Failure fuel cell
Fuel cells already have proven designs in both automotive industry [4] as in aircraft designs[5]. The fuel cell for the Greenliner however needs to produce a significantly higher performance, at different operating conditions. Since such a fuel cell has no proven flight design yet, a possibility of fuel cell failure is present, which decreases the reliability of the aircraft.

Hydrogen transport systems
Liquid hydrogen is stored at 20 degrees Kelvin, which provides a challenge in the handling of the liquid hydrogen. As discussed in chapter subsection 5.6.1, both the transport systems materials as the insulation of it have to be designed such that they prevent failure of the system. However, these systems are not widely applied in aircraft, thus the performance of operating it in aircraft conditions is not completely certain. This can lead to unexpected failures, thus decreases the aircraft reliability.

Hydrogen sensors
Small leaks in the hydrogen tank can have severe consequences, so they need to be noted in time so that the tank can be repaired. For this reason a hydrogen sensor is placed inside the fuselage part where the tank is placed. Advanced sensors can already detect a presence of 0.01% hydrogen in the air [90]. The pilot or maintenance mechanic will then get a sign that somethings is malfunctioning and can act upon it.

Internal wall slosh
Due to the unconventional tank design for liquid hydrogen compared to conventional kerosene tanks, the internal wall slosh has to be re-evaluated. The internal wall slosh prevention is done by putting baffles in the tank [6]. Sloshing can have an impact on the centre of gravity position, when an aircraft takes-off all the fuel moves to the back. Due to the hydrogen tank location in the back of the aircraft, this change on the centre of gravity can be significant due the larger arm with respect to the original centre of gravity. Thus, the internal wall slosh can lead to a decrease in reliability of the aircraft.

Technology Readiness Level
Summarising, the unconventional aspects of the Greenliner design will provide the largest challenge in terms of reliability. This challenge mainly occurs due to the technology readiness level of the unconventional aspects, which lead to uncertainty in terms of performance. When more testing is performed the technology readiness level will increase, which also increases the reliability.

10.4.1. Availability
The system availability is a measure of what percentage of its operational lifetime the Greenliner is actually available to be used. This is for example influenced by the time it may take to perform refuelling or to do the maintenance required after each operational cycle.
Every cycle the Greenliner needs to undergo a turnaround. As explained in section 10.1 this concerns refuelling, quick maintenance/check, cleaning and boarding passengers. Regular turnaround procedures are expected to take a similar amount of time as for conventional aircraft. So for inspecting the new turnaround time only refuelling, warm-up of the fuel cells and inspection is considered, as these involve new procedures.

Refuelling
Refuelling the aircraft with hydrogen is a new concept with respect to current aviation. The hydrogen needs to be held at very low temperatures, which might be considered as dangerous or difficult to handle. However, there already exist multiple hydrogen fuelling stations for cars, which actually work similar to the conventional gas stations [7]. They are fully equipped with the necessary devices to safely transfer the hydrogen to the vehicle. Next to that, for cars the fuelling time of hydrogen is similar to that of conventional fuel [89]. The difference between these fuelling stations for cars and the fuelling station needed for the aircraft is the state of the hydrogen. The cars referred to use compressed

---

[4]Retrieved from `http://fsec.ucf.edu/en/publications/pdf/fsec-cr-1987-14.pdf`, accessed 29 June 2018
[5]Retrieved from `https://newatlas.com/hy4-hydrogen-fuel-cell-passenger-plane-test-flight/45687/`, accessed on 29 June 2018
[6]Retrieved from `https://www.physicsforums.com/threads/how-aircraft-reduce-fuel-splashes-inside-a-wing.813847/` [cited on 28-06-2018]
[7]Retrieved from `http://blog.toyota.co.uk/how-to-refuel-a-hydrogen-car` [on 29-06-2018]

hydrogen gas, while the Greenliner uses liquid hydrogen with significantly less compression. Because of this, the main principle of the refuelling will stay similar, but different materials are needed in order to handle the low temperatures of the liquid hydrogen. However, this still is a promising feature for the refuelling procedures and time of the aircraft. For this reason it is assumed that the refuelling time will be comparable to the conventional refuelling time.

Heat Management

Heat management of fuel cells still a bit of a challenge as seen in [55]. It also states that heating up the fuel cells can already be performed within six minutes. The Greenliner is equipped with a heating system for the incoming air via the air inlet. Then the active air intake can be activated just before taxiing to the runway, first on the GPU later on the APU. The incoming air is then heated to 80°and led past the fuel cell. Consecutively, the fuel cells are booted up, which then also start producing heat. Then during taxiing the fuel cells will reach the required temperature for take-off. Taking all of this into account, the heat up of the fuel cells will not give a significant delay to the turnaround time and can be executed during boarding the passengers.

Checks

Concerning checks, it mostly consists of regular inspections of the different parts of the aircraft. An important component, however, which should be checked are the fuel cells. If its performance goes down it should be checked for clogging or contamination.

Maintenance

Furthermore, the aircraft is not available during maintenance, the time this will take will be assessed in subsection 10.4.2. From this it can be concluded that the Greenliner has a similar turnaround time as the reference aircraft, which is 1 hour. However, this must be researched more thoroughly to give an an actual number.

10.4.2. Maintainability

The maintainability criterion focuses on the amount of effort it takes to repair or replace certain parts in case of damage or failure. This includes, amongst others, the time the aircraft is inoperative due to the maintenance and the accessibility and ease for doing maintenance on or replacements of parts.

The main unconventional aspects of the Greenliner which require more attention in terms of maintainability is the fuel cell system, the hydrogen tank and the electric motors. Thus next to the conventional maintenance checks, these subsystems require additional inspection.

Fuel Cell system

The fuel cell performance depends both on the performance of the systems supplying the air and hydrogen as on the status of the fuel cell itself. Therefore, the whole system needs to be inspected regularly. For the air intake, the filters are most important since they prevent harmful particles from imposing permanent damage to the fuel cell. For the hydrogen supply, the valves and circulation systems are most important, since malfunctioning would stop the fuel cell from working. For the fuel cell itself, regular performance inspections have to be performed in order to prevent it from malfunctioning mid-flight. Access for fuel cell inspection is provided by hatches in the wings. Due to the stack configuration of the fuel cells, separate stacks can be taken out for inspection, improving the maintainability. Besides, the air intakes can be accessed from the outside of the aircraft and the hydrogen supply from the inside of the aircraft. The accessibility reduces the time needed for maintenance, thus improves the maintainability.

Tank

The hydrogen storage tank experiences different load cases throughout its lifetime, due to external temperature differences and internal pressure differences of the stored hydrogen. Due to this changing loading fatigue can occur, thus the tank has to be inspected after each flight. Besides, the hydrogen storage tank is one of the largest safety risks as will be discussed in the next subsection. Access for maintenance of the hydrogen tank is well provided, however access for replacing the hydrogen tank can be more difficult. The maintenance time and ease thus are dependent on the severity of the maintenance, and on whether the tank has to be replaced.

Electric motors

As elaborated upon in the reliability part of this section, the electric motors will operate at significantly lower temperatures than conventional. This does not necessarily restrict the electric motor performance, however regular inspection is needed in order to prevent motor malfunctioning. The motors can't be accessed from the inside of the aircraft, thus maintenance hatches have to be installed near the electrical motors in order to be able to perform the inspections and

maintenance. However, the amount of motors, as discussed in the reliability part, provide redundancy for single point failure. Less inspection thus is needed than for the fuel cell system and the hydrogen tank.

Maintenance operations

Maintenance checks in aircraft are categorised based on their level of occurrence [8]. Line maintenance (LM) takes place every operational cycle, in total this would take about 12 hours per week. Check A takes place every eight to ten weeks and takes between six and 24 hours. Check B takes place every six to eight months and takes one to three days. Check C takes place every 18 months or two years and takes three weeks. Check D takes place every six to 12 years and takes three to six weeks.

Based on the maintainability of both conventional aircraft subsystems as on the unconventional subsystems designed, an outline is made based on scheduled maintenance activities. Table 10.1 shows the different subsystems and their assigned maintenance check category.

Table 10.1: Overview of maintenance category per subsystem

Subsystem	Check Category
Fuel cell system	LM, A, D
Outside Fuselage	LM, B, D
Hydrogen Tank	LM, D
Motors	A, D
Propellers	A, D
Emergency equipment	A, D
Control Systems and Surfaces	A, D
On-board Sensors	A, D
Wing	A, D
Empennage	D
Inside Fuselage	D
Landing gear	D

10.4.3. Safety

Due to the unconventional subsystems chosen for the Greenliner design, safety is of greater concern than for conventional aircraft. The biggest safety risks are briefly elaborated upon, where only unconventional subsystems are discussed.

Tank rupture

Tank rupture is one of the main safety issues of the Greenliner. Even with the smallest leak this can already lead to issues. When liquid hydrogen escapes the tank, it will rapidly expand due to the temperature difference and ultimately the tank might explode. To mitigate the chance of rapid expansion, the fuselage wall around the tank is insulated such that the temperature goes down with the temperature of the leaking hydrogen and at a certain temperature this prevents the hydrogen from expanding even more. Furthermore, hydrogen might reach the passenger cabin and suffocate them. This is mitigated by putting the tank in a separate compartment of the fuselage, which does not let any gasses pass. The pilot will already have noted that hydrogen has escaped and will try to land as soon as possible to fix the tank. It is important to check the tank frequently for cracks to prevent disasters. The schedule for these checks is included in subsection 10.4.2.

Tank puncture

Tank puncture can occur when sharp objects hit the hydrogen tank, which leads to a leakage. As explained in the previous part about tank rupture, even a small leak can already lead to failure of the system. Although tank puncture is rarely occurring, a safety measure can be taken by using a layer of puncture-resistant material (for example Dyneema or Kevlar fibres could be used [9] [10]). Such a layer will provide the necessary protection against for example a sharp

---

[8] retrieved from `https://www.qantasnewsroom.com.au/roo-tales/the-a-c-and-d-of-aircraft-maintenance/` accessed on 29 June 2018

[9] retrieved from `http://www.dsm.com/products/dyneema/en_GB/technologies/dyneema-form-factors/fabric.html` accessed on 2 July 2018

[10] retrieved from `http://www.dupont.com/products-and-services/fabrics-fibers-nonwovens/fibers/brands/kevlar.html` ac-

aircraft part breaking, or in an extreme case, even a bullet fired at the hydrogen tank.

Fuel cell clogging

Fuel cell clogging can cause a decrease in performance of the fuel cell [3]. At a certain point this will lead to a failure of the fuel cells and thus a shut down of the motors. Therefore, the airflow should always be filtered by several redundant filters and should be checked at every turnaround. The hydrogen side of the fuel cell should be purged of nitrogen and should have a sensor for measuring the amount of nitrogen, giving a signal when this is above the allowed amount.

Propeller blade breakage

In extreme load cases, a propeller blade can break off. Due to the amount of propellers, the failure of one propeller won't lead to failure of the mission. On the opposite, if a propeller blade punctures the fuselage, more damage is done. The blade can puncture a motor, which would lead to more propellers being inoperative. However even if more motors or propellers become inoperative, the aircraft will still be able to safely land. Besides, the propellers are located at the non-pressurised part of the fuselage, thus no depressurisation will occur when a blade punctures the fuselage.

Lightning

The influence of lighting on aircraft is always a subject of discussion as it scares passengers when it hits the aircraft. However, lightning has minor impacts on the aluminium body. The current enters the fuselage, then travels through the outer shell of the fuselage and then exits the fuselage at another part. Rarely, the aircraft is damaged by the lightning and in case it happens, this only affects the exterior part. [11] However, there should be enough resistance against the high temperatures, reached by the current, especially in the fuselage part around the hydrogen tank. When this is accounted for, there is no risk that the hydrogen might be affected by lightning.

---

cessed on 2 July 2018

[11] Retrieved from `https://www.telegraph.co.uk/travel/travel-truths/what-happens-when-lightning-hits-a-plane/` [cited on 29-06-2018]

Sustainability Assessment & Compliance

In chapter 3, an approach to sustainability was developed. After applying this approach throughout the design process, it must now be assessed whether the Greenliner meets the imposed sustainability goals. In section 11.1, these goals are analysed and a comparison is given to a reference aircraft. A score is then applied for each criterion. These scores are presented in a spider map in section 11.2.

11.1. Sustainability Analysis

The sustainability of the Greenliner is assessed based on the three sustainability pillars: Environmental, Social and Financial sustainability. This section evaluates the Greenliner's sustainability with different criteria within these three pillars. Then the Greenliner performance is compared to a conventional aircraft. The analysis is done for the year 2030, when the Greenliner is planned to be operational (see chapter 12). For each criterion, the aircraft is scored for 1 to 5, as catastrophic, poor, adequate, good and excellent. In subsection 11.1.1, subsection 11.1.2 and subsection 11.1.3, the score for each criterion is provided with proper motivation. In the end, the result is summarised in Figure 11.1.

11.1.1. Environmental Principle

Recycling of Materials

The process of converting waste materials into new materials or products is called recycling. This process is a very important method to reduce waste. Furthermore, materials can be reused multiple times if treated correctly, therefore, the mining of raw materials can be reduced. The energy consumed to produce a product when using recycled materials is lower than when using raw materials [45]. Therefore, the recycling of the aircraft materials is considered for the Greenliner. In order to analyse the recyclability of the aircraft, the different materials used in the design and their recyclability are accessed. These materials can be categorised in metals, composites and graphite.

The majority of the Greenliner is built out of metal, which is mostly easy to recycle. The metal recycling procedure includes collecting, sorting, compacting, shredding, separating and purification. Collecting aircraft metals would take place when the aircraft is at its end-of-life phase or certain parts are broken beyond repair. An aircraft metal sorting process should remove the non-metallic materials such as the fabric for seats, plastic for the galley, so that the collected materials have a very high percentage of metal. Then, the remaining metallic parts of the aircraft are shredded and crushed. The shredding process breaks the metal into small pieces, such that the melting process requires less energy. Next, different types of metals are separated. First, the separation between ferrous and non-ferrous metals is done by using a large magnet. Then among the non-ferrous materials, there are leftover non-metal particles such as paint or plastics, which can be removed by simply blowing hot air through the shredded materials. Lastly, the purification starts with melting the materials. After this process, each type of metal can be split and they can then be reused for other purposes.

The metal types used for Greenliner include aluminium, stainless steel, titanium and platinum. All these materials are not used in their pure form, instead they are combined with other metals to provide a better performance structure, conductivity, thermal or other aspects. For instance, for the fuselage, wing and tails, aluminium alloyed with copper is used. In the Greenliner, the LH2 storage tank also consists of the aluminium alloy 2219, which has contains 92% aluminium, 6% copper, 0.3% iron and some other metals. Nearly more than 75 % of aluminium produced is still in use today. Therefore, aluminium alloys are used for Greenliner application. Therefore, further separation and pretreatment process are necessary before aluminium can be molten. Although stainless steel and titanium are applied in the LH2 transfer lines and the landing gear, these constitute only a small portion of the complete application of metals. Furthermore, the fuel cell catalyst platinum is also recyclable.

The non-metallic materials such as graphite, rubber, or foam have different degrees of recyclablity. Graphite material, used in the fuel cells, can be recycled and after doing so maintain 90% of its electrochemical performance [82]. On the other hand, other materials such as foam fillings or the rubber tyres cannot be easily recycled. These will be used for other applications, or will be simply disposed of.

The Greenliner can be given a score of 4.5 in terms of recyclability, because of its widespread use of easily recyclable materials. For the Dornier 228 however, some composites are used for parts such as the propeller, which lowers the recyclabilityk, resulting in a score of 4.

Reuse of Aircraft Parts

The reuse of the aircraft parts can be divided into three parts: The reuse for other aircraft in general, the reuse for other Greenliners and not reusable at all.

Interior parts, such as seats, cabin lighting, cabin temperature management systems and lavatory can all be reused in other aircraft, as these are most likely bought from other companies. It should be noted that for visible components such as the seats, it might be hard to sell them as second hand products, as many airlines prefer to have a modern and comfortable interior of the passenger cabin. Apart from these interior parts, the propellers and motors (especially if properly maintained) could also be reused on other aircraft, although it might not be likely since they have been specifically designed for the Greenliner.

Some parts are specifically designed for the Greenliner, such that they cannot be reused in other aircraft. These parts would be the hydrogen tank, cockpit instrumentation, hydrogen and oxygen pressurisation system, oxygen humidifier and the door. If their lifetime exceeds that of a Greenliner unit, these parts can easily be reused if properly maintained.

During the lifetime of the Greenliner there is a number of systems that cannot be reused in other aircraft. These systems include all structural, load carrying parts, such as the wings, the landing gears, the tail, the fuselage shell and the gears of the engines, which wear off during operations. These parts are subject to recycling. Apart from these parts, also the fuel cell system and APU cannot be reused, since the fuel cell system and APU degrade over time and need replacement.

It should be noted that it is planned to build only a few hundred units of the Greenliner, which is low compared to other companies. Most commercial aircraft are built in units that range in the thousands, which means that those companies have enough money to design a lot of their subsystems themselves. This is not the case for the Greenliner, and therefore most of the parts must be bought from partners. For the sake of sustainability, the possibility of buying used parts for new Greenliners will be examined.

It can be expected that many parts of the Greenliner can be reused. Therefore, a 4.5 is given in this category. A similar rating is applied for the Dornier 228, because there are around 370 aircraft built in total.

Emissions

The main goal in the design of the Greenliner is the absence of harmful emissions. It must therefore be shown that the two types of emissions that the aircraft does produce, hydrogen and water, do not have a significant harmful effect on the environment. As for the emission of water, which is about 1 cup per second, will not significantly influence the environment, as cloud formation and water precipitation are natural phenomena. When the use of hydrogen as a fuel is adapted by other aircraft manufacturers, it is however recommended that the effect of water emission on the environment is more closely researched.

As for the hydrogen, there are some sources that state that hydrogen is an indirect greenhouse gas itself because it reduces the amount of hydroxyl in the air, and therefore increasing the lifetime of direct greenhouse gases such as methane [1]. Although proper research should still be conducted into the effects of hydrogen emissions, it should be acknowledged that no direct greenhouse gasses are produced during operation.

The operation of the Greenliner requires oxygen particles from the air to complete the electrochemichal reaction that happens in the fuel cell. It could be said that due to this effect the oxygen in the air would be depleted. This is however not true, because during the production of hydrogen from electrolysis with water, oxygen is created. Therefore the netto usage of oxygen is zero, given that the hydrogen is produced from a process similar to electrolysis.

To ensure an emission free aircraft while using hydrogen as a fuel, it must be guaranteed that the hydrogen is produced in an emission free process. A possible method would be to create hydrogen from electrolysis at the aircraft, using electricity generated by a solar cell or wind energy power-plant located at, or near the airport.

---

[1] Retrieved from `http://www.ghgonline.org/otherhydrogen.htm` on June 28 2018

Apart from emissions during the operational phase of the aircraft, it must be mentioned that during aircraft production the emissions will be kept as low as possible. Since the company building the Greenliner is a small company, it will most likely have a single location and not use energy on the intermediate transportation of parts. It is however deemed that in the foreseeable future, aircraft production cannot be done completely on green energy.

In terms of emissions, the Greenliner outperforms Dornier 228 because the Greenliner is designed to have zero harmful emissions. Therefore, The scores given are a 5 and a 1.

11.1.2. Social Principle

Technical readiness level

The technical readiness level (TLR) of the Greenliner is lower than that of a conventional aircraft because of the use of an unconventional propulsion method and fuel type. It is however a conventional aircraft in the sense that it has an expected configuration with a wing and tail. The TLR of the Greenliner is therefore lower than that of the reference aircraft. Although this will be improved once the first complete prototypes are conducted and test in flight, this will require a lot of investments. The technical readiness level could therefore also be improved by doing tests on the unconventional subsystems of the Greenliner.

Once the propulsion system is validated after doing wind tunnel tests, the technical readiness level will already have improved. For the fuel cell system the air intake should be tested in a wind tunnel, and the fuel cell itself should be built and tested under multiple operating pressures to validate the model, which would further improve the TRL. In order for the Greenliner to become a product trusted by the society and the customers, the technical readiness level should attain the same level as for conventional aircraft. This is also important in order to make the product accessible to everyone.

In terms of the TRL, the Greenliner still performs badly at the present moment. However, when forcasting until 2030, it is expected that the technology related will have improved, thereforea 4 can be assigned. As for the Dornier 228, which has been in service since 1981, the TRL merits a score of 5.

Regulations

For any new technology that is developed in aviation, regulations must be adapted or created accordingly. Although the Greenliner could mostly already operate in the current regulatory framework, it is expected that the relevant authorities will adapt to the technological advancements, as it was for instance the case for unmanned aerial vehicles, with the regulation referred to as Operation and Certification of Small Unmanned Aircraft Systems by the FAA [64]. It can therefore be expected, that new regulations for the use of hydrogen in aviation or the use of distributed propulsion will be established. However, for more general topics such as noise regulations, it can be expected that the Greenliner will fulfill these, which is also important with respect to the public acceptance of the product.

It can be expected that at the entry into service of the Greenliner, the relevant regulations will exist, such that they can be taken into account in the final design phase. Therefore, both the Greenliner and the reference aircraft receive a score of 4 with respect to the regulations.

Noise

The difference between the Greenliner and a conventional aircraft in terms of noise is that the Greenliner uses electric motors instead of combustion engines, which already reduces the amount of noise that is produced. However, the Greenliner is using 23 propellers, which is a lot more than regular aircraft. The propeller must therefore be designed such that a configuration with 23 propellers will still comply with the noise regulations from ICAO [71]. In section 7.5 it is explained in more detail how the Greenliner complies with the ICAO regulations. Achieving low noise is particularly important for a new technology, as society expects positive results, instead of additional nuisance.

11.1.3. Financial Principle

The financial sustainability of the Greenliner will be assessed in this subsection.

Production Cost

From the project objective statement shown in chapter 1 it is clear that the production cost of the Greenliner must be competitive with conventional aircraft. In chapter 12 an analysis of the production cost is given, where it is stated that the unit cost will be 9.6 million USD. This concludes that the Greenliner has a higher production cost than Dornier 228. Hence scores of 3 and 4 are given to these two designs.

DOC

From requirement **GF-SYS-EXT.1.1-1** (see chapter 13) it is clear that the operational cost of the Greenliner shall not exceed the operational cost of a conventional aircraft. With a cheaper cost of LH2, the Greenliner scores a 4 in DOC, while Dornier 228 scores a 3 as it uses conventional fuel (see section 12.4).

Disassembly and Dismantling

During the disassembling and dismantling processes at the end-of-life of an aircraft, a lean approach should be aimed for to optimise this process by decreasing waste, reducing disassembling time and reducing the cost.

Before starting disassembling aircraft parts, the valuable parts of the aircraft should be identified. This is closely related to the customers requirements and how they want to reuse the parts in the aircraft. For the Greenliner, there are a few special parts that might be considered valuable to the customer, which include the fuel cell, propeller because of the high purchase price of these parts, related to the materials used.

It should be noted that, for the Greenliner, it is expected that the disassembly of certain parts is different from the reference aircraft. For instance, the removal of the hydrogen tank poses an additional challenge as it must be removed from the inside of the fuselage. On the other hand, the aircraft features a conventional configuration, which means that similar procedures or even accessing tools can be used. Furthermore, it can be expected that the operators will be able to deal with these challenge with proper support from the manufacturer. Therefore, both designs are given a 4.

Maintenance

Just as for the direct operational cost, there is a requirement regarding the maintenance cost of the Greenliner. **GF-SYS-EXT.1.1-2** states that the average maintenance cost shall not exceed that of a conventional aircraft. In section 12.4 the maintenance cost is estimated to be similar to that of a conventional aircraft, while for engine labour and materials the maintenance cost is estimated to be even lower. Therefore, a 4 is given for both aircraft.

11.2. Sustainability Spider Map

From the analyses made in section 11.1 a spider map was set-up in Figure 11.1. This map graphically depicts and compares the performance in sustainability of both the Greenliner and the Dornier 228 in the year 2030.
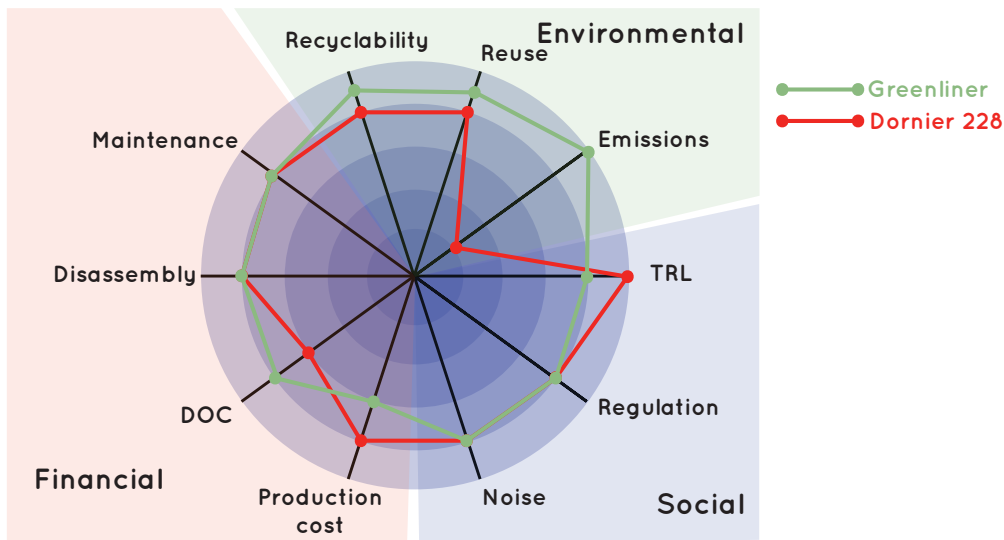

Figure 11.1: Sustainability analysis summary for the Greenliner and Dornier 228 in 2030

<div align="right"># 12</div>

Financial Analysis

In this chapter, a financial analysis of the Greenliner design concept is provided. First, in section 12.1 the current and future markets are analysed. Then, in section 12.2 the investments necessary for the development and construction of the aircraft are presented. This is followed by estimations of the return of investment in section 12.3, the direct operational costs in section 12.4 and finally the airport adaption costs in section 12.5.

12.1. Market Analysis

In this section the market price, the market volume and the achievable market share are discussed.

Most 19 seaters that are currently in scheduled passenger operation are mostly designed over 30 years ago[1], which is why the unit price for a new aircraft in this class can not be directly determined by a direct relationship to the price of these older aircraft. Therefore a different approach is taken. Instead, newer aircraft are taken as a reference, up to the size of the Airbus A318. As one can observe in Table 12.1, the cost for each aircraft is divided by the number of passengers in standard configurations. After scaling these values to 19 passengers and averaging, it is concluded that a modern 19 seater can be expected to have a retail price of about 9.6 million USD. To compare, this is relatively close to the retail price of 9 million USD of the Do 228NG, which is one of the 19 seaters currently in production[2].

Table 12.1: Cost comparison of similar aircraft

Aircraft	Unit price [million USD]	Passengers in standard configuration [-]	Cost per passenger [million USD]	Unit price scaled to 19 passengers [million USD]
Dornier Do228 [103]	9	19	0.47	9
Embraer ERJ 145[3]	21	45	0.47	8.93
ATR 42[4]	19.5	50	0.39	7.41
Mitsubishi Regional Jet[5]	46.3	69	0.67	12.73
Bombardier CRJ200[6]	21	50	0.42	7.98
Airbus A318 [4]	77.4	107	0.72	13.7
Boeing 737 [14]	32	85	0.38	7.22
Average				**9.6**

The client determined that the unit price of the Greenliner shall exceed the price of a conventional aircraft in the same class by at most 25%, which results in a unit price of 12 million USD. The higher price could be justified by several reasons, such as the public image or extra government funding[7]. Then, assuming that the operations of small regional aircraft will, again for the sake of sustainability, completely shift to the class of 19 seat aircraft, the predicted 600 units result in a total market value of 12 million USD · 600 = 7.2 billion USD.

---

[1]Retrieved from `https://en.wikipedia.org/wiki/Regional_jet` [accessed 14 june 2018]

[2]Retrieved from `https://www.ainonline.com/aviation-news/air-transport/2011-10-10/ruag-shows-nextgen-dornier-do228ng` [accessed 8 May 2018]

[3]Retrieved from `https://www.aircraftcompare.com/helicopter-airplane/Embraer-ERJ-145/122` [accessed 8 May 2018]

[4]Retrieved from `https://www.airfinancejournal.com/articles/3160018/Aircraft-Profile-ATR-42-500` [accessed 8 May 2018]

[5]Retrieved from `https://www.thenational.ae/business/mitsubishi-s-jet-set-for-push-into-middle-east-1.153824` [accessed 8 May 2018]

[6]Retrieved from `https://www.aircraftcompare.com/helicopter-airplane/bombardier-crj-200/92` [accessed 8 May 2018]

[7]Retrieved from `http://www.cleansky.eu/clean-sky-2-budget` [accessed 14 june 2018]

As the Greenliner-concept is (one of) the first emission-free aircraft, it is expected that, besides operating in the current market, it creates a market for itself. It is hard to estimate the potential of this aircraft, but it is expected that if the Greenliner is the first zero-emission aircraft on the market it can capture a significant portion of it. Therefore, the ambition is to take a similar part of the market that the main players have today, about 25% (the three largest regional plane manufacturers: ATR, Embraer and bombardier each cover between 20% and 25% of the market)[8]. It is therefore assumed that for the first version of this aircraft $25\% \cdot 600 = 150$ aircraft can be sold. After analysing the competition, the Zunum Aero Jet is the largest threat. They are planning to have a hybrid 19 seater flying by 2020 - 2025 [101], therefore it is expected that if the Greenliner is introduced in 2030, it will be the first all-electric aircraft to fly. As summarised in Figure 12.1, the Greenliner concept has a lot of potential.
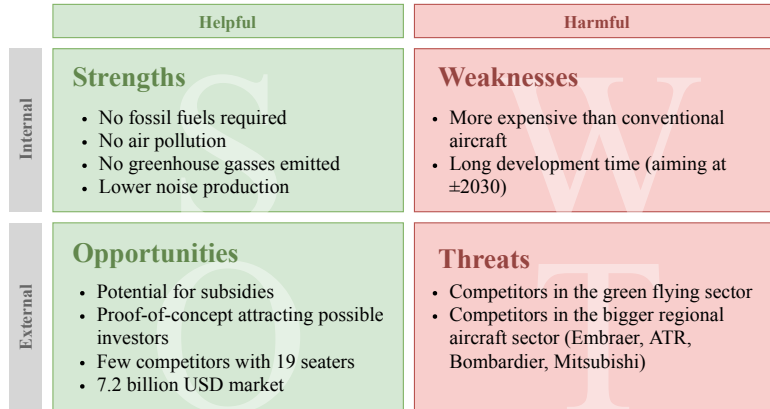

Figure 12.1: Market position SWOT Diagram

12.2. Investments

In order to produce an aircraft, money has to be invested first. In this section, these costs are analysed: they are broken down in development, manufacturing and test costs. In a conceptual design phase it is hard to have a good estimation of these values: a statistical method is adopted [105] for the development , manufacturing and test costs.

Since the statistical methods makes use of averages, a high level breakdown with just three levels is adopted (Figure 12.2). If these costs are known, the theoretical profit can be calculated if the selling price is determined. As one can observe, all subsystems play a role in both the development and the manufacturing costs. The final assembly, material costs and acquisition costs are only part of the manufacturing costs. Finally the test costs consists of using testing software and the certification costs.
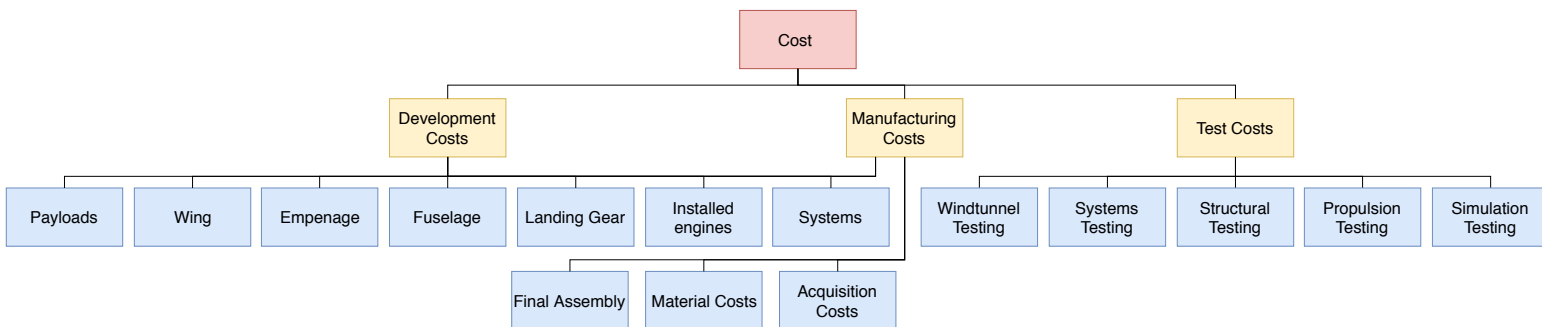

Figure 12.2: Cost Breakdown Pre Operations

---

[8]Retrieved from https://blog.forecastinternational.com/wordpress/long-term-growth-projected-for-regional-aircraft-market/ [accessed 24 June 2018]

12.2.1. Development and Manufacturing Costs

For the development and manufacturing costs the model presented by Willcox [105] and Markish [56] is used. It specifies the projected development costs for the aircraft subsystem per expected kilo at operation empty weight and can be observed in Table 12.2 and Table 12.3. These values were estimated based on public domain data and tools plus expert testimony and mostly based on the Boeing 777-200 [56]. It is a crude approximation, but since this is only conceptual design it is not wise to go into depth at this moment: if a more complex model is used it would use non-linear cost estimating relationships and require to have a lot of details of the design [56].

Table 12.2: Developing costs per kg (OEW) in USD (2002) of aircraft components

	Engineering	Material & equipment	Tool design	Tool fabrication	support	total
Wing	15637	3909	4105	13605	1836	39093
Empennage	45993	11499	12073	40014	5404	114983
Fuselage	28301	7075	7430	24624	3325	70753
Landing gear	2202	551	578	1916	258	5505
Installed engines	7666	1916	2013	6669	899	19163
Systems	30254	7564	7941	26321	3554	75634
Payloads	9491	2372	2491	8259	1116	23728

Table 12.3: Manufacturing costs per kg (OEW) in USD (2002) of aircraft components

	labor	materials	other	total
Wing	1343	450	194	1986
Empennage	3558	1067	514	5139
Fuselage	1497	419	216	2132
Landing gear	236	216	35	487
Installed engines	547	201	79	827
Systems	694	201	101	996
Payloads	893	220	130	1243
Final assembly	128	9	7	143

Because of harsh competition, aircraft manufacturers tend to keep these numbers close to the chest and it is therefore very hard to verify and validate above tables. It is therefore assumed this method is verified and validated by the creators, but since this process is not repeatable it was decided to check the final values with industry professionals to give perspective. It is recommended that for the final cost estimation more research is conducted.

Furthermore, while the 777 is not comparable in size to the Greenliner, it was the first Boeing aircraft to use fly-by-wire and the first to be entirely designed on a computer. In the case of the Greenliner the novelty is the propulsion system. In this early stage of the process it is therefore assumed that this method is applicable to the Greenliner.

Finally, the values in the model are from 2002, a correction factor of 40%[9] must be added to the total value.
The results are observable in Table 12.4. As can be seen, the total investment costs are more than 300 million USD, while the initial cost price is about 10 million.

12.2.2. Testing Costs

To estimate the testing costs, a method provided by Roskam[81] is used. For this method, the following test costs are included: windtunnel testing, systems testing, structural testing, propulsion testing and simulation testing (flight software).
The test cost can be estimated with Equation 12.1

$$C_{test} = 0.008325 \cdot W_{ampr}^{0.873} \cdot V_{cruise}^{1.890} \cdot N_{test}^{0.346} \cdot IC \cdot F_{diff} \qquad (12.1)$$

[9] Retrieved from `https://www.officialdata.org/2002-dollars-in-2018` [accessed 15 June 2018]

Table 12.4: Greenliner development cost (corrected the total value with the inflation)

	Weight [kg]	Development per kg [$]	Cost per part [$]
Wing	885	39,093	34,596,927
Empennage	179	114,983	20,581,902
Fuselage	975	70,753	68,984,490
Landing gear	105	5,505	578,022
Installed engines	1119	19,163	21,443,039
Systems	948	75,634	71,701,396
Payloads	200	23,728	4,745,695
		total & corrected 2018	311,684,060

Table 12.5: Greenliner unit price cost (corrected the total value with the inflation)

	Weight [kg]	Development per kg [$]	Cost per part [$]
Wing	885	1986	1,757,942
Empennage	179	5139	919,881
Fuselage	975	2132	2,078,584
Landing gear	105	487	51,159
Installed engines	1119	827	925,120
Systems	948	996	944,677
Payloads	200	1243	248,683
Final assembly	4411	143	632,102
		total & corrected 2018	10,581,406

In which W_{ampr} can be estimated with Equation 12.2, V_{cruise} is the equivalent airspeed (kts) during cruise, $N_{test} = 2$[81] are the amount of prototypes built for testing, IC = 6.47 is the inflation index with respect to 1970[10], $F_{diff} = 2$[81] corresponds to difficulty level 2: "programs involving very aggressive use of new technologies"

$$W_{ampr} = invlog[0.1936 + 0.8645 log(W_{to})] \tag{12.2}$$

When calculated, the testing costs are C_{test} = 5,810,000 USD.

12.3. Return on Investment

The initial unit price is 10,581,000 USD. For typical aircraft manufacturing processes, the cost are reduced by a factor 0.9 every time the production doubles [105]. Using this relationship the unit cost price is calculated for all 150 units, this can be observed in Figure 12.3a. Since the aircraft is sold for 12 million USD, this means an initial profit of 12,000,000 - 10,581,000 = 1,419,000 USD, because of the learning curve, this reaches a profit of 4,989,000 USD. Since the invenstment is $C_{development} + C_{test}$ = 311,684,000 + 5,810,000 = 317,749,000 USD, it takes time to make a profit, as can be observed in Figure 12.3b, the break even point occurs in 2038, nine years after the first unit was sold. After all 150 unit have been sold, the total profit is USD 370,227,000.

12.4. Direct Operational Costs (DOC)

According to NASA[51] the direct operational costs splits in the components observable in Figure 12.4.

In order to assess the direct operational cost, the Greenliner is compared to similar conventional aircraft (Dornier 288 and DH Twin Otter):

Depreciation Since the Greenliner is valued at 125% the price of a conventional aircraft and since it is assumed that the lifetime is the same, the depreciation will be 25% higher.

Insurance Since insurance is mainly concerned with value, it is expected that also insurance is 25% as expensive.

Interest If a company finances their aircraft by taking out a 25% higher loan, the interest will be 25% higher as well (it is assumed the interest rate will be the same).

---

[10]Retrieved from `https://www.bls.gov/cpi/` [Accessed 19 June 2018]

(a) Learning curve for production
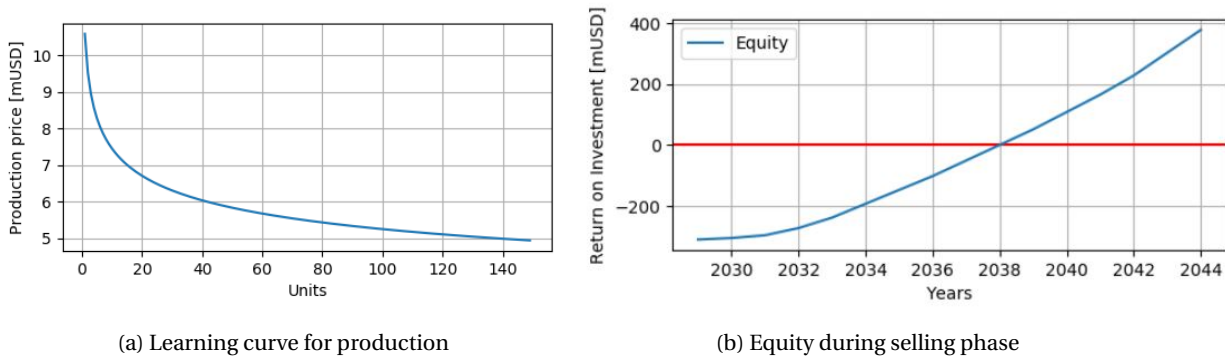

(b) Equity during selling phase

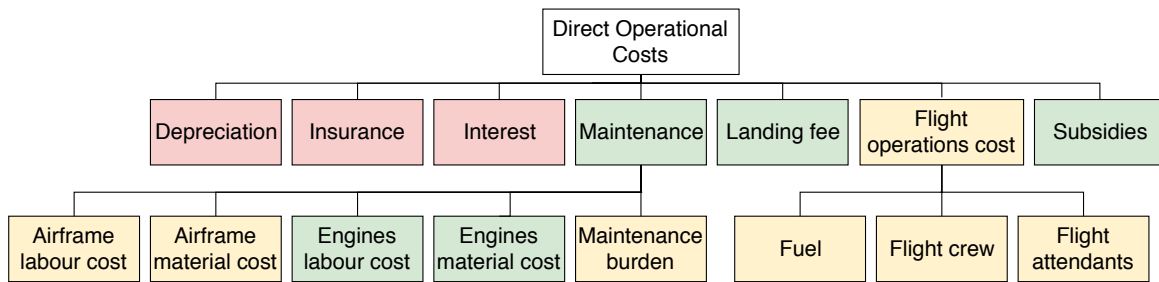Figure 12.3: Financial analysis Greenliner

Figure 12.4: Direct operation cost distribution: Red; worse than conventional aircraft, yellow; equal to conventional aircraft, green; better performing than regular aircraft

Maintenance Maintenance consists of airframe labour cost, airframe material cost, engines labour cost, engine material cost and maintenance burden:

  Airframe labour cost Since the Greenliner fuselage is comparable to reference aircraft, it is assumed that the labour costs of maintaining the airframe will be the same.

  Airframe material cost For the Greenliner the same material is used as for comparable aircraft, therefore it is expected that the metrial cost for maintenance is similar.

  Engines labour cost Since electric engines are way less complex than airbreathing engines, it is expected that this part of the operational costs will be lower for the Greenliner option.

  Engines material cost For the same reasons as for the labour cost plus the fact that electrical engines are relatively cheap, the material cost will also be lower.

  Maintenance burden Maintenance burden covers overhead costs such as controlling, monitoring, planning, testing and administration. It is expected that these overhead costs will not be different for the Greenliner.

Landing fee The landing fee is based upon maximum take off weight and additional fees for NO_x-emissions and noise. Since the Greenliner is completely emission free and low in noise, it is expected to have a lower landing fee

Flight operations costs The flight operation costs consists of the fuel, flight crew and flight attendants.

  Fuel At today's price, the liquid hydrogen is very expensive, but the price is expected to drop to €1/kg in 2030 [99], therefore not making it more expensive than using kerosene.

  Flight crew & Flight attendants The greenliner design does not affect the flight crew & attendants costs.

Subsidies The European Union has a research programme, funded by Horizon 2020, with a programme budget of 4 billion euros. This programme aims to help reaching the ACARE goals[11]:

---

[11]http://www.acare4europe.org/sria/flightpath-2050-goals/protecting-environment-and-energy-supply-0, [accessed on 26 June 2018]

- In 2050 technologies and procedures available allow a 75% reduction in CO2 emissions per passenger kilometre and a 90% reduction in NOx emissions.The perceived noise emission of flying aircraft is reduced by 65%. These are relative to the capabilities of typical new aircraft in 2000.
- Aircraft movements are emission-free when taxiing.
- Air vehicles are designed and manufactured to be recyclable.
- Europe is established as a centre of excellence on sustainable alternative fuels, including those for aviation, based on a strong European energy policy.
- Europe is at the forefront of atmospheric research and takes the lead in the formulation of a prioritised environmental action plan and establishment of global environmental standards.

The Greenliner helps reaching all these goals, therefore it is expected that some subsidy can be allowed.

The requirements stated that the operational costs cannot exceed 125% of the operational cost of a comparable aircraft. As can be seen in Figure 12.4, only the depreciation, insurance, interest and fuelcost increase. The first three are linearly related to selling price, meaning they do not exceed the 25% extra. To compare the fuel cost, it is calculated how much the fuel costs for the Twin Otter and the Dornier 228 are compared to the liquid hydrogen the Greenliner uses. The result can be found in Table 12.6. To conclude; it will be cheaper to use liquid hydrogen than to use kerosene when the Greenliner hits the market.

Table 12.6: Fuel price comparison

Aircraft	Fuel consumption	Cost	Total costs two hr flight [$]
Twin Otter	650 lb/h[12] = 97 gallons/h lb/h	$2.16/gallon[13]	210
Dornier 228	575 lb/h[14] = 86 gallons/h	$2.16/gallon	186
Greenliner	60 kg/h	$0.90/kg (in 2030)[99]	108
		$2.75/kg (in 2020)[99]	330

Taking into account all the direct operation costs,

12.5. Airport Adaptation Costs

It is assumed that either the liquid hydrogen is produced off-site and transported to the airport or that it is produced on-site. In the case of off-site production, this implies no additional costs to existing airports. If the hydrogen is produced on-site, it is assumed that an external company will take care of it and it will not cost the airport extra money.

---

[12]Retrieved from `https://www.vikingair.com/twin-otter-information/operating-costs` [Accessed on 26 June 2018]

[13]Retrieved from `https://www.indexmundi.com/commodities/?commodity=jet-fuel` [Accessed on 26 June 2018]

[14]Retrieved from `https://www.tenderned.nl/tenderned-web/aankondiging/detail/documenten/document/7331845aa5a6781cba5356d74a6af60f/pageId/D909C` [Accessed on 26 June 2018]

13

Compliance with Requirements

In this section the compliance matrix is presented in Table 13.1. It shows whether or not each requirement is fulfilled by the Greenliner. In the first two columns the requirement IDs and the actual requirements are stated. In the third column it is indicated what the status of the requirement is. The check mark (✓) indicates that the design complies with the requirement, the tilde (~) means that it is assessed in the report but that it requires some more research, the cross means (X) that it is not considered and still needs to be assessed in future detailed design. In the last column the relevant sections are presented and comments are given, if necessary, to substantiate the reasoning.

Table 13.1: Compliance Matrix

Requirement ID	Requirement	✓ / ~ / X	Relevant Section(s) & Comments
GF-SYS-INT.1-1	In the standard cabin configuration, the aircraft shall seat 19 passengers such that 100 kg are dedicated to each passenger, of which 20kg are dedicated for luggage.	✓	section 5.1 & chapter 6
GF-SYS-INT.2-2-n	The aircraft shall have a nominal cruise range of at least 500 nautical miles at maximum payload.	✓	section 4.2 & section 7.1: The range requirement is one of the main parameters on which the design is based.
GF-SYS-INT.3-1	The aircraft shall be minimally able to fly at FL245.	✓	section 7.1 & subsection 7.1.1
GF-SYS-INT.3-2-n	The aircraft shall be able to reach any destination within 500 nautical miles in 2 hours at standard atmospheric conditions.	✓	chapter 6: The time to fly is expressed in cruise velocity and range, which yield a flight duration of 1.8 hours.
GF-SYS-INT.3-3	The aircraft shall require a maximum runway length of 1500 meters to complete its take off.	✓	section 5.10
GF-SYS-INT.3-4	The aircraft shall require a maximum runway length of 1500 meters to complete its landing.	✓	section 5.10
GF-SYS-INT.3-5	The propulsion system shall be an exchangeable unit.	✓	Equation 5.5.2 & section 10.4: The propulsion system concerns propellers, electric motors & fuel cells.
GF-SYS-EXT.1-1-n	The aircraft shall comply with the applicable regulations declared by EASA and ICAO.	~	section 7.5: Only a few regulations have been considered, in the next phase all the regulations should be checked on compliance.
GF-SYS-EXT.1-2	The aircraft flight operations must be completed successfully without the dependency on exterior influences such as external energy sources.	✓	section 5.8 & section 5.6: the fuel cells do require energy for start up, however this can be supplied by the APU, which afterwards can be charged by the fuel cell for the next take-off.

GF-SYS-EXT.2-1	The development and manufacturing cost per aircraft shall be such that the maximum retail price of one aircraft is 12.5 million USD.	✓	section 12.1: The unit price is, after the market analysis, expected to be 12 million USD, however this is only based on assumptions and expectations and should be investigated more closely in the detailed design phase.
GF-SYS-EXT.1.1-1	The average operational costs shall not exceed those of conventional similar aircraft.	✓	section 12.4: Same reasoning as for GF-SYS-EXT.2-1
GF-SYS-EXT.1.1-2	The average maintenance costs shall not exceed those of conventional similar aircraft.	✓	section 12.4: Same reasoning as for GF-SYS-EXT.2-1
GF-SYS-EXT.1.1-3	The aircraft shall perform within regulations for a duration of at least 35,000 cycles.	~	section 10.4: This is not explicitly assessed in this report, it is a consideration for the detailed design phase.
GF-SYS-EXT.1.1-4	The airport shall not have to spend more than TBD million USD on adaptations in order to be able to operate the aircraft from the airport.	✓	section 12.5
GF-SYS-EXT.1.2-1	The airline shall be able to choose between at least two different interior designs.	~	section 5.1: The current interior design is flexible, seats can be relocated and the exit door can be moved. However, an actual second interior design is not included yet, this is more relevant for the detailed design phase and will therefore be assessed then.
GF-SYS-EXT.1.2-3	The aircraft shall have a nominal turnaround time of no more than one hour.	✓	section 10.1 & section 10.4
GF-SYS-EXT.1.3-1	The aircraft shall not produce any harmful emissions.	✓	section 11.1
GF-SYS-EXT.1.3-2	The amount of harmful emissions emitted during manufacturing shall not exceed the amount of harmful emissions during manufacturing of similar conventional aircraft.	~	section 11.1: It is considered that the emissions will not be marginal during production relative to similar aircraft, however no actual research is performed in the emissions from production of the innovative parts. Therefore this requirement should first be investigated in more detail in a later phase before it can be checked for compliance.
GF-SYS-EXT.1.3-3	The aircraft shall be designed such that at least 85% of its parts are recyclable.	✓	section 10.3 & section 11.1

Conclusion & Recommendations

In this last chapter, a conclusion of the complete report is provided in chapter 14, followed by a list of recommendations for the future development of the Greenliner in section 14.2.

14.1. Conclusion

Up to today, the aircraft industry has shown itself to be incapable of adopting the necessary changes to reduce climate change effects and prevent the exhaustion of our natural resources. Since aviation is crucial to the modern globalised world, a viable alternative to fossil fuels must be found.

To reach this goal, new technology must be investigated. Research must be conducted in order to create a promising design and bring it to life, with a strong focus on sustainability. The mission statement is formulated as follows:
Assess the possibility of emission free flying in a commercial passenger aircraft, while competing with existing aircraft in total cost of ownership.
In order to fulfill this mission, the present design project was set up, with the goal of designing a 19 seat emission free regional airliner. After research into state-of-the-art technologies and a requirements-driven trade-off, a concept was selected that combines liquid hydrogen (LH2) energy storage with Proton Exchange Membrane Fuel Cells (PEM-FCs), to provide power to the Distributed Electrical Propulsion system (DEP). A conventional aircraft configuration was chosen to incorporate this concept, leading to the finalised conceptual design of the Greenliner aircraft.

To generate the Greenliner conceptual design, use was made of an iterative design method. This method was validated by comparing results to output values of parametric estimation methods by Raymer and Torenbeek, as well as design parameters of reference aircraft: the Dornier Do228 and the DHC-6 Twin Otter. The final design parameters of the Greenliner concept are shown in Table 14.1 and Table 14.2:

Table 14.1: General Greenliner characteristics

Crew	two pilots
Capacity	19 passengers
Payload	1900 kg
Length	16.7 m
Wingspan	16.1 m
Wing area	25.9 m^2
Airfoil	NACA 23018
Empty weight	4412 kg
Max. takeoff weight	6461 kg
Fuel	Liquid hydrogen
Max. fuel	151 kg
Powerplant	Magnax AXF185
Fuel cell type	PEMFC
Propellers	23 Greenliner props (26 kW each)
Propeller diameter	0.32 m

Table 14.2: Greenliner performance parameters

Cruise speed	137 m/s
Stall speed, clean conf.	51 m/s
Range	500 nmi
Service ceiling	12000 m
Rate of climb, average	3000 ft/min
Wing loading, cruise	2.45 kN/m^2
Take-off	1500 m
Landing	1500 m

The design methods and their outcomes were evaluated in extensive verification and validation procedures. As a whole, the design methods are considered verified, and the concept is validated. Room for improvement was found most notably in the modelling of the velocity field and the weight estimation for the fuel cell model. Additionally, due

to the complexity and novelty of distributed electric propulsion, it is imperative that more extensive research is done into the propulsion subsystem.

A sustainability assessment was done on the final concept, based on three main principles: environmental, social and financial sustainability. The Greenliner was compared on these principles to the Dornier 228. The Greenliner scores similarly to the Dornier on financial and social sustainability, but outperforms it in every environmental aspect.

Financial analysis predicts that with an initial investment of 320 million USD and a unit selling price of 12 million USD, the breakeven point occurs in 2038, with the expectation that the first unit is sold in 2029. The direct operating costs depend largely on the production cost of liquid hydrogen. Governments and airports are expected to invest in infrastructure for hydrogen production in the future.

To evaluate the expected performance of the Greenliner, compliance with requirements was examined. There are no requirements that are expected to remain unfulfilled. However, more research must be done to make sure certain requirements are indeed fully met. These include most notably: complete compliance with EASA and ICAO regulations, a lifetime of 35,000 cycles, and an amount of emissions during manufacturing that does not exceed that of similar conventional aircraft.

Looking back at the mission statement, the Greenliner conceptual design certainly shows the possibility of emission free flying. Even as industry experts claim large electric aircraft may not fly before 2050, the Greenliner shows a real opportunity for developing a sustainable, cost competitive airliner that can enter the market as early as 2030.

14.2. Recommendations for Further Research and Development

Recommendations for further reasearch and development regarding the most important subsystems of the Greenliner are presented below.

Fuel cell system

The fuel cell system design is one of the most complex features of the Greenliner concept. While the technology of fuel cells has been around for some time, it has never been applied in aerospace, which means that further research is needed. The key recommendations with respect to the fuel cell system are listed here.

1. **Investigate fuel cell startup time**
   Currently the startup time of the fuel cell system is estimated quite roughly. More research would improve the degree of certainty on the reliability of the system.

2. **Improve and extend the current model**
   Due to time and computing power constraints, the resolution and depth of the model are at this stage limited. It is recommended that additional modelling is done to improve the accuracy of predictions on fuel cell system performance. The main points of improvement for the current model are the velocity field accuracy and the total weight estimation.

3. **Prototype and test the fuel cell system**
   While improving the computational fuel cell model can improve confidence of the results, it should be validated in detailed design by experimental results. The recommendation is therefore to build a prototype of the fuel cell system and do extensive testing under all conditions it may encounter. Especially the influence of operational pressure should be evaluated in detail.

4. **Research fuel cell wall material alternatives**
   The current fuel cell design incorporates expanded graphite as the channel wall material. While graphite is commonly used in fuel cells, its application in automotive and aerospace engineering brings with it two main complications. Firstly, the high material cost, and secondly the brittleness of the material. Therefore, research into alternatives such as titanium nitride is recommended.

5. **Evaluate inlet filter performance**
   It is assumed at this stage that all particles that are harmful to the fuel cell can be filtered at the air inlet. However, no detailed research has yet been done into air filters and their operation at the required airspeed and mass flow levels. Therefore, air filter performance under these conditions should be evaluated in the next stage of the design.

6. **Introduce redundancy for the tank pump system**
   The current hydrogen circulation system does not incorporate redundancy explicitly into the design. This means it is currently a single point of failure, which should be avoided in aircraft design. Therefore, detailed design of the tank and pumps should focus on introducing redundancy.

Propulsion

In validating the propulsion subsystem design, a number of issues arose that deserve attention in the next phase of the Greenliner development. Recommendations for further design are listed here.

1. **Conduct additional research into boundary layer velocity profiles.**
   Turbulent flow along boundary layers is a complex phenomenon that is hard to predict precisely. Here for example one assumed incompressible flow. However, if the budget for time and computing power allows it, a Computational Fluid Dynamics (CFD) analysis would produce a larger degree of certainty on the flow conditions encountered by the propellers in the boundary layer. Additionally, a better estimate can be made for the beneficial effect of wake filling on drag reduction. To validate any CFD models, wind tunnel testing is also recommended.

2. **Investigate feasibility of ducted propellers**
   Early on in the design process, the option of using ducted propellers was discarded, because literature research showed no benefit to conventional propeller efficiency at the cruise speed the Greenliner flies at. However, in the context of BLI propulsion, placing ducts could have benefits, most notably creating a more uniform flow into the propellers [76] [87].

3. **Investigate influence of propulsion system on stability and controllability**
   Propeller engines are seeing a resurgence in interest, because of the potential of increasing efficiency both for electric and combustion-driven systems. However, it is recognised that the complex slipstream profile of a propeller can influence the stability and controllability of an aircraft [13]. For detailed sizing of especially the tail surfaces, this effect needs to be studied and taken into account. If the effect of the propulsion system on the tail proves to be detrimental, one possible solution could be to switch to a T-tail design. While this would incur a weight penalty due to increased structural complexity, it would keep the horizontal tail surface out of the wake of the propellers.

4. **Investigate feasibility of propulsive empennage**
   Because the emphasis of the Greenliner conceptual design has been on proving feasibility of the combination of fuel cells and electrical propulsion, the overall airframe design has been conservative. Conventional wing and tail configurations have been chosen, because they provide reliable and predictable performance at this stage of the design. However, the choice for DEP has some additional potential benefits that can be investigated. One of the more promising concepts is that of propulsive empennage: longitudinal and lateral stability and control can be provided by a thrust differential of the motors. This would remove the need for conventional tail surfaces and reduce drag. Additionally, this would of course solve the potential problem of propeller exhaust influence on tail surfaces. Because the Greenliner utilises 23 motors in total, this concept could readily be incorporated in the current design by individual control of each motor. A current example of research into propulsive empennage is the Delft University Unconventional Concept [33] [98].

5. **Analyse motor heat management in detail** The chosen motors are claimed to be effective in cooling by their manufacturer. However, detailed design will require more in depth calculations and modelling to properly design the complete cooling system.

6. **Increase propeller area to reach service ceiling**
   An assessment of the service ceiling proved the margin for manoeuvring at cruise altitude is insufficient. This issue can be resolved by increasing the total effective propeller area.

7. **Power several propellers with one motor for the whole or only part of the configuration**
   As discussed in section 5.5, one can get a better configuration when not matching the number of motors with the number of propellers.

8. **Update propeller configuration and sizing**
   As discussed in the Verification and Validation, the propeller configuration and sizing should be updated to reflect the validated sizing model. This means changing the number of propellers to 18, with each a radius of 19 cm. Of course, this update needs to also be included in a new complete design iteration to ensure it is taken into account in the complete subsystem sizing.

Additional Recommendations

The main focus of the Greenliner conceptual design has been on designing the fuel cell and propulsion subsystems. However, a number of recommendations can also be done with respect to the other features of the design. These recommendations are as follows:

1. **Recover energy during descent and braking**
   A potential additional benefit of operating an electric aircraft is the possibility of recovering kinetic energy by essentially letting the propellers function as turbines. The recovered energy can then be stored in the APU batteries. This is a topic of current research, and the benefits can be evaluated in detailed design.

2. **Research the effect of emitting water into the atmosphere**
   While water is not classified as a greenhouse gas, the effect of emitting water is debated in the scientific community. Seeing as the vision for the future includes large scale operation of hydrogen powered aircraft, this effect should be studied.

3. **Conduct additional research on implementation of solar panels**
   The investigation of solar panel feasibility for the Greenliner has been cursory. To determine the potential benefit with more confidence, a complete assessment should be done of the implications of including this feature in the Greenliner design. For example, there will be additional complications with regard to structural and electrical integration. A detailed assessment will show whether it is worth it to include solar panels in the final design.

4. **Improve the estimation of Return on Investment**
   As was mentioned in the report, an estimation of the Research & Development costs has proved to be more difficult than expected. The result is that this estimate has a low degree of confidence, which in turn means the Return on Investment is uncertain. The best course of action for further development is therefore to analyse the R&D costs in more detail.

5. **Evaluate integral cryogenic tank**
   The non-integrated tank design option is used in the Greenliner. Meanwhile, the advantage of using integrated tank design is not investigated. When the cryogenic tank is integrated with the fuselage, a stronger tank is required as structural loading of the fuselage is exerted onto the tank. More research can be conducted with regard to the different performance between integral and non-integral tank design for a hydrogon powered aircraft.

6. **Model LH2 boil-off loss during operation**
   For a short operating period, the small amount of boil-off loss of LH2 is accounted for by carrying extra 5% of hydrogen. In order to correctly estimate the DOC, the LH2 loss during transport, refilling and flight should be modelled.

7. **Investigate on an insulation compartment**
   In case of a hydrogen leakage, the cryogenic temperature will reduce the internal fuselage structure integrity when come into contact. This leakage may occur when the tank has a crack or a small whole. Therefore, the internal space of the tank compartment should be installed with insulation materials. This insulation compartment should be studied and designed such that in case of a large amount of hydrogen leakage, the fuselage structure will not fail immediately.

8. **Investigate lightning protection system**
   Lightning is likely to struck the aircraft for every 1,000 flight hours. Therefore, the lightning protection system is important to ensure the safety during operation. Especially when LH2 is used on board, the protection on the fuel system should be

Acknowledgements

Bibliography

search, 31(1):29–55, 1 2007. ISSN 1099-114X. doi: 10.1002/er.1226. URL http:https://doi.org/10.1002/er.1226.

[1] I. H. Abbott. *Theory of wing sections*. Dover publications, 1959.

[2] Central Intelligence Agency. The world factbook. https://www.cia.gov/library/publications/the-world-factbook/fields/2244.html#xx, 2017.

[3] R.K. Ahluwalia and X. Wang. Buildup of nitrogen in direct hydrogen polymer-electrolyte fuel cell stacks. *Journal of Power Sources*, 171(1):63 – 71, 2007. ISSN 0378-7753. Scientific Advances in Fuel Cell Systems, Turin, Italy, 13-14 September 2006.

[4] Airbus. Airbus aircraft: 2018 average list prices. Technical report, Airbus Press Office, 2018.

[5] Elisa Alonso, Frank R. Field, and Randolph E. Kirchain. Platinum availability for future automotive technologies. *Environmental Science & Technology*, 46(23):12986–12993, 2012.

[6] J.D. Anderson. *Aircraft Performance and Design*. McGraw-Hill, 2010.

[7] J.D. Anderson. *Fundamentals of aerodynamics*. McGraw-Hill Education, 2016.

[8] European Regions Airline Association. Eraa yearbook, 2018.

[9] R. Chouikh A. Guizani B. Larbi, W. Alimi. Effect of porosity and pressure on the pem fuel cell performance. *International journal of hydrogen energy*, pages Pages 8542–8549, 2012.

[10] Bacou-Dalloz. A– and c–weighted noise measurements. *Sound Source*, page 2, 2005.

[11] B.Blunier and A.Miraoui. *Air Management in PEM Fuel Cells: State-of-the-Art and Prospectives*. IEEE, 2007.

[12] Roland Berger. Aircraft electrical propulsion - the next chapter of aviation?, 2017.

[13] T. Bouquet. Modelling the propeller slipstream effect on the longitudinal stability and control. Master's thesis, Delft University of Technology, Delft, January 2016.

[14] Peter M. Bowers. *Boeing Aircraft since 1916*. Naval Institute Press, 1989. Page 495.

[15] G.D. Brewer. *Hydrogen Aircraft Technology 1st ed.* John Wiley & Sons, Inc., 1991.

[16] P. C. Carman. Fluid flow through granular beds. *Chemical Engineering Research and Design Journal*, pages S32–S48, 1997.

[17] M. J. Crocker. *Handbook of noise and vibration control*. John Wiley & Sons, Inc., 2007.

[18] N.S. Currey. *Aircraft Landing Gear Design*. AIAA, 1988.

[19] M. W. Verbrugge D. M. Bernardi. Mathematical model of a gas diffusion electrode bonded to a polymer electrolyte. *AIChE Journal*, pages Pages 1151–1163, 1991.

[20] M. Delgado Gosálvez, J. van Ham, S. Joosten, D. Juschus, G. Nieuwerth, T. van Pelt, L. Smit, M. Takken, Y. Wang, and T. Ziere. Green flying baseline report. Unpublished project report, May 2018.

[21] M. Delgado Gosálvez, J. van Ham, S. Joosten, D. Juschus, G. Nieuwerth, T. van Pelt, L. Smit, M. Takken, Y. Wang, and T. Ziere. Green flying midterm report. Not online available, June 2018.

[22] Ibrahim Dincer. Environmental and sustainability aspects of hydrogen and fuel cell systems. *International Journal of Energy Re-

[23] U.S. DRIVE Partnership. U.S. DRIVE. Hydrogen delivery technical team roadmap. P35, June 2013.

[24] European Aviation Safety Agency (EASA). Certification specifications and acceptable means of compliance for large aeroplanes cs-23 amendment 5, 2017.

[25] European Aviation Safety Agency (EASA). Certification specifications and acceptable means of compliance for large aeroplanes cs-25 amendment 21, 2018. replaced on 17/04/2018 without change to its content.

[26] Ricardo Energy & Environment. Heathrow airport 2015 emission inventory. *Heathrow Airport Limited*, 2015.

[27] H.J.Steiner et al. Multi-disciplinary design and feasibility study of distributed propulsion systems, 2012.

[28] J.Jimenez et al. The dynamic identity fusion index. *SAGE*, page 15, 2015.

[29] Federal Aviation Administration (FAA). *Aviation Maintenance Technician Handbook–Airframe*. Department of Transportation, 2012.

[30] R. Faye, R. Laprete, and R. Winter. Blended winglets for improved airplane performance. Boeing Aero magazine, January 2002.

[31] E. Gill. Systems engineering methods. Slides Systems Engineering and Aerospace Design (AE3211-I), 02 2018.

[32] L. Gipson. Reduce fuel burn with a dose of bli. https://www.nasa.gov/aero/reduce-fuel-burn-with-a-dose-of-bli, August 2017.

[33] K.J.M. Hameeteman. Unconventional propulsive empennage - future or fiction? Master's thesis, Delft University of Technology, Delft, September 2017.

[34] H.D.Kim. Distributed propulsion vehicles, 2010.

[35] Frederic Hecht. *Freefem++*. Laboratoire Jacques-Louis Lions, Universite Pierre et Marie Curie, 3rd edition, 2018.

[36] N.C. Heerens. Landing gear design in an automated design environment. Master of science thesis, TU Delft, 2014.

[37] Martin Hepperle. Javafoil. https://www.mh-aerotools.de/airfoils/javafoil.htm, 1996–2018.

[38] M. Hirscher. *Handbook of Hydrogen Storage: New Materials for Future Energy Storage*. 978-3-527-32273-2. WILEY-VCH, 2010.

[39] M Holweg. The genealogy of lean production. *Journal of Operations Management*, page 18, 2006.

[40] Y. SHIRAI N. ARIYASU I. INAGAKI, T. TAKECHI. Application and features of titanium for the aerospace industry. Technical report, NIPPON STEEL & SUMITOMO METAL, 2014.

[41] R. Lingwood I. Towle, C. Johnston and P.S. Grant. The aircraft at end of life sector: a preliminary study, 2004.

[42] J. Jean, A. Wang, and V. Bulovic. In situ vapor-deposited parylene substrates for ultra-thin, lightweight organic solar cells. *Organic Electronics*, 2016.

[43] M.L. Jetzer. S-ii lh2 tank construction. https://history.nasa.gov/afj/s-ii/s-ii-insulation.html, 2010.

[44] L. Decker K. Ohlig. The latest developments and outlook for hydrogen liquefaction technology. *American Institute of Physics*, 2014.

[45] P. Koltun. Materials and sustainable development. *Progress in Natural Science: Materials International Volume 20*, pages Pages 16–29, 2010.

[46] Ayça Kolukısa. Evaluating aircraft turnaround process in the

framework of airport design and airline behaviour, 2010.

[47] J. Kozeny. Über kapillare leitung des wassers im boden. *Sitzungs-bericht*, pages 271–306, 1927.

[48] I Kroo and A Shevell. *Aircraft Design: Synthesis and Analysis*, volume 0.99. Desktop Aeronautics, Inc., P.O. Box 20384 Stanford, CA 94309, January 2001.

[49] A. Lanz, J. Heffel, and C. Messer. *Hydrogen Fuel Cell Engines*. College of the Desert, Palm Desert, CA, USA, December 2001.

[50] P. L. Lasagna, K. G. Mackall, F. W. Burcham, and T. W. Putnam. Landing approach airframe noise measurements and analysis. *Scientific and Technical Information Office*, page 36, 1980.

[51] R. H. Liebeck. *Advanced subsonic airplane design & economic studies*. National Aeronautics and Space Administration, Lewis Research Center, 1995.

[52] Lilium. The lilium jet, the world's first electric vertical take off and landing jet. `https://lilium.com/`, 2018.

[53] L.Noels. Aircraft structures: Design example. `http://www.ltas-cm3.ulg.ac.be/MECA0028-1/StructAeroDesignExample.pdf`, 2014.

[54] S. Rowshanzamir M. Haghayegh, M. H. Eikani. Modelling and simulation of a proton exchange membrane fuel cell using computational fluid dynamics. *International journal of hydrogen energy*, pages Pages 21944–21954, 2017.

[55] D. Dickinson M. Nasri. Thermal management of fuel cell-driven vehicles using ht-pem and hydrogen storage. *EVER*, page 6, 2014.

[56] J. Markish. Valuation techniques for commercial aircraft program design. Master's thesis, Massachusetts Institute of Technology, 2002.

[57] J. E. Marte and D. W. Kurtz. A review of aerodynamic noise from propellers, rotors, and lift fans. *Jet Propulsion Laboratory*, page 58, 1970.

[58] S. K. Mital, S. M. Arnold J. Z. Gyekenyesi, R. M. Sullivan, J. M. Manderscheid, and P.L.N. Murthy. Review of current state of the art and key design issues with potential solutions for liquid hydrogen cryogenic storage tank structures for aircraft applications. *Scientific and Technical Information Office*, page 5, 2006.

[59] M.D. Moore. Distributed electric propulsion aircraft, Oktober 2015.

[60] J.A. Mulder, W.H.J.J. van Staveren, J.C. van der Vaart, E. de Weerdt, C.C. de Visser, A.C. in 't Veld, and E. Mooij. Flight dynamics. Slides Flight Dynamics (AE3202), 02 2018.

[61] A Nishizawa. Feather project in jaxa and toward future electric aircraft. *Next Generation Aeronautical Innovation Hub Center*, page 41, 2016.

[62] P. Nithiarasu O. Zienkiewicz, R. Taylor. *The Finite Element Method For Fluid Dynamics*. Butterworth-Heinemann, 5th edition, 2005.

[63] U.S. Department of Energy. Cost estimating guide. Technical report, U.S. Department of Energy, 2011.

[64] DEPARTMENT OF TRANSPORTATION of the U.S. Aerospace automation stretches beyond drilling and filling, 2016.

[65] R. O'Hayre, C. Suk-Won, W. Colella, and F.B. Prinz. *Fuel Cell Fundamentals*. John Wiley & Sons, 3rd edition, 2016.

[66] F. Oliviero. Aerospace design and systems engineering elements ii. Slides on Fundamentals on Wing Aerodynamics, 2015.

[67] F. Oliviero. Aerospace design and systems engineering elements ii. Slides on Lift and Drag estimation, 2015.

[68] F. Oliviero. Aerospace design and systems engineering elements ii. Slides on Mobile Surfaces on the Wing, 2015.

[69] National Research Council (US) Committee on Airliner Cabin Air Quality. *The Airliner Cabin Environment and the Health of Passengers and Crew*. National Academy of Sciences (US), 1986.

[70] Committee on Emergency and Continuous Exposure Guidance Levels for Selected Submarine Contaminants. *Emergency and Continuous Exposure Guidance Levels for Selected Submarine Contaminants: Volume 2*. National Academies Press (US), 2008.

[71] International Civil Aviation Organization. Environmentalprotection - annex 16 - volume i - aircraft noise, 2011. supersedes all previously released versions from before 17th November 2011.

[72] T. Page. Composites materials and their recycling. *imanager's Journal on Material Science*, pages 37–51, 2016.

[73] V. Pardee. Up in the air: How airplane carbon pollution jeopardizes global climate goals. `https://www.biologicaldiversity.org/programs/climate_law_institute/transportation_and_global_warming/airplane_emissions/pdfs/Airplane_Pollution_Report_December2015.pdf`, 2015.

[74] Joane Perry. End-of-life solutions: Retirement is not what it used to be, 2011.

[75] J. Ihonen P.Koski, L.C. Pérez. *Comparing Anode Gas Recirculation with Hydrogen Purge and Bleed in a Novel PEMFC Laboratory Test Cell Configuration*. VTT - Technical Research Centre of Finland, April 2015.

[76] A. P. Plas, M. A. Sargeant, V. Madani, D. Crichton, E. M. Greitzer, T. P. Hynes, and C. A. Hall. Performance of a boundary layer ingesting (bli) propulsion system. `http://silentaircraft.org/object/download/1922/doc/AIAA-2007-450-464.pdf`, January 2007.

[77] D.P. Raymer. *Aircraft Design: a Conceptual Approach*. American Institute of Aeronautics and Astronautics, 3rd edition, 1999.

[78] Dr. Jan Roskam. *Component Weight Estimation*. DARcorporation, 1997.

[79] Dr. Jan Roskam. *Airplane design Part III: Layout Design of Cockpit, Fuselage, Wing and Empennage: Cutaways and Inboard Profiles*. DARcorporation, 1997.

[80] Dr. Jan Roskam. *Airplane design Part IV: Layout of Landing Gear and Systems*. DARcorporation, 6th edition edition, 2010.

[81] Dr. Jan Roskam. *Airplane design Part VIII: Airplane Cost Estimation: Design, Development, Manufacturing and Operating*. DARcorporation, 6th edition edition, 2010.

[82] S. Rothermel, M. Evertz, J. Kasnatscheew, X. Qi, and Winter S. Nowak M. Grützke and. M. Graphite recycling from spent lithium-ion batteries. *CHEMSUMCEM Volume9, Issue24*, pages 3473–3484, 2016.

[83] P. Neksab S. Krasae, J.H. Stang. Development of large-scale hydrogen liquefaction processes from 1898 to 2009. *International Journal of Hydrogen Energy Volume 35, Issue 10*, pages 4524–4533, May 2010.

[84] M. H. Sadraey. *Aircraft Design: A Systems Engineering Approach*. John Wiley & Sons Ltd, 1 edition, 2013.

[85] D. Scholz. An optional apu for passenger aircraft. *5th CEAS Air and Space Conference 2015*, September 2015.

[86] Anja Schütz. maxon dc motors take to the air. *Maxon Motor Australia*, 2013.

[87] A. Sharma. Design of inlet for boundary layer ingestion in a blended wing body aircraft. Master's thesis, Delft University of Technology, Delft, January 2015.

[88] Sineton. A37k154 - electric motor. Technical report, Sineton Research and Development, 2016.

[89] P. Speers. Hydrogen mobility europe (h2me): Vehicle and hydro-

gen refuelling station deployment results. *World Electric Vehicle Journal*, page 11, 2018.

[90] G. Black U. Banach T. Hübert, L. Boon-Brett. Hydrogen sensors – a review. *Elsevier*, page 24, 2011.

[91] R. Tirnovan and S. Giurgea. Efficiency improvement of a pemfc power source by optimization of the air management. *International Journal of Hydrogen Energy*, 37(9):7745 – 7756, 2012. ISSN 0360-3199. doi: 10.1016.2012.02.029.

[92] E. Torenbeek. *Synthesis of subsonic airplane design: an introduction to the preliminary design of subsonic general aviation and transport aircraft, with emphasis on layout, aerodynamic design, propulsion and performance.* Kluwer, 1982.

[93] E. TZIMAS, C. FILIOU, S.D. PETEVES, and J.B. VEYRET. Hydrogen storage: State-of-the-art and future perspective. *"Audiovisual Library European Commission*, pages 29–33, 2003.

[94] S. Um, C.Y. Wang, and K. S. Chen. Computational fluid dynamics modeling of proton exchange membrane fuel cells. *Journal of The Electrochemical Society*, 2000.

[95] Unique. Aircraft apu emissions at zurich airport, 2005.

[96] Masatoshi Uno, Takanobu Shimada, and Koji Tanaka. Reactant recirculation system utilizing pressure swing for proton exchange membrane fuel cell. *Journal of Power Sources*, 196(5):2558 – 2566, 2011. ISSN 0378-7753. doi: https://doi.org/10.1016/j.jpowsour.2010.10.094. URL http://www.sciencedirect.com/science/article/pii/S037877531001894X.

[97] J. M. Urlacher. Electric circuits. *Pilotweb*, page 8, 2015.

[98] N.H.M. van den Dungen. Synthesis of an aircraft featuring a ducted-fan propulsive empennage. Master's thesis, Delft University of Technology, Delft, April 2017.

[99] Prof. Ad van Wijk. Green hydrogen economy in the northern netherlands. https://www.waterstofnet.eu/_asset/_public/powertogas/Conference/8-Ad-Van-Wijk_TUDelft_Green-hydrogen-economy_in-the-Northern-Netherlands.pdf, 2018.

[100] W. Verhagen and E. Mooij. Project management and systems engineering in dse. Slides PM/SE, spring 2018.

[101] G. Warwick. Boeing, jetblue back hybrid-electric regional startup. *Aviation Week & Space Technology*, 2017.

[102] P. Waurzyniak. Aerospace automation stretches beyond drilling and filling. *Advanced Manufacturing*, page 74, 2015.

[103] H. Weisberger. Ruag shows off nextgen dornier do228ng. https://www.ainonline.com/aviation-news/air-transport/2011-10-10/ruag-shows-nextgen-dornier-do228ng, October 2011. Accessed on April 2018.

[104] L. Werfelman. Thin skinned. *Aerosafety World*, 2011.

[105] K. Willcox. Aircraft systems engineering, lectureslides. MIT Aerospace Computational Design Laboratory, 2004.

[106] C. Winnefeld, T. Kadyk, B. Bensmann, U. Krewer, and H. Hanke-Rauschenbach. Modelling and designing cryogenic hydrogen tanks for future aircraft applications. *Energies*, pages 1–9, 2018.

[107] H-F Xu, X Wang, Z-G Shao, and I-M Hsing. Recycling and regeneration of used perfluorosulfonic membranes for polymer electrolyte fuel cells. *Journal of Applied Electrochemistry*, 32, 12 2002.

[108] X. Yan, M. Hou, H. Zhang, F. Jing, P. Ming, and B. Yi. Performance of pemfc stack using expanded graphite bipolar plates. *Journal of Power Sources*, 2006.

[109] S. Yourkowski. 777 tour fun facts & data. https://courses.washington.edu/ie337/Boeing%20Tour%20Facts.pdf, March 2003.

[110] R Zuber, Christian Hagelüken, K Seitz, R Privette, and K Fehl. Recycling of precious metals from fuel cell components, 2004.

[111] S. A. Zulkifli. *Energy Recovery from Landing Aircraft*. PhD thesis, Loughborough University, Loughborough, 2012.

[112] I. Čavka, O. Čokorilo1, and L. Vasov2. Energy efficiency in aircraft cabin environment: Safety and design. *Energy and Buildings Volume 115*, pages 63–68, 2016.